KATHOLIEKE UNIVERSITEIT LEUVEN
FAKULTEIT DER TOEGEPASTE WETENSCHAPPEN
DEPARTEMENT ELEKTROTECHNIEK
Afdeling ESAT
Kardinaal Mercierlaan 94, B-3030 Leuven (Heverlee), België

ADAPTIVE FILTERING AND ITS APPLICATIONS IN ECHO CANCELLATION AND BIOMEDICAL SIGNAL PROCESSING

Jury:
Prof. Dr. Ir. J. Berlamont, vice-dekaan, voorzitter
Prof. Dr. Ir. J. Vandewalle, promotor
Prof. Dr. Ir. W. Sansen
Dr. Ir. A. Barbé
Dr. Ir. D. Van Compernolle
Prof. Dr. G. Vantrappen
Prof. Dr. J. Janssens

Proefschrift voorgedragen tot
het behalen van het doctoraat
in de Toegepaste Wetenschappen

door

Jiande CHEN

U.D.C. 681.3 * C3

April 1989

Preface

Five years ago when I arrived at Leuven, alone, only with a letter from Prof. J. Vandewalle and a letter of permission to register at Katholieke Universiteit Leuven I did not dare to imagine that, one day, I could complete my doctoral study and have published about 20 papers. The accomplishment of this work would have been impossible without contributions from many people.

First of all I would like to express my heartfelt gratitude to my promotor Prof. J. Vandewalle for his continuous stimulation, encouragement and careful supervision during the development of this work. His patient guidance and broad scientific knowledge have not only made important contributions to this thesis but also influenced me on carrying out future scientific research. Special thanks to him for his supporting me to participate in many international conferences and for his courtesy of using English language in all activities carried out in our SISTA group.

With a great pleasure I wish to thank Prof. W. Sansen, Prof. G. Vantrappen and Prof. J. Janssens. They, together with my promotor, have constantly instructed me for the work presented in chapter 5 of this thesis. I am extremely grateful to Prof. G. Vantrappen and Prof. J. Janssens for their initiation of interesting research topics on the electrogastrography and for their providing me with necessary facilities in the acquisition of biomedical data.

Many thanks go to Dr. A Barbé and Dr. D. Van Compernolle for their critical review and constructive comments which made this thesis more readable.

I would also like to thank Prof. A. Oosterlinck and Prof. R. Govaerts for their kind concern to create a stimulating working environment and Prof. J. Peperstraete for the courses he gave.

Contributions from many other people are deeply appreciated. Parts of chapter 4 have been developed in cooperation with H. Bes and his colleagues from Siemens–ATEA. His ideas are reflected in this thesis. My acknowledgement goes to Ir. D. Sallaerts from Bell Telephone Company for his initiation of research on the nonlinear echo cancellation and for his constructive discussions. I would also like to express my feeling of thanks to D. Vandeputte, M. Vandeurzen, Dr. E. Vancutsem, A. Degreef, G. Tijskens, F. Debondt for their assistances in one way or another.

Very specially, I am indebted to my dear colleagues and ex-colleagues L. Vandenberghe, M. Moonen, Dr. S. Van Huffel, W. Mommaerts, Dr. B. De Moor, D. Callaerts, Dr. Shaohua Tan, J. Swevers, J. Vanderschoot and F. Meulemans. They have created a cheerful research environment in our SISTA group which made me happy to expect more SISTA seminars and meetings. Their kindness, especially in speaking English for me, is extremely appreciated. Without their cooperation I would have been isolated.

For the past years I have received both technical and daily aids from many people at Departement Elektrotechniek, particularly, I would like to thank I. Tokka, M. Elsen, L. Schol, D. Vermetten and G. Debuisson.

My acknowledgement also goes to Prof. Jiaruo Wan and Prof. Kai Wang both from East China Normal University who initiated my study in Belgium.

Continuous financial support from Katholieke Universiteit Leuven and ESAT laboratory is appreciated. I am particularly indebted to Mr. R. Vanermen from International Center for his generous help.

Finally I would like to take the opportunity to give my profound thanks to my parents for their education and their spiritual support. I also wish to thank our little son Tian-tian who always refreshes me with his endless and naive questions. I have found no words to express my appreciation to my wife Xiuxia for what she has done for me for the past many years. Her love, her incentive and her endurance have made many contributions to this work.

Jiande Chen
Leuven, April 1989

Dedicated to Xiuxia and Di

Contents

1 Introduction 1
- 1.1 Motivation and main results of the work . . . 1
- 1.2 Structures Algorithms and Applications . . . 4
  - 1.2.1 Structures . . . 4
  - 1.2.2 Algorithms . . . 7
  - 1.2.3 Applications . . . 8
- 1.3 Brief Historical Survey of Adaptive Filter . . . 12
  - 1.3.1 Development of Adaptive Algorithms . . . 12
  - 1.3.2 Progress in Applying Adaptive Filters . . . 14
- 1.4 Outline of the thesis . . . 15

2 LMS Adaptive FIR Filters 17
- 2.1 Introduction . . . 17
- 2.2 LMS Adaptive FIR Filter . . . 18
- 2.3 Properties of LMS Adaptive Filter . . . 20
  - 2.3.1 Convergence condition . . . 21
  - 2.3.2 Convergence rate . . . 21
  - 2.3.3 Weight vector noise . . . 23
  - 2.3.4 Misadjustment . . . 23
  - 2.3.5 Performance in a nonstationary environment . . . 24
- 2.4 Experiments With the LMS Algorithm . . . 25
  - 2.4.1 Effect of the step-size in a stationary environment . 26
  - 2.4.2 Effect of the SNR of the primary input . . . 29
  - 2.4.3 Effect of the step-size in a nonstationary environment 31
- 2.5 μ-Vector LMS Adaptive System . . . 32
  - 2.5.1 ALE as a pre-processor . . . 33
  - 2.5.2 μ-vector LMS algorithm . . . 34
  - 2.5.3 Simulations with the μ-vector LMS algorithm . . . 36
  - 2.5.4 Application . . . 37
- 2.6 Adaptive Lattice Filter . . . 38

  - 2.6.1 Introduction . . . 38
  - 2.6.2 Lattice structure . . . 38
  - 2.6.3 Applications of the lattice filter . . . 39
  - 2.6.4 Stochastic gradient lattice algorithm . . . 40
- 2.7 Lattice Form TSAF . . . 41
  - 2.7.1 Time-sequenced adaptive filter . . . 41
  - 2.7.2 Lattice form TSAF . . . 44
  - 2.7.3 Simulation results with lattice TSAF . . . 45
- 2.8 Conclusion . . . 48

3 Adaptive IIR Filters 49
- 3.1 Introduction . . . 49
- 3.2 Constrained and Recursive Adaptive IIR Filters . . . 50
  - 3.2.1 Constrained adaptive IIR filter . . . 50
  - 3.2.2 Recursive Adaptive Filter . . . 52
- 3.3 Adaptive ARMA Filter . . . 54
- 3.4 Adaptive LMS-ARMA Spectral Analysis . . . 57
  - 3.4.1 Introduction . . . 57
  - 3.4.2 Adaptive LMS-AR spectral estimation . . . 58
  - 3.4.3 Adaptive LMS-ARMA spectral analysis . . . 60
  - 3.4.4 Experiment with LMS-ARMA method . . . 61
- 3.5 Adaptive RLS-ARMA Spectral Analysis . . . 62
  - 3.5.1 RLS algorithm for adaptive ARMA filter . . . 62
  - 3.5.2 Experiment with RLS-ARMA method . . . 66
- 3.6 Comparison of Adaptive FIR and IIR Filters . . . 67
  - 3.6.1 Convergence . . . 67
  - 3.6.2 Performance comparison . . . 68
- 3.7 Conclusion . . . 71

4 Adaptive Echo Cancellation 73
- 4.1 Introduction . . . 73
- 4.2 Line Echo Cancellation . . . 75
  - 4.2.1 Echo on telephone network . . . 75
  - 4.2.2 Traditional methods of echo control . . . 78
  - 4.2.3 Adaptive echo cancellation . . . 79
  - 4.2.4 Some potential alternatives to LMS . . . 81
  - 4.2.5 Design criteria for echo canceller . . . 83
- 4.3 Acoustic Echo Cancellation . . . 86
  - 4.3.1 Introduction . . . 86
  - 4.3.2 Approaches for AAEC . . . 88
  - 4.3.3 Subband acoustic echo canceller . . . 91
  - 4.3.4 No-delay structure . . . 95

4.3.5 Simulation with the no-delay structure 97
4.4 Design of A No-delay Subband AAEC 98
4.4.1 General structure of the AAEC 98
4.4.2 Optimal number of subbands 102
4.4.3 Design consideration 104
4.4.4 Simulation results 105
4.4.5 Summary of the no-delay subband AAEC 110
4.5 Nonlinear Echo Cancellation 111
4.5.1 Echoes in full duplex data transmission system . . . 112
4.5.2 Nonlinear echo cancellation 113
4.5.3 Wiener scheme 115
4.5.4 Volterra expansion method 116
4.6 Design of A Nonlinear Echo Canceller 118
4.6.1 Model of simulation 119
4.6.2 Simulations with Volterra expansion approach 121
4.6.3 Simulations with Wiener scheme 124
4.6.4 Comparison of Volterra expansion and Wiener scheme 127
4.6.5 Design of an NEC with Volterra expansion 129
4.7 Conclusion 132

5 Adaptive Gastric Signal Processing 137
5.1 Introduction 137
5.2 Electrical Activities in the Stomach 138
5.2.1 Anatomy of the stomach 139
5.2.2 Electrical signaling in nerve or muscle cells 140
5.2.3 Slow wave (electrical control activity) 141
5.2.4 Contraction related activities 143
5.3 Electrogastrography 146
5.3.1 Measurement of EGG 147
5.3.2 Characteristics of EGG 147
5.4 Adaptive Enhancement of EGG 151
5.4.1 Principle of adaptive signal enhancement 152
5.4.2 Adaptive enhancement system 153
5.4.3 Performance analysis 157
5.4.4 Result and application 164
5.4.5 Summary 165
5.5 Adaptive Cancellation of Respiratory Artifact 166
5.5.1 Measurement 167
5.5.2 Adaptive cancellation of the respiratory artifact . . . 168
5.5.3 Results 170
5.5.4 Discussion and Conclusion 171
5.6 Information Available to be Extracted 172

5.6.1 Simulation of internal gastric signal 173
5.6.2 Transfer from the stomach to the abdomen 174
5.6.3 Simulation with contractions 178
5.6.4 Discussion and conclusion 181
5.7 Detection of Slow Wave Propagation 181
5.7.1 Localization of the stomach 182
5.7.2 Running cross correlation 183
5.7.3 Results 183
5.7.4 Discussion and Conclusion 185
5.8 Adaptive Spectral Analysis 186
5.8.1 Gastric dysrhythmias 187
5.8.2 Adaptive spectral analysis 188
5.8.3 Postprandial EGG spectral analysis 190
5.9 Conclusion 193

6 Conclusions 195

List of Figures

1.1 Block diagram of an acoustic echo canceller 2
1.2 Digital filter 4
1.3 Adaptive transversal FIR filter 5
1.4 IIR structure of an adaptive filter 6
1.5 Lattice structure of an adaptive filter 7
1.6 4-wire and 2-wire connection 9
1.7 Adaptive noise canceller 9
1.8 Adaptive line enhancer 10

2.1 Learning curves with different step-size 27
2.2 Performance of the adaptive filter with different step-size . 28
2.3 Square errors of 10 independent runs with a small step-size 29
2.4 Square errors of 10 independent runs with a large step-size 30
2.5 Simulated nonstationary signal in the primary input 32
2.6 Performance of adaptive filter with different step-size in a nonstationary environment 33
2.7 Performance comparison of the μ-vector LMS and the LMS algorithms 37
2.8 Time variation of error performance surfaces 42
2.9 Illustration of a time-sequenced adaptive filter 43
2.10 Lattice form time-sequenced adaptive filter 45
2.11 Comparison between TSAF and AF 46
2.12 Comparison between original and modified TSAF 47
2.13 Comparison among AF, TSAF and lattice form TSAF . . . 48

3.1 Block diagram of the recursive filter 53
3.2 Adaptive ARMA filter 55
3.3 Estimation of two sinusoids ($f_1 = 0.1Hz$, $f_2 = 0.2Hz$) . . . 62
3.4 Estimation of two sinusoids ($f_1 = 0.1Hz$, $f_2 = 0.11Hz$) . . 63
3.5 Spectral estimation of a biomedical signal using RLS-ARMA method 67

3.6 Simulation system for adaptive echo cancellation 69
3.7 Performance comparison in adaptive noise cancellation . . . 70
3.8 Performance comparison in adaptive line enhancement . . . 71
3.9 Performance comparison in spectral estimation 72

4.1 Detail of the hybrid 76
4.2 Echoes on a telephone line 77
4.3 An echo suppressor 78
4.4 Adaptive cancellation of echo on a telephone line 80
4.5 Transform-domain adaptive echo canceller 83
4.6 Impulse response 87
4.7 FIR–IIR implementation of an AAEC 89
4.8 Adaptive pole-zero echo canceller 90
4.9 Conventional structure of the subband AAEC 91
4.10 2-subband QMF analysis/synthesis scheme 93
4.11 No-delay subband AAEC 96
4.12 Convergence of the no-delay AAEC 98
4.13 ECho cancellation output with the new structure 99
4.14 General structure of an no-delay subband AAEC 100
4.15 Frequency response of the prototype lowpass filter 101
4.16 Computational reduction of the proposed AAEC 103
4.17 Convergence of the subband AAEC 106
4.18 Echo cancellation performance of the proposed subband AAEC 107
4.19 Echo cancellation performance of full-band AAEC 108
4.20 ERLE vs. adaptations in real-time simulation 109
4.21 The influence of open/close the door 110
4.22 The influence of **some one walking** 111
4.23 Echoes in full duplex data transmission system 112
4.24 Nonlinear echo canceller with the Wiener scheme 115
4.25 Analog subtraction NEC with the Wiener scheme 117
4.26 Simulation model based on U-interface on ISDN 119
4.27 Comparison of a linear EC and a nolinear EC of Volterra expansion 122
4.28 Comparison of linear EC and NEC of Wiener scheme 124
4.29 Learning curves of the NEC with different μ_a 126
4.30 Influence of the far-end signal on the NEC 128
4.31 ERLE of the NEC with a training period 131
4.32 Effect of the finite wordlength of weights 134
4.33 Effect of length M on performance and complexity of the NEC 135

5.1 The anatomy of the stomach 139
5.2 Ion concentration gradient and voltage gradient 141

5.3 The triggering of an action potential 142
5.4 The propagation of electrogastric signal in the stomach . . . 144
5.5 Configuration of gastric potentials 145
5.6 Relation between intra-cellular, extra-cellular electrical activities and contractile force 146
5.7 Block diagram of the overall system 147
5.8 Cutaneous electrogastrographies 148
5.9 Power spectrum (dB) of an EGG 149
5.10 A cutaneous EGG 150
5.11 Power spectrum of a tachygastrial EGG 152
5.12 An adaptive signal enhancer 153
5.13 Adaptive system of EGG signal enhancment 154
5.14 Pre-processing result 155
5.15 Simulated signals 159
5.16 Convergence of the system 160
5.17 Performance of the system 162
5.18 Effect of the pre-processing 164
5.19 Performance of the system in a stationary environment . . . 165
5.20 Comparison of the input signal waveform and the output signal waveform 166
5.21 Results of the adaptive enhancement of the EGG 167
5.22 Cutaneous (a) and intraluminal (b) electrogastric signals and respiratory signal (c) 168
5.23 Power spectrum of the cross correlation between the cutaneous and the intraluminal gastric signals 169
5.24 Power spectrum of the cross correlation between the cutaneous EGG and the respiratory signal 170
5.25 Adaptive system for the cancellation of respiratory disturbance 171
5.26 Cancellation of the respiratory artifact in the cutaneous EGG 172
5.27 Cancellation of the respiratory artifact in the intraluminal recording 173
5.28 Cancellation of the respiratory artifact (time domain) . . . 174
5.29 Simuled gastric signals in the stomach 175
5.30 Simulated cutaneous electrogastric signals 178
5.31 Configurations of gastric signals in the antrum 179
5.32 Simulated cutaneous electrogastric signals when contractions occur in the stomach 180
5.33 Positions of electrodes 182
5.34 Four channel cutaneous electrogastric signals 185
5.35 A portion of the filtered signals shown in Fig.5.34 186
5.36 Time lags among different channel EGG signals 187
5.37 Tachygastrial EGG signal 188

5.38 Running power spectra of a normal EGG 190
5.39 Running power spectra of a tachygastrial EGG 191
5.40 Running power spectra of a postprandial EGG 192

List of Tables

2.1 Effect of the step-size on the filter performance 30
2.2 Effect of the SNR on the filter performance 31

4.1 Comparison of algorithms 85
4.2 Influence of the length M on the NEC 123
4.3 Influence of the nonlinearity 123
4.4 The influence of step-size μ_w 125
4.5 The influence of step-size μ_a 125
4.6 Influence of the nonlinearities (Wiener scheme) 127

5.1 Composition of cutaneous EGG 149
5.2 Effect of μ' on the system performance with nonstationary inputs 161
5.3 Effect of β on the system performance 161
5.4 Effect of SNR of the primary input on the system performance 161
5.5 Effect of time variations of the frequency and the amplitude of the signal on the system performance 163
5.6 Conductivity of biological tissues 176

Abbreviations and Notations

Abbreviatoins

- AAEC: Adaptive Acoustic Echo Canceller
- A/D: Analog/Digital convertor
- AF: Adaptive Filter
- AFB: Adaptive Filters in Subbands
- ALE: Adaptive Line Enhancer
- AR: Auto-Regressive
- ARMA: Auto-Regressive Moving Average
- D/A: Digital/Analog converter
- EC: Echo Canceller
- ECG: Electrocardiography
- EGG: Electrogastrography
- ERL: Echo Return Loss
- ERLE: Echo Return Loss Enhancement
- FB(A): Analysis Filter Bank
- FB(S): Synthesis Filter Bank
- FFT: Fast Fourier Transform
- FIR: Finite Impulse Response
- HP: Highpass Filter
- IIR: Infinite Impulse Response
- ISDN: Integrated Services Digital Network
- LEC: Adaptive Linear Echo Canceller
- LMS: Least Mean Square

- LP: Lowpass Filter
- MMSE: Minimum Mean Square Error
- MSE: Mean Square Error
- NEC: Adaptive Nonlinear Echo Canceller
- RLS: Recursive Least Square
- SNR: Signal-to-Noise Ratio
- TSAF: Time-Sequenced Adaptive Filter

Notations

- j: Time index
- $P_x(\omega)$: Power of a time series x_j
- $E[\ ]$: Expectation
- $Cov[\ ]$: Covariance
- Fs: Sampling frequency
- f_s: Signal frequency
- z^{-1}: One sample delay
- $\triangle$: Number of delay

Adaptive filters

- x_j: Single channel Input of the adaptive filter
- d_j: Primary input
- y_j: Output of the adaptive filter
- e_j: Residual error of the adaptive filter
- w_{ij}: ith weight of the adaptive filter at time j
- μ: Step-size of the LMS algorithm
- N: Order of the adaptive filter (number of taps)

- X_j: Input vector of the adaptive filter at time j
- W_j: Weight vector at time j
- $P = E[d_j X_j]$: Cross-correlation vector
- $R = E[X_j X_j^T]$: Auto-correlation matrix
- W^*: Optimal (or MMSE) solution
- ϵ_j: Mean square error at time j
- ϵ_{min}: Minimum mean square error
- β: Nonstationary factor in the μ-vector LMS algorithm

Lattice filter

- k_p: Reflection coefficient on pth stage
- e^f_{pj}: pth stage forward error at time j
- e^b_{pj}: pth stage backward error at time j

Adaptive nonlinear echo canceller

- (n): Order of the Volterra expansion
- N: Number of linear coefficients of the nonlinear echo canceller
- M: Length of nonlinear memory
- $h^{(n)}_{k_1,\ldots,k_n}(j)$: Coefficients of nonlinear echo canceller with Volterra expansion method
- P_1: Power of the second order harmonic
- P_2: Power of the third order harmonic

Chapter 1

Introduction

1.1 Motivation and main results of the work

Signal enhancement, noise cancellation and spectral estimation are common and important subjects in telecommunications and in signal processing. The conventional methods, such as digital filtering and Fourier transform, are very useful tools for these purposes in situations where the statistics of signals are known a priori. However, many problems encountered in daily engineering activities involve extracting relevant information from some physical processes which are unknown or nonstationary or possibly both. An appropriate technique well suited for these problems is *adaptive filtering.*

For example, in telecommunication and hands-free telephone systems one may encounter the following annoying problem. There is unwanted coupling between a loudspeaker and a microphone installed in a same room or device called acoustic echo. In this situation both the talker's speech picked up by the microphone to be transmitted (the signal) and the acoustic echo, i.e., the speech from the loudspeaker picked up by the microphone (the noise) have the same characteristics. Conventional digital filtering is then obviously not applicable. However, an adaptive echo canceller shown in Fig.1.1 can remove the acoustic echo. The echo canceller is composed of an adaptive filter which simulates the acoustic echo path and produces a replica, y_j, of the echo n_j. This replica is then subtracted from the signal d_j.

It is impossible to know the characteristic of an acoustic echo path in advance. It is determined by lots of factors, such as the room size, the positions of the loudspeaker and the microphone, the reflection factor of the wall etc. Any movement of objects in the room, such as the gesture of

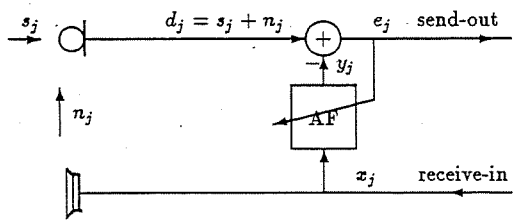


Figure 1.1: Block diagram of an acoustic echo canceller

the speaker, will cause the characteristic changes of the acoustic echo path, resulting in nonstationarity. The echo canceller, however, will adjust its coefficients to match the unknown characteristic of the acoustic echo path and follow its changes.

Another example is the cancellation of respiratory disturbance in a cutaneously measured biomedical signal in which the frequency of the respiratory disturbance may overlap with that of a relevant signal component. An adaptive noise canceller can deal with that problem if a reference input exists which is not correlated with the signal component but correlated with the respiratory disturbance. The adaptive noise canceller estimates the respiratory disturbance from the reference input and subtracts it from the measurement in the same way as an echo canceller does.

The third example we would like to give is the spectrum estimation of a time series which has changing frequency, such as a frequency modulated signal. A time series can be modeled as an autoregressive (AR) or autoregressive moving-average (ARMA) process and an adaptive filter can estimate the parameters of the AR or ARMA model. The power spectrum can therefore be calculated from these parameters. Since these parameters are iteratively adapted, the changing frequency of the input signal can well be traced.

Conventional digital filtering in the frequency domain is not suitable for the above applications. In the first example, the characteristic of the acoustic echo path is unknown and changing. It is not possible to use a digital filter with fixed weights. In the second example the overlap of the signal and noise frequencies makes the conventional digital filter design impractical. A running Fourier transform may be applied to estimate the instantaneous frequency in example 3. But it should be limited to applications where the change of the signal frequency is relatively slow, or in other words, there should be no significant change within the length of the window when a

fast Fourier transform is performed.

In summary, conventional digital filtering techniques are not suitable in either of the following situations:

1. The characteristic of an input signal to be processed is unknown.
2. The statistics of an input signal or a physical process are time-varying.
3. The frequency of a relevant signal component overlaps with that of the noise to be eliminated.

The adaptive filtering techniques to be discussed in this thesis are, however, suitable to the above situations. It has been a research subject for decades and has been especially active since the late 1970's. Fundamental adaptive filtering theory has been developed and it has found a great deal of applications in communications and signal processing.

The motivation of this work is to present developments of new algorithms and new applications.

During several years of research numerous results have been obtained and the main contributions of our work on the adaptive filter are as follows:

1. New algorithms for nonstationary signal processing. One is called the μ–vector least mean square (LMS) algorithm and the other is the lattice form time-sequenced algorithm, both presented in chapter 2.
2. Adaptive infinite impulse response (IIR) filters in chapter 3. A new structure of the adaptive IIR filter is proposed and LMS and recursive least square (RLS) algorithms are derived. A systematic treatment of adaptive IIR filters is provided. The comparison between the adaptive IIR filters and the adaptive FIR filter is given.
3. Applications of the adaptive filter in acoustic echo cancellation in teleconferencing and hands-free telephone systems and in nonlinear echo cancellation in data transmission systems. A new structure for the subband acoustic echo canceller is proposed and a subband acoustic echo canceller using the structure is designed. A nonlinear echo canceller for an ISDN line is designed and its performance is thoroughly investigated.
4. Adaptive biomedical signal processing. The applications of adaptive filter in electrogastric signal detection and processing are well exploited. Several adaptive techniques have been developed. Based on these techniques some important problems in the research community of electrogastrography have been solved and some important new results on the electrogastrography have been obtained.

5. Adaptive ARMA spectrum estimation. The adaptive IIR filter and its algorithms presented in chapter 3 have been successfully applied to estimate power spectra of sinusoids in white noise and of biomedical signals with changing frequencies.

1.2 Adaptive Filters: Structures, Algorithms and Applications

A digital filter is shown in Fig.1.2 where x_j is its input at time instant j, y_j is its output and $H(z)$, its transfer function. The output of the filter depends linearly on its input and its internal structure, i.e., the implementation of $H(z)$. The coefficients of the filter are specially designed and are time invariant.

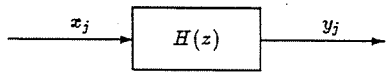


Figure 1.2: Digital filter

An adaptive digital filter is an adaptive version of the digital filter. It has the same representation as in Fig.1.2 but with an important distinction – the coefficients of the adaptive filter can be adjusted according to some algorithm to control the transfer function over a useful range in order to match the statistical properties of the input and to follow its changes.

Adaptive filters can be classified into different categories according to its structures and algorithms. What is meant by structure is the particular way of realizing the filter. What is meant by algorithm is the adaptation algorithm which enables the filter transfer function to track some statistical changes of its external environment based on a certain performance measure.

1.2.1 Structures

According to the expression of a filter transfer function there are two structures: finite impulse response (FIR) and infinite impulse response (IIR). According to the realization of the transfer function, however, each can be divided into transversal (direct realization) and lattice structures.

FIR and IIR Structures

The most commonly employed structure for an adaptive filter is the FIR filter as depicted in Fig.1.3. z^{-1} in the figure stands for a delay unit. The tapped delay line, $x_j, x_{j-1}, ..., x_{j-N+1}$ is adaptive filter input at time j, N is the order of the adaptive filter and $w_{kj}\,(k = 1, N)$ are the adjustable filter weight coefficients. The output of the adaptive filter is represented by a difference equation:

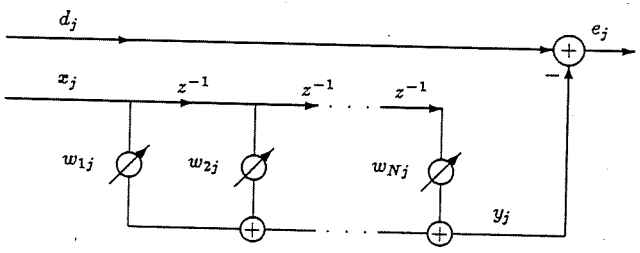


Figure 1.3: Adaptive transversal FIR filter

$$y_j = \sum_{k=1}^{N} w_{kj} x_{j-k+1} \tag{1.1}$$

The transfer function at time j can then be written as:

$$H_j(z) = \sum_{k=1}^{N} w_{kj} z^{1-k} \tag{1.2}$$

Since the filter coefficients are changing over time, the transfer function is also changing, therefore a time index j is needed.

Another possible structure for an adaptive filter is the IIR filter. Fig.1.4 illustrates one of possible structures. In this structure a feedback loop is added and another tapped delay line is included.

The output of this adaptive IIR filter is expressed by the following equation:

$$y_j = \sum_{k=1}^{p} a_{kj} x_{j-k+1} + \sum_{k=1}^{q} c_{kj} y_{j-k} \tag{1.3}$$

where $a_{kj}\ (k = 1, 2, ..., p)$ and $c_{kj}\ (k = 1, 2, ..., q)$ are weight coefficients of the adaptive filter.

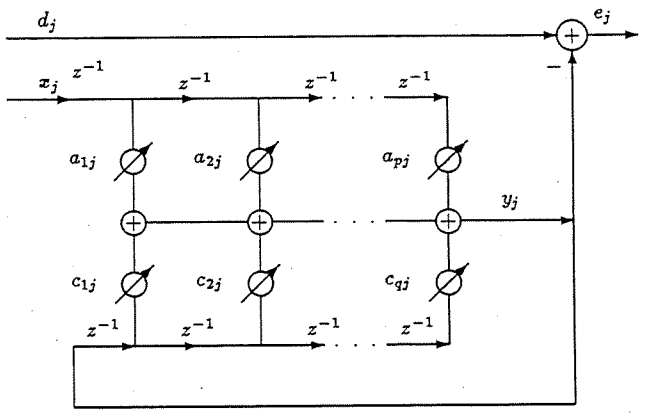


Figure 1.4: IIR structure of an adaptive filter

Taking z-transform the above equation can be written as:

$$\begin{aligned} Y_j(z) &= X_j(z)(a_{1j} + a_{2j}z^{-1} + ..., +a_{pj}z^{-p+1}) \\ &\quad +Y_j(z)(c_{1j}z^{-1} + c_{2j}z^{-2} + ..., +c_{qj}z^{-q}) \end{aligned} \tag{1.4}$$

By defining

$$A_j(z) = a_{1j} + a_{2j}z^{-1} + ..., +a_{pj}z^{-p+1} \tag{1.5}$$

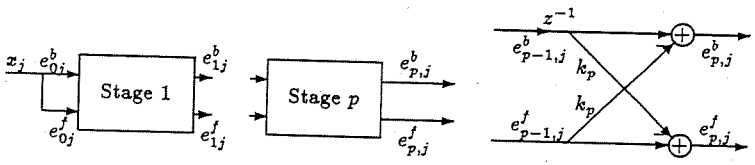
$$C_j(z) = 1 - c_{1j}z^{-1} - c_{2j}z^{-2} - ..., -c_{qj}z^{-q} \tag{1.6}$$

the transfer function of the filter is:

$$H_j(z) = \frac{A_j(z)}{C_j(z)} \tag{1.7}$$

Transversal and Lattice Structures

The realization of the adaptive FIR and adaptive IIR filters shown in Fig.1.3 and Fig.1.4 is called *transversal* structure which is universally utilized. Another implementation of the adaptive filter is the *lattice* structure. A lattice adaptive FIR filter is shown in Fig.1.5. e^f_{pj} and e^b_{pj} are called forward and backward errors on the pth stage at time j. $k_p\ (p = 1, 2, ..., N)$ are commonly called reflection or PARCOR (PARtial CORrelation) coefficients (Markel 1976).



(a) Block diagram (b) Structure of the pth stage

Figure 1.5: Lattice structure of an adaptive filter

An adaptive filter in the lattice structure involves both time- and order-updates. It has a rapid convergence, is robust and efficient in computations.

1.2.2 Algorithms

Unlike the conventional digital filter, the coefficients of an adaptive filter can be adjusted iteratively in order to follow the statistic changes of an external environment. Once the filter structure has been chosen, an adaptation algorithm must be chosen. The selection of the adaptation algorithm is generally based on the following main factors:

1. Computational complexity of the algorithm.

2. Convergence speed of the adaptation.

3. Accuracy of the transfer function in the steady-state.

A simple and commonly used adaptation algorithm is the least mean-square (LMS) algorithm which is the main subject of this dissertation. The LMS algorithm is based on the steepest descent method. It avoids explicit solution of a set of linear equations. Therefore it is the simplest and the most widely utilized algorithm. Its disadvantages are slow convergence and sub-optimal performance.

In practice where fast adaptation and better performance are needed, the recursive least square (RLS) algorithm can be used. Compared with the LMS algorithm the RLS algorithm is much more complicated in computations, especially when the order of the adaptive filter is high because of the involved matrix computation.

1.2.3 Applications

The main advantage of the adaptive filter, i.e., the ability to operate efficiently in an unknown and/or changing environment, makes it very attractive in many applications, such as in telecommunications, in biomedical signal processing, in geophysical signal processing, in the elimination of radar clutter and in sonar processing. Some applications related to our work are outlined in the following paragraphs.

Echo cancellation

The application of the adaptive filter in echo cancellation can be classified into three categories:

1. Acoustic echo cancellation in teleconferencing and hands-free telephone systems.

2. Linear echo cancellation on telephone networks and in data transmission systems.

3. Nonlinear echo cancellation in data transmission systems.

The acoustic echo results from the unwanted coupling between the loudspeaker and microphone in teleconferencing or hands-free telephone systems. It has been described at the beginning of this chapter and will be discussed in detail in chapter 4.

The echo in a telephone network is produced by a hybrid which performs the conversion from two-wire to four-wire and vice versa. Fig.1.6 illustrates the connection through the hybrid (H) for a long distance telephone network. The hybrid attempts to couple the signal energy from the far-end talker to the subscriber, such that no energy is reflected back to the far-end. Due to some uncertainties, such as unknown loop length, component variance etc., however, these impedances can hardly be matched completely. Consequently not all of the signal energy is directed to the subscriber and some is returned along the four-wire as an echo n_j.

To overcome this problem a similar adaptive echo canceller (EC) as depicted in Fig.1.1 can be inserted in the network and the echo can be cancelled in the same way as in Fig.1.1.

Nonlinear echo is only a small portion of an echo. It is originated from some nonlinear components in the telephone network, mainly A/D and D/A convertors. The cancellation of this nonlinear effect can be achieved by using a nonlinear echo canceller.

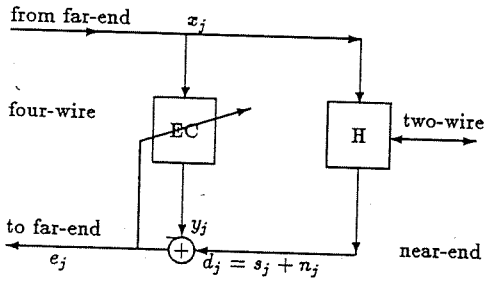


Figure 1.6: 4-wire and 2-wire connection on a telephone network

Adaptive Noise Cancellation

In digital signal processing practice, one often encounters the following problem: A measurement is a mixture of an interesting signal and noise and their frequencies overlap, such as, 50 Hz interference in an electrocardiographic signal and background noise in a speech signal.

The structure of an adaptive noise canceller is shown in Fig.1.7. The input, d_j, to the summation (called primary input) consists of a signal s_j and noise n_j. They are assumed to be uncorrelated with each other. The input to the adaptive filter (called reference input) x_j is composed of noise n'_j which is only related to n_j in the primary input.

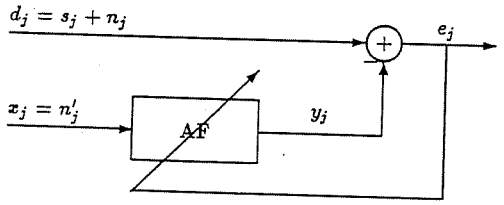


Figure 1.7: Adaptive noise canceller

The adaptive filter produces an output y_j which is an estimate of the noise n_j and subtracts it from the primary input.

The echo canceller is, in fact, an example of the adaptive noise canceller.

Adaptive Line Enhancer

A very simple and popular application of the adaptive filter is the adaptive line enhancer (ALE). The ALE can be applied to detect a low level sine wave (or periodic signals in general) in a background of additive noise with a broadband spectrum, such as white noise.

The ALE is illustrated in Fig.1.8. It consists of a bulk delay element $\triangle$ and an adaptive filter (AF). The input of the adaptive filter is a delayed version of primary input d_j and its output y_j is subtracted from signal d_j to produce an estimation error e_j. The estimation error is, in turn, used to adaptively control the weights of the adaptive filter. The delay element $\triangle$ should be chosen large enough to remove the correlation between the noise component in the primary input and the noise component in the adaptive filter input, i.e., $E[n_j n_{j-\triangle}] = 0$. The ALE can suppress broadband noise contained in the primary input, while passing correlated narrow-band components with little attenuation.

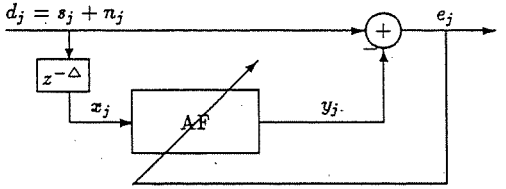


Figure 1.8: Adaptive line enhancer

The name of adaptive line enhancer results from the fact that it can *enhance* the presence of a sine wave whose spectrum consists of harmonic *lines* in an *adaptive* manner.

Adaptive Spectrum Estimation

The power spectrum is a very useful measure of a discrete time series in frequency domain. There are two ways of estimating the power spectrum: nonparametric spectral analysis and parametric spectral analysis. In parametric methods a certain model is assumed for a time process. Two commonly used models are autoregressive (AR) and autoregressive moving-average (ARMA) models. In the following paragraphs an outline of the applications of the adaptive filter in adaptive AR and ARMA spectrum estimations is presented.

a) Adaptive AR Spectrum Estimation

In the AR model, a time series is modeled as the output of a linear filter excited by a white noise process as follows:

$$x_j = -\sum_{k=1}^{N} a_k x_{j-k} + n_j \tag{1.8}$$

where a_k $(k = 1, 2, ..., N)$ are autoregressive parameters and n_j is an uncorrelated random process of power σ_n^2.

The excitation n_j can be written as the nonpredictable portion of the signal or the innovation of the AR process:

$$n_j = x_j + \sum_{k=1}^{N} a_k x_{j-k} \tag{1.9}$$

Once the parameters of the AR model are known the power spectrum of the process can be calculated as

$$P_x(\omega) = \frac{\sigma_n^2}{|1 + \sum_{k=1}^{N} a_k e^{-i\omega k}|^2} \tag{1.10}$$

i in the above equation stands for an imaginary number, $i = \sqrt{-1}$.

In the application of adaptive spectrum estimation, the data sample x_j is available and it is desired to compute an AR power spectrum of the underlying signal process from the data sample x_j. It can be shown that an adaptive filter provides a simple way of computing the power spectrum.

In Fig.1.8 if $\triangle$ is chosen to be one sample, the estimation error e_j is given by

$$e_j = x_j - \sum_{k=1}^{N} w_{kj} x_{j-k} \tag{1.11}$$

where w_{kj} $(k = 1, 2, ..., N)$ are the adaptive filter coefficients. e_j can be proven to be an uncorrelated random process, thus the similarity between EQ(1.9) and (1.11) is very clear. That is, after the convergence of the adaptation algorithm $-w_{kj}$ will approach the true values of a_k in Eq(1.8). The power spectrum can then be calculated from the coefficients w_{kj} $(a_k = -w_{kj},\ k = 1, 2, ..., N)$.

b) Adaptive ARMA Spectrum Estimation

A more general model for a time series x_j is the ARMA model. It assumes that the time series x_j can be modeled as the output of a p pole and q zero filter excited by a white noise process:

$$x_j = -\sum_{k=1}^{p} a_k y_{j-k} + \sum_{k=0}^{q} c_k n_{j-k} \tag{1.12}$$

where n_j is white noise and $c_0 \equiv 1$, $a_k (k = 1, 2, ..., p)$ and $c_k (k = 1, 2, ..., q)$ are parameters of the ARMA model.

Once these parameters are identified the power spectrum of the time series x_j can be calculated:

$$P_x(\omega) = \frac{\sigma_n^2 |1 + \sum_{k=1}^{q} c_k e^{-i\omega k}|^2}{|1 + \sum_{k=1}^{p} a_k e^{-i\omega k}|^2} \tag{1.13}$$

where, $i = \sqrt{-1}$.

1.3 Brief Historical Survey of Adaptive Filter

The adaptive filtering techniques have a long history. The recent rapid development of integrated circuit, especially the very large scale integrated circuit (VLSI) and the availability of digital signal processors have made practical implementations of adaptive algorithms possible and has intensified the research in this subject. In this section we present a brief historical review of the developments of the adaptive filter in the areas which are closely related to the subject matter of this thesis. These areas involve adaptive algorithms including least mean square algorithm, recursive least mean-square algorithm, adaptive IIR filter, adaptive noise cancellation and adaptive spectrum analysis.

1.3.1 Development of Adaptive Algorithms

The earliest derivation of the **least mean-square algorithm** can be traced back to the late 1950's. During that time a number of researchers were working independently on different applications of adaptive filters. The LMS algorithm was devised by Widrow and Hoff in 1959 in their work on the adaptive linear threshold logic element (Widrow and Hoff, 1960).

The LMS algorithm is a stochastic gradient algorithm. It iterates each weight coefficient of the adaptive filter in the direction of the gradient of the squared amplitude of a residual error signal with respect to that coefficient.

During the late 1970's several versions of the LMS algorithm were developed. These include block implementation (Clark 1981) of the LMS algorithm and the frequency domain LMS algorithm (Dentino 1978, Mansour 1982). They are more efficient in computations since the weight vector is only adapted once for a block of input samples.

For nonstationary signal processing several LMS-based algorithms have been developed. Ferrara and Widrow proposed a time-sequenced LMS algorithm (Ferrara 1981). The algorithm performs better than the conventional LMS algorithm for nonstationary signals having recurring statistical characteristics. The convergence of that algorithm is, however slower than the conventional one. A variable step (VS) LMS algorithm was developed in (Harris 1986). The difference between this algorithm and the LMS is that the step-size is not a constant but a variable, which makes the algorithm more suitable for nonstationary environment at the expense of computations. In chapter 2 we present a μ-vector LMS algorithm which has the same computational complexity as the conventional one but produces better performance with nonstationary inputs (Chen 1988c).

The performance of the LMS adaptive filter in stationary and nonstationary environments has been analyzed in (Barbe 1971, Widrow 1975, 1976, Zeidler 1978, Treichler 1979, Rickard 1979, Bershad 1980, Morgan 1983, Anderson 1983).

The original reference on the *recursive least square* (RLS) algorithm seems to be Plackett (Plackett, 1950) although it has been derived independently by several investigators. The RLS algorithm usually converges much faster than the LMS algorithm at the expense of the increased computational complexity. One very active objective in the research on RLS filter has been to derive computationally efficient algorithms. Some computationally efficient algorithms can be found in the literature, such as the "fast Kalman" method (Ljung 1978 and Falconer 1978), vector space approaches (Cioffi 1983, 1984) and the lattice form predictor (Morf 1978).

The *adaptive IIR filter* was originally proposed in (White 1975), known as the recursive adaptive digital filter. In this kind of adaptive IIR filter the feedback is taken from the output of the adaptive filter. Various simplifications and improvements to the recursive LMS algorithm have been proposed in (Feintuch 1976, David 1981, Hsia 1981 and Larimore 1980). A general algorithm for the recursive adaptive filter is given in (Widrow 1985).

Another form of the adaptive IIR filter where the feedback is taken from the residual error between the primary input and the adaptive filter output, was proposed (Friedlander 1982). He used that structure and the maximum likelihood algorithm to estimate the power spectrum of an input time series. Recently we derived an LMS algorithm and an RLS algorithm

for this type of adaptive filter (Chen 1987d). It will be discussed in chapter 3.

1.3.2 Progress in Applying Adaptive Filters

The adaptive line enhancer was originally proposed by Widrow and his colleagues. The first attempt was made in 1965 to cancel 60 Hz interference in an electrocardiographic recording. In 1975, Widrow et al. published a very comprehensive paper with different examples on adaptive noise cancellation.

The adaptive echo canceler was first proposed in (Sondhi 1967 and Kelly 1970). It is a successful application of the adaptive filter to eliminate echoes in telephone networks. Different algorithms have been applied to the adaptive echo canceler. Most of them are based on LMS algorithm because it is simple and easy for hardware implementation.

It appears that Kellermann (Kellermann 1985) first used the adaptive subband filtering technique in acoustic echo cancellation. The acoustic echo path usually has a very long impulse response and heavy computations would be involved if the conventional echo canceler is applied. A new structure for subband acoustic echo canceler will be shown in chapter 4, with which we have avoided the problem of introducing delays in the transmission line (Chen 1988a and 1988d).

The first attempt to cancel the nonlinear distortion in the echo path was made by Thomas (Thomas, 1971), in which the Volterra representation of nonlinear systems was applied to the echo control problem. Different methods have been proposed, such as the table look-up method (Holte 1981), the distributed arithmetic architecture (Peled 1974 and Sicuranza 1986), the Wiener scheme (Corredera 1985) and the Volterra expansion (Agazzi 1982). Recently we have designed an adaptive nonlinear echo canceller using a 3rd order Volterra expansion (Chen 1989a and 1989d).

Compared with the applications of the adaptive filter in other fields, the progress of applications of the adaptive filter in biomedical signal processing has been slow although the first application of the adaptive noise canceler was for the elimination of 60 Hz interference in electrocardiography.

In the research of the electrogastrography (cutaneous electrogastric measurement) it has been claimed that the conventional digital filtering technique should not be used because the frequency or harmonics of the interesting gastric signal component overlap with the frequency of the noise. Kentie et al. (Kentie 1981) proposed a simple adaptive filtering scheme, but no satisfactory results were obtained. During previous years, however, we have made a lot of efforts on this field – adaptive gastric signal processing. A number of results have been obtained (Chen 1987b, 1988e, 1988f

KATHOLIEKE UNIVERSITEIT LEUVEN
FAKULTEIT DER TOEGEPASTE WETENSCHAPPEN
DEPARTEMENT ELEKTROTECHNIEK
Afdeling ESAT
Kardinaal Mercierlaan 94, B-3030 Leuven (Heverlee), België

ADAPTIVE FILTERING AND ITS APPLICATIONS IN ECHO CANCELLATION AND BIOMEDICAL SIGNAL PROCESSING

Jury:
Prof. Dr. Ir. J. Berlamont, vice-dekaan, voorzitter
Prof. Dr. Ir. J. Vandewalle, promotor
Prof. Dr. Ir. W. Sansen
Dr. Ir. A. Barbé
Dr. Ir. D. Van Compernolle
Prof. Dr. G. Vantrappen
Prof. Dr. J. Janssens

Proefschrift voorgedragen tot
het behalen van het doctoraat
in de Toegepaste Wetenschappen

door

Jiande CHEN

U.D.C. 681.3 * C3

April 1989

Preface

Five years ago when I arrived at Leuven, alone, only with a letter from Prof. J. Vandewalle and a letter of permission to register at Katholieke Universiteit Leuven I did not dare to imagine that, one day, I could complete my doctoral study and have published about 20 papers. The accomplishment of this work would have been impossible without contributions from many people.

First of all I would like to express my heartfelt gratitude to my promotor Prof. J. Vandewalle for his continuous stimulation, encouragement and careful supervision during the development of this work. His patient guidance and broad scientific knowledge have not only made important contributions to this thesis but also influenced me on carrying out future scientific research. Special thanks to him for his supporting me to participate in many international conferences and for his courtesy of using English language in all activities carried out in our SISTA group.

With a great pleasure I wish to thank Prof. W. Sansen, Prof. G. Vantrappen and Prof. J. Janssens. They, together with my promotor, have constantly instructed me for the work presented in chapter 5 of this thesis. I am extremely grateful to Prof. G. Vantrappen and Prof. J. Janssens for their initiation of interesting research topics on the electrogastrography and for their providing me with necessary facilities in the acquisition of biomedical data.

Many thanks go to Dr. A Barbé and Dr. D. Van Compernolle for their critical review and constructive comments which made this thesis more readable.

I would also like to thank Prof. A. Oosterlinck and Prof. R. Govaerts for their kind concern to create a stimulating working environment and Prof. J. Peperstraete for the courses he gave.

Contributions from many other people are deeply appreciated. Parts of chapter 4 have been developed in cooperation with H. Bes and his colleagues from Siemens–ATEA. His ideas are reflected in this thesis. My acknowledgement goes to Ir. D. Sallaerts from Bell Telephone Company for his initiation of research on the nonlinear echo cancellation and for his constructive discussions. I would also like to express my feeling of thanks to D. Vandeputte, M. Vandeurzen, Dr. E. Vancutsem, A. Degreef, G. Tijskens, F. Debondt for their assistances in one way or another.

Very specially, I am indebted to my dear colleagues and ex-colleagues L. Vandenberghe, M. Moonen, Dr. S. Van Huffel, W. Mommaerts, Dr. B. De Moor, D. Callaerts, Dr. Shaohua Tan, J. Swevers, J. Vanderschoot and F. Meulemans. They have created a cheerful research environment in our SISTA group which made me happy to expect more SISTA seminars and meetings. Their kindness, especially in speaking English for me, is extremely appreciated. Without their cooperation I would have been isolated.

For the past years I have received both technical and daily aids from many people at Departement Elektrotechniek, particularly, I would like to thank I. Tokka, M. Elsen, L. Schol, D. Vermetten and G. Debuisson.

My acknowledgement also goes to Prof. Jiaruo Wan and Prof. Kai Wang both from East China Normal University who initiated my study in Belgium.

Continuous financial support from Katholieke Universiteit Leuven and ESAT laboratory is appreciated. I am particularly indebted to Mr. R. Vanermen from International Center for his generous help.

Finally I would like to take the opportunity to give my profound thanks to my parents for their education and their spiritual support. I also wish to thank our little son Tian-tian who always refreshes me with his endless and naive questions. I have found no words to express my appreciation to my wife Xiuxia for what she has done for me for the past many years. Her love, her incentive and her endurance have made many contributions to this work.

Jiande Chen
Leuven, April 1989

Dedicated to Xiuxia and Di

Contents

1 Introduction 1
- 1.1 Motivation and main results of the work . . . 1
- 1.2 Structures Algorithms and Applications . . . 4
  - 1.2.1 Structures . . . 4
  - 1.2.2 Algorithms . . . 7
  - 1.2.3 Applications . . . 8
- 1.3 Brief Historical Survey of Adaptive Filter . . . 12
  - 1.3.1 Development of Adaptive Algorithms . . . 12
  - 1.3.2 Progress in Applying Adaptive Filters . . . 14
- 1.4 Outline of the thesis . . . 15

2 LMS Adaptive FIR Filters 17
- 2.1 Introduction . . . 17
- 2.2 LMS Adaptive FIR Filter . . . 18
- 2.3 Properties of LMS Adaptive Filter . . . 20
  - 2.3.1 Convergence condition . . . 21
  - 2.3.2 Convergence rate . . . 21
  - 2.3.3 Weight vector noise . . . 23
  - 2.3.4 Misadjustment . . . 23
  - 2.3.5 Performance in a nonstationary environment . . . 24
- 2.4 Experiments With the LMS Algorithm . . . 25
  - 2.4.1 Effect of the step-size in a stationary environment . 26
  - 2.4.2 Effect of the SNR of the primary input . . . 29
  - 2.4.3 Effect of the step-size in a nonstationary environment 31
- 2.5 μ-Vector LMS Adaptive System . . . 32
  - 2.5.1 ALE as a pre-processor . . . 33
  - 2.5.2 μ-vector LMS algorithm . . . 34
  - 2.5.3 Simulations with the μ-vector LMS algorithm . . . 36
  - 2.5.4 Application . . . 37
- 2.6 Adaptive Lattice Filter . . . 38

  - 2.6.1 Introduction . . . 38
  - 2.6.2 Lattice structure . . . 38
  - 2.6.3 Applications of the lattice filter . . . 39
  - 2.6.4 Stochastic gradient lattice algorithm . . . 40
- 2.7 Lattice Form TSAF . . . 41
  - 2.7.1 Time-sequenced adaptive filter . . . 41
  - 2.7.2 Lattice form TSAF . . . 44
  - 2.7.3 Simulation results with lattice TSAF . . . 45
- 2.8 Conclusion . . . 48

3 Adaptive IIR Filters 49
- 3.1 Introduction . . . 49
- 3.2 Constrained and Recursive Adaptive IIR Filters . . . 50
  - 3.2.1 Constrained adaptive IIR filter . . . 50
  - 3.2.2 Recursive Adaptive Filter . . . 52
- 3.3 Adaptive ARMA Filter . . . 54
- 3.4 Adaptive LMS-ARMA Spectral Analysis . . . 57
  - 3.4.1 Introduction . . . 57
  - 3.4.2 Adaptive LMS-AR spectral estimation . . . 58
  - 3.4.3 Adaptive LMS-ARMA spectral analysis . . . 60
  - 3.4.4 Experiment with LMS-ARMA method . . . 61
- 3.5 Adaptive RLS-ARMA Spectral Analysis . . . 62
  - 3.5.1 RLS algorithm for adaptive ARMA filter . . . 62
  - 3.5.2 Experiment with RLS-ARMA method . . . 66
- 3.6 Comparison of Adaptive FIR and IIR Filters . . . 67
  - 3.6.1 Convergence . . . 67
  - 3.6.2 Performance comparison . . . 68
- 3.7 Conclusion . . . 71

4 Adaptive Echo Cancellation 73
- 4.1 Introduction . . . 73
- 4.2 Line Echo Cancellation . . . 75
  - 4.2.1 Echo on telephone network . . . 75
  - 4.2.2 Traditional methods of echo control . . . 78
  - 4.2.3 Adaptive echo cancellation . . . 79
  - 4.2.4 Some potential alternatives to LMS . . . 81
  - 4.2.5 Design criteria for echo canceller . . . 83
- 4.3 Acoustic Echo Cancellation . . . 86
  - 4.3.1 Introduction . . . 86
  - 4.3.2 Approaches for AAEC . . . 88
  - 4.3.3 Subband acoustic echo canceller . . . 91
  - 4.3.4 No-delay structure . . . 95

4.3.5 Simulation with the no-delay structure 97
4.4 Design of A No-delay Subband AAEC 98
4.4.1 General structure of the AAEC 98
4.4.2 Optimal number of subbands 102
4.4.3 Design consideration 104
4.4.4 Simulation results 105
4.4.5 Summary of the no-delay subband AAEC 110
4.5 Nonlinear Echo Cancellation 111
4.5.1 Echoes in full duplex data transmission system . . . 112
4.5.2 Nonlinear echo cancellation 113
4.5.3 Wiener scheme 115
4.5.4 Volterra expansion method 116
4.6 Design of A Nonlinear Echo Canceller 118
4.6.1 Model of simulation 119
4.6.2 Simulations with Volterra expansion approach 121
4.6.3 Simulations with Wiener scheme 124
4.6.4 Comparison of Volterra expansion and Wiener scheme 127
4.6.5 Design of an NEC with Volterra expansion 129
4.7 Conclusion 132

5 Adaptive Gastric Signal Processing 137
5.1 Introduction 137
5.2 Electrical Activities in the Stomach 138
5.2.1 Anatomy of the stomach 139
5.2.2 Electrical signaling in nerve or muscle cells 140
5.2.3 Slow wave (electrical control activity) 141
5.2.4 Contraction related activities 143
5.3 Electrogastrography 146
5.3.1 Measurement of EGG 147
5.3.2 Characteristics of EGG 147
5.4 Adaptive Enhancement of EGG 151
5.4.1 Principle of adaptive signal enhancement 152
5.4.2 Adaptive enhancement system 153
5.4.3 Performance analysis 157
5.4.4 Result and application 164
5.4.5 Summary 165
5.5 Adaptive Cancellation of Respiratory Artifact 166
5.5.1 Measurement 167
5.5.2 Adaptive cancellation of the respiratory artifact . . . 168
5.5.3 Results 170
5.5.4 Discussion and Conclusion 171
5.6 Information Available to be Extracted 172

5.6.1 Simulation of internal gastric signal 173
5.6.2 Transfer from the stomach to the abdomen 174
5.6.3 Simulation with contractions 178
5.6.4 Discussion and conclusion 181
5.7 Detection of Slow Wave Propagation 181
5.7.1 Localization of the stomach 182
5.7.2 Running cross correlation 183
5.7.3 Results 183
5.7.4 Discussion and Conclusion 185
5.8 Adaptive Spectral Analysis 186
5.8.1 Gastric dysrhythmias 187
5.8.2 Adaptive spectral analysis 188
5.8.3 Postprandial EGG spectral analysis 190
5.9 Conclusion 193

6 Conclusions 195

List of Figures

1.1 Block diagram of an acoustic echo canceller 2
1.2 Digital filter 4
1.3 Adaptive transversal FIR filter 5
1.4 IIR structure of an adaptive filter 6
1.5 Lattice structure of an adaptive filter 7
1.6 4-wire and 2-wire connection 9
1.7 Adaptive noise canceller 9
1.8 Adaptive line enhancer 10

2.1 Learning curves with different step-size 27
2.2 Performance of the adaptive filter with different step-size . 28
2.3 Square errors of 10 independent runs with a small step-size 29
2.4 Square errors of 10 independent runs with a large step-size 30
2.5 Simulated nonstationary signal in the primary input 32
2.6 Performance of adaptive filter with different step-size in a nonstationary environment 33
2.7 Performance comparison of the μ-vector LMS and the LMS algorithms 37
2.8 Time variation of error performance surfaces 42
2.9 Illustration of a time-sequenced adaptive filter 43
2.10 Lattice form time-sequenced adaptive filter 45
2.11 Comparison between TSAF and AF 46
2.12 Comparison between original and modified TSAF 47
2.13 Comparison among AF, TSAF and lattice form TSAF . . . 48

3.1 Block diagram of the recursive filter 53
3.2 Adaptive ARMA filter 55
3.3 Estimation of two sinusoids ($f_1 = 0.1Hz$, $f_2 = 0.2Hz$) . . . 62
3.4 Estimation of two sinusoids ($f_1 = 0.1Hz$, $f_2 = 0.11Hz$) . . 63
3.5 Spectral estimation of a biomedical signal using RLS-ARMA method 67

3.6 Simulation system for adaptive echo cancellation 69
3.7 Performance comparison in adaptive noise cancellation . . . 70
3.8 Performance comparison in adaptive line enhancement . . . 71
3.9 Performance comparison in spectral estimation 72

4.1 Detail of the hybrid 76
4.2 Echoes on a telephone line 77
4.3 An echo suppressor 78
4.4 Adaptive cancellation of echo on a telephone line 80
4.5 Transform-domain adaptive echo canceller 83
4.6 Impulse response 87
4.7 FIR–IIR implementation of an AAEC 89
4.8 Adaptive pole-zero echo canceller 90
4.9 Conventional structure of the subband AAEC 91
4.10 2-subband QMF analysis/synthesis scheme 93
4.11 No-delay subband AAEC 96
4.12 Convergence of the no-delay AAEC 98
4.13 ECho cancellation output with the new structure 99
4.14 General structure of an no-delay subband AAEC 100
4.15 Frequency response of the prototype lowpass filter 101
4.16 Computational reduction of the proposed AAEC 103
4.17 Convergence of the subband AAEC 106
4.18 Echo cancellation performance of the proposed subband AAEC 107
4.19 Echo cancellation performance of full-band AAEC 108
4.20 ERLE vs. adaptations in real-time simulation 109
4.21 The influence of open/close the door 110
4.22 The influence of **some one walking** 111
4.23 Echoes in full duplex data transmission system 112
4.24 Nonlinear echo canceller with the Wiener scheme 115
4.25 Analog subtraction NEC with the Wiener scheme 117
4.26 Simulation model based on U-interface on ISDN 119
4.27 Comparison of a linear EC and a nolinear EC of Volterra expansion 122
4.28 Comparison of linear EC and NEC of Wiener scheme 124
4.29 Learning curves of the NEC with different μ_a 126
4.30 Influence of the far-end signal on the NEC 128
4.31 ERLE of the NEC with a training period 131
4.32 Effect of the finite wordlength of weights 134
4.33 Effect of length M on performance and complexity of the NEC 135

5.1 The anatomy of the stomach 139
5.2 Ion concentration gradient and voltage gradient 141

5.3 The triggering of an action potential 142
5.4 The propagation of electrogastric signal in the stomach . . . 144
5.5 Configuration of gastric potentials 145
5.6 Relation between intra-cellular, extra-cellular electrical activities and contractile force 146
5.7 Block diagram of the overall system 147
5.8 Cutaneous electrogastrographies 148
5.9 Power spectrum (dB) of an EGG 149
5.10 A cutaneous EGG 150
5.11 Power spectrum of a tachygastrial EGG 152
5.12 An adaptive signal enhancer 153
5.13 Adaptive system of EGG signal enhancment 154
5.14 Pre-processing result 155
5.15 Simulated signals 159
5.16 Convergence of the system 160
5.17 Performance of the system 162
5.18 Effect of the pre-processing 164
5.19 Performance of the system in a stationary environment . . . 165
5.20 Comparison of the input signal waveform and the output signal waveform 166
5.21 Results of the adaptive enhancement of the EGG 167
5.22 Cutaneous (a) and intraluminal (b) electrogastric signals and respiratory signal (c) 168
5.23 Power spectrum of the cross correlation between the cutaneous and the intraluminal gastric signals 169
5.24 Power spectrum of the cross correlation between the cutaneous EGG and the respiratory signal 170
5.25 Adaptive system for the cancellation of respiratory disturbance 171
5.26 Cancellation of the respiratory artifact in the cutaneous EGG 172
5.27 Cancellation of the respiratory artifact in the intraluminal recording 173
5.28 Cancellation of the respiratory artifact (time domain) . . . 174
5.29 Simuled gastric signals in the stomach 175
5.30 Simulated cutaneous electrogastric signals 178
5.31 Configurations of gastric signals in the antrum 179
5.32 Simulated cutaneous electrogastric signals when contractions occur in the stomach 180
5.33 Positions of electrodes 182
5.34 Four channel cutaneous electrogastric signals 185
5.35 A portion of the filtered signals shown in Fig.5.34 186
5.36 Time lags among different channel EGG signals 187
5.37 Tachygastrial EGG signal 188

5.38 Running power spectra of a normal EGG 190
5.39 Running power spectra of a tachygastrial EGG 191
5.40 Running power spectra of a postprandial EGG 192

List of Tables

2.1 Effect of the step-size on the filter performance 30
2.2 Effect of the SNR on the filter performance 31

4.1 Comparison of algorithms 85
4.2 Influence of the length M on the NEC 123
4.3 Influence of the nonlinearity 123
4.4 The influence of step-size μ_w 125
4.5 The influence of step-size μ_a 125
4.6 Influence of the nonlinearities (Wiener scheme) 127

5.1 Composition of cutaneous EGG 149
5.2 Effect of μ' on the system performance with nonstationary inputs 161
5.3 Effect of β on the system performance 161
5.4 Effect of SNR of the primary input on the system performance 161
5.5 Effect of time variations of the frequency and the amplitude of the signal on the system performance 163
5.6 Conductivity of biological tissues 176

Abbreviations and Notations

Abbreviatoins

- AAEC: Adaptive Acoustic Echo Canceller
- A/D: Analog/Digital convertor
- AF: Adaptive Filter
- AFB: Adaptive Filters in Subbands
- ALE: Adaptive Line Enhancer
- AR: Auto-Regressive
- ARMA: Auto-Regressive Moving Average
- D/A: Digital/Analog converter
- EC: Echo Canceller
- ECG: Electrocardiography
- EGG: Electrogastrography
- ERL: Echo Return Loss
- ERLE: Echo Return Loss Enhancement
- FB(A): Analysis Filter Bank
- FB(S): Synthesis Filter Bank
- FFT: Fast Fourier Transform
- FIR: Finite Impulse Response
- HP: Highpass Filter
- IIR: Infinite Impulse Response
- ISDN: Integrated Services Digital Network
- LEC: Adaptive Linear Echo Canceller
- LMS: Least Mean Square

- LP: Lowpass Filter
- MMSE: Minimum Mean Square Error
- MSE: Mean Square Error
- NEC: Adaptive Nonlinear Echo Canceller
- RLS: Recursive Least Square
- SNR: Signal-to-Noise Ratio
- TSAF: Time-Sequenced Adaptive Filter

Notations

- j: Time index
- $P_x(\omega)$: Power of a time series x_j
- $E[\ ]$: Expectation
- $Cov[\ ]$: Covariance
- Fs: Sampling frequency
- f_s: Signal frequency
- z^{-1}: One sample delay
- $\triangle$: Number of delay

Adaptive filters

- x_j: Single channel Input of the adaptive filter
- d_j: Primary input
- y_j: Output of the adaptive filter
- e_j: Residual error of the adaptive filter
- w_{ij}: ith weight of the adaptive filter at time j
- μ: Step-size of the LMS algorithm
- N: Order of the adaptive filter (number of taps)

- X_j: Input vector of the adaptive filter at time j
- W_j: Weight vector at time j
- $P = E[d_j X_j]$: Cross-correlation vector
- $R = E[X_j X_j^T]$: Auto-correlation matrix
- W^*: Optimal (or MMSE) solution
- ϵ_j: Mean square error at time j
- ϵ_{min}: Minimum mean square error
- β: Nonstationary factor in the μ-vector LMS algorithm

Lattice filter

- k_p: Reflection coefficient on pth stage
- e^f_{pj}: pth stage forward error at time j
- e^b_{pj}: pth stage backward error at time j

Adaptive nonlinear echo canceller

- (n): Order of the Volterra expansion
- N: Number of linear coefficients of the nonlinear echo canceller
- M: Length of nonlinear memory
- $h^{(n)}_{k_1,\ldots k_n}(j)$: Coefficients of nonlinear echo canceller with Volterra expansion method
- P_1: Power of the second order harmonic
- P_2: Power of the third order harmonic

Chapter 1

Introduction

1.1 Motivation and main results of the work

Signal enhancement, noise cancellation and spectral estimation are common and important subjects in telecommunications and in signal processing. The conventional methods, such as digital filtering and Fourier transform, are very useful tools for these purposes in situations where the statistics of signals are known a priori. However, many problems encountered in daily engineering activities involve extracting relevant information from some physical processes which are unknown or nonstationary or possibly both. An appropriate technique well suited for these problems is *adaptive filtering*.

For example, in telecommunication and hands-free telephone systems one may encounter the following annoying problem. There is unwanted coupling between a loudspeaker and a microphone installed in a same room or device called acoustic echo. In this situation both the talker's speech picked up by the microphone to be transmitted (the signal) and the acoustic echo, i.e., the speech from the loudspeaker picked up by the microphone (the noise) have the same characteristics. Conventional digital filtering is then obviously not applicable. However, an adaptive echo canceller shown in Fig.1.1 can remove the acoustic echo. The echo canceller is composed of an adaptive filter which simulates the acoustic echo path and produces a replica, y_j, of the echo n_j. This replica is then subtracted from the signal d_j.

It is impossible to know the characteristic of an acoustic echo path in advance. It is determined by lots of factors, such as the room size, the positions of the loudspeaker and the microphone, the reflection factor of the wall etc. Any movement of objects in the room, such as the gesture of

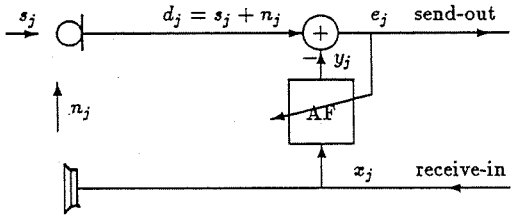


Figure 1.1: Block diagram of an acoustic echo canceller

the speaker, will cause the characteristic changes of the acoustic echo path, resulting in nonstationarity. The echo canceller, however, will adjust its coefficients to match the unknown characteristic of the acoustic echo path and follow its changes.

Another example is the cancellation of respiratory disturbance in a cutaneously measured biomedical signal in which the frequency of the respiratory disturbance may overlap with that of a relevant signal component. An adaptive noise canceller can deal with that problem if a reference input exists which is not correlated with the signal component but correlated with the respiratory disturbance. The adaptive noise canceller estimates the respiratory disturbance from the reference input and subtracts it from the measurement in the same way as an echo canceller does.

The third example we would like to give is the spectrum estimation of a time series which has changing frequency, such as a frequency modulated signal. A time series can be modeled as an autoregressive (AR) or autoregressive moving-average (ARMA) process and an adaptive filter can estimate the parameters of the AR or ARMA model. The power spectrum can therefore be calculated from these parameters. Since these parameters are iteratively adapted, the changing frequency of the input signal can well be traced.

Conventional digital filtering in the frequency domain is not suitable for the above applications. In the first example, the characteristic of the acoustic echo path is unknown and changing. It is not possible to use a digital filter with fixed weights. In the second example the overlap of the signal and noise frequencies makes the conventional digital filter design impractical. A running Fourier transform may be applied to estimate the instantaneous frequency in example 3. But it should be limited to applications where the change of the signal frequency is relatively slow, or in other words, there should be no significant change within the length of the window when a

fast Fourier transform is performed.

In summary, conventional digital filtering techniques are not suitable in either of the following situations:

1. The characteristic of an input signal to be processed is unknown.
2. The statistics of an input signal or a physical process are time-varying.
3. The frequency of a relevant signal component overlaps with that of the noise to be eliminated.

The adaptive filtering techniques to be discussed in this thesis are, however, suitable to the above situations. It has been a research subject for decades and has been especially active since the late 1970's. Fundamental adaptive filtering theory has been developed and it has found a great deal of applications in communications and signal processing.

The motivation of this work is to present developments of new algorithms and new applications.

During several years of research numerous results have been obtained and the main contributions of our work on the adaptive filter are as follows:

1. New algorithms for nonstationary signal processing. One is called the μ–vector least mean square (LMS) algorithm and the other is the lattice form time-sequenced algorithm, both presented in chapter 2.
2. Adaptive infinite impulse response (IIR) filters in chapter 3. A new structure of the adaptive IIR filter is proposed and LMS and recursive least square (RLS) algorithms are derived. A systematic treatment of adaptive IIR filters is provided. The comparison between the adaptive IIR filters and the adaptive FIR filter is given.
3. Applications of the adaptive filter in acoustic echo cancellation in teleconferencing and hands-free telephone systems and in nonlinear echo cancellation in data transmission systems. A new structure for the subband acoustic echo canceller is proposed and a subband acoustic echo canceller using the structure is designed. A nonlinear echo canceller for an ISDN line is designed and its performance is thoroughly investigated.
4. Adaptive biomedical signal processing. The applications of adaptive filter in electrogastric signal detection and processing are well exploited. Several adaptive techniques have been developed. Based on these techniques some important problems in the research community of electrogastrography have been solved and some important new results on the electrogastrography have been obtained.

5. Adaptive ARMA spectrum estimation. The adaptive IIR filter and its algorithms presented in chapter 3 have been successfully applied to estimate power spectra of sinusoids in white noise and of biomedical signals with changing frequencies.

1.2 Adaptive Filters: Structures, Algorithms and Applications

A digital filter is shown in Fig.1.2 where x_j is its input at time instant j, y_j is its output and $H(z)$, its transfer function. The output of the filter depends linearly on its input and its internal structure, i.e., the implementation of $H(z)$. The coefficients of the filter are specially designed and are time invariant.

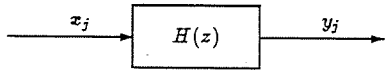


Figure 1.2: Digital filter

An adaptive digital filter is an adaptive version of the digital filter. It has the same representation as in Fig.1.2 but with an important distinction – the coefficients of the adaptive filter can be adjusted according to some algorithm to control the transfer function over a useful range in order to match the statistical properties of the input and to follow its changes.

Adaptive filters can be classified into different categories according to its structures and algorithms. What is meant by structure is the particular way of realizing the filter. What is meant by algorithm is the adaptation algorithm which enables the filter transfer function to track some statistical changes of its external environment based on a certain performance measure.

1.2.1 Structures

According to the expression of a filter transfer function there are two structures: finite impulse response (FIR) and infinite impulse response (IIR). According to the realization of the transfer function, however, each can be divided into transversal (direct realization) and lattice structures.

FIR and IIR Structures

The most commonly employed structure for an adaptive filter is the FIR filter as depicted in Fig.1.3. z^{-1} in the figure stands for a delay unit. The tapped delay line, $x_j, x_{j-1}, ..., x_{j-N+1}$ is adaptive filter input at time j, N is the order of the adaptive filter and $w_{kj}\,(k = 1, N)$ are the adjustable filter weight coefficients. The output of the adaptive filter is represented by a difference equation:

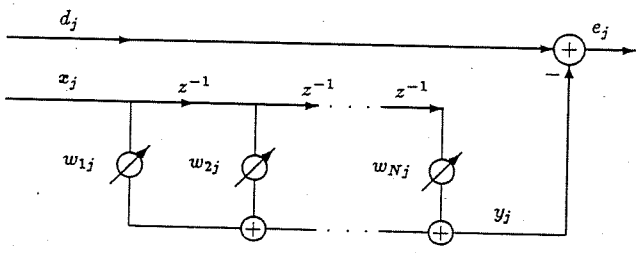


Figure 1.3: Adaptive transversal FIR filter

$$y_j = \sum_{k=1}^{N} w_{kj} x_{j-k+1} \tag{1.1}$$

The transfer function at time j can then be written as:

$$H_j(z) = \sum_{k=1}^{N} w_{kj} z^{1-k} \tag{1.2}$$

Since the filter coefficients are changing over time, the transfer function is also changing, therefore a time index j is needed.

Another possible structure for an adaptive filter is the IIR filter. Fig.1.4 illustrates one of possible structures. In this structure a feedback loop is added and another tapped delay line is included.

The output of this adaptive IIR filter is expressed by the following equation:

$$y_j = \sum_{k=1}^{p} a_{kj} x_{j-k+1} + \sum_{k=1}^{q} c_{kj} y_{j-k} \tag{1.3}$$

where $a_{kj}\ (k = 1, 2, ..., p)$ and $c_{kj}\ (k = 1, 2, ..., q)$ are weight coefficients of the adaptive filter.

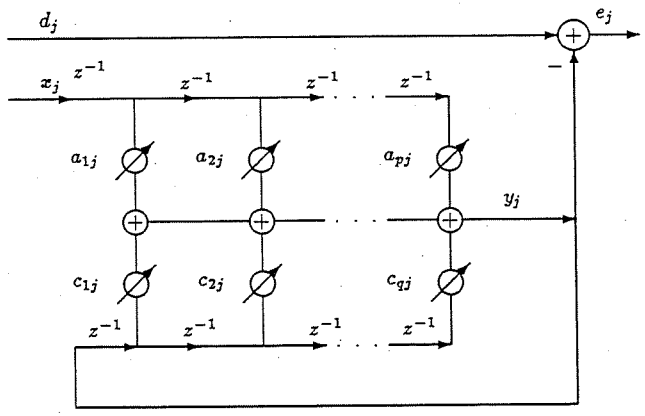


Figure 1.4: IIR structure of an adaptive filter

Taking z-transform the above equation can be written as:

$$\begin{aligned} Y_j(z) &= X_j(z)(a_{1j} + a_{2j}z^{-1} + ..., +a_{pj}z^{-p+1}) \\ &\quad +Y_j(z)(c_{1j}z^{-1} + c_{2j}z^{-2} + ..., +c_{qj}z^{-q}) \end{aligned} \tag{1.4}$$

By defining

$$A_j(z) = a_{1j} + a_{2j}z^{-1} + ..., +a_{pj}z^{-p+1} \tag{1.5}$$

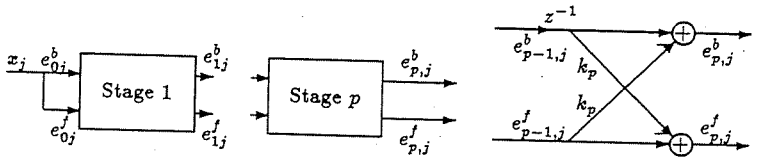
$$C_j(z) = 1 - c_{1j}z^{-1} - c_{2j}z^{-2} - ..., -c_{qj}z^{-q} \tag{1.6}$$

the transfer function of the filter is:

$$H_j(z) = \frac{A_j(z)}{C_j(z)} \tag{1.7}$$

Transversal and Lattice Structures

The realization of the adaptive FIR and adaptive IIR filters shown in Fig.1.3 and Fig.1.4 is called *transversal* structure which is universally utilized. Another implementation of the adaptive filter is the *lattice* structure. A lattice adaptive FIR filter is shown in Fig.1.5. e^f_{pj} and e^b_{pj} are called forward and backward errors on the pth stage at time j. $k_p\ (p = 1, 2, ..., N)$ are commonly called reflection or PARCOR (PARtial CORrelation) coefficients (Markel 1976).



(a) Block diagram (b) Structure of the pth stage

Figure 1.5: Lattice structure of an adaptive filter

An adaptive filter in the lattice structure involves both time- and order-updates. It has a rapid convergence, is robust and efficient in computations.

1.2.2 Algorithms

Unlike the conventional digital filter, the coefficients of an adaptive filter can be adjusted iteratively in order to follow the statistic changes of an external environment. Once the filter structure has been chosen, an adaptation algorithm must be chosen. The selection of the adaptation algorithm is generally based on the following main factors:

1. Computational complexity of the algorithm.

2. Convergence speed of the adaptation.

3. Accuracy of the transfer function in the steady-state.

A simple and commonly used adaptation algorithm is the least mean-square (LMS) algorithm which is the main subject of this dissertation. The LMS algorithm is based on the steepest descent method. It avoids explicit solution of a set of linear equations. Therefore it is the simplest and the most widely utilized algorithm. Its disadvantages are slow convergence and sub-optimal performance.

In practice where fast adaptation and better performance are needed, the recursive least square (RLS) algorithm can be used. Compared with the LMS algorithm the RLS algorithm is much more complicated in computations, especially when the order of the adaptive filter is high because of the involved matrix computation.

1.2.3 Applications

The main advantage of the adaptive filter, i.e., the ability to operate efficiently in an unknown and/or changing environment, makes it very attractive in many applications, such as in telecommunications, in biomedical signal processing, in geophysical signal processing, in the elimination of radar clutter and in sonar processing. Some applications related to our work are outlined in the following paragraphs.

Echo cancellation

The application of the adaptive filter in echo cancellation can be classified into three categories:

1. Acoustic echo cancellation in teleconferencing and hands-free telephone systems.

2. Linear echo cancellation on telephone networks and in data transmission systems.

3. Nonlinear echo cancellation in data transmission systems.

The acoustic echo results from the unwanted coupling between the loudspeaker and microphone in teleconferencing or hands-free telephone systems. It has been described at the beginning of this chapter and will be discussed in detail in chapter 4.

The echo in a telephone network is produced by a hybrid which performs the conversion from two-wire to four-wire and vice versa. Fig.1.6 illustrates the connection through the hybrid (H) for a long distance telephone network. The hybrid attempts to couple the signal energy from the far-end talker to the subscriber, such that no energy is reflected back to the far-end. Due to some uncertainties, such as unknown loop length, component variance etc., however, these impedances can hardly be matched completely. Consequently not all of the signal energy is directed to the subscriber and some is returned along the four-wire as an echo n_j.

To overcome this problem a similar adaptive echo canceller (EC) as depicted in Fig.1.1 can be inserted in the network and the echo can be cancelled in the same way as in Fig.1.1.

Nonlinear echo is only a small portion of an echo. It is originated from some nonlinear components in the telephone network, mainly A/D and D/A convertors. The cancellation of this nonlinear effect can be achieved by using a nonlinear echo canceller.

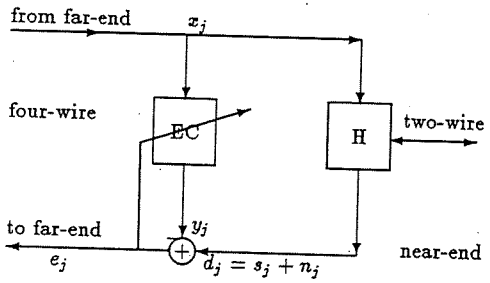


Figure 1.6: 4-wire and 2-wire connection on a telephone network

Adaptive Noise Cancellation

In digital signal processing practice, one often encounters the following problem: A measurement is a mixture of an interesting signal and noise and their frequencies overlap, such as, 50 Hz interference in an electrocardiographic signal and background noise in a speech signal.

The structure of an adaptive noise canceller is shown in Fig.1.7. The input, d_j, to the summation (called primary input) consists of a signal s_j and noise n_j. They are assumed to be uncorrelated with each other. The input to the adaptive filter (called reference input) x_j is composed of noise n'_j which is only related to n_j in the primary input.

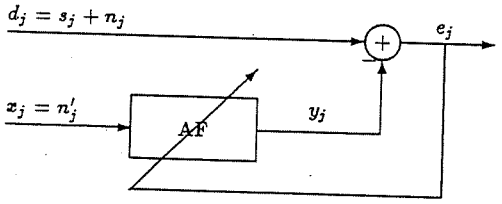


Figure 1.7: Adaptive noise canceller

The adaptive filter produces an output y_j which is an estimate of the noise n_j and subtracts it from the primary input.

The echo canceller is, in fact, an example of the adaptive noise canceller.

Adaptive Line Enhancer

A very simple and popular application of the adaptive filter is the adaptive line enhancer (ALE). The ALE can be applied to detect a low level sine wave (or periodic signals in general) in a background of additive noise with a broadband spectrum, such as white noise.

The ALE is illustrated in Fig.1.8. It consists of a bulk delay element $\triangle$ and an adaptive filter (AF). The input of the adaptive filter is a delayed version of primary input d_j and its output y_j is subtracted from signal d_j to produce an estimation error e_j. The estimation error is, in turn, used to adaptively control the weights of the adaptive filter. The delay element $\triangle$ should be chosen large enough to remove the correlation between the noise component in the primary input and the noise component in the adaptive filter input, i.e., $E[n_j n_{j-\triangle}] = 0$. The ALE can suppress broadband noise contained in the primary input, while passing correlated narrow-band components with little attenuation.

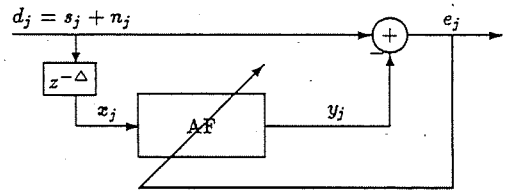


Figure 1.8: Adaptive line enhancer

The name of adaptive line enhancer results from the fact that it can *enhance* the presence of a sine wave whose spectrum consists of harmonic *lines* in an *adaptive* manner.

Adaptive Spectrum Estimation

The power spectrum is a very useful measure of a discrete time series in frequency domain. There are two ways of estimating the power spectrum: nonparametric spectral analysis and parametric spectral analysis. In parametric methods a certain model is assumed for a time process. Two commonly used models are autoregressive (AR) and autoregressive moving-average (ARMA) models. In the following paragraphs an outline of the applications of the adaptive filter in adaptive AR and ARMA spectrum estimations is presented.

a) Adaptive AR Spectrum Estimation

In the AR model, a time series is modeled as the output of a linear filter excited by a white noise process as follows:

$$x_j = -\sum_{k=1}^{N} a_k x_{j-k} + n_j \tag{1.8}$$

where a_k $(k = 1, 2, ..., N)$ are autoregressive parameters and n_j is an uncorrelated random process of power σ_n^2.

The excitation n_j can be written as the nonpredictable portion of the signal or the innovation of the AR process:

$$n_j = x_j + \sum_{k=1}^{N} a_k x_{j-k} \tag{1.9}$$

Once the parameters of the AR model are known the power spectrum of the process can be calculated as

$$P_x(\omega) = \frac{\sigma_n^2}{|1 + \sum_{k=1}^{N} a_k e^{-i\omega k}|^2} \tag{1.10}$$

i in the above equation stands for an imaginary number, $i = \sqrt{-1}$.

In the application of adaptive spectrum estimation, the data sample x_j is available and it is desired to compute an AR power spectrum of the underlying signal process from the data sample x_j. It can be shown that an adaptive filter provides a simple way of computing the power spectrum.

In Fig.1.8 if $\triangle$ is chosen to be one sample, the estimation error e_j is given by

$$e_j = x_j - \sum_{k=1}^{N} w_{kj} x_{j-k} \tag{1.11}$$

where w_{kj} $(k = 1, 2, ..., N)$ are the adaptive filter coefficients. e_j can be proven to be an uncorrelated random process, thus the similarity between EQ(1.9) and (1.11) is very clear. That is, after the convergence of the adaptation algorithm $-w_{kj}$ will approach the true values of a_k in Eq(1.8). The power spectrum can then be calculated from the coefficients w_{kj} $(a_k = -w_{kj},\ k = 1, 2, ..., N)$.

b) Adaptive ARMA Spectrum Estimation

A more general model for a time series x_j is the ARMA model. It assumes that the time series x_j can be modeled as the output of a p pole and q zero filter excited by a white noise process:

$$x_j = -\sum_{k=1}^{p} a_k y_{j-k} + \sum_{k=0}^{q} c_k n_{j-k} \tag{1.12}$$

where n_j is white noise and $c_0 \equiv 1$, $a_k (k = 1, 2, ..., p)$ and $c_k (k = 1, 2, ..., q)$ are parameters of the ARMA model.

Once these parameters are identified the power spectrum of the time series x_j can be calculated:

$$P_x(\omega) = \frac{\sigma_n^2 |1 + \sum_{k=1}^{q} c_k e^{-i\omega k}|^2}{|1 + \sum_{k=1}^{p} a_k e^{-i\omega k}|^2} \tag{1.13}$$

where, $i = \sqrt{-1}$.

1.3 Brief Historical Survey of Adaptive Filter

The adaptive filtering techniques have a long history. The recent rapid development of integrated circuit, especially the very large scale integrated circuit (VLSI) and the availability of digital signal processors have made practical implementations of adaptive algorithms possible and has intensified the research in this subject. In this section we present a brief historical review of the developments of the adaptive filter in the areas which are closely related to the subject matter of this thesis. These areas involve adaptive algorithms including least mean square algorithm, recursive least mean-square algorithm, adaptive IIR filter, adaptive noise cancellation and adaptive spectrum analysis.

1.3.1 Development of Adaptive Algorithms

The earliest derivation of the **least mean-square algorithm** can be traced back to the late 1950's. During that time a number of researchers were working independently on different applications of adaptive filters. The LMS algorithm was devised by Widrow and Hoff in 1959 in their work on the adaptive linear threshold logic element (Widrow and Hoff, 1960).

The LMS algorithm is a stochastic gradient algorithm. It iterates each weight coefficient of the adaptive filter in the direction of the gradient of the squared amplitude of a residual error signal with respect to that coefficient.

During the late 1970's several versions of the LMS algorithm were developed. These include block implementation (Clark 1981) of the LMS algorithm and the frequency domain LMS algorithm (Dentino 1978, Mansour 1982). They are more efficient in computations since the weight vector is only adapted once for a block of input samples.

For nonstationary signal processing several LMS-based algorithms have been developed. Ferrara and Widrow proposed a time-sequenced LMS algorithm (Ferrara 1981). The algorithm performs better than the conventional LMS algorithm for nonstationary signals having recurring statistical characteristics. The convergence of that algorithm is, however slower than the conventional one. A variable step (VS) LMS algorithm was developed in (Harris 1986). The difference between this algorithm and the LMS is that the step-size is not a constant but a variable, which makes the algorithm more suitable for nonstationary environment at the expense of computations. In chapter 2 we present a μ-vector LMS algorithm which has the same computational complexity as the conventional one but produces better performance with nonstationary inputs (Chen 1988c).

The performance of the LMS adaptive filter in stationary and nonstationary environments has been analyzed in (Barbe 1971, Widrow 1975, 1976, Zeidler 1978, Treichler 1979, Rickard 1979, Bershad 1980, Morgan 1983, Anderson 1983).

The original reference on the *recursive least square* (RLS) algorithm seems to be Plackett (Plackett, 1950) although it has been derived independently by several investigators. The RLS algorithm usually converges much faster than the LMS algorithm at the expense of the increased computational complexity. One very active objective in the research on RLS filter has been to derive computationally efficient algorithms. Some computationally efficient algorithms can be found in the literature, such as the "fast Kalman" method (Ljung 1978 and Falconer 1978), vector space approaches (Cioffi 1983, 1984) and the lattice form predictor (Morf 1978).

The *adaptive IIR filter* was originally proposed in (White 1975), known as the recursive adaptive digital filter. In this kind of adaptive IIR filter the feedback is taken from the output of the adaptive filter. Various simplifications and improvements to the recursive LMS algorithm have been proposed in (Feintuch 1976, David 1981, Hsia 1981 and Larimore 1980). A general algorithm for the recursive adaptive filter is given in (Widrow 1985).

Another form of the adaptive IIR filter where the feedback is taken from the residual error between the primary input and the adaptive filter output, was proposed (Friedlander 1982). He used that structure and the maximum likelihood algorithm to estimate the power spectrum of an input time series. Recently we derived an LMS algorithm and an RLS algorithm

for this type of adaptive filter (Chen 1987d). It will be discussed in chapter 3.

1.3.2 Progress in Applying Adaptive Filters

The adaptive line enhancer was originally proposed by Widrow and his colleagues. The first attempt was made in 1965 to cancel 60 Hz interference in an electrocardiographic recording. In 1975, Widrow et al. published a very comprehensive paper with different examples on adaptive noise cancellation.

The adaptive echo canceler was first proposed in (Sondhi 1967 and Kelly 1970). It is a successful application of the adaptive filter to eliminate echoes in telephone networks. Different algorithms have been applied to the adaptive echo canceler. Most of them are based on LMS algorithm because it is simple and easy for hardware implementation.

It appears that Kellermann (Kellermann 1985) first used the adaptive subband filtering technique in acoustic echo cancellation. The acoustic echo path usually has a very long impulse response and heavy computations would be involved if the conventional echo canceler is applied. A new structure for subband acoustic echo canceler will be shown in chapter 4, with which we have avoided the problem of introducing delays in the transmission line (Chen 1988a and 1988d).

The first attempt to cancel the nonlinear distortion in the echo path was made by Thomas (Thomas, 1971), in which the Volterra representation of nonlinear systems was applied to the echo control problem. Different methods have been proposed, such as the table look-up method (Holte 1981), the distributed arithmetic architecture (Peled 1974 and Sicuranza 1986), the Wiener scheme (Corredera 1985) and the Volterra expansion (Agazzi 1982). Recently we have designed an adaptive nonlinear echo canceller using a 3rd order Volterra expansion (Chen 1989a and 1989d).

Compared with the applications of the adaptive filter in other fields, the progress of applications of the adaptive filter in biomedical signal processing has been slow although the first application of the adaptive noise canceler was for the elimination of 60 Hz interference in electrocardiography.

In the research of the electrogastrography (cutaneous electrogastric measurement) it has been claimed that the conventional digital filtering technique should not be used because the frequency or harmonics of the interesting gastric signal component overlap with the frequency of the noise. Kentie et al. (Kentie 1981) proposed a simple adaptive filtering scheme, but no satisfactory results were obtained. During previous years, however, we have made a lot of efforts on this field – adaptive gastric signal processing. A number of results have been obtained (Chen 1987b, 1988e, 1988f

and 1989b).

A very classical spectral estimation method named as periodogram was introduced at the turn of this century (Schuster 1898). Being aware of erratic results often obtained by the periodogram method, Yule (Yule 1927) and Wold (Wold 1938) proposed an autoregressive model for the spectral analysis. Burg (Burg 1967 and 1975) introduced the maximum entropy method which estimates the power spectrum directly from the available time series.

In 1975 Griffiths extended the application of the autoregressive model to estimate the instantaneous frequency of a nonstationary stochastic process by the LMS adaptive filter (Griffiths 1975). The parameters of the AR model are iteratively calculated for each newly available input sample. Consequently, the estimated power spectrum is a function of both frequency and time. This method has been successfully applied to estimate the instantaneous frequency of a sine wave with rapid variations of the frequency.

In chapter 3 we expand Griffiths' method by introducing a feedback from the estimated error and by adding another tapped delay line. Therefore an adaptive ARMA model is formulated for the power spectral estimation (Chen 1987d).

1.4 Outline of the thesis

This thesis contains two main parts: theory and algorithms of the adaptive filter (Chapter 2 and 3) and their applications in telecommunications (chapter 4) and in biomedical signal processing (chapter 5).

Chapter 2 gives basic principles and important properties of the adaptive filter. The LMS Algorithm is derived and its properties in both stationary and nonstationary environments are outlined based on Widrow et al's work. A new LMS algorithm, called the μ-vector LMS algorithm, is proposed and its performance is investigated. The adaptive lattice filter is introduced, a lattice form TSAF is proposed and its advantage of fast convergence is shown.

Chapter 3 gives a systematic treatment on the transversal LMS adaptive IIR filter. Three sorts of the adaptive IIR filter are discussed: constrained adaptive IIR filter, recursive adaptive filter and adaptive ARMA filter. Their performances and stabilities are compared with the adaptive FIR filter.

The adaptive auto-regressive method proposed by Griffiths is first described, which is based on the transversal adaptive FIR filter. Adaptive ARMA spectral estimation methods are proposed by applying LMS and

RLS algorithms. Experimental results on the proposed new methods are shown.

In Chapter 4 one can find the applications of the adaptive filter in the adaptive echo cancellation. A general description of the adaptive echo cancellation is given in section 4.2. In section 4.3, problems with the acoustic echo are pointed out and possible solutions are outlined. A new acoustic echo canceller which introduces no delay on the transmission line is designed. The detailed discussion can be found in section 4.4. Section 4.5 gives an overview on the nonlinear echo cancellation followed by a thorough experimental study on the adaptive nonlinear echo cancellation with the Wiener scheme and with the Volterra expansion method.

Chapter 5 shows the applications of the adaptive filter in biomedical signal processing, particularly in gastric signal processing. At the beginning of the chapter, electric activities in the stomach are described. Afterwards, the measurement method and the characteristics of the gastric signal are discussed. Finally, the applications of the adaptive filtering techniques in the gastric signal processing are shown: the adaptive enhancement of the gastric signal, the adaptive cancellation of the respiratory artifact and the adaptive spectral estimation of cutaneous gastric measurements.

Conclusions and remarks can be found in the last chapter of the thesis, where the main contributions of our work to the adaptive filter and its applications are summarized. The further work on the related interesting subjects is

Chapter 2

LMS Adaptive FIR Filters

2.1 Introduction

In chapter 1 we have mentioned that adaptive filters can be classified into several categories. According to the type of the filter transfer function they can be divided into finite impulse response (FIR) and infinite impulse response (IIR) filters. According to the realization of the adaptive filter, they can be classified as the transversal (direct implementation) structure and the lattice structure. According to the algorithm used to adapt the coefficients of the adaptive filter, each selected structure may have different versions. Two commonly used algorithms are the least mean square (LMS) algorithm and the recursive least square (RLS) algorithm. Based on these two, various adaptation algorithms for different applications have been developed.

In this chapter we present the LMS adaptive transversal and lattice FIR filters. The basic principles of the LMS adaptive filter and of the adaptive lattice filter are briefly introduced. Our contributions to the adaptive algorithm are discussed at length: the μ-vector LMS algorithm (Chen 1988c) and the lattice form time sequenced adaptive filter (Chen 1987a). Simulation results of the proposed algorithms are presented.

The chapter is structured as follows: In section 2.2 the LMS adaptive filter originally proposed in (Widrow 1960) is introduced. Its main properties, such as the convergence condition, the convergence rate, the weight vector noise and the misadjustment are briefly reviewed (Widrow 1976) in section 2.3. Section 2.4 presents some experimental results on the LMS

adaptive filter. The effects of the step-size of the LMS algorithm on the adaptive filter with both stationary and nonstationary inputs are investigated. In section 2.5 a μ-vector LMS algorithm (Chen 1988c) is proposed. Its performance is investigated in comparison with the LMS algorithm. Its applications in biomedical signal processing (Chen 1987c, Chen 1989c) are mentioned, and the detailed discussion can be found in chapter 5. The adaptive lattice filter (Markel 1976) and the stochastic gradient algorithm for the adaptive lattice filter are introduced in section 2.6. In section 2.7 we propose a lattice form TSAF (Chen 1987a) which significantly improves the convergence rate of the transversal TSAF proposed in (Ferrara 1981).

2.2 LMS Adaptive FIR Filter

The basic structure of a transversal FIR filter is illustrated in Fig.1.3, where j stands for the time instant, z^{-1} for a unit delay, w_{kj} $(k = 1, 2, ..., N)$ are the weights of the adaptive filter and N is the order (number of taps) of the adaptive filter. The input to the adaptive filter weights is composed of a tapped delay line, $x_j, x_{j-1}, ..., x_{j-N+1}$. The output of the adaptive filter at time j is denoted by y_j which is the summed multiplication between the tap inputs and the corresponding weights:

$$y_j = \sum_{k=1}^{N} w_{kj} x_{j-k+1} \tag{2.1}$$

The purpose of the adaptive filter can be described as:

> Given a primary input signal d_j (see Fig.1.3) for an available input signal to the adaptive filter x_j, applying a certain criterion, produce an output which is an estimate of the primary input d_j in such a way that the residual error between d_j and the output of the adaptive filter y_j is made as small as possible in a statistical sense.

The residual error e_j in the figure can be written as

$$e_j = d_j - y_j \tag{2.2}$$

To derive the solution of the adaptive filter, some criterion for the optimization is needed. Since the error e_j can have both positive and negative values, the square error e_j^2 is a better criterion and is very widely used. However, when the process under consideration is stochastic, the statistical

property of the square error signal, which is well suited as a performance criterion, is the ensemble average or mean as defined as follows:

$$\varepsilon_j = E[e_j^2] \tag{2.3}$$

where E[.] stands for the expectation operator and ε_j is called the mean square error.

Define W_j as the weight vector:

$$W^T = [w_{1j}, w_{2j}, ..., w_{jN}] \tag{2.4}$$

and X_j as the adaptive filter input vector at time j:

$$X_j^T = [x_j, x_{j-1}, ..., x_{j-N+1}] \tag{2.5}$$

where the superscript T stands for transposition. The output of the adaptive filter y_j can then be written as:

$$y_j = X_j^T W_j \tag{2.6}$$

and the estimation error e_j as:

$$e_j = d_j - X_j^T W_j \tag{2.7}$$

Assuming that the two input signals d_j and x_j are wide-sense stationary and have zero mean, and substituting Eq(2.7) in Eq(2.3) we have the expression of the mean square error:

$$\varepsilon_j = \sigma_d^2 - 2W_j^T P + W_j^T R W_j \tag{2.8}$$

with

$$\sigma_d^2 = E[d_j^2] \tag{2.9}$$

$$P = E[d_j X_j] \tag{2.10}$$

$$R = E[X_j X_j^T] \tag{2.11}$$

where σ_d^2 is the variance of the primary input d_j, P is N-by-1 cross-correlation vector between the adaptive filter input vector X_j and the primary input d_j and R is N-by-N auto-correlation matrix of the input vector X_j.

Eq(2.8) states that the mean square error ε is a quadratic function of the filter weight vector W_j. Geometrically the mean square error is a bowl-shaped surface. This surface is often called the **error performance surface**.

In a stationary environment, the MSE is a constant and thus the error performance surface has a fixed shape and a fixed minimum. Differentiating

the MSE ε_j in Eq(2.8) with respect to the weight vector W and setting the result to zero one attains,

$$RW^* = P \tag{2.12}$$

Eq(2.12) is called normal equation and its solution W^* is called MMSE solution (or optimal solution). The corresponding filter is called MMSE filter (or optimal filter) which operates at the minimum point of the error performance surface (Widrow 1975).

The main drawback of the MMSE filter is, however, that the statistics of the input signals d_j and x_j should be known a priori. In many real applications, they are unknown and/or changing and the filter should work based on available data samples.

An adaptive algorithm, which is well suited in situations where the statistics of the inputs are unknown or changing, is the LMS algorithm. Due to its simplicity, the LMS algorithm is the most widely used adaptive algorithm in currently implemented systems.

Applying the steepest descent method (Murray 1972) and using a noisy gradient to approximate the true gradient,

$$W_{j+1} = W_j - \mu \nabla_j \quad \text{(steepest descent method)} \tag{2.13}$$

$$\hat{\nabla}_j = \frac{\partial e_j^2}{\partial W_j} \quad \text{(noisy gradient)} \tag{2.14}$$

one can have the Widrow-Hoff LMS algorithm (Widrow 1960):

$$W_{j+1} = W_j + 2\mu e_j X_j \quad \text{(LMS algorithm)} \tag{2.15}$$

The parameters μ in the above LMS algorithm is called the step-size (or feedback factor, gain factor, convergence factor) which controls the convergence of the LMS algorithm.

The LMS algorithm states that the next weight vector is equal to the current weight vector plus a change proportional to an estimate of the negative gradient of the error performance surface.

The initial value of the weight vector can be arbitrarily chosen, usually zero. The order (N) of the LMS adaptive filter required is generally equal to twice the ratio of the total signal bandwidth to the frequency resolution of the adaptive filter, i.e., enough information of the interesting frequency components should be stored in the filter weights (Widrow 1975).

2.3 Properties of LMS Adaptive Filter

This section gives the main properties of the LMS adaptive filter. The detailed discussion can be found in (Widrow 1976). Some notations used

in this section are listed as follows:

$$R = Q\Lambda Q^T \qquad \Lambda = diag[\lambda_1, \lambda_2, ..., \lambda_N]$$

$$V_j = W_j - W^* \qquad V_j' = Q^{-1}V$$

2.3.1 Convergence condition

The convergence (mean value of the weight vector) of the LMS algorithm is guaranteed as long as the following condition is satisfied:

$$0 < \mu \leq \frac{1}{\text{total input power to AF}} \tag{2.16}$$

This leads to

$$\lim_{j\to\infty} E[W_j] = W^* \tag{2.17}$$

That is, the mean of the weight vector of the LMS adaptive filter converges to the MMSE solution if Eq(2.16) is satisfied. It should be pointed out that Eq(2.16) is a sufficient (not necessary) condition for the convergence of the mean value of the weight vector as shown in (Barbe 1971). It was also shown in (Barbe 1971) that when the step-size is chosen to be a large value, the adaptive filter may operate at a point far away from the minimum point of the error performance surface although the mean of the weight vector converges to the MMSE solution.

In practical applications we often choose the value of the step-size as follows:

$$0 < \mu << \frac{1}{\text{total input power to AF}} \tag{2.18}$$

Under the above condition the operation of the adaptive filter near the MMSE solution can be guaranteed. The effect of the step-size μ on the performance of the LMS adaptive filter will be shown in section 2.4.

2.3.2 Convergence rate

Starting with any initial value, the weight vector of the adaptive filter undergoes a transient during the adaptation to reach its optimal value. The time constant of the kth weight coefficient is given by (Widrow 1976):

$$\tau_k = \frac{1}{2\mu\lambda_k} \qquad k = 1, 2, ..., N \tag{2.19}$$

where λ_k is the kth eigenvalue of the auto-correlation matrix R.

Eq(2.19) shows the time constant for an individual filter weight coefficient. It can be seen that the convergence rate is related to the step-size μ. A large μ results in a faster convergence and vice versa. The weight coefficient corresponding to the largest eigenvalue has the highest convergence rate and the weight coefficient corresponding to the smallest eigenvalue has the lowest convergence rate. The overall time constant τ for any weight is bounded by

$$\frac{1}{2\mu\lambda_{max}} \leq \tau \leq \frac{1}{2\mu\lambda_{min}} \tag{2.20}$$

From the above equation we see that the convergence rate of the LMS algorithm is limited by the smallest eigenvalue.

Assume that different values of the step-size μ_k are chosen for different weights, the highest convergence rate is attained if

$$\mu_k\lambda_k = \text{fixed constant for each k}$$

In reality this is not feasible, i.e., λ_k $(k = 1, 2, ..., N)$ are unknown since the correlation matrix R is not calculated during the adaptation.

Let's define the eigenvalue spread as the ratio between the largest and smallest eigenvalues:

$$\text{eigenvalue spread} = \frac{\lambda_{max}}{\lambda_{min}} \tag{2.21}$$

The convergence rate decreases as the eigenvalue spread increases. To explain this, let's consider two cases as follows:

1. $\lambda_{min} = \lambda_{max} = \lambda$. In this case the fastest convergence can be obtained by setting the step-size:

$$\mu = \frac{1}{2\lambda}$$

This leads to

$$\tau' = \frac{1}{2\mu\lambda} = 1 \tag{2.22}$$

2. $\lambda_{max} > \lambda_{min}$. The largest possible value of μ in this case is $1/(2\lambda_{max})$. The bound of the overall convergence rate is

$$\tau'' = \frac{1}{2\mu\lambda_{min}} = \frac{\lambda_{max}}{\lambda_{min}} \tag{2.23}$$

Comparing Eq(2.22) and (2.23) we see that the time constant for the second case is $\lambda_{max}/\lambda_{min}$ times larger than that for the first case, and that the time constant is proportional to the eigenvalue spread. Therefore, with

the largest possible value of the step-size the convergence rate is inversely proportional to the eigenvalue spread. It means that the adaptive filter converges slowly if the auto-correlation matrix R of the input signal x_j has a large eigenvalue spread. This is the main drawback of the transversal LMS adaptive filter. This problem can be overcome either by using the lattice structure or by using the recursive least square algorithm.

2.3.3 Weight vector noise

In Eq(2.15) we can see that the second term on the right hand side is a noise term in the steady-state. It generates noise in the weight vector.

Assume that the LMS adaptive filter has converged to a steady-state and operates near the minimum point of the error performance surface. It was shown in (Widrow 1976) that the covariance of the weight vector noise is equal to

$$\text{Cov}[V_j'] = \mu\varepsilon_{min} I \tag{2.24}$$

Eq(2.24) states that near the minimum point of the error performance surface in the steady-state, the covariance of the weight vector noise is proportional to the step-size and the minimum mean square error.

2.3.4 Misadjustment

The LMS adaptive filter operates near the minimum point of the error performance surface. In real situations it does not reach this point and therefore $W_j \neq W^*$, and $\varepsilon_j \neq \varepsilon_{min}$. The random noise in the weight vector produces an excess mean square error. That is, the weight vector is "mis-adjusted".

The misadjustment M serves as a good performance indication. It is defined as the ratio between the average excess mse and the minimum mean square error.

$$M \triangleq \frac{\text{average excess } mse}{\varepsilon_{min}} \tag{2.25}$$

In a stationary environment the misadjustment can be expressed as (Widrow 1976):

$$M = \frac{\text{average excess } mse}{\varepsilon_{min}} = \mu \text{ (total input power to AF)} \tag{2.26}$$

Eq(2.26) states that the misadjustment increases as the step-size and/or the total input power to the adaptive filter increase(s). It is clearly indicated in this equation that faster adaptation (a larger μ) results in larger misadjustment. Better performance in the steady-state can be obtained with slower adaptation.

2.3.5 Performance in a nonstationary environment

We know that in a stationary environment, the error performance surface has a fixed minimum point. At this minimum point, the weight vector has its optimum value W^*. The adaptive process of the weight vector searches this point and updates its value to be as close to the optimum value as possible. In a nonstationary environment, however, the minimum point of the error performance surface is changing over time.

The nonstationary environment may involve the following three cases (Chen 1988c):

1. Only the primary input signal d_j is nonstationary. In this case the cross correlation vector is time-varying but the input auto-correlation matrix remains fixed.
2. Only the filter input signal x_j is nonstationary. In this case, both the cross correlation vector and the input auto-correlation matrix are time-varying.
3. Both the primary input and filter input are nonstationary.

Now assume the filter input signal x_j is nonstationary, the cross correlation vector and the input correlation matrix are written as

$$P_j = E[d_j X_j] \tag{2.27}$$

$$R_j = E[X_j X_j^T] \tag{2.28}$$

From these equations we see that both P_j and R_j are time dependent. In analogy with Eq(2.8), the mean square error in the nonstationary environment is written as

$$\varepsilon_j = E[d_j^2] - 2W_j^T P_j + W_j^T R_j W_j \tag{2.29}$$

Because P_j and R_j are time-varying the error performance surface is changing over time. Accordingly the optimum weight vector W_j^* is time-varying too. This requires the adaptive process to track the optimum weight vector W_j^* as well as its time variation. Therefore the weight vector tracking error $W_j - W_j^*$ at time j consists of two parts: the gradient noise and the weight vector lag.

$$W_j - W_j^* \triangleq (W_j - E[W_j]) + (E[W_j] - W_j^*) = V_{1j} + V_{2j} \tag{2.30}$$

where the expectations are averaged over the ensemble.

The first part on the right side of Eq(2.30) is the weight vector gradient noise. It is the difference between an individual weight vector and the

ensemble mean due to the gradient noise. The second part is the weight vector lag. It is the difference between the ensemble mean of the weight vectors and the optimum value W_j^* due to the mis-track of the changes of the optimum weight vector W_j^* over time.

The covariance of the weight vector gradient noise can be evaluated by the gradient noise covariance in the stationary case as shown in Eq(2.24). The covariance of the weight vector lag is shown in (Widrow 1976) to be inversely proportional to the step-size μ:

$$\text{Cov}[E[W_j] - W_j^*] \propto \frac{1}{\mu} \tag{2.31}$$

It says that slow adaptation (small μ) results in large weight vector lag. This is understandable because slower adaptation makes the adaptive filter less able to track the time variation of the optimum weight vector.

The average excess *mse* in a nonstationary environment can be expressed as (Widrow 1976):

$$\text{average excess } mse = E[V_{1j}'^T \Lambda V_{1j}'] + E[V_{2j}'^T \Lambda V_{2j}'] \tag{2.32}$$

The first part on the right hand side of Eq(2.32) results from the weight vector gradient noise and the second part from the weight vector lag. It is shown (Widrow 1976) that the average excess *mse* due to the weight vector gradient noise is proportional to the step-size μ and that due to the weight vector lag is inversely proportional to the step-size μ (for small value of μ). It suggests that the optimum value of μ which results in the minimum value of the total misadjustment exists when the two parts are equal. This implies that there is always a compromise between faster adaptation (being able to track the time variation of the input signal) and better performance.

2.4 Experiments With the LMS Algorithm

In the previous section the LMS algorithm and its characteristics in stationary and nonstationary environments have been outlined. In this section we present some computer simulation results of the LMS adaptive filter applied. The experiments (Chen 1988c) investigate the effects of different values of the step-size μ on the performance of the adaptive filter. More experiments on adaptive signal enhancing system and on adaptive noise cancellation system can be found in (Chen 1989b and Chen 1989c) and in chapter 5.

The experimental system is the adaptive line enhancer (also called linear predictor) shown in Fig.1.8. The input to the adaptive filter x_j is a delayed

version of the primary input d_j. The adaptive filter produces an estimated output of the primary input signal d_j. $\triangle$ is a bulk delay. It should be properly chosen to decorrelate the noise (not the interesting signal) in the primary input. In the following experiments it is set equal to 1. In the case that the signal d_j consists of a periodic signal, such as a sinusoid, in white noise, the adaptive line enhancer produces an enhanced output without or with less noise. The principle of the ALE will be explained in detail in the next section.

2.4.1 Effect of the step-size in a stationary environment

In section 2.3 we stated that the convergence rate is proportional to the value of the step-size (see Eq(2.19)). In a stationary environment, a large step-size results in fast convergence, but causes large misadjustment. The following experiments demonstrate these properties (Chen 1988c).

The primary input d_j consists of a sinusoid s_j in a uniformly distributed (-0.5,0.5) white noise n_j.

$$d_j = s_j + b_n n_j = sin(\omega j) + b_n n_j$$

where b_n is a constant controling the SNR of the signal d_j and n_j is a uniformly distributed (-0.5, 0.5) white noise.

The frequency of the sinusoid is equal to 0.05 Hz. The sampling frequency is 1 Hz. Unless otherwise mentioned $b_n = 2$. The order of the adaptive filter is set to 30 ($30 > 1/(\text{interesting freq,}) = 1/0.05 = 20$). To compare the performance of the ALE with different values of the step-size, a large μ (μ_1) and a small μ (μ_2) are chosen:

$$\mu_1 = \frac{0.1}{\text{total input power}} \qquad \mu_2 = \frac{0.025}{\text{total input power}}$$

The learning curves (the mean square error vs. the number of adaptations) averaged over 100 independent runs (to have a smooth learning curve) are shown in Fig.2.1. It should be pointed out that in this thesis the mean square error instead of the square error is often used to illustrate the convergence of the adaptive filter. This is because the error signal e_j usually contains the white noise n_j passing from the primary input. To cancel its random effect on the square error, e_j^2, the best way is to use the mean square error. Solid line results from $\mu = \mu_1$ and crossed line from $\mu = \mu_2$. From this figure we can observe that the large step-size μ_1 results in a faster convergence than the small step-size. On the other hand, however, the large step-size μ_1 generates larger mean square error in the steady state.

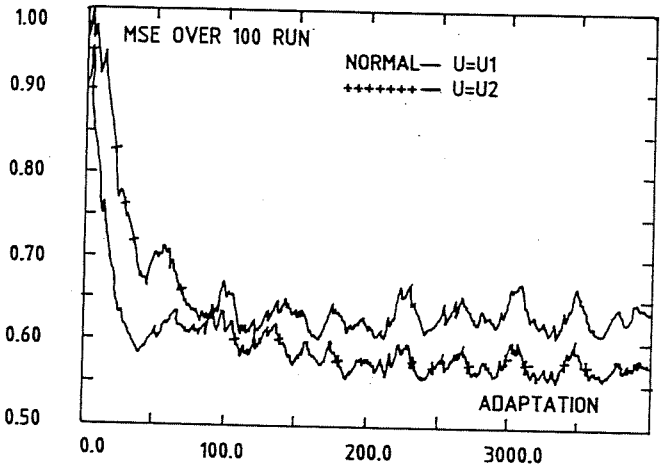


Figure 2.1: Learning curves with different step-size. $N = 30$, $Fs = 1\ Hz$, $\triangle = 1$, $b_n = 2$; Normal curve: $\mu = \mu_1$; Curve with crosses: $\mu = \mu_2$.

The noise cancellation performance of the adaptive line enhancer is illustrated in Fig.2.2. Curve 1 shows the power spectrum of the primary input signal (512 data samples) and curve 2 and 3 show the power spectra of the output signal e_j of the adaptive line enhancer with $\mu = \mu_1$ and $\mu = \mu_2$, respectively. The power spectra of the outputs are calculated from 512 data samples after the convergence of the adaptive filter (one single run).

From this figure we see that the signal component (0.05 Hz) is not affected by the adaptive line enhancer but the noise power is significantly reduced. Comparing curve 2 and curve 3 we can conclude that in a stationary environment a small value of the step-size produces a better performance for the noise cancellation than that with a large μ.

To see the effect of the step-size on the performance of the adaptive filter for an individual run, the square error between the signal s_j and the filter output y_j (should be a replica of s_j) for each individual run is calculated (to eliminate the white noise effect the square error $(s_j - y_j)^2$

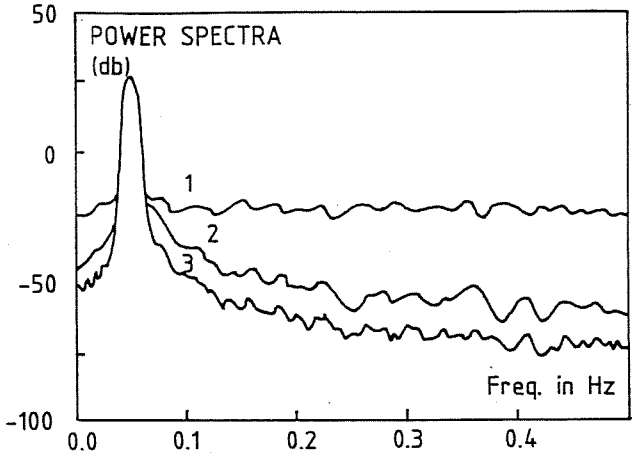


Figure 2.2: Performance of the adaptive filter with different step-size. $N = 30$, $Fs = 1\ Hz$, $\triangle = 1$, $b_n = 2$. Curve 1: input power spectrum (512s); Curve 2: output power spectrum with $\mu = \mu_1$; Curve 3: output power spectrum with $\mu = \mu_2$.

instead of the square error e_j is calculated). The square errors, $(s_j - y_j)^2$ of 10 independent runs are shown in Fig.2.3 (with $\mu = \mu_2$) and Fig.2.4 (with $\mu = \mu_1$). The line with stars in the figures shows the square error of one individual run. From Fig.2.3 we can see that with the small step-size, the adaptive filter converges in each individual run after about 100 adaptations. In the steady-state, the maximum square error is about 0.3 and the mean square error, $\overline{(s_j - y_j)^2}$, is about 0.03 (see table 2.1). With the large step-size, however, we can see in Fig.2.4 that the deviation of the square error from its mean value is much larger than that resulting from the small step-size. This shows that with large step-size the adaptive filter may operate quite far away from the minimum point of the error performance surface. It was shown in (Barbe 1971) that with a large step-size the filter weight vector of an individual run may not converge although its mean converges. To guarantee the convergence of the adaptive filter for each individual run to the optimal solution, the step-size should be chosen

according to Eq(2.18).

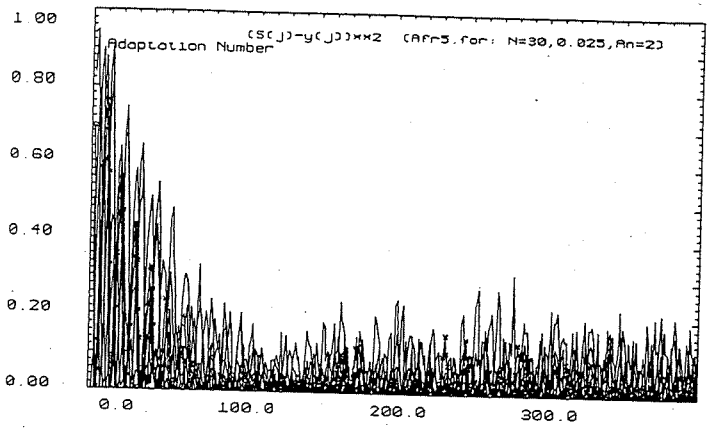


Figure 2.3: Square errors of 10 independent runs with a small step-size. $N = 30$, $Fs = 1\ Hz$, $\triangle = 1$, $b_n = 2$, $\mu = \mu_2$ Curve with stars results from one of the runs

In table 2.1 we show the effect of different values of the step-size on the performance of the adaptive filter. The first row in the table shows the values of μ and the second row, the time averaged square error between the signal s_j and the filter output y_j in an individual run calculated as follows:

$$\overline{(s_j - y_j)^2} = \frac{1}{200} \sum_{j=4800}^{5000} (s_j - y_j)^2$$

It can be observed in the table that as the step-size decreases, the time averaged square error becomes smaller and smaller, i.e., the performance becomes better and better.

2.4.2 Effect of the SNR of the primary input

Recall the LMS algorithm,

$$W_{j+1} = W_j + 2\mu e_j X_j$$

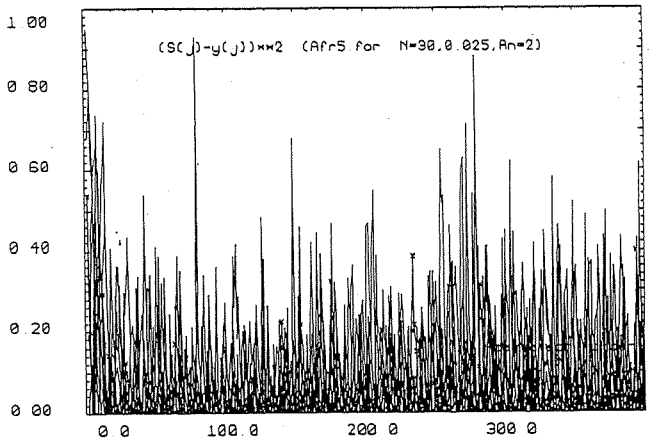


Figure 2.4: Square errors of 10 independent runs with a large step-size. $N = 30$, $Fs = 1\ Hz$, $\triangle = 1$, $b_n = 2$, $\mu = \mu_1$ Curve with stars results from one of the runs

It can be written as follows:

$$\begin{aligned} W_{j+1} &= W_j + 2\mu(d_j - y_j)X_j \\ &= W_j + 2\mu(s_j - y_j)X_j + 2\mu n_j X_j \end{aligned} \tag{2.33}$$

It is obvious that the last term on the right hand side of Eq(2.33) is a noise term, which degrades the performance of the adaptive filter. Its effect is shown in table 2.2, where the first row presents the level of the white noise in the primary input signal, the second row, the time averaged square error, $\overline{(s_j - y_j)^2}$ in an individual run. It can be observed that as the SNR gets higher (b_n smaller), the performance of the adaptive filter becomes better.

Table 2.1: Effect of the step-size on the filter performance

step-size μ	0.2	0.1	0.05	0.025	0.0125	0.01
$\overline{(s_j - y_j)^2}$	0.081	0.057	0.044	0.03	0.02	0.016

Table 2.2: Effect of the SNR on the filter performance

level of white noise b_n	6	5	4	3	2	1
$(s_j - y_j)^2$	0.131	0.112	0.085	0.043	0.030	0.007

2.4.3 Effect of the step-size in a nonstationary environment

The LMS adaptive filter operating in a nonstationary environment has two tasks: one is to search for the optimum weight vector and the other is to track the time variation of this optimum weight vector. The optimal choice of the value of the step-size is a compromise between fast adaptation and better performance (slow adaptation). The following experiments are designed to show the effect of its different values on the adaptive line enhancer performance (Chen 1988c).

The primary input signal d_j to the adaptive line enhancer consists of a simulated nonstationary signal s_j and a uniformly distributed (-0.5, 0.5) white noise n_j.

$$d_j = s_j + b_n n_j \tag{2.34}$$

The nonstationary signal s_j is a sequence of the following signals:

$$s_j = b_s sin(\frac{2\pi j}{T_s}(1 + \frac{j}{200})) \tag{2.35}$$

each considered over one full period. The amplitude b_s and the period T_s of each signal vary as:

$$b_s = b(d_a n' + 1)$$

$$T_s = T(d_T n' + 1)$$

where b and T are constants, n' is a uniformly distributed (-0.5,0.5) white noise, d_a and d_f are the factors determining the deviations of the amplitude and of the period of the signal s_j, respectively.

In the following simulations, the sampling frequency is 1 Hz, $T = 20$, $b = 1$, $b_n = 2$, $d_a = d_f = 50\%$. A portion of the simulated nonstationary signal s_j (with $d_a = d_f = 0$) is shown in Fig.2.5. Simulation results are shown in Fig.2.6, where curve 1 is the input power spectrum (512s data) curve 2 and curve 3 are the output power spectra (data are collected after the convergence of the algorithm) of the adaptive line enhancer with a large step-size $\mu = 0.1/$(total input power) and with a small step-size $\mu = 0.0125/$(total input power), respectively. From the figure we observe

that the dominant frequency component (highest peak in Fig.2.6) is not affected by the adaptive line enhancer but the other frequency components are attenuated. The small step-size (see curve 3) results in better noise removal but, on the other hand, introduces more signal attenuation than the large step-size (see curve 2). This follows from the characteristics of the LMS algorithm discussed in the previous section: slow adaptation is less able to track the time variation of the optimum weight vector in a nonstationary environment, causing larger weight vector lag, and therefore results in more attenuation of the signal components.



Figure 2.5: Simulated nonstationary signal in the primary input

For particular nonstationary input signals, there exists an optimal value of the step-size which results in minimum MSE in the steady-state. One example can be found in (Chen 1989b) and will be shown in chapter 5.

2.5 μ-Vector LMS Adaptive System

The effect of the step-size μ on the performance of the LMS adaptive filter has been discussed in the previous sections. It has been shown that in a stationary environment a better performance in the steady-state results from a small value of the step-size. In a nonstationary environment the optimal choice of the step-size is a compromise between fast and slow adaptations. Smaller μ produces less gradient noise but causes larger weight vector lag. In order to have better performance in a nonstationary environment we propose in this section a two stage adaptive system and a μ-vector LMS algorithm (Chen 1988c).

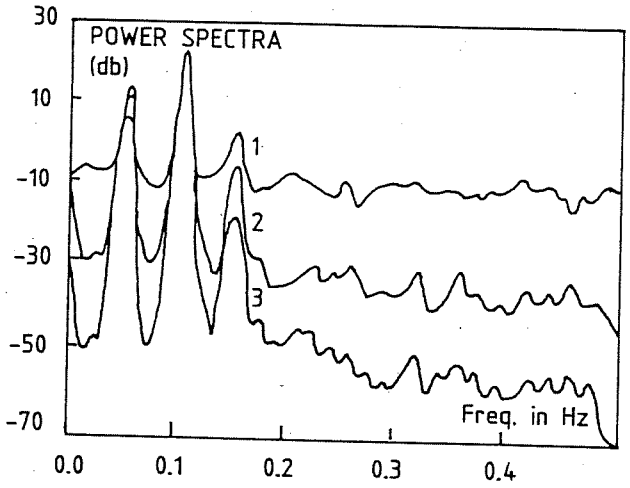


Figure 2.6: Performance of adaptive filter with different step-size in a non-stationary environment. $N = 30$, $Fs = 1\ Hz$, $\triangle = 1$, $b_n = 2$, Curve 1: input power spectrum (512s); Curve 2: output power spectrum with $\mu = \mu_1$; Curve 3: output power spectrum with $\mu = \mu_2$

2.5.1 ALE as a pre-processor

From Eq(2.24) we see that the covariance of the gradient noise in the weight vector is proportional to the value of the step-size and the minimum mean square error. For the LMS adaptive filter operating in a nonstationary environment, the total weight vector error is composed of the weight vector gradient noise and the weight vector lag expressed by Eq(2.31). In order to reduce the weight vector lag, the value of the step-size should be large enough. But from the Eq(2.24) we see that a large step-size will cause large gradient noise. One possible way to compensate this increase is to reduce the minimum mean square error ε_{min}.

For the adaptive line enhancer, ε_{min} consists of the noise power in the primary input and the noise component at the output of the adaptive filter. Accordingly the value of ε_{min} decreases if the primary input has less noise, or in other words, the minimum mean square error ε_{min} decreases as the input SNR increases (Chen 1988c).

A constructive way of increasing the SNR of the input is to use an adaptive line enhancer as a pre-processor. The principle of the adaptive line enhancer is explained as follows (see Fig.1.8).

Assume that the input signal d_j consists of a signal s_j and noise n_j, which are uncorrelated with each other. The bulk delay $\triangle$ is chosen to be large enough such that n_j and $n_{j-\triangle}$ are uncorrelated with each other while s_j and $s_{j-\triangle}$ are still correlated.

The error signal e_j is expressed as

$$e_j = s_j + n_j - y_j \tag{2.36}$$

The mean square error

$$\varepsilon_{min} = E[(s_j - y_j)^2] + E[n_j^2] + 2E[n_j(s_j - y_j)] \tag{2.37}$$

Considering that n_j is not correlated with s_j and y_j, the last term on the right side of the above equation turns out to be zero and

$$\varepsilon_{min} = E[(s_j - y_j)^2] + E[n_j^2] \tag{2.38}$$

Since $E[n_j^2]$ is not affected during the adaptation, the necessary and sufficient condition of minimizing the mean square error is

$$E[(s_j - y_j)^2] = 0$$

This states that the adaptive filter output y_j is a minimum mean square error estimate of the signal s_j.

From the above discussion we can conclude that if an input signal to be processed consists of a periodic (or highly correlated) signal and an uncorrelated noise, such as a white noise, the noise will be eliminated at the output of the adaptive filter. That is to say, an adaptive line enhancer can improve the SNR of the noisy signal, and therefore relieves the burden of the next processing stage, meaning that fast adaptation without introducing heavy gradient noise is made possible.

The results of the ALE used as a pre-processor have already been shown in Fig.2.2 and Fig.2.6. From these figures we know that the use of the ALE as a pre-processor leads to nice performance for stationary signals but caution should be made for nonstationary signals, that is, the adaptation rate should not be too low in order to avoid the attenuation of the interesting signal (Chen 1988c).

2.5.2 μ-vector LMS algorithm

The μ-vector LMS algorithm (Chen 1988c) to be proposed in this section is an extension of the LMS algorithm. It will be shown that the μ-vector

LMS algorithm produces better performance than the conventional LMS algorithm for nonstationary signal processing (Chen 1987c, 1989c). Being different from the conventional LMS algorithm it uses different values of the step-size for different filter input samples. It gives more recent samples larger values than the past samples in order to track the statistical changes of the input signal.

The μ-vector LMS algorithm is described as follows (Chen 1988c):

The adaptation of the weight vector W_{j+1} at time $j+1$

$$W_{j+1} = W_j + 2\vec{\mu}_j e_j X_j \tag{2.39}$$

where $\vec{\mu}_j$ is a diagonal matrix described as

$$\vec{\mu}_j = \begin{bmatrix} \mu_{1j} & & & \\ & \mu_{2j} & & \\ & & \ddots & \\ & & & \mu_{Nj} \end{bmatrix} \tag{2.40}$$

The ith element of $\vec{\mu}_j$ at time j is expressed as

$$\mu_{ij} = (1-\beta)^{i-1} q_j \tag{2.41}$$

where q_j is the normalized step-size which is given to the most recent sample x_j.

$$q_j = \mu'/(G_j + G_0) \tag{2.42}$$

and G_j is estimated by

$$G_j = (1-\alpha)G_{j-1} + \alpha x_j^2 \tag{2.43}$$

In the above equations β is a nonstationary factor (or forgetting factor) less than 1. For stationary inputs β could be chosen to be zero, which implies that the μ-vector LMS algorithm becomes the LMS algorithm with normalized step-size.

The parameter μ' is now the factor which together with the nonstationary factor β controls the convergence of the algorithm. G_j is the estimation of the total input power to the adaptive filter. G_0 is a small constant used to prevent μ_{ij} from getting too large when the input signal gets very small. α is a small constant less than 1, usually equal to $1/N$ (N – the order of the adaptive filter).

Since

$$\mu_{1j} > \mu_{kj}, \quad k = 2, 3, ..., N$$

the algorithm always converges if the the condition

$$0 < \mu_{1j} < \frac{1}{\text{total input power}} \tag{2.44}$$

is satisfied.

Since

$$\mu_{1j} = (1-\beta)^0 q_j = \frac{\mu'}{G_j + G_0} < \frac{\mu'}{\text{total input power}}$$

it follows that the convergence of the proposed algorithm is guaranteed if

$$0 < \mu' < 1 \tag{2.45}$$

is satisfied.

2.5.3 Simulations with the μ-vector LMS algorithm

The performance of the proposed μ-vector LMS algorithm is investigated by simulations in comparison with the conventional LMS algorithm (Chen 1988c). One of the results is shown in Fig.2.7. The experimental system is an adaptive line enhancer with the bulk delay Δ equal to 1 sample. The input to the ALE is a nonstationary signal, the same as the one described in Eq(2.34) and (2.35). The parameters are chosen as follows:

$$N = 30, \; G_0 = \sum_{j=1}^{30} x_j^2, \; \mu' = 0.1$$

Curve 1 in Fig.2.7 shows the input power spectrum. Curve 2 is the power spectrum of the ALE output by applying the conventional LMS algorithm (or $\beta = 0$ in the proposed algorithm) and curve 3 is that by applying the proposed algorithm with $\beta = 0.05$. It is observed from the figure that the μ-vector LMS algorithm results in a better performance than the conventional one, that is, the same amount of attenuation of the signal components as the conventional one but more noise reduction than the conventional LMS algorithm. More results showing the performance of the μ-vector LMS algorithm can be found in (Chen 1989c) and in chapter 5.

The nonstationary factor β can be optimized for particular nonstationary signals. One example was shown in (Chen 1989c) and it will be presented in chapter 5.

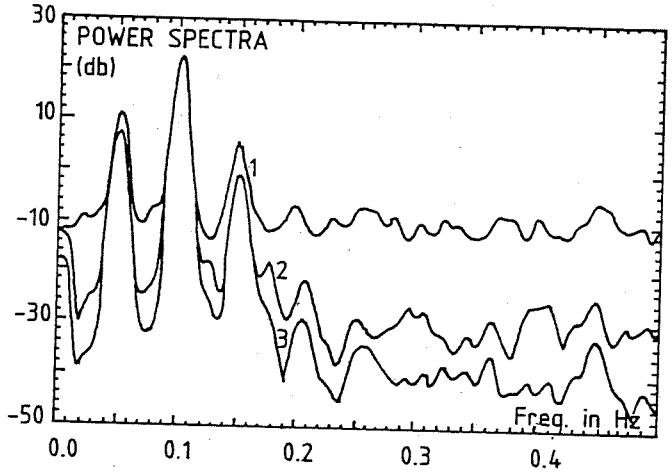


Figure 2.7: Performance comparison of the μ-vector LMS and the LMS algorithms. $N = 30$, $Fs = 1\ Hz$, $\triangle = 1$, $b_n = 2$, $\mu' = 0.1$, $G_0 = x_1^2 + ..., + x_{30}^2$. Curve 1: input power spectrum (512s); Curve 2: output power spectrum with $\beta = 0$; Curve 3: output power spectrum with $\beta = 0.05$

2.5.4 Application

The proposed two stage adaptive system has been applied with success in the cancellation of respiratory artifacts in biomedical signals (Chen 1987b, 1989b). In these applications the adaptive system is composed of an ALE followed by an adaptive noise canceler (ANC). It is shown in the applications that the introduction of an ALE as a pre-processor does result in better performance.

The μ-vector LMS algorithm has been applied in enhancing nonstationary biomedical signals, where the adaptive system consists of an ALE and a modified multi-channel adaptive enhancer (Chen 1988e and 1989c).

The detailed description of the applications can be found in chapter 5.

2.6 Adaptive Lattice Filter

2.6.1 Introduction

We have discussed in the previous sections the adaptive transversal FIR filters using the LMS algorithms. The LMS adaptive transversal FIR filter is mostly used in signal processing and telecommunications because of its simplicity and stability. Its main disadvantage is, however, that the convergence speed is related to the eigenvalue spread of the auto-correlation matrix of the input signal. The convergence is very slow when the eigenvalue spread is very large or the signal is highly correlated. Another problem with the adaptive transversal filter is that the roundoff noise resulting from the finite wordlength representation of the filter weights in fixed point increases as the width of the passband of the signal gets narrow.

The lattice structure was well developed in (Markel 1976) while the adaptive lattice filter was originally proposed in (Griffiths 1977) for the purpose of noise cancellation. It was applied in speech coding (Markel 1976, Carter 1978) and channel equalizing (Satorius 1979) to achieve rapid convergence. The applications to radar signal processing can be found in (Haykin 1985). The convergence properties of the gradient adaptive lattice filter have been well analyzed by many researchers, as in (Gibson 1980, Medaugh 1981 and Honig 1981).

Using vector space concepts, the least square lattice (LSL) adaptive algorithm has been derived. This is, however not the topic of this chapter. The basic structure for the LSL algorithm was proposed in (Morf 1978, Lee 1981). An excellent tutorial paper on the derivation and the applications of the LSL can be found in (Friedlander 1982). The book of Honig and Messerschmitt gives a detailed discussion on both gradient lattice filters and least square lattice filters (Honig 1984).

In this and the next sections we present the basic principles of the adaptive lattice filter and our contributions to the adaptive lattice filter, respectively. The structure, the advantages and the stochastic gradient (or LMS) algorithm of the adaptive lattice filter will be introduced in this section. These materials are based on the literature.

2.6.2 Lattice structure

The lattice structure is illustrated in Fig.1.5 and is expressed as (Markel 1976):

$$e^f_{p,j} = e^f_{p-1,j} - k_p e^b_{p-1,j-1} \tag{2.46}$$

$$e^b_{p,j} = e^b_{p-1,j-1} - k_p e^f_{p-1,j} \tag{2.47}$$

where, e^f_{pj} and e^b_{pj} are respectively the pth stage forward and backward errors at time j. k_p is called the pth reflection coefficient (Markel 1976).

The stability of the lattice filter is always guaranteed if the following condition holds (Honig 1984):

$$|k_p| < 1, \quad 1 \leq p \leq N \tag{2.48}$$

2.6.3 Applications of the lattice filter

The lattice filter was derived based on the Levinson-Durbin algorithm (Levinson 1947 and Durbin 1959). The strategy of the Levinson-Durbin algorithm is to express the optimal pth order predictor based on the knowledge of the $(p-1)$st order predictor. The lattice structure has several advantages over the transversal structure.

The optimal reflection coefficients k_p are independent of the filter order N. Thus, successive lattice stages may be added to or subtracted from existing stages without the necessity of recalculating already existing reflection coefficients. The coefficients of the transversal prediction filter, however all change when the order N of the filter is modified (Honig 1984).

The derivation of the higher order predictor in the lattice structure is based upon the lower order predictors, Thus, in some applications where the order of the predictor required to achieve a given error is not known in advance, successive orders of the prediction errors can be calculated while monitoring the mean square error.

In some applications to be discussed in the following, the lattice structure offers very attractive features.

Lattice joint process estimator In a joint process estimator, a primary input d_j and a reference input x_j are provided (see Fig.2.10) In the transversal structure the input to the adaptive filter is composed of a tapped delay line $x_j, x_{j-1}, ..., x_{j-N+1}$. The lattice joint process estimator is constructed when the reference input x_j is connected to the lattice filter and the backward errors are fed to the adaptive filter, i.e., the tapped delay line is replaced by the lattice structure.

In the lattice joint process estimator the backward errors e^b_{pj} $(p = 1, 2, ..., N)$ are uncorrelated with each other (Makhoul 1978). When these errors constitute the input to the joint LMS adaptive filter, the convergence speed is significantly improved because of the whiteness of the backward errors.

However, this advantage disappears when the reference input signal is already a white process, such as in the application of echo cancellation in data transmission systems, where the input signals are transmitted data that are mostly random.

Lattice linear predictive coder The lattice filter is almost universally used in speech analysis and synthesis (Markel 1975, Rabiner 1978, Makhoul 1981). The lattice linear predictive coder has several advantages: 1) The solution of a set of linear equations using the Levinson-Durbin algorithm is eliminated; 2) Reduced precision is required in the calculation since the coefficients k_p require considerably less precision (Honig 1984); 3) Easier for quantization since $|k_p| < 1$; 4) Easier for stability check after quantization.

Spectral estimation We mentioned in chapter 1 that a time series can be modeled as the output of a linear filter excited by a white noise process. The lattice filter is, in fact, a linear predictor. Its input is the time series x_j while the output is a white noise. That is, the lattice filter is a whitening filter or an inverse filter. Thus, once the lattice converges, the power spectrum can be calculated from its coefficients k_p using the Levinson-Durbin algorithm.

2.6.4 Stochastic gradient lattice algorithm

The procedure of deriving the stochastic gradient algorithm is similar to that of deriving the LMS algorithm. To recursively update the reflection coefficients first apply the steepest descent method and then replace the mean square errors by square errors (this method is often called stochastic gradient method (Ljung 1983)):

$$W_{j+1} = W_j - \mu \nabla_w E[e_j^2] \tag{2.49}$$

For the lattice filter there are two error sequences as described previously. The most popular way of adapting the reflection coefficients k_p is to minimize the sum of the forward and the backward errors. Following the gradient approach, one attains,

$$k_{p,j+1} = k_{pj} - \mu \nabla_{k_p} (E[(e^f_{pj})^2 + (e^b_{pj})^2] \tag{2.50}$$

In the same way as in the derivation of the LMS algorithm, simply ignoring the expectation in Eq(2.50), one gets,

$$k_{p,j+1} = k_{pj} - 2\mu(e^f_{pj}\frac{\partial e^f_{pj}}{\partial k_p} + e^b_{pj}\frac{\partial e^b_{pj}}{\partial k_p}) \tag{2.51}$$

Substituting Eq(2.49) and (2.50) into (2.51), the stochastic gradient lattice algorithm is derived (Satorius 1979):

$$k_{p,j+1} = k_{pj} + 2\mu(e^f_{pj}e^b_{p-1,j-1} + e^b_{pj}e^f_{p-1,j}) \tag{2.52}$$

where μ is the step-size which controls the convergence of the stochastic gradient lattice algorithm. Its value must be properly chosen to guarantee

the stability. In order to avoid the problem associated with filter instability a time-varying value of μ is usually chosen as follows (Satorius 1979):

$$q_{pj} = (1-\alpha)q_{p,j-1} + (e^f_{pj})^2 + (e^b_{pj})^2 \tag{2.53}$$

where α is a small constant ($<< 1$).

Then, the stochastic gradient lattice algorithm becomes:

$$k_{p,j+1} = k_{pj} + \frac{1}{q_{pj}}(e^f_{pj}e^b_{p-1,j-1} + e^b_{pj}e^f_{p-1,j}) \tag{2.54}$$

Eq(2.54) is the normalized gradient lattice algorithm. $1/q_{pj}$ is called the normalized step-size which is updated recursively according to Eq(2.53).

From Eq(2.53) an important property can be observed: the normalized step-size $1/q_{pj}$ increases for small prediction error. This is quite desirable since low prediction error implies a high degree of accuracy in the prediction, or the linear filter has indeed formed an adequate model of the system under consideration. Thus any increase in the prediction errors should be due to a change in system parameters, and it is desirable to have the lattice adjust to this new system very quickly. On the other hand, if the processing environment consists of a high white noise level in addition to any signal, then the prediction error could be quite large. This causes the normalized step-size to be fairly small. Therefore, the adaptive lattice will not respond very rapidly to a high noise environment.

2.7 Lattice Form TSAF

The transversal TSAF proposed in (Ferrara 1981) has an attractive performance for the processing of some nonstationary signals. Its drawback is, however slow convergence of the adaptation due to the fact that in the TSAF several instead of one weight vectors are used and only one is adapted for each input sample.

In this section we propose a lattice form TSAF (Chen 1987a). It results in significant improvement in the convergence speed since the backward errors of the lattice structure, which are used as the inputs of the TSAF, are uncorrelated with each other.

2.7.1 Time-sequenced adaptive filter

From Eq(2.8) we know that the mean square error, ϵ_j of the adaptive transversal filter is a quadratic function of the weight vector.

$$\epsilon_j = E[d_j^2] - 2W_j^T P_j + W_j^T R_j W_j \tag{2.55}$$

With stationary inputs, the cross correlation vector P_j and the auto-correlation matrix R_j are constants , That is, $P_j = P$ and $R_j = R$. Therefore the mean square error has a single fixed minimum point at which the weight vector has its optimum value. After sufficiently long adaptations the weight vector approaches this optimum value.

With nonstationary inputs, however, P_j and R_j are changing over time and the minimum point, the curvature and the orientation of the mean square error surface are also changing. Consequently the optimal weight vector is time-varying. In this case the adaptive filter introduces an extra misadjustment due to the fact that the adaptation of the weight vector can not follow well the time variation of the optimum solution. Fig. 2.8 illustrates the error performance surfaces in the nonstationary environment. At different time instants, the error surface has different locations (Chen 1987a).

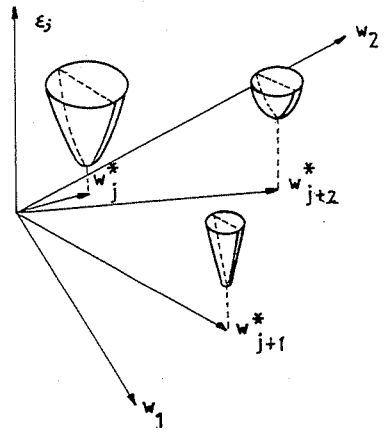


Figure 2.8: Time variation of error performance surfaces for a nonstationary process

But for some nonstationary signals having a *a recurring statistical character*, e.g., recurring pulse in noise and a periodic signal in noise, there exist a finite number of different error performance surfaces which also recur in time. The TSAF (Ferrara 1981) is especially developed for the processing

of that sub-set of nonstationary signals.

The TSAF uses multiple (M) adjustable weight vectors, denoted by $W_1, W_2, ..., W_M$. Each weight vector is assumed to associate with a corresponding error performance surface. For each input sample, according to an external time-sequenced signal t_j, one and only one weight vector is selected and adapted towards the minimum point of the corresponding error performance surface by the LMS algorithm. In this way each weight vector becomes an expert in filtering a particular portion of the interval between recurring points and after a long enough adaptation each weight vector approaches the optimum value of the corresponding error performance surface.

Fig.2.9 shows the TSAF. It can be considered to have M adaptive filters. At a particular time instant or interval, only one adaptive filter is connected to the input signal x_j by the switch t_j and adapted. At another time instant or interval the switch points to another filter. At each recurring point the switch goes back to its original position and the successive process is repeated.

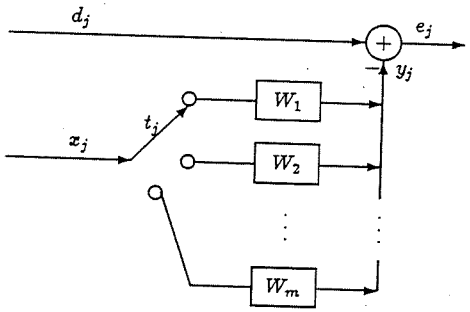


Figure 2.9: Illustration of a time-sequenced adaptive filter. W_k – the weight vectors; t_j – the time-sequenced signal (should be available)

Mathematically, the LMS TSAF is described as follows (Chen 1987a):
$j < L$:

$$y_j = X_j^T W_{1j} \tag{2.56}$$

$$W_{1,j+1} = W_{1j} + 2\mu e_j X_j \tag{2.57}$$

$j = L$:

$$W_{kj} = W_{1j} \quad k = 2, 3, ..., M \tag{2.58}$$

$j > L$:

$$y_j = X_j^T W_{t_j,j} \tag{2.59}$$

$$\begin{aligned} W_{k,j+1} &= W_{kj} + 2\mu e_j X_j \quad k = t_j \\ &= W_{kj} \qquad\qquad\quad \text{otherwise} \end{aligned} \tag{2.60}$$

where W_{kj} is the kth weight vector at time j. M is the number of the weight vectors used. t_j is an externally available time-sequenced signal (an integer number). It switches the adaptation to a right weight vector at each particular time. The meaning of L is explained in the next paragraph.

The algorithm described above is a slightly modified version of that in (Ferrara 1981). Instead of assuming all initial weight vectors to be zero, we start with the adaptation of only one weight vector W_1 for the first L samples, see Eq(2.57). This adapted value is then assigned as the initial values of the other weight vectors, see Eq(2.58). This means that for the first L input samples the conventional LMS algorithm is applied and after that the time-sequenced LMS algorithm is used.

The performance of the TSAF in comparison with the conventional LMS adaptive filter was investigated in (Ferrara 1981, 1982 and Chen 1986). It has been shown that for nonstationary signals which have recurring statistical character, less waveform distortion is introduced by the TSAF than by the conventional adaptive filter.

The computational complexity of the TSAF is the same as that of the conventional adaptive filter since at each time instant only one weight vector is adapted. But the convergence of the LMS-TSAF is much slower than that of the LMS adaptive filter. The more weight vectors are used, the slower the convergence of the TSAF is.

2.7.2 Lattice form TSAF

In order to speed up the convergence, we propose to implement the TSAF in a lattice structure, where the tapped delay inputs are replaced by the lattice structure as illustrated in Fig.2.10 (Chen 1987a). The time-switching to the different weight vectors of the TSAF is not shown in the figure for simplicity. The subtraction takes a recursive form and the adaptation of the pth element of the kth weight vector at time j, $w_{k,p,j}$ is controlled by the residual error e_{pj} on the corresponding stage. d_j is the primary input and x_j is the reference input. The adaptation of the reflection coefficients k_p $(1 \le p \le N-1)$ is based on the normalized stochastic gradient lattice algorithm in section 4.3.3.

The backward errors e_{pj}^b $(1 \le p \le N-1)$ are used as the inputs to the TSAF. These backward errors have been proved to be uncorrelated

with each other once the lattice has converged (Makoul 1977). Thus fast convergence is provided.

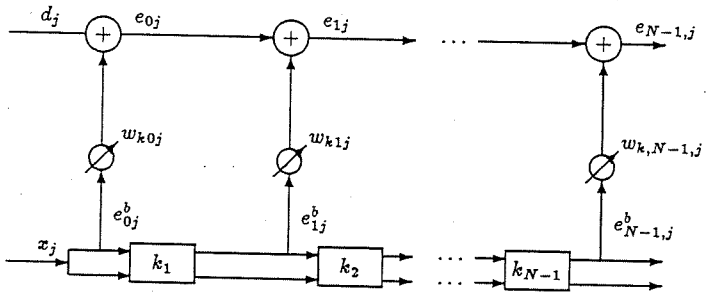


Figure 2.10: Lattice form time-sequenced adaptive filter

The adaptation algorithm for the pth weight coefficient of the kth weight vector at time j, $w_{k,p,j+1}$, is expressed as follows:

$$0 \le p \le N-1: \quad \begin{aligned} w_{k,p,j+1} &= w_{kpj} + \tfrac{1}{q^2_{pj}} e_{pj} e^b_{pj} \quad k = t_j \\ &= w_{kpj} \qquad\qquad\qquad \text{otherwise} \end{aligned} \tag{2.61}$$

where the residual error e_{pj} $(0 \le p \le N-1)$:

$$e_{0j} = d_j - w_{t_j,0,j} x_j \tag{2.62}$$

$$e_{pj} = e_{p-1,j} - w_{t_j,p,j} e^b_{pj}, \quad 1 \le p \le N-1 \tag{2.63}$$

and q^2_{pj} is the normalized step-size expressed as:

$$q^2_{pj} = (1-\alpha_q) q^2_{p,j-1} + (e^b_{pj})^2, \quad 0 \le p \le N-1 \tag{2.64}$$

2.7.3 Simulation results with lattice TSAF

Computer simulations have been conducted to investigate the convergence property of the proposed lattice form TSAF and to compare it with the time-sequenced LMS algorithm and the conventional LMS algorithm (Chen 1987a).

The system used in the simulations is an adaptive line enhancer. The input signal d_j consists of a nonstationary sinusoidal signal (its frequency is fixed at 0.05 Hz, but its amplitude is randomly changing from one period to another with a deviation of 50%) in a uniformly distributed (-0.5,0.5) white noise with SNR equal to 6 dB. The sampling frequency is 1 Hz. The delay $\triangle$ is chosen to be one sample. The adaptive filter is realized either by the transversal structure or by the lattice structure according to the purposes of the simulation. The filter order is set to be 20. Four learning curves (averaged over 200 independent runs) are shown in Fig.2.11 to Fig.2.13.

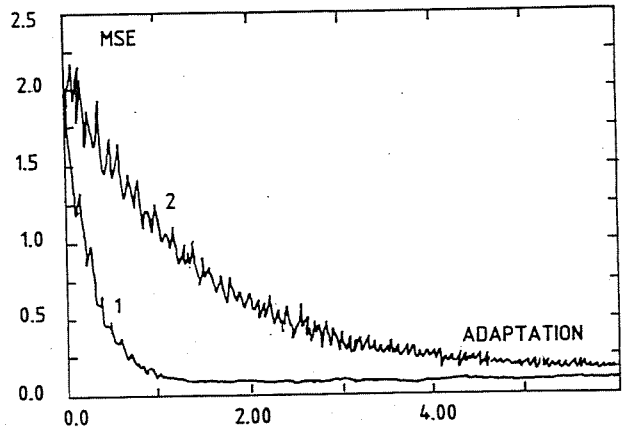


Figure 2.11: Comparison between TSAF and AF. Curve 1: learning curve (200 runs) from the conventional adaptive filter; Curve 2: from the TSAF

1. Curve 1 results from the conventional LMS adaptive filter with the convergence factor μ equal to 0.02/(total filter input energy)
2. Curve 2 is obtained by applying the TSAF proposed in (Ferrara 1981) 10 weight vectors (just an arbitrary value) are used and all initial values are assumed to be zero.
3. Curve 3 is obtained under the same conditions as curve 2 but the modified algorithm (Chen 1987a) is used, that is, for the first $L = 20$ input samples the conventional LMS algorithm is used and only one weight vector is adapted. Its value is then assumed to be the initial value of the other weight vectors.
4. Curve 4 is the result of the proposed lattice form TSAF with 10 weight vectors as in the previous two simulations and $q_{p0} = 20$ $(0 \le p \le N-1)$, $\alpha = \alpha_q = 0.01$.

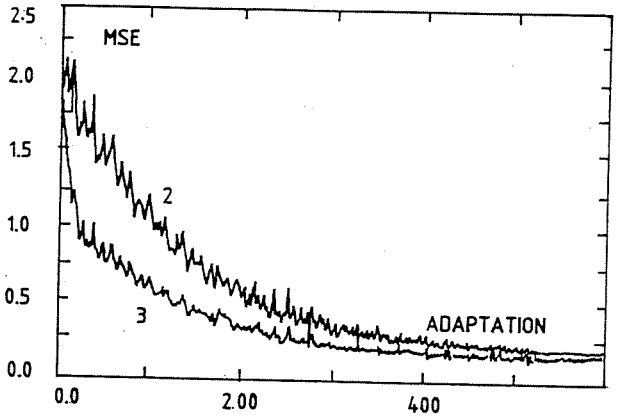


Figure 2.12: Comparison between original and modified TSAF. Curve 1: learning curve (200 runs) from original TSAF; Curve 3: from the modified TSAF

The values of the parameters α, μ and q_{p0} were chosen based on experiments, resulting in a better performance.

The comparison of the convergence rate between the time-sequenced LMS and the conventional LMS algorithms is illustrated in Fig.2.11. The drawback of the time-sequenced LMS algorithm is clearly observed from this figure. It converges much slower than the conventional LMS algorithm. The advantage of the initial weight vector modification of the time-sequenced LMS algorithm is shown in Fig.2.12, where curve 2 results from the original TSAF and curve 3, from the modified one. The slightly modified algorithm does increase the convergence speed.

Fig.2.13 shows the important result of this section. Comparing learning curve 2 (TSAF) and curve 4 (lattice form TSAF) we can observe the dramatic increase of the convergence speed by using the lattice structure. As we mentioned in the previous discussion this improvement results from the orthogonality of the lattice structure in its backward errors. We can also observe from this figure that the proposed lattice form TSAF converges even faster than the conventional LMS algorithm (curve 1). Definitely it will make the TSAF more applicable in practice.

From curve 4 we may also observe that it has a peak at about the $20th$ iteration. This results from the fact that for the first 20 samples the

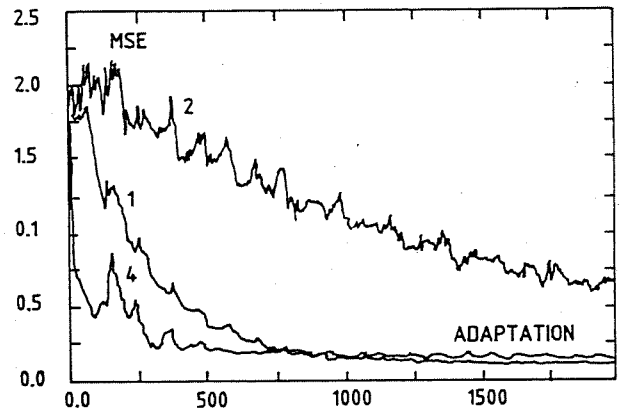


Figure 2.13: Comparison among AF, TSAF and lattice form TSAF. Curve 1 and 2 are the same as in the previous figures; Curve 4: from the lattice form TSAF

conventional LMS algorithm is applied and only after that time instant the time sequenced LMS algorithm is used.

2.8 Conclusion

In this chapter, the LMS adaptive filter was introduced. Some important properties of the adaptive LMS filter were outlined. Experimental results showing the performance of the adaptive filter were given. A new LMS algorithm was proposed. It has been shown that the new algorithm performs better than the conventional LMS algorithm for nonstationary signal processing.

The TSAF produces a better performance than the conventional LMS algorithm in filtering some nonstationary signals having recurring characteristics. Its main drawback is, however, the very low convergence, which may hinder some of its applications. We implemented the TSAF in a lattice from. This significantly improves the convergence of the TSAF due to the orthogonality of the lattice structure in its backward errors. Simulation results were presented and the improvement was shown.

Chapter 3

Adaptive IIR Filters

3.1 Introduction

The transversal adaptive FIR filter has been discussed in the preceding chapter. It consists of a tapped delay line and its weights are adaptively adjusted according to the LMS algorithm. The adaptive FIR filter has found a great deal of applications in situations where the statistics of the input signal or system are unknown or changing or both. In chapter 4 and 5 its applications in the cancellation of echoes in telecommunication systems and in biomedical signal processing will be exploited at length. Yet, sometimes in practice, one encounters situations where a system has recursive characteristics or in other words, the system has both poles and zeroes. In this case, the adaptive FIR filter which is of all-zero form is inefficient in computations. For example, to identify or model a system with both poles and zeroes, the use of the adaptive FIR filter leads to heavy computation. That is, high order is required by the adaptive FIR filter.

To solve this problem, adaptive infinite impulse response (IIR) filters have been proposed. Different structures and algorithms for the adaptive IIR filter can be found in the literature. One of the purposes of this chapter is to give a systematic treatment of the adaptive IIR filters.

Three sorts of adaptive IIR filters are to be presented in the chapter:

1. Constrained adaptive IIR filter. In this sort of the adaptive filter, the tapped delay line is replaced by a conventional IIR filter in which some of the parameters are adjustable (Hush 1986, Stoica 1988, Rao 1988).

2. Recursive adaptive filter. This sort of adaptive filter consists of two tapped delay lines: a forward tapped delay line which is the same as in the adaptive FIR filter and a backward tapped delay line of which the input is a

feedback taken from the output of the adaptive filter (White 1975, Feintuch 1976).

3. Adaptive autoregressive moving average (ARMA) filter (Chen 1987d, Chen1988b). It is similar to the recursive adaptive filter except that the feedback is taken from the residual error between the primary input and the filter output. It was proposed for ARMA spectral analysis (Chen 1987d) and is therefore given this name.

The derivation of the adaptive algorithm is much more difficult for the adaptive IIR filter than for the adaptive FIR filter because of the recursive structure of the filter transfer function. The LMS or simplified LMS algorithm is commonly used for the adaptation of the filter weights.

The immediate reward of the adaptive IIR filter lies in the substantial decrease in computations. However, its applications are limited because of the following:

- It becomes unstable if the poles move outside the unit circle during the adaptive process.
- The error performance surface of the adaptive IIR filter is generally nonquadratic and may have local minima.
- The analysis of its performance is rather difficult.

This chapter is structured as follows: In section 3.2 we introduce the constrained adaptive IIR filter and the recursive adaptive filter which have already existed in the literature. In section 3.3 we propose the adaptive ARMA filter. A simplified LMS algorithm is developed for the adaptation of the filter weights. The applications of the LMS adaptive ARMA filter in spectral estimation is presented in section 3.4. The adaptive RLS-ARMA spectral estimation method is discussed in section 3.5. Comparisons can be found in section 3.5 between the adaptive FIR filter and the adaptive IIR filters.

3.2 Constrained and Recursive Adaptive IIR Filters

3.2.1 Constrained adaptive IIR filter

In this thesis, the term " adaptive IIR filter" is used as a general term for all sorts of adaptive IIR filters with feedback or with pole-zero form. One of the adaptive IIR filters to be discussed in this section is called "constrained adaptive IIR filter". In the literature one may encounter terms, "adaptive

IIR filter," "constrained adaptive IIR filter" and so on (Thompson 1978, Hush 1986, Stoica 1988, Rao 1988)

In the constrained adaptive IIR filter, the tapped delay line is replaced by a conventional IIR filter expressed as:

$$H(z) = \frac{A(z)}{C(z)} \tag{3.1}$$

It has both zeroes and poles which are determined by the functions $A(z)$ and $C(z)$. It is known that if the poles move outside the unit circle, the filter becomes unstable. To avoid this problem some constraints are imposed on the parameters of $A(z)$ and $C(z)$. Thus it is called constrained adaptive IIR filter. The main trick is, therefore, how to impose the constraints on the parameters of the IIR filter according to particular applications.

The following example gives an idea how this sort of adaptive filter is derived.

Assume the primary input signal is a sinusoid in white noise and the purpose is to extract the sinusoid. Thus, the ALE with $\triangle = 1$ can be applied.

$$x_j = d_{j-1} \text{ and } d_j = b_s \cdot sin(f_0 j) + n_j$$

where, n_j is white noise, j is the time index. Choose the IIR filter as follows (Hush 1986):

$$H(z) = \frac{(\frac{1-f^2}{1+f^2})w - (1-f^2)z^{-1}}{1 - wz^{-1} + f^2 z^{-2}} \tag{3.2}$$

where,

$$-2f < w < 2f \tag{3.3}$$

With the above constraints it is easy to verify that the poles of $H(z)$ are constrained to be complex and to be within the unit circle on the z-plane. Therefore, the stability of $H(z)$ is guaranteed.

It can also be shown that the magnitude response of $z^{-1}H(z)$ is that of a bandpass filter which peaks at the angular frequency:

$$f = cos^{-1}(\frac{w}{1+f^2}) \tag{3.4}$$

and thus $z^{-1}H(z)$ has unity gain and zero phase shift. That is, the output y_j of $H(z)$ is guaranteed to be identical to the sinusoid in the primary input d_j.

Assume that f is fixed and w is adaptive. The adaptation algorithm for w is not difficult to develop using the LMS algorithm:

$$\begin{aligned} w_{j+1} &= w_j - 2\mu e_j \frac{\partial e_j}{\partial w_j} \\ &= w_j + 2\mu e_j \frac{\partial y_j}{\partial w_j} \end{aligned} \tag{3.5}$$

The filter output y_j can be written as (Hush 1986):

$$y_j = w(\frac{1-f^2}{1+f^2})x_{j-1} - (1-f^2)x_{j-2} + wy_{j-1} - f^2 y_{j-2} \tag{3.6}$$

Substituting Eq(3.6) into (3.5), the LMS algorithm for the adaptation of w_j can be derived.

From the above example we see that the stability of the constrained adaptive IIR filter can always be guaranteed by imposing constraints on some parameters of the IIR filter. But some knowledge of the input signal should be known in advance.

The constrained adaptive IIR filter has found applications in the enhancement of narrow band signals in broad-band noise, especially in extracting sinusoidal signals in white noise (Hush 1986, Rao 1988 and Stoica 1988).

3.2.2 Recursive Adaptive Filter

The recursive adaptive filter consists of two tapped delay lines: a forward tapped delay line and a backward tapped delay line as shown in Fig.1.4 (Feintuch 1976).

The forward part is the same as the adaptive FIR filter with length p. The backward tapped delay line consists of $y_{j-1}, ..., y_{j-q}$. Fig.3.1 illustrates the block diagram of the recursive adaptive filter, where,

$$A(z) = a_{1j} + a_{2j}z^{-1} + \cdots + a_{pj}z^{-p+1} \tag{3.7}$$

$$C(z) = c_{1j}z^{-1} + c_{2j}z^{-2} + \cdots + c_{qj}z^{-q} \tag{3.8}$$

The transfer function of the IIR filter is then:

$$H(z) = \frac{A(z)}{1 - C(z)} \tag{3.9}$$

The LMS algorithm for the recursive adaptive filter was derived in (Widrow 1985). It is summarized here.

From Fig.1.4, the adaptive filter output y_j is expressed as:

$$y_j = \sum_{k=1}^{p} a_{kj}x_{j-k+1} + \sum_{k=1}^{q} c_{kj}y_{j-k} \tag{3.10}$$

Define an input vector U_j and a weight vector W_j, given by

$$U_j^T = [x_j, ..., x_{j-p+1}, y_{j-1}, ..., y_{j-q}] \tag{3.11}$$

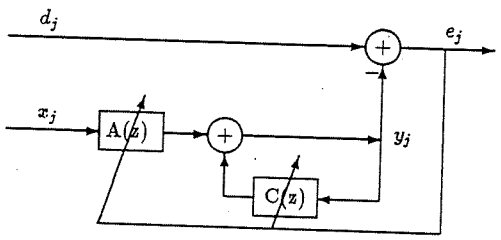


Figure 3.1: Block diagram of the recursive filter

$$W_j^T = [a_{1j}, ..., a_{pj}, c_{1j}, ..., c_{qj}] \tag{3.12}$$

Then, the output y_j can be written as,

$$y_j = W_j^T U_j \tag{3.13}$$

The error signal e_j in Fig.1.4 is equal to,

$$e_j = d_j - y_j = d_j - W_j^T U_j \tag{3.14}$$

Eq(3.14) is quite similar to the expression of the residual error in the adaptive FIR filter except that U_j here is a generalized input vector which contains not only the input data samples but also the feedbacks.

Assume $p = q$. Applying the steepest descent method and using the square error to approximate the mean square error, the LMS algorithm can be derived, which is summarized as follows (Widrow 1985):

$$\begin{array}{lll} \textit{Initialization}: & W_0 = \text{null vector} & \\ & \alpha_{k0} = \beta_{k0} = 0 & (1 \le k \le p) \\ \textit{Adaptation}: & y_j = W_j^T U_j & \\ & W_{j+1} = W_j + 2\tilde{\mu} e_j \tilde{\nabla}_j & \\ & \alpha_{kj} = x_{j-k+1} + \sum_{l=1}^{p} c_{lj} \alpha_{k,j-l} & (1 \le k \le p) \\ & \beta_{kj} = y_{j-k} + \sum_{l=1}^{p} c_{lj} \beta_{k,j-l} & (1 \le k \le p) \end{array} \tag{3.15}$$

where,

$$\begin{array}{ll} \tilde{\nabla}_j^T & = [\alpha_{1j}, ..., \alpha_{pj}, \beta_{1j}, ..., \beta_{pj}] \\ U_j^T & = [x_j, x_{j-1}, ..., x_{j-p+1}, y_{j-1}, y_{j-2}, ..., y_{j-p}] \\ W_j^T & = [a_{1j}, a_{2j}, ..., a_{pj}, c_{1j}, c_{2j}, ..., c_{pj}] \\ \tilde{\mu} & = diag[\mu_a, ..., \mu_a, \mu_c, ..., \mu_c] \end{array} \tag{3.16}$$

The above general version of the LMS algorithm is, in general complicated for real applications. Various recursive LMS algorithms such as SHARF and Feintuch's algorithms proposed in (Feintuch 1976, Larimore 1980, Hsia 1981) can be considered as simplified versions of the general LMS algorithm.

The convergence of the SHARF algorithm in some applications has been proved (Johnson 1981) and applications in noise cancellation and in adaptive prediction can be found in (Larimore 1978a, 1978b).

The Feintuch's algorithm is the simplest one in the family of the recursive LMS algorithms.

Recalling from Eq(3.10), it is obvious that the second term on the right of the equation is also a function of the weight vector W_j, which makes the derivation of the LMS algorithm complicated. However, in the derivation of Feintuch's algorithm, this fact was simply ignored. This results in the simplest recursive LMS algorithm as follows (Feintuch 1976):

$$\begin{array}{l} y_j = W_j^T U_j \\ e_j = d_j - y_j \\ W_{j+1} = W_j + 2\mu e_j U_j \end{array} \tag{3.17}$$

From Eq(3.17) we can see that the forward weights and the backward weights are separately adapted. The adaptation algorithm for each is exactly the same as that for the adaptive FIR filter.

3.3 Adaptive ARMA Filter

In section 3.2 the recursive adaptive filter was discussed. In that sort of the adaptive IIR filter, the feedback is taken from the output of the adaptive filter. The LMS algorithm is derived by applying the steepest descent method. The resulting recursive adaptive filter is efficient in computations for the identification of a system with recursive nature. In this section we propose another adaptive IIR filter: an adaptive ARMA filter (Chen 1987d) which has a similar structure as the recursive adaptive filter. The main difference is that in the adaptive ARMA filter, the feedback is taken from the residual error signal e_j between the primary input d_j and the adaptive filter output y_j. It is especially suited for ARMA spectral analysis and thus called adaptive ARMA filter. In a slightly different way, the LMS algorithm will be derived for the adaptive ARMA filter based on a similar approximation made in the derivation of the Feintuch's algorithm.

The structure of the adaptive ARMA filter is shown in Fig.3.2, where the adaptive filter consists of two tapped delay lines. The feedback is taken from the residual error signal e_j. The parameter sets a_{kj} $(k = 1, 2, ..., p)$ and

c_{kj} $(k = 1, 2, ..., q)$ are feed-forward and feedback weights of the adaptive filter, respectively. This structure was first proposed in (Friedlander 1982b) where the maximum likelihood method was applied to estimate the power spectrum of a time series. The LMS algorithm of the adaptive ARMA filter was derived in (Chen 1987d) and is described as follows (see Fig.3.2):

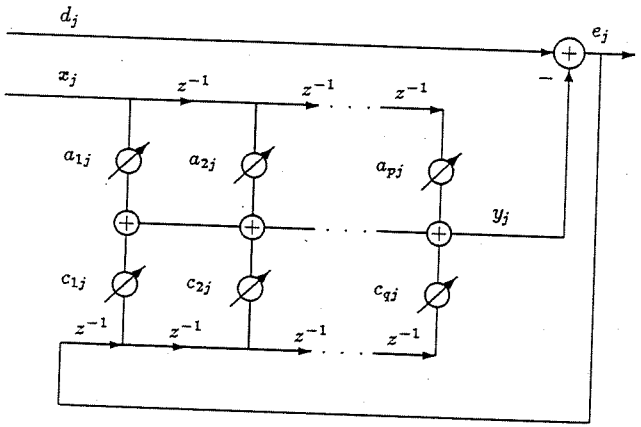


Figure 3.2: Adaptive ARMA filter

The output of the adaptive filter y_j equals:

$$y_j = A_j^T X_j + C_j^T \mathrm{e}_j \tag{3.18}$$

where,

$$A_j^T = [a_{1j}, a_{2j}, ..., a_{pj}] \quad C_j^T = [c_{1j}, c_{2j}, ..., c_{qj}]$$

$$X_j^T = [x_j, x_{j-1}, ..., x_{j-p+1}] \quad \mathrm{e}_j^T = [e_{j-1}, e_{j-2}, ..., e_{j-q}]$$

Assume the input signals d_j and x_j are wide-sense stationary, the mean square error can be expressed as:

$$E[e_j^2] = E[d_j^2] + A_j^T R_{xx} A_j + C_j^T R_{ee} C_j - 2A_j^T P_{dx} - 2C_j^T P_{de} + 2A_j^T R_{xe} C_j \tag{3.19}$$

where P_{dx} and P_{de} are cross-correlation vectors, R_{xx} and R_{ee} are auto-correlation matrices and R_{xe} is cross correlation matrix defined as:

$$P_{dx} = E[d_j X_j] \quad P_{de} = E[d_j \mathrm{e}_j]$$

$$R_{xx} = E[X_j X_j^T] \quad R_{ee} = E[\mathrm{e}_j \mathrm{e}_j^T]$$

$$R_{xe} = E[X_j \mathrm{e}_j^T]$$

Assume the above second order statistics are known a priori, the MMSE solution can be obtained by minimizing the mean square error with respect to the filter weight vectors, A_j and C_j, and setting them to zero.

$$\nabla_A [E(e_j^2)] = 2R_{xx}A - 2P_{dx} + 2R_{xe}C = 0 \tag{3.20}$$

$$A = R_{xx}^{-1}(P_{dx} - R_{xe}C) \tag{3.21}$$

$$\nabla_C [E(e_j^2)] = 2R_{ee}C - 2P_{de} + 2R_{xe}A = 0 \tag{3.22}$$

$$C = R_{ee}^{-1}(P_{de} - R_{xe}A) \tag{3.23}$$

In most of real applications, however, these statistics are not known a priori. Thus the gradient method is applied for the adaptation of the filter weights:

$$A_{j+1} = A_j - \mu_a \nabla_A [E(e_j^2)] = A_j - 2\mu_a(R_{xx}A_j - P_{dx} + R_{xe}C_j) \tag{3.24}$$

$$C_{j+1} = C_j - \mu_c \nabla_C [E(e_j^2)] = C_j - 2\mu_c(R_{ee}C_j - P_{de} + R_{xe}A_j) \tag{3.25}$$

According to the LMS algorithm (see section 2.3.2), above unknown matrices and vectors are replaced by instantaneous estimations of their values, i.e., R_{xx} is estimated by $X_j X_j^T$, R_{ee} by $\mathrm{e}_j \mathrm{e}_j^T$, P_{dx} by $d_j X_j$, P_{de} by $d_j \mathrm{e}_j$ and R_{xe} by $X_j \mathrm{e}_j^T$. Consequently, the LMS algorithm can be obtained as follows:

$$A_{j+1} = A_j + 2\mu_a e_j X_j \tag{3.26}$$

$$C_{j+1} = C_j + 2\mu_c e_j \mathrm{e}_j \tag{3.27}$$

where μ_a and μ_c are constants controlling the convergence of the algorithm.

The proposed adaptive ARMA filter has a very attractive property in modelling a time series. We will see later in section 3.4 that the output of the ARMA filter y_j is an ARMA estimate of the input signal d_j. After convergence the parameters a_{kj} and c_{kj} of the adaptive filter should be close to those of the ARMA model. Thus the adaptive ARMA filter is suitable for spectral analysis. The detailed discussion on the spectral estimation can be found in section 3.4 and 3.5 and its application to the adaptive spectral estimation of biomedical signals can be found in chapter 5.

3.4 Adaptive LMS-ARMA Spectral Analysis

3.4.1 Introduction

The power spectral density estimation of a discretely sampled deterministic or stochastic process is a frequently encountered problem in digital signal processing. Conventional methods of spectral estimation are based on fast Fourier transform (FFT) techniques. They are generally efficient in computations and produce reasonable results for stationary signals. These FFT based approaches, however, have several disadvantages:

- The problem of leakage in frequency domain, i.e., the energy in the main lobe of a spectral response leaks into sidelobes, masking adjacent spectral responses that are present. This is due to the implicit windowing of the data when processed. Careful selection of windows can reduce the sidelobe leakage, but always at the expense of reduced resolution.

- The limitation of tracking time-varying spectra due to the block processing of the FFT.

- Inefficiency in estimating a signal with only few data samples available.

In order to avoid the problems resulting from the FFT, modern spectral estimation techniques have been proposed since the 1970's (Kay 1981). Unlike the FFT based methods (non-parametrized method), modern techniques are all parametrized: First a relevant model is assumed and then the parameters of the model are calculated from data samples and the power spectrum is computed according to the parameters. Generally, modern spectral techniques provide better performance in spectral resolution and in signal detectability. But these performance advantages are strongly dependent on the SNR. For low enough SNR modern spectral estimations are often no better than those obtained from FFT processing. Commonly used modern estimation techniques are the AR and ARMA methods. A nice survey on the modern analysis methods can be found in (Kay 1981). In this section we propose an adaptive LMS-ARMA spectral method (Chen 1987d). An adaptive ARMA spectral analysis method using a RLS algorithm is discussed in the next section.

3.4.2 Adaptive LMS-AR spectral estimation

In chapter 1 we indicated that a time series can be modeled as the output of a linear filter $H(z)$ excited by a white noise process:

$$x_j = -\sum_{k=1}^{N} a_k x_{j-k} + n_j \tag{3.28}$$

where a_k $(k = 1, 2, ..., N)$ are AR parameters, n_j is an uncorrelated random process with power σ^2.

The transfer function between the input n_j and the output x_j for the AR process is expressed as

$$H(z) = \frac{1}{A(z)} \tag{3.29}$$

with

$$A(z) = \sum_{k=0}^{N} a_k z^{-k} \tag{3.30}$$

where $a_0 = 1$. The AR model is also termed all-pole model according to Eq(3.29).

Once the parameters of the AR model are known, the power spectrum of the process can be calculated as (Kay 1981):

$$P_x(\omega) = \frac{\sigma^2}{|1 + \sum_{k=1}^{N} a_k e^{-i\omega k}|^2} \tag{3.31}$$

To calculate the parameters of the AR model, an adaptive LMS-AR method was proposed in (Griffiths 1975). In Fig.1.8 let's assume the primary input is a time series x_j while the filter input is a one sample delayed $(\triangle = 1)$ version of the primary input. Thus the output of the adaptive filter is a linear predictor of the time series x_j:

$$y_j = \hat{x}_j = \sum_{k=1}^{N} w_{kj} x_{j-k} \tag{3.32}$$

Comparing Eq(3.32) with (3.28) we can see that the output $\hat{x}_j$ is an AR estimate of x_j with estimation error e_j expressed by

$$e_j = x_j - \hat{x}_j \tag{3.33}$$

Apply the LMS algorithm to adapt the adaptive filter weights, after convergence, the power spectrum of x_j can be calculated from the weights according to (3.31), where $a_k = -w_{kj}$ $(k = 1, 2..., N)$.

Simulation results can be found in (Griffiths 1975).

The advantages of this method are: 1) Unlike non-adaptive AR spectral methods (Ulrych 1975, Burg 1975, Marple 1975), auto-correlation estimates are avoided. The AR parameters are adapted for each input sample. The computational complexity is reduced from $o(N^2)$ to only $o(2N)$. 2) The non-adaptive AR methods require autocorrelation estimates and, as a result, presuppose that the data are stationary during the time window in which autocorrelation measurements are taken. Thus, in the case that a time series has a rapid time varying frequency such as, a frequency modulated signal, the time variation may be masked because the window size used to compute the correlation values exceeds the period of these variations. With the adaptive method, however, this problem is avoided as long as the time variation of an input signal is slower than the convergence rate of the LMS algorithm.

The drawback of this adaptive method is that the AR parameters are available for the calculation of the power spectrum only after the algorithm has converged. Thus it is not suitable for the estimation of the power spectrum of a signal with only few data available. One way to alleviate the problem associated with the short data recording is to process the input data several times, using the final values of filter weights of the last processing as initial values for the next processing.

Both the adaptive and non-adaptive AR spectral estimation methods have higher resolution than the FFT based techniques with a relatively high SNR. For a low SNR, however the resolution is no better than that of the conventional periodogram (Oppenheim 1975). The reason for the degradation is that the all-pole model assumed in the AR spectral estimation is no longer valid when observation noise is present. The power spectrum of a noise corrupted signal is, in fact, characterized by poles and zeros. The inconsistency of the AR model leads to the degradation. This can be explained as follows: The dynamic range of the power spectral density of a time series x_j is affected by the noise. Since the linear predictor (also called inverse filter) attempts to whiten the power spectrum, it is obvious that due to the present noise, the power spectrum is already flat and so the transfer function of the linear predictor will not significantly whiten the power spectrum any further.

To avoid or reduce the degradation of the AR spectral estimation in the presence of noise, the following approaches may be applied:

- ARMA spectral estimation.
- AR spectral estimation with large order.
- Filtering the data to reduce the noise before spectral analysis.

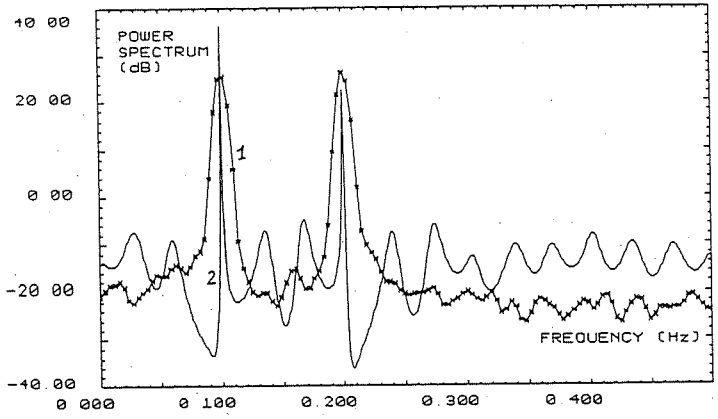


Figure 3.3: Estimation of two sinusoids. Real frequencies: $f_1 = 0.1Hz$, $f_2 = 0.2Hz$, Sampling frequency: 1 Hz. Curve 1: spectral estimation by the periodogram method; Curve 2 by the proposed method

The second simulation is designed to investigate the ability of distinguishing two very close spectral lines. The input time series has the same composition as in the previous simulation but the frequencies of the two sinusoids are equal to $0.1Hz$ and $0.11Hz$, respectively. The results are shown in Fig.3.4, where curve 1 shows the spectral estimation by the periodogram method, one can see that the two spectral responses merged into one. The estimation by the proposed method is shown in curve 2 where two different spectral responses are well recognizable.

3.5 Adaptive RLS-ARMA Spectral Analysis

3.5.1 RLS algorithm for adaptive ARMA filter

Suppose the adaptive ARMA filter shown in Fig.3.2 is implemented as a 1-step ahead linear predictor with input signal x_j. A recursive least square (RLS) algorithm is developed as follows.

In Fig.3.2 let's define

$$U_j^T = [x_{j-1}, x_{j-2}, ...x_{j-p}, e_{j-1}, ..., e_{j-q}] \tag{3.41}$$

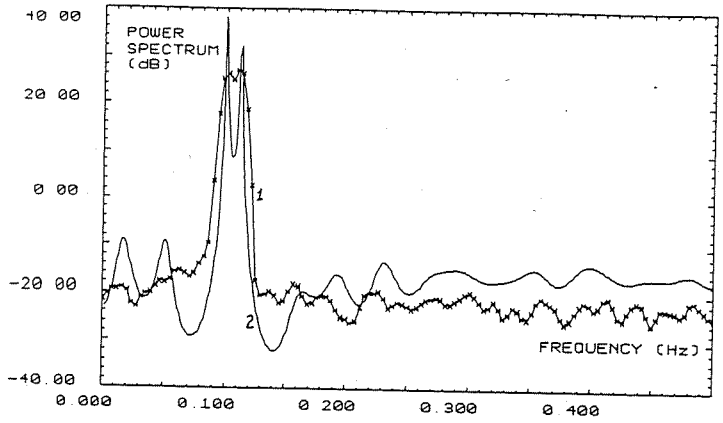


Figure 3.4: Estimation of two sinusoids. Real frequencies: $f_1 = 0.1Hz$, $f_2 = 0.11Hz$, Sampling frequency: 1 Hz. Curve 1: spectral estimation by the periodogram method; Curve 2 by the proposed method

$$W_j^T = [a_{1j}, ..., a_{pj}, c_{1j}, ...c_{qj}] \tag{3.42}$$

The error in predicting the kth input sample x_k using W_j is defined as

$$e_{k/j} = x_k - U_k^T W_j \tag{3.43}$$

The solution to the RLS problem is to minimize a cumulative square error ϵ_j

$$\varepsilon_j = \sum_{k=1}^{j} \lambda^{j-k} e_{k/j}^2 \tag{3.44}$$

Substituting (3.43) into (3.44) one can find the optimal solution. The parameter $\lambda(0 < \lambda \leq 1)$ in (3.44) is termed forgetting factor which may be used to give the recent data heavier weight in the RLS computations. For stationary data, it is often set to 1, which means that all data are equally weighted in the computation of filter weights.

To derive the RLS algorithm, set the gradient of Eq(3.44) to zero

$$\frac{\partial}{\partial W_j} \varepsilon_j = 0 \tag{3.45}$$

It can be observed that in Eq(3.43) the filter input vector U_j is also a function of the filter weight vector W_j This makes the derivation of the

algorithm very complicated. For simplicity we assume that the vector U_j is independent of the filter weight vector W_j. Based on this assumption an RLS algorithm for the adaptive ARMA filter can be developed.

Solving Eq(3.45) one attains the following equation:

$$R_j W_j = P_j \text{ or } W_j = R_j^{-1} P_j \tag{3.46}$$

with:

$$R_j = \sum_{k=1}^{j} \lambda^{j-k} U_k U_k^T \tag{3.47}$$

$$P_j = \sum_{k=1}^{j} \lambda^{j-k} x_k U_k \tag{3.48}$$

where R_j is the sample autocorrelation matrix with dimension $N \times N (N = p + q)$ and P_j is the sample cross-correlation vector with N elements. One might have noticed the difference between the sample autocorrelation matrix (or sample cross-correlation vector) and the autocorrelation matrix R (or cross correlation vector) described in chapter 2. For stationary, ergodic data and with $\lambda = 1$,

$$\lim_{j \to \infty} \frac{1}{j} R_j = R \tag{3.49}$$

the sample autocorrelation matrix becomes the true autocorrelation matrix. Eq(3.46) is very similar to the optimal solution described in chapter 2. To obtain the optimal weight vector W_j, the inverse matrix R_j^{-1} is involved, which requires massive amounts of computations. The direct matrix inverse needs $o(N^3)$ operations and $o(N^3)$ storage locations. It is surely too expensive.

Assuming that at time $j-1$, Eq(3.46) is valid and the solution is known

$$W_{j-1} = R_{j-1}^{-1} P_{j-1} \tag{3.50}$$

Eq(3.46) can then be solved in a recursive way.

Since the quantities at the previous time $j-1$ in (3.50) are assumed to be known, the sample autocorrelation matrix and the sample cross-correlation vector at time j can be calculated as follows:

$$R_j = \sum_{k=1}^{j-1} \lambda^{j-k} U_k U_k^T + U_j U_j^T = \lambda R_{j-1} + U_j U_j^T \tag{3.51}$$

$$P_j = \lambda P_{j-1} + x_j U_j \tag{3.52}$$

Note that the second term on the right-hand side of Eq(3.51) is also an matrix with dimension $N \times N$ and what we need is the recursive update

for the inverse matrix R_j^{-1} in terms of the previous inverse R_{j-1}^{-1}. Thus the matrix inverse lemma can be applied, which is written as follows:

$$if \;\; H = A + \mathbf{b}\mathbf{c}^T \tag{3.53}$$

$$then \;\; H^{-1} = A^{-1} - A^{-1}\mathbf{b}(1 + \mathbf{c}^T A^{-1}\mathbf{b})\mathbf{c}^T A^{-1} \tag{3.54}$$

where H and A are $N \times N$ matrices, $\mathbf{b}$ and $\mathbf{c}$ are vectors with N elements.

Comparing (3.51) with (3.53) and using the result in (3.54) one attains

$$R_j^{-1} = \frac{1}{\lambda}[R_{j-1}^{-1} - \frac{R_{j-1}^{-1} U_j U_j^T R_{j-1}^{-1}}{\lambda + \gamma_j}] \tag{3.55}$$

where γ_j is a scalar defined as

$$\gamma_j = U_j^T R_{j-1}^{-1} U_j \tag{3.56}$$

Eq(3.55) indicates that if R_{j-1}^{-1} is assumed to be known, R_j^{-1} can be calculated since all information required is available.

To simplify the algorithm further we define an $N \times N$ matrix B_j as

$$B_j = R_j^{-1} \tag{3.57}$$

and an $N \times 1$ gain vector $\mathbf{g}_j$ as

$$\mathbf{g}_j = \frac{B_{j-1} U_j}{\lambda + \gamma_j} \tag{3.58}$$

Then the recursion in (3.55) becomes

$$B_j = \frac{1}{\lambda}[B_{j-1} - \mathbf{g}_j U_j^T B_{j-1}] \tag{3.59}$$

Now substituting Eq(3.57), (3.59) and (3.48) into (3.46) and simplifying we obtain:

$$\begin{aligned} W_j &= \tfrac{1}{\lambda}(B_{j-1} - \mathbf{g}_j U_j^T B_{j-1})(\lambda P_{j-1} + x_j U_j) \\ &= W_{j-1} + \mathbf{g}_j(x_j - U_j^T W_{j-1}) \end{aligned} \tag{3.60}$$

Finally using Eq(3.43) we have

$$W_j = W_{j-1} + \mathbf{g}_j e_{j/j-1} \tag{3.61}$$

Despite the complexity of the RLS algorithm its similarity to the LMS algorithm can be observed. That is, the new weight vector equals the old weight vector plus a modification vector. However, the update terms in the

two algorithms are substantially different. This is because different criteria are used for the optimizing process.

In the derivation of the LMS algorithm, a mean square error measure is used and it is not a function of the input data, but is dependent on the statistical characterization of the data instead. In the derivation of the RLS algorithm, however, a cumulative square error criterion is used and it is really a function of the actual data vectors which will be used in the prediction. Moreover, from Eq(3.44) we can see that a new error criterion is recomputed and then re-optimized for every time instant j. This makes the convergence of the RLS algorithm much faster than the simple LMS method. For spectral estimation, the property of fast convergence means that the ARMA parameters can be obtained from a short data recording. We'll demonstrate this later. On the other hand, the cumulative square error criterion makes the algorithm more complicated, i.e., higher computational complexity. In the LMS algorithm only $2N$ operations are required for each input sample. In the RLS algorithm, however, $7N^2$ operations are required.

To reduce the complexity fast transversal filters have been proposed which require $7 - 10N$ operations. A brief discussion on the comparison between different algorithms can be found in section 4.2.4.

3.5.2 Experiment with RLS-ARMA method

Experiments with simulated two sinusoids in gaussian noise have shown that the RLS method produces the same performance as the LMS method except that considerably less adaptations are needed for the RLS algorithm.

Fig.3.5 shows one of the results, where the input data contains 65 samples of a cutaneous gastric signal with a sampling frequency of 2 Hz (see chapter 5 for more about the signal). In the experiment with the RLS-ARMA method, p is chosen to be 10 and q to be 3. The curve in the figure shows the estimated power spectrum (in dB) after 65 adaptations, starting with a null weight vector. In the figure two peaks can be clearly observed. The first one from the left is a signal originating from the human stomach and the second is respiratory artifact. From the figure we can be convinced that the RLS-ARMA method is very powerful for the spectral estimation of a short data recording. For the gastric signal, its frequency is around 0.04-0.05 Hz (slow time-varying). With a sampling frequency of 2 Hz its period is 40-50 samples. In our experiment only 65 samples are used for the estimation, which covers one and a half period of the signal. Based on experiments with the LMS-ARMA method, this is impossible since the LMS algorithm has not yet converged after 65 adaptations.

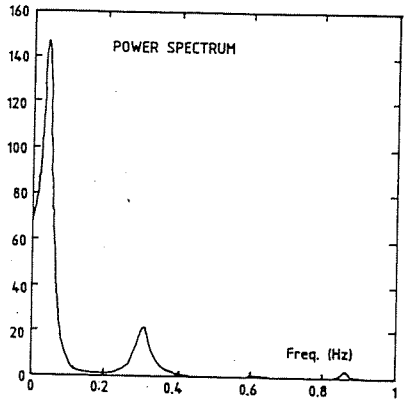


Figure 3.5: Spectral estimation of a biomedical signal using RLS-ARMA method. Power spectrum (dB) vs. frequency. Sampling frequency: 2 Hz. $p = 10$, $q = 3$. Power spectrum calculated after 65 adaptations.

3.6 Comparison of Adaptive FIR and IIR Filters

In this section the adaptive IIR filters will be compared with the adaptive FIR filter on convergence and on performance (Chen 1988b).

3.6.1 Convergence

From the discussion in chapter 2 we know that the mean square error of the adaptive FIR filter is a quadratic function of the filter weight vector. The error performance surface has only one minimum. Starting with any initial values, the filter weights are adapted according to the LMS algorithm to reach the optimum values. The convergence (mean of the weight vector) of the adaptive FIR filter is always guaranteed as long as the following condition holds:

$$0 < \mu < \frac{1}{\lambda_{max}} \tag{3.62}$$

For a constrained adaptive filter, it was shown in section 3.2 that the stability and the convergence can be guaranteed by imposing proper constraints on the IIR filter coefficients (Rao 1988, Stoica 1988).

The convergence of the recursive adaptive filter and the adaptive ARMA filter is, however not guaranteed. In (Stearn 1981) a conjecture was made on the recursive adaptive filter that under wide-band signal conditions the error performance surface of the recursive adaptive filter has only a single global minimum if the transfer function $H(z)$ has at least as many zeros and poles as the system to be identified. But a counterexample can be found in (Fan 1988).

The convergence of the LMS algorithm for the adaptive ARMA filter has not yet been proved. However, according to our experience with the recursive adaptive filter and with the adaptive ARMA filter, the convergence is guaranteed if the step-size is chosen as follows:

$$0 < \mu_a, \mu_c << \frac{1}{\text{total input power}} \tag{3.63}$$

To understand the behavior of these two sorts of the adaptive IIR filters, more efforts still have to be made.

3.6.2 Performance comparison

Several experiments have been done on adaptive line enhancement, adaptive noise cancellation and spectral estimation in order to compare the performance of the adaptive IIR filter with that of the adaptive FIR filter (Chen 1988d).

The experiment of the adaptive noise cancellation is based on a system shown in Fig.3.6, where the filter input x_j is a simulated ARMA process. The desired signal d_j is a filtered version of the signal x_j. The filter $F(z)$ consists of 100 taps. The values of its taps are equal to those of an approximately simulated impulse response of the echo path on a long distance telephone network. The adaptive filter is implemented as either an adaptive FIR filter or a recursive adaptive filter.

Fig.3.7a shows the square error e_j^2 resulting from an adaptive FIR filter with the filter order equal to 100 and Fig.3.7b shows that resulting from a recursive adaptive filter with $p = 100$ and $q = 1$. Comparing these two figures we observe that adding a feedback with only one tap from the filter output increases the convergence rate in this application. They have the same performance in steady-state. Experiments have been set up to apply the recursive adaptive filter with $p+q < 100$ (this implies less computations) in this application. The results show that a recursive adaptive filter with $p < 100$ can not produce satisfactory results.

Fig.3.8 shows the comparative results of their application in adaptive line enhancement. The desired signal d_j consists of a sinusoid in white

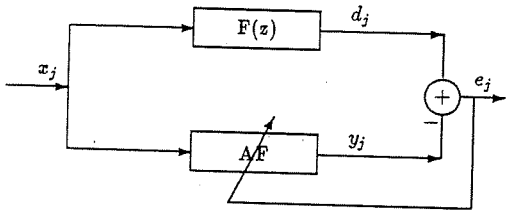


Figure 3.6: Simulation system for adaptive echo cancellation

noise (it is not an ARMA process). The filter input is a one-sample delayed version of d_j. The figure shows the mean square error over 200 independent runs versus the adaptation number. Curve 1 results from an adaptive FIR filter with $N = 20$ and curve 2 from a recursive adaptive filter with $p = 18$, $q = 2$ ($p + q = N$ means the same computational complexity for the two adaptive filters). We can see from this figure that the recursive adaptive filter converges faster than the adaptive FIR filter at the same cost (the same number of taps). The steady-state performance is the same for these two adaptive filters.

The last experiment is on spectral estimation. The input signal is a biomedical signal (see chapter 5 for more). The result is shown in Fig.3.9. Curve 1 is the true power spectrum. Curve 2 is the power spectrum estimated by the adaptive FIR filter, from which we observe that the information on the frequency components with lower power is missing. The estimated spectrum by the adaptive ARMA filter is shown in curve 3, from which we see it provides all information on the different frequency components. This experiment shows that the adaptive ARMA filter produces better performance than the adaptive FIR filter in the spectral estimation of the cutaneous gastric signal.

From these experiments we have shown that in contrast to the conclusion made in the literature (Widrow 1985) the recursive adaptive filter may have higher convergence rate than the adaptive FIR filter for the adaptive line enhancement and the adaptive noise cancellation. However, we have found that the adaptive IIR filter does not improve the performance in the steady-state for these cases.

The proposed adaptive ARMA filter can provide better performance on spectral estimation than the adaptive FIR filter (AR method) if a time

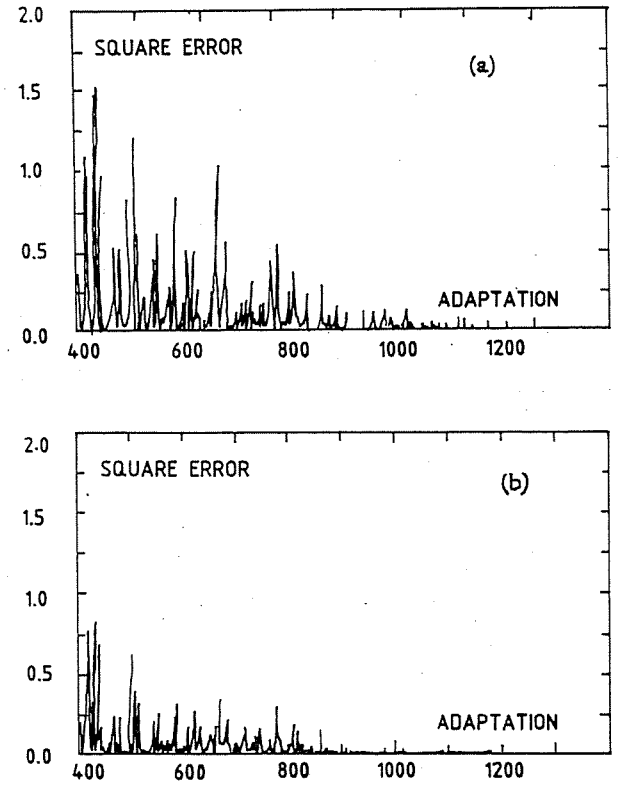


Figure 3.7: Performance comparison in adaptive noise cancellation. (a) Square error vs. adaptation number resulting from an adaptive FIR filter (N=100); (b) Square error vs. adaptation number resulting from a recursive adaptive filter (p=100, q=1).

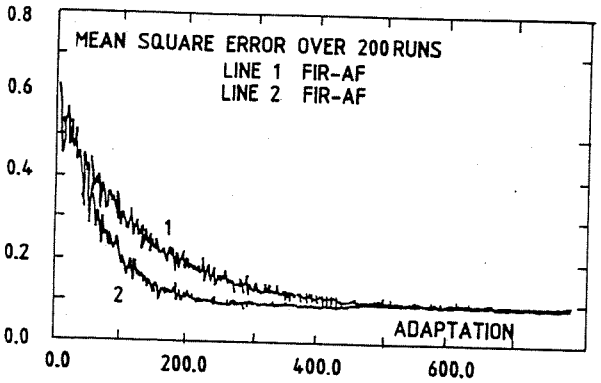


Figure 3.8: Performance comparison in adaptive line enhancement. Curve 1: MSE over 200 runs vs. adaptations resulting from an adaptive FIR filter (N=20); Curve 2: from a recursive adaptive filter (p=18, q=2)

series is an ARMA process.

The main problem with the recursive adaptive filter and the adaptive ARMA filter is the possible divergence since no mathematical formula is available that guarantees the convergence of the LMS algorithm.

3.7 Conclusion

A systematic treatment was given in this chapter on adaptive IIR filters. Three sorts of adaptive IIR filters and their LMS algorithms were discussed. Some comparisons between the adaptive IIR filters and the adaptive FIR filter on convergence and on performance have been given.

The recursive adaptive filter has an attractive property in identifying a system with recursive nature. It has also been applied in the adaptive noise cancellation and in the adaptive line enhancement and our simulations show that it may result in faster convergence than the adaptive FIR filter in some cases.

The problem with the recursive adaptive filter and the adaptive ARMA filter is that the convergence can not be guaranteed. However, experiments have shown that they are stable if the step-size is carefully chosen (small enough).

The proposed adaptive ARMA filter can generate an ARMA estimation of an input time series. Thus it is very useful in signal modelling and in

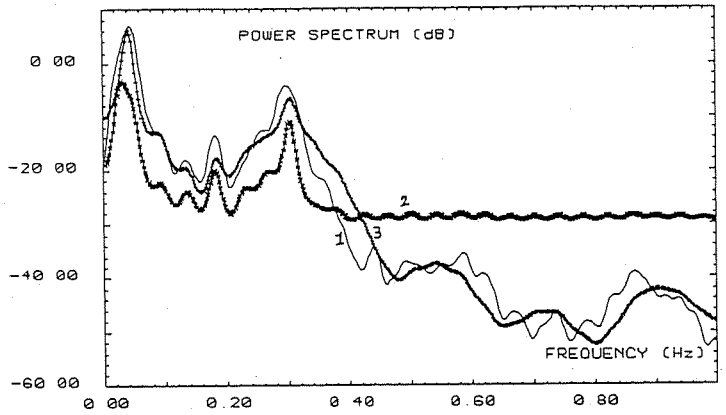


Figure 3.9: Performance comparison in spectral estimation (power spectra in dB vs. frequency in Hz. Input: a biomedical signal. Curve 1: estimated by the periodogram method; Curve 2 by the adaptive AR method; Curve 3 by the LMS-ARMA method.

signal analysis. The application of the proposed adaptive ARMA filter in ARMA spectral analysis has been discussed. Both the LMS and the RLS algorithm for the adaptation of the filter weights have been derived. Simulation results have shown that the proposed adaptive LMS-ARMA and RLS-ARMA spectral analysis methods produce better performance than the FFT based periodogram method and than the LMS-AR method for a time series which can be better modeled by an ARMA process. It has also been shown that the adaptive RLS-ARMA spectral analysis method is very efficient for short data recordings.

Chapter 4

Adaptive Echo Cancellation

4.1 Introduction

Adaptive filters have found a great deal of applications in telecommunications. Among them two very attractive ones are adaptive echo cancellation and adaptive channel equalization.

The adaptive channel equalization is a widespread application of the adaptive filtering technique in data transmission systems to eliminate the intersymbol interference. A common need for high speed data transmission to furnish computer communications is to utilize the widespread network of voice bandwidth channels developed for voice communications. A modulator-demodulator (MODEM) is then required to carry digital signals over these analog passband channel by translating binary data to voice frequency signals and back. In data transmission systems, the binary data is first encoded and modulated by the transmitter and then sent over the telephone line. At the receiver, it is demodulated and decoded. However, in efficient digital communication systems the effect of each symbol transmitted over a time dispersive channel extends beyond the time interval used to represent that symbol. The distortion caused by the resulting overlap of the received symbols is called inter-symbol interference.This distortion is one of major obstacles to reliable high speed data transmission over low background noise channels of the limited bandwidth. The adaptive equalizer adjusts adaptively its coefficients to compensate for the inter-symbol interference. More detailed discussion on the adaptive channel equalization can be found in (Lucky 1968 and Proakis 1983).

In speech and data transmission systems, the echo is introduced in the hybrid when the impedances are not perfectly matched, which is often the case. Some nonlinearities should be considered in the echo because of the nonlinear behavior of the analog/digital (A/D) and D/A conversions and the asymmetry between transmitted positive and negative pulses. In the hand-free telephone and teleconferencing systems, the acoustic echo is generated by the unwanted coupling between the loudspeaker and the microphone. These echoes are often annoying problems and should be cancelled by applying certain techniques.

In order to solve the echo problem in the long distance transmission system, an echo suppressor (Clark 1925) was proposed. It utilizes the voice switch technique. It has been noticed, however, that some voice quality degradation can not be avoided, principally because of the voice switching operating during the double-talking stage or at the beginning and final parts of a conversation. As a result of research on voice and signal processing an echo canceller was considered to solve the above mentioned problem.

The idea of the adaptive echo canceller was first proposed in (Sondhi 1967, Kelly 1970). The echo canceller models the echo path, produces a replica of the echo and subtracts it from the echo-combined incoming signal to obtain the signal alone.

Since the first invention of the echo cancellation a lot of efforts have been expended to improve of the adaptive echo canceller such as, increasing the convergence speed and obtaining high echo reduction. Various algorithms have been developed for the echo canceller and different methods of the implementation of the echo canceller have been proposed (Sondhi 1980, Gritton 1984, Messerschmitt 1984).

Echo canceller has found various applications in telecommunications, mainly,

1. Echo cancellation on the analog customers' loop, i.e., speech transmission.

2. Echo cancellation on the digital customers' loop, i.e., full duplex data transmission. It is more difficult since the echo level is much higher than the incoming signal and therefore the nonlinear effects in the echo path should be taken into account.

3. Acoustic echo cancellation in the teleconferencing and hand-free telephone systems. It is also very difficult since the acoustic echo has very long impulse response.

In this chapter we present our research results on the acoustic echo cancellation and on the nonlinear echo cancellation for a full-duplex data

transmission system. In the next section we discuss the cancellation of the echo in a long distance telephone network. The source of the echo, the basic principle of the echo cancellation, adaptive algorithms available for the echo canceller and design criteria are discussed in that section.

Section 3 presents the acoustic echo cancellation in the teleconferencing and hand-free telephone systems. The main difference between the line echo and the acoustic echo is that the acoustic echo path has much longer impulse response. Nevertheless the acoustic echo canceller has heavy computational burden. According to our experience the subband acoustic echo canceller seems to be a good solution for this problem. The detailed discussion of the subband method is presented (Chen 1988a).

In section 4 we present an acoustic echo canceller using the subband method for the teleconferencing and hand-free telephone systems. A new structure of the subband acoustic echo canceller proposed in section 3 is applied. Both off-line simulation results on the computer and real time simulation results on the DSP processor environment are presented (Chen 1988d).

The cancellation of the nonlinear echo in the data transmission system is described in section 5. Two methods, Wiener scheme and Volterra series expansion are discussed. Their performances are compared by means of simulations (Chen 1989a). Results showing the effects of the nonlinearity of the echo path, far-end signal and finite word length are presented. A nonlinear echo canceller for a U-interface circuit on the integrated service digital network (ISDN) is proposed and the improvement of the system over the linear one is shown in section 6 (Chen 1989d).

4.2 Line Echo Cancellation

4.2.1 Echo on telephone network

Echo is a phenomenon almost every one encounters in daily life. When conversations take place, one hears echoes of his speech waves reflected by the wall, the floor and other neighboring objects. It is not noticeable if the time delay between the speech and the echo is short. But it becomes annoying if that delay is long. Generally speaking, the longer the echo is delayed, the more it should be attenuated before it becomes untolerable.

On a telephone network or in a data transmission system, echoes may be generated too. As shown in figure 4.1, the telephone network is composed of two-wire line, four-wire line and hybrids which perform the transformation between the two-wire and the four-wire lines. Every telephone set in a given geographical area is connected to a central office by a two-wire line

(called the customers' loop). The two-wire line serves for communication in either direction. For long distance communication four-wire line is applied because of the following reasons: 1) The long distance network requires amplification while the amplifiers are one-way devices; 2) For reasons of economy, most long distance calls are multiplexed, i.e., a number of calls use portions of one wide-band transmission channel. Multiplexing requires that signals in the two directions be sent over different slots.

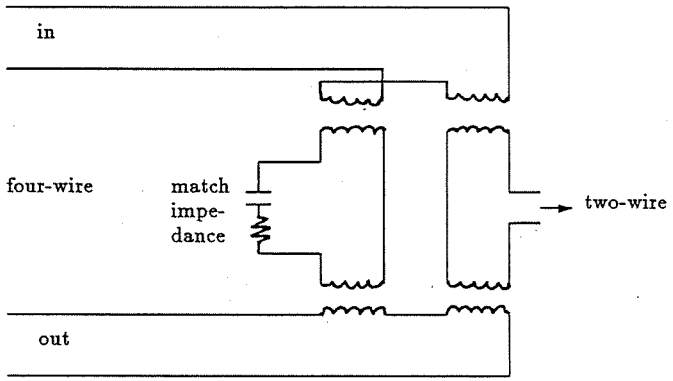


Figure 4.1: Detail of the hybrid

The transformation between the two-wire and four-wire lines is performed by the hybrid shown in figure 4.1. The four-wire consists of the two "in" wire and two "out" wire, each serves for communication for one direction. The connection between the hybrid and the talker is made by the two-wire which is balanced by an artificial network (called matching impedance). From this figure we see that the hybrid is basically a bridge circuit. Ideally, the two transformers are identical and the matching impedance is exactly equal to the impedance of the two-wire circuit at all frequencies. Under such conditions it is clear that any signal originating on the "in" side of the four-wire circuit gets coupled to the two-wire circuit, while producing no response in the "out" side of the four-wire circuit. A signal originating in the two-wire circuit couples to both paths of the four-wire circuit, but it has no effect on the "in" side because the amplifiers there are only for the opposite direction.

In reality, however the hybrid, which is a part of the four-wire circuit,

may be connected to any one of a large number of different two-wire circuits terminated in the customers' loops and the customers' loops are extremely variable in length, in the type of wire, in the number of extension phones in use, etc. Generally the impedance of the two-wire circuit can not be perfectly matched by the matching impedance and the "in" side is coupled to the "out" side of the hybrid, thus giving rise to an **echo**!

Two sorts of echoes may be encountered on a telephone line as illustrated in figure 4.2, where a) shows the talker's echo which results in the talker hearing a delayed version of his or her own voice owing to feed-through at the hybrid at the far-end of the connection; b) shows the listener's echo. The listener hears the original and a delayed version of the talker's speech because the echo signal travels the four-wire twice.

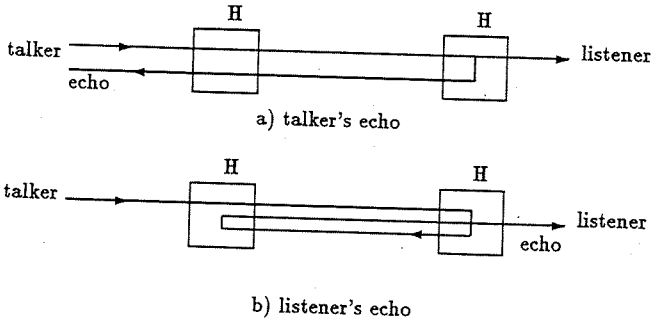


Figure 4.2: Echoes on a telephone line

The effect of the echo depends on the transmission delay and the effective transfer function around the four-wire path. If the delay is short the talker's echo represents an insignificant impairment because it is indistinguishable from the normal sidetone in the telephone. Delay of a few milliseconds or more with insufficient echo attenuation, however will make the conversation very difficult. In the case of the listener' echo, short delay results in an overall frequency response with peaks and valleys owing to the destructive and constructive interference at different frequencies. Subjectively, the effect is as if the talker spoke into a rain barrel.

4.2.2 Traditional methods of echo control

In the control of the echo on the telephone line there are several commonly used methods. These include net-loss, echo suppression and echo cancellation. The first two methods are described as follows.

Net-loss is the simplest way of attenuating the echo. From figure 4.2 we see that the talker's echo travels through the four-wire line twice and the listener's echo passes through the line three times. So the idea is to introduce insertion loss into the telephone connection, say L dB. Consequently, the signal, the talker's echo and the listener's echo are respectively attenuated L dB, $2L$ dB and $3L$ dB. Therefore the signal to noise ratio (SNR) is improved. Since the signal is also attenuated in this method it is not adequate for a long distance network, where either echo suppressor or echo canceller may be applied.

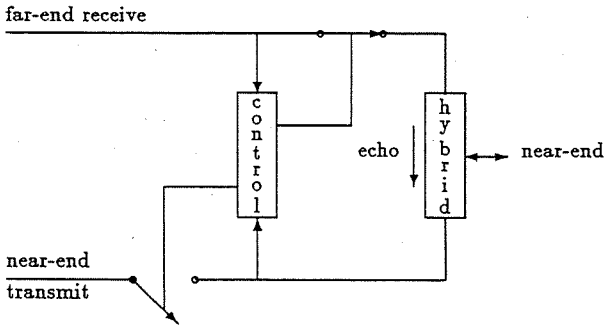


Figure 4.3: An echo suppressor

Echo suppressor is shown in figure 4.3. Its principle is to insert a large attenuation, but only in the direction of the transmission that is not currently carrying conversations. It dynamically changes the connection based on a determination of who is talking. When the far-end talker is speaking, the path used to transmit the near-end speech is opened so that the echo is prevented. When the near-end talker speaks, the same switch is closed and a symmetric one on the far-end speech path is opened. This approach works well, but it has three main problems (Sondhi 1980):

1. It introduces the problems of clipping speech sounds and of impairing interruption. For example, if the near-end talker is initially listening

to the far-end but suddenly wants to interject a point, it is quite likely that the switch preventing his speech from being transmitted will not close quickly and the far-end talker may not receive all of the message.

2. Dead effect. Usually conversations take place with one end active (speaking) and the other end passive (listening) but with very short response just to indicate that he is listening. Due to the clipping effect, the talker may not hear anything from the listener and thus may have feeling of talking on a dead line.

3. Double-talk. In a situation where both directions contain speech (both ends are speaking) it becomes very difficult for the echo suppressor to handle. It is completely useless in a full duplex data transmission system where both directions of the transmission must be utilized simultaneously.

4.2.3 Adaptive echo cancellation

The structure of the adaptive echo canceller for the telephone line is illustrated in figure 4.4. x_j is the received signal from the far-end talker on the four-wire line. n_j is the echo generated by the hybrid, s_j is the near-end talker's speech signal, e_j is supposed to be the echo-free near-end signal to be sent to the far-end. Ideally, $e_j = s_j$ the far-end talker will not hear his or her own speech, that is, the talker's echo is cancelled. It is also clear that the near-end will not hear the delayed version of the far-end talker's speech. That is, the listener's echo (see figure 4.2) is automatically eliminated if the the talker's echo is cancelled.

The echo canceller models the echo path, produces a replica of the echo and subtracts this replica from the echo-combined near-end signal d_j to generate an echo-free speech.

The design of the adaptive echo canceller involves two steps: system identification and residual error minimization. The echo path, namely the echo transfer function of the hybrid in combination with the transmission facility (omitted in figure 4.4) between the hybrid and the echo canceller, is generally considered to be linear. It is usually represented by the impulse response and therefore the adaptive FIR filter is applied as an echo canceller.

The echo path may also be modeled as a pole-zero system. Then the adaptive IIR filter may be used, which will be discussed later. Here we only consider the echo canceller realized by the adaptive FIR filter.

Once the echo path is modeled, the following procedure is how to minimize the residual error signal e_j, which will lead to different algorithms.

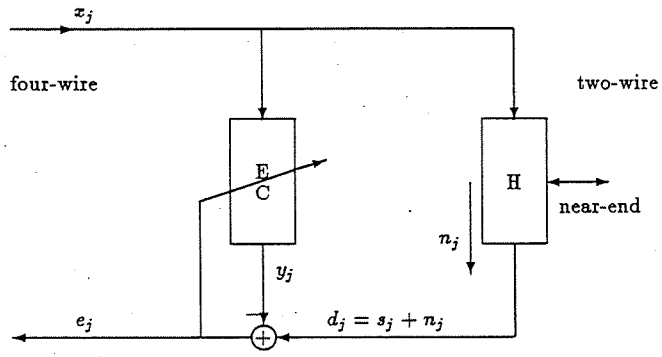


Figure 4.4: Adaptive cancellation of echo on a telephone line. H – Hibrid, EC – Adaptive echo canceller, x_j – received signal from the four-wire, n_j – echo, s_j – signal from the two-wire to be transmitted.

The most commonly used algorithm is the LMS algorithm:

$$y_j = \sum_{k=1}^{N} w_{kj} x_{j-k+1} \tag{4.1}$$

$$e_j = d_j - y_j = s_j + (n_j - y_j) \tag{4.2}$$

$$W_{j+1} = W_j + 2\mu_j e_j X_j \tag{4.3}$$

where $W_j = [w_{1j}, ..., w_{Nj}]^T$, $X_j = [x_j, ..., x_{j-N+1}]^T$. W_j is the weight vector of the echo canceller (or adaptive FIR filter with order of N). The step-size μ is usually normalized as follows:

$$\mu_j = \mu / q_j \tag{4.4}$$

$$q_j = (1 - \frac{1}{N}) q_{j-1} + \frac{x_j^2}{N} \tag{4.5}$$

Some important issues on the adaptive echo canceller are summarized below:

- Number of taps. The number of taps required for the transversal adaptive filter depends on the effective length of the impulse response of the hybrid and the transmission delay from the echo canceller to the hybrid.

- Convergence rate. The echo path is usually time varying, the convergence of the adaptive echo canceller should be fast enough to follow the changes of the echo path. Generally the time variation of the echo path on the telephone line is very slow and thus small value of μ could be used in order to have better echo cancellation performance.
- Double-talk. How to handle the double-talk is another important issue in the design of the echo canceller. The near-end speech s_j is "true" error signal (see Eq(4.2)) and is usually strong. According to the analysis of the LMS algorithm in chapter 2 we know that this true error signal s_j will result in gradient noise in the weight vector. Since s_j is much stronger than the effective residual $(x_j - y_j)$ the fluctuation of the weight vector is very large. Consequently, the adaptive echo canceller may exhibit unacceptable behavior. Thus a double-talk detector is required. It simply ceases the adaptation of the echo canceller when double-talk is detected. The detailed description of the double-talk detector is beyond our interests and can be found in (Minami 1985)

4.2.4 Some potential alternatives to LMS

Transversal LMS adaptive filter is the most commonly used for the adaptive echo cancellation because of its simplicity (easiness for implementation) and the well-understood stability. Some potential alternatives to the LMS are briefly described as follows:

Sign LMS algorithm

A simplified version of the LMS algorithm is the sign algorithm which uses the sign of the instantaneous error signal e_j rather than its value. The algorithm then becomes

$$W_{j+1} = W_j + 2\mu[sgn(e_j)]X_j \tag{4.6}$$

The introduction of the sign operation $sgn(\cdot)$ complicates the theoretical analysis of the algorithm's behavior and leads to slow convergence. Its advantage is the saving of the computation. The multiplications required for the adaptation of the weight vector are eliminated if the step-size μ is chosen a power of 2.

Block LMS algorithm

Block algorithm is another simplified version of the LMS algorithm. It adjusts the weight vector once every M input samples,

$$W_{j+1} = W_j + 2\mu \sum_{k=1}^{M} e_{j-k+1}X_{j-k+1} \tag{4.7}$$

In the same way as the sign algorithm, the block LMS algorithm reduces the computational complexity at the costs of the slow convergence and lower performance.

Least square algorithm

Instead of minimizing the mean square error, it is possible to minimize the sum of the squared instantaneous error as shown in section 3.5. This leads to the RLS algorithm:

$$W_{j+1} = W_j + Q_{j+1}e_{j+1}X_{j+1} \tag{4.8}$$

where Q_j is a complicated expression involving matrix manipulations (Ljung 1983). The advantage of the RLS algorithm is the fast convergence. It was proved that the RLS algorithm converges in N iterations for pseudo-random signals (Salz 1983). But the computational complexity is increased to $o(N^2)$.

Fast RLS algorithm

The RLS algorithm converges rapidly but requires considerable computations. An optimization algorithm exists, which uses the fact that the input signal vector at any time is that of the previous sampling instant delayed by one or more samples added. Proper mathematical manipulations of the feature leads to fast algorithm with only around $10N$ operations for the same convergence condition as the RLS algorithm (Falconer 1978 and Cioffi 1983)

Adaptive lattice filter

The fast RLS algorithm has the advantages of fast convergence and less computations than the RLS algorithm. However, it has the problem of possible numerical instability. The adaptive lattice filter discussed in chapter 2 may also be applied as an adaptive echo canceller. Its convergence speed is high, owing to the orthogonalization of the lattice structure. Since the reflection coefficients of the adaptive lattice filter are less than 1, it is numerically stable and the finite wordlength representation of the coefficients has less effect on the filter performance.

Frequency domain algorithm

The frequency domain approach can be cast into a large class called the transform domain approach (Narayan 1983). Two types of the transform domain echo canceller are shown in figure 4.5. In type a) only the input signal to the echo canceller is transformed, while in type b) both incoming signals are transformed (Dentino 1978 and Mansour 1982). Type b) has been applied in the acoustic echo cancellation (Kellermann 1983, Gilloire 1987, Chen 1988a & 1988d) and will be discussed later in detail.

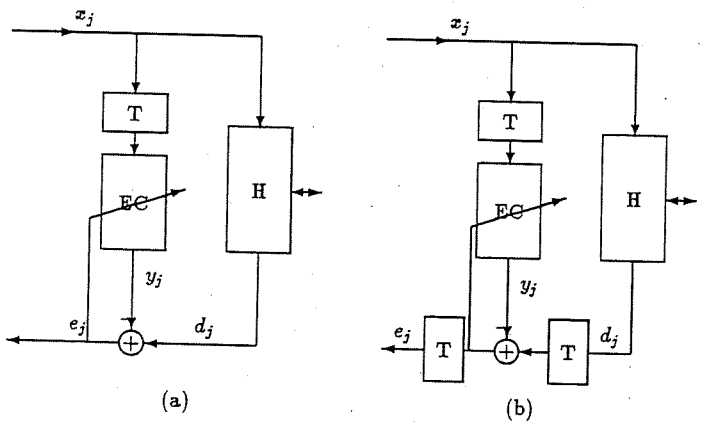


Figure 4.5: Transform-domain adaptive echo canceller. T – Transform.

One advantage of performing such a transform is that the step-size of the adaptation for each frequency component can be separately normalized according to the signal power in that frequency, resulting in better performance for the whole frequency bands. This advantage will become evident in following sections.

4.2.5 Design criteria for echo canceller

For the design of an adaptive echo canceller to operate in a certain environment, following main design factors should be considered:

Structure and algorithm
Subtraction configuration
Selection of number of bits

Selections of the structure and the algorithm

The first thing one has to do in the design of an echo canceller is the selection of the adaptive filter structure and the adaptation algorithm. In the selection, following main features should be kept in mind: stability, convergence rate, residual error in steady-state, computational complexity and the resulting circuit complexity.

We mentioned at the beginning of section 4.2 that an echo path can generally be modeled as an FIR filter, but it may be modeled as an IIR filter too. That is, both adaptive FIR filter and adaptive IIR filter may be applied. Because of the possible instability of the adaptive IIR filter, the preferential choice is the adaptive FIR filter. Due to potential advantage of the computational efficiency in modelling a noisy signal and a system with a recursive nature, however, the research on the adaptive IIR filter and its application to the echo canceller is becoming more active.

Lattice structure has the advantage of breaking down the transmitted signal into uncorrelated components before it enters the adaptive filter. It's worth using the lattice structure for the speech transmission since speech samples are correlated, although the correlation characteristics change rapidly with time. In a data transmission system, however it is not necessary to implement an echo canceller in the lattice structure due to the fact that the transmitted data are, in general, uncorrelated.

The RLS algorithm has the fastest convergence and lowest residual error in the steady-state. Fast RLS algorithm has the same performance as the RLS but with less computations. In situations where fast convergence speed is required by an echo canceller, for example, the echo path has characteristic of fast time-variations, these algorithms are good candidates if there are no problems with the circuit complexity and if the time interval between two successive samples is long enough to carry out the adaptations.

The convergence speed of the LMS algorithm is related to the statistical properties of the signals and to the step-size μ. In data transmission system, the signal is usually uncorrelated and the time variation of the echo path is slow, the LMS algorithm is a good candidate. When the LMS algorithm is utilized a compromised value of the step-size μ must be chosen. It happens very often that a large value of μ is chosen for a training period or for the half-duplex start-up time and a small value is chosen when the far-end signal is present, which will be shown later in this chapter. The LMS algorithm is usually chosen for the echo canceller in a speech transmission system because of its simplicity.

In applications where the simplicity of the computation outweights the importance of fast convergence and low steady-state error, the sign algorithm and the block algorithm may be used.

Table 4.1 shows two main features of several algorithms: the number of operations (multiplication and division) and the convergence speed. From this table we can see the increase of the computational complexity from the sign algorithm to the RLS algorithm. With the increase of the complexity the convergence speed of the algorithm increases too. Thus, an adequate choice should be based on the compromise between these two features.

Table 4.1: Comparison of algorithms

algorithm	*operation*	*convergence*
Sign	N	very slow
LMS	2N	slow
Gradient lattice	10N	fast
Fast RLS	10N	very fast
RLS	N^2	very fast

The complexity of an adaptive echo canceller circuit is related to the order N of the adaptive filter in use. This is dependent on the effective length of the echo path. As the value of N increases the algorithms with fast convergence become impractical or difficult for the implementation.

Subtraction configuration

The replica of the echo produced by the echo canceller is digital, while the incoming signal being analog. Thus, for the subtraction of the echo replica and echo-combined incoming signal, an A/D or a D/A conversion is required according to subtraction configurations: analog subtraction and digital subtraction.

In the case of analog signal subtraction, a D/A convertor is needed at the output of the adaptive filter to transfer the digital echo replica y_j into an analog one. This analog echo replica is then subtracted from the incoming analog signal d_j. At the output of the analog subtractor, an A/D convertor is located to generate a digital error signal required by the adaptation.

For the digital signal subtraction, the incoming signal d_j must be sampled and quantified before being input to the subtractor. the digital output of the adaptive filter y_j is directly subtracted from the converted digital incoming signal.

Selection of the number of bits

Another important factor should be considered in the design of the echo canceller is the word-length, i.e., the accuracy with which every variable is presented in the echo canceller. One of the main parameters influencing this accuracy is the A/D (or D/A) convertor. It must have sufficient bits to cover the dynamic range of the signals.

Another important factor is the number of bits used to represent the filter weights. It is associated with the performance of the echo canceller. The required word-length for the filter weights is given by the following

equation (Widrow 1987):

$$B = Log2(0.5 * \frac{\lambda_{max}}{\lambda_{min}} * \frac{1+\gamma}{\gamma} * N * ERL) \tag{4.9}$$

where, B is the number of bits required to represent the weights, $\lambda_{max}/\lambda_{min}$ is the eigenvalue spread of the auto-correlation matrix of the input signal x_j, γ is a safety factor to guarantee the convergence, N is the order of the filter (number of taps) and ERL is the echo return loss in dB, which is defined as the ratio of the returned echo after echo cancellation and the echo before the echo canceller.

The operation precision, especially on the multiplication, should also be taken into account. In some cases the multiplication does not affect the accuracy, for example, multiplication by +1 or -1 just means sign change. In speech echo cancellation, some unnecessary multiplications can be avoided by choosing the step-size μ as a power of 2. In this way the multiplication by μ is simply replaced by a shift, which saves time and avoids lowering the precision.

4.3 Acoustic Echo Cancellation

In the previous section the echo cancellation was discussed in general. In this section we concentrate on the acoustic echo cancellation for teleconferencing and hand-free telephone systems.

4.3.1 Introduction

In the teleconferencing and hand-free telephone systems, public loudspeaker and microphone are used as shown in figure 4.4. The microphone picks up not only the talker's speech signal s_j but also the echo n_j of the received far-end signal x_j, owing to the direct propagation of signal x_j from the loudspeaker to the microphone and the reflected waves by the wall, floor and other objects in the room. The acoustic echo resulting from this unwanted coupling between the loudspeaker and the microphone may be very annoying since the far-end talker will hear his own voice.

The acoustic echo is more difficult to control than that on the speech/data transmission system because of the following reasons:

1) The acoustic echo path can usually be characterized by its impulse response. The length of the impulse response equals the multiplication of the reverberation time and the sampling frequency. In general, a comparatively small conference room in which about ten participants can be gathered will have a reverberation time of about 0.3 – 0.4 second. Usually the sampling

frequency is chosen to be about 8 KHz for hand-free telephone system. For teleconferencing wider bandwidth is required to achieve broadcast quality transmission, the sampling frequency is often chosen to be about 16 KHz. The unwanted coupling between the loudspeaker and the microphone is stronger in the hand-free telephone system than in the teleconferencing system due to the fact that the distance between the loudspeaker and the microphone is shorter in the hand-free telephone device than in the teleconferencing room. Generally speaking, to achieve sufficient echo cancellation an acoustic echo canceller requires more than 750 taps for teleconferencing system and more than 1000 taps for hand-free telephone system.

Fig.4.6 shows an impulse response measured in a normal office with size of $3 \times 3 \times 2.7\ m^3$. The distance between the loudspeaker and the microphone is 30 cm and the sampling frequency is 8 KHz. a) shows the impulse response; b) shows the decay of energy in dB as a function of the number of taps. From this figure we can see that the echo path has long impulse response. To achieve an attenuation of 35 dB, 1500 taps must be implemented for the acoustic echo canceller. This proves that the acoustic echo canceller has very heavy computational burden.

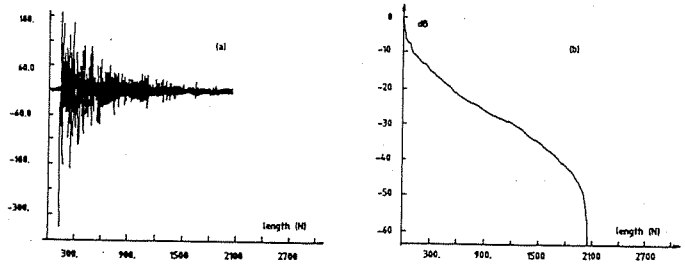


Figure 4.6: Impulse response. (a) Impulse response of an echo path measured in a normal office. (b) Decay of energy (dB) as a function of the number of taps.

2) The acoustic echo path is a nonstationary channel. The movement of the speaker or other object in the room modifies significantly the impulse response of the echo path. This possible fast time-varying character of the echo path requires that the convergence speed of the acoustic echo

canceller must be as fast as possible. However, adaptive algorithms with fast convergence are complicated in computations. For example, the fast RLS algorithm has operations with an order of $10N$. Since the number of the taps required for the acoustic echo canceller is extremely large, these fast algorithms become almost unapplicable.

3) Because of the heavy computational burden, the LMS algorithm is a good candidate for the acoustic echo canceller. However, as it is well known that the convergence rate of the LMS algorithm is related to the statistical property (eigenvalue spread) of the input signal which is the speech from a remote room or a far-end talker. The LMS algorithm is badly suited for the speech signal since the speech signal is nonstationary and has non-flat power spectrum.

In summary, some approaches to be applied for the acoustic echo canceller should have a convergence which is as fast as possible and have a computational burden which is as low as possible. This is, of course too idealized to solve. In practice we make more efforts on the reduction of the computational complexity while keeping the requirement of fast convergence in mind.

4.3.2 Approaches for AAEC

Unlike the adaptive echo cancellation for speech or data transmission systems, not many publications can be found on the design of the AAEC. Only few methods have been shown to be adequate (Horna 1982, Furuya 1985, Kellermann 1985, Gilloire 1987, Chen 1988a and 1988d). It should be mentioned that among the approaches to be described in the following only some have been really implemented or tested. Some of them are just our primitive ideas (Chen 1989f).

Full-band AAEC A direct way of realizing the AAEC is to use a transversal adaptive FIR filter to model the acoustic echo path as the line echo canceller does. For an acoustic echo path with the impulse response shown in Fig.4.6, a transversal adaptive FIR filter with 1500 taps can be applied as the AAEC to achieve 35 dB echo cancellation. For the implementation, several commercially available adaptive filters with length of hundreds for each can be cascaded to achieve the sufficient attenuation. If the number of taps required is around 1000, a single chip implementation is possible, applying certain techniques (Hsu 1986).

The advantage of this method is that no special effort has to be made for the design. Its main disadvantages are heavy computational burden and bad convergence performance for the whole band, which will be shown later.

FIR–IIR method Another possible way of designing an AAEC is to use a combination of the adaptive FIR filter and the adaptive IIR filter. The structure is illustrated in Fig.4.7. The adaptive FIR filter with length of N_1 is used to model the first N_1 taps of the impulse response of the echo path and the adaptive IIR filter is used to model the weak tail of the impulse response. Since the IIR filter has a longer impulse response than the FIR filter for any fixed number of coefficients. The total taps of the FIR and IIR filters together may be less than that by applying the full-band method.

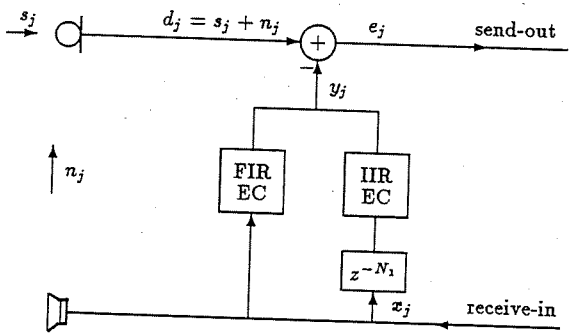


Figure 4.7: FIR–IIR implementation of an AAEC. N_1 – tap number of the adaptive FIR echo canceller.

In (Fuch 1988) the above method was simulated with different values of N_1 and different orders of the adaptive IIR filter. The results show that the value of N_1 is rather sensitive to the performance of the AAEC and the adequate value is unknown. It's likely that the adaptive IIR filter may only model the tail (with limited taps) of the impulse response of the echo path.

Our conclusion is that the FIR–IIR method has attractive feature of possibly saving the computations but more efforts still have to be made to investigate the performance of this method.

Pole-zero method The pole-zero adaptive echo canceller proposed in (Giltin 1976) is shown in Fig.4.8. It accounts for poles as well as zeroes in the echo path. The transfer function of the echo canceller can be written as:

$$H(z) = \frac{A(z)}{1 - B(z)} \tag{4.10}$$

where A(z) is the zero filter

$$A(z) = a_0 + a_1 z^{-1} + \cdots + a_p z^{-p} \tag{4.11}$$

and $1 - B(z)$ is the pole filter

$$1 - B(z) = 1 - b_1 z^{-1} - \cdots - b_q z^{q} \tag{4.12}$$

These two filters are adapted to minimize the equation error e'_j (Ljung 1983) using the LMS adaptation algorithm:

$$A_{j+1} = A_j + 2\mu_a e'_j X_j \tag{4.13}$$

$$B_{j+1} = B_j + 2\mu_b e'_j D_j \tag{4.14}$$

where,

$$X_j^T = [x_j, x_{j-1}, \cdots, x_{j-p}] \tag{4.15}$$

$$D_j^T = [d_j, d_{j-1}, \cdots, d_{j-q}] \tag{4.16}$$

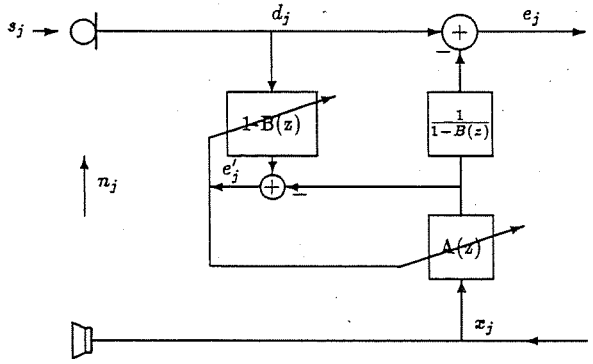


Figure 4.8: Adaptive pole-zero echo canceller

The basic idea of this method is to replace the problem of directly minimizing the echo by the problem of identifying the model parameters of echo path.

The residual error e_j and the equation error e'_j are correlated by the following z-transform:

$$E(z) = \frac{E'(z)}{1 - B(z)} \tag{4.17}$$

If the identification is accurate enough that e'_j is zero, the residual error e_j, in the absence of the near-end speech and noise, is also zero.

Simulations with different echo path models were conducted in (Long 1987). Unfortunately, in the room acoustic application it was found that the required order of the adaptive pole-zero echo canceller may be so large that no computational saving can be achieved over the transversal full-band echo canceller.

Subband method the most attractive method for the acoustic echo canceller, in our opinion, is the subband method (Kellermann 1983, Gilloire 1987, Chen 1988a). It is illustrated in Fig.4.9, where FB(A)/FB(S) is the analysis/synthesis filter bank and AFB is the adaptive filters implemented in subbands. Two analysis filter banks divide the incoming signals d_j and x_j into several subbands. In each subband, a complex adaptive filter is applied, operating in the same way as the conventional adaptive filter but at decimated rate. The residual error signal is fed into a synthesis filter bank and then transmitted. The detailed discussion on this method is the subject of the following sections.

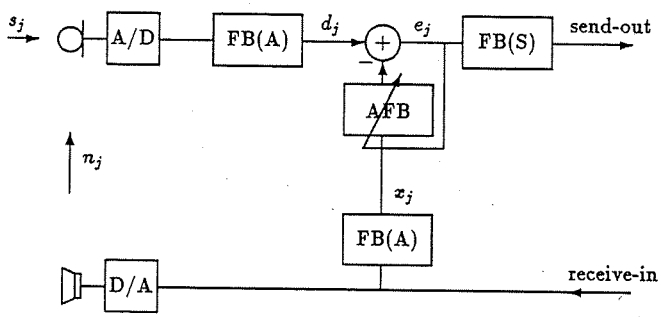


Figure 4.9: Conventional structure of the subband AAEC. FB(A) – analysis filter bank, FB(S) – synthesis filter bank, AFB – adaptive filter bank in subbands.

4.3.3 Subband acoustic echo canceller

The basic idea behind the subband method is to divide the signal into several subbands and then to apply an adaptive filter in each subband,

operating at a decimated rate.

Decimation and Interpolation

In order to explain the basic principle of the analysis/synthesis filter banks used in the subband AAEC, we present an example to show how a signal is divided into 2 frequency subbands, decimated, interpolated after adaptive filtering and finally reconstructed.

Fig.4.10 shows a conventional 2 subband quadrature mirror filter (QMF) analysis/synthesis scheme. A signal x_j sampled at frequency f_s ($f_s = \frac{1}{\tau} = \frac{\omega_s}{2\pi}$) is going to be split into two half band channels with cutoff frequency of $f_s/4$ (see Fig.4.10a). The lower half-band channel is derived by lowpass filtering the input signal x_j with a lowpass FIR filter H with impulse response h_j and z-transform $H(z)$. The higher half-band channel is derived by an FIR high-pass filter $H(-z)$ with impulse response $(-1)^j h_j$. Two sub-sampled channels ${}^1x_j$ and ${}^2x_j$ with z-transform ${}^1X(z)$ and ${}^2X(z)$ are derived from x_j lowpass and high-pass filtering followed by a decimation with a factor of 2. Hence their z-transform may be expressed by

$$ {}^1X(z) = \frac{1}{2}[H(z^{1/2})X(z^{1/2}) + H(-z^{1/2})X(-z^{1/2})] \qquad (4.18) $$

$$ {}^2X(z) = \frac{1}{2}[H(-z^{1/2})X(z^{1/2}) + H(z^{1/2})X(-z^{1/2})] \qquad (4.19) $$

where $X(z)$ is the z-transform of the signal x_j.

After the intermediate processing, adaptive filtering for our purpose, these two channel signals have to be reconstructed. It's done as in Fig.4.10b, first by interpolating with a factor of 2 (inserting one zero-valued sample between each sample of the channel signals), then by filtering at the rate f_s with the same lowpass or high-pass filter as the one before the decimation and finally by summing the resulting two channel signals. The reconstructed signal is denoted $\tilde{x}_j$ and its z-transform $\tilde{X}(z)$ defined by

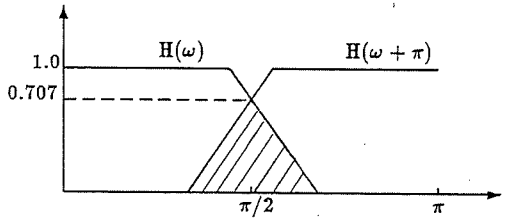
$$ \begin{aligned} \tilde{X}(z) &= \tfrac{1}{2}[H(z)X(z) + H(-z)X(-z)]H(z) \\ &\quad -\tfrac{1}{2}[H(-z)X(z) + H(z)X(-z)]H(-z) \end{aligned} \qquad (4.20) $$

$$ \tilde{X}(z) = \frac{1}{2}X(z)[H^2(z) - H^2(-z)] \qquad (4.21) $$

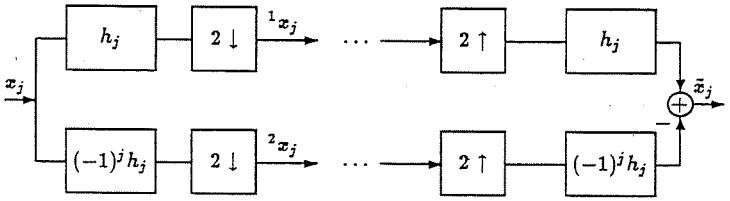
It may be noted that by subtracting second channel from the first one instead of addition, the aliasing terms corresponding to $X(-z)$ are cancelled. Thus the only condition which should be met to achieve perfect reconstruction is that of having a flat frequency response.

Now rewrite Eq(4.21) as (on the unit circle):

$$ \tilde{X}(e^{i\omega T}) = \frac{1}{2}X(e^{i\omega T})[H^2(e^{i\omega T}) - H^2(e^{i(\omega+\omega_s/2)T})] \qquad (4.22) $$



a) Half-band spliting



b) Decimation and interpolation

Figure 4.10: 2-subband QMF analysis/synthesis scheme

Assume H is a symmetrical N-tap FIR filter and its Fourier transform is defined by

$$H(e^{i\omega T}) = H(\omega)e^{-i(N-1)\pi(\omega/\omega_s)} \tag{4.23}$$

Substituting Eq(4.23) into (4.22) yields

$$\tilde{X}(e^{i\omega T}) = \frac{1}{2}X(e^{i\omega T})e^{-i2\pi(N-1)(\omega/\omega_s)}[H^2(\omega) - H^2(\omega + \frac{\omega_s}{2})e^{-i(N-1)\pi}] \tag{4.24}$$

If N is even the above equation becomes

$$\tilde{X}(e^{i\omega T}) = \frac{1}{2}X(e^{i\omega T})e^{-i2\pi(N-1)(\omega/\omega_s)}[H^2(\omega) + H^2(\omega + \frac{\omega_s}{2})] \tag{4.25}$$

Eq(4.25) states that the signal $\tilde{x}_j$ is a perfect replica of the signal x_j delayed by $N-1$ samples and multiplied by $1/2$ if the following condition

is met:

$$H^2(\omega) + H^2(\omega + \frac{\omega_s}{2}) = 1 \tag{4.26}$$

With the above example we have explained the basic principle of the analysis/synthesis filter banks. The detailed discussions on K-subband analysis/synthesis methods are too much involved. Two common approaches are QMF and DFT structures which can be found in (Galand 1984, Millar 1985, Bellanger 1976, Vary 1983 and Crochiere 1983).

Advantage of subband acoustic echo canceller

Now let's go back to the subband acoustic echo canceller again (see Fig.4.9). Assume the impulse response of the echo path has effective length of N taps. the signals are divided into K subbands and the critical sampling rate is applied, that is, the signals are decimated with a factor of $M = K$. Thus, K adaptive filters with length of N/M each are required to operate at the decimated sampling frequency of f_s/M. This leads to the total multiplications required by the subband acoustic echo canceller:

$$O_{sub} = K(2\frac{N}{M}\frac{1}{K}) + O_{FB} = \frac{2N}{K} + O_{FB} \tag{4.27}$$

where O_{FB} is the operations required by the filter banks.

Comparing Eq(4.27) with the multiplications required by the full-band acoustic echo canceller, $O_{full} = 2N$, we can see that as the number of the subbands K and the number of the taps N increase, more and more computational reduction may be achieved. In section 4.4 we will discuss this in detail and will see the computational efficiency of the subband method.

Another important advantage of the subband structure is its better performance than the full-band method. In the subband acoustic echo canceller, the adaptive filtering is performed in subbands. Thus the step-size of the adaptation in a particular subband can be optimized according the statistical property of the signal within that frequency band, resulting in better convergence in the whole frequency range. A simulation result showing this advantage will be presented.

We have mentioned before that the acoustic echo path has a long impulse response and the input signals are speech having non-flat power spectra, the convergence of the full-band AAEC with LMS algorithm may be very slow. By applying the subband structure we may observe that the signal in each subband has a flat or nearly flat power spectrum if the number of the subbands is large, i.e.,

$$\lim_{k\to\infty} \frac{\lambda_{max}}{\lambda_{min}} = 1 \tag{4.28}$$

Thus the subband AAEC will result in faster convergence than the full-band method.

Problems

The existing problem of the filter bank structure shown in Fig.4.9 is the delay introduced in the transmission line because the FB(A) and FB(S) are inserted in the line. The prototype filter used in the filter bank either with the QMF structure or with DFT structure is usually an FIR filter because of the requirement of linear phase character. The FIR filter with a order of L generates a delay of $L/2$ samples. Thus, generally speaking, the total delay in samples introduced in the line equals the order of the FIR filter (or the number of its taps). If more substantial computational reduction is desired, the signals must be divided into more subbands, i.e., the bandwidth of each subband should be narrower and the prototype FIR filter requires higher order. Accordingly, more delay in the transmission line is produced. In real applications this additional delay should be avoided. A new structure is proposed in the next section to avoid the problem (Chen 1988a).

Another problem with the subband AAEC, in the case where the critical decimation is applied, is the aliasing. It was shown in (Gilloire 1987) that the echo canceller seems to be ineffective at the boundary frequencies of two adjacent subbands if the critical decimation is utilized. In (Gilloire 1988) an interesting method was proposed, where additional adaptive filters operating in a cross-bands manner are introduced. In the design of the subband AAEC we apply oversampling method to avoid the aliasing problem, which will be shown in section 4.4 (Chen 1988d).

4.3.4 No-delay structure

A new structure (Chen 1988a) without introducing any delay in the transmission line is proposed and illustrated in Fig.4.11. Comparing this new structure with the conventional one in Fig.4.9 one can find two differences. First, the analysis and the synthesis filter banks in the transmission line are removed and second, an additional adaptive filter (called compensating adaptive filter) denoted as AF' is introduced. The compensating adaptive filter operates in the full-band at the original sampling frequency f_s. It produces the replica of the acoustic echo together with the adaptive filters in the subbands.

In order to explain the behavior of the new structure subband AAEC, we assume that the filter banks are just delay units which do not perform any filtering action but only a shift of $L/2$ samples. Then we can observe at the summation point in Fig.4.11 that y_j arrives L samples later than the echo

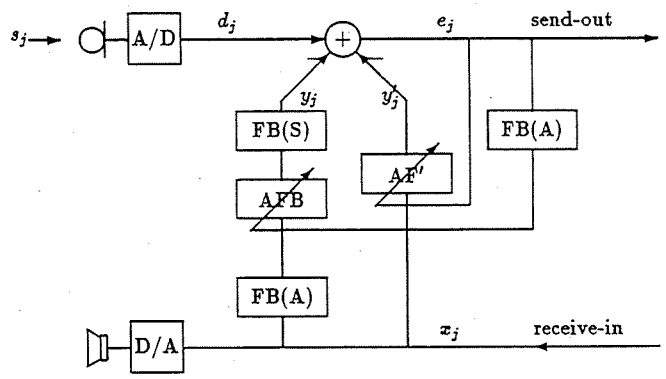


Figure 4.11: No-delay subband AAEC. AF' – compensating afaptive filter.

itself n_j. (It should be pointed out that in the conventional subband structure shown in Fig.4.9, they arrive simultaneously since both are delayed with the same number of samples.) This delay may result in instability of the subband AAEC. Thus the additional adaptive filter is introduced to compensate that delay. It is clear that the required number of taps of the compensating adaptive filter should be equal to the total delay generated by the analysis and the synthesis filter banks, L.

For the adaptive filters in the subbands of the new structure, one may have found a severe problem: the residual error signal e_j used to control the adaptation of the filter weights is also delayed, which will cause the divergence of the conventional LMS algorithm. Therefore the LMS algorithm should be modified to cope with the delay.

For each adaptive filter operating in the subband, the adaptation of the filter weights is modified as follows (Chen 1988a):

$$W_{k,j+1} = W_{k,j} + 2\mu e_{j-L/2} x_{j-L/2-k+1-L/2} \quad k = 1, 2, \cdots N \tag{4.29}$$

where,

$$e_j = s_j + n_j - y_j - y'_j \tag{4.30}$$

N is the number of taps of the adaptive filters in the subbands and $L/2$ is the delay produced by the analysis/synthesis filter bank.

Eq(4.29) states that for the adaptation of the filter weights, since the error signal is delayed in $L/2$ samples before being used for the adaptation,

the input signal to the adaptive filter, $x_{j-L/2}$ should first be delayed in the same number of samples. Simulations have shown that the convergence of the new structure AAEC using the modified LMS algorithm (4.29) is guaranteed under the same condition as the LMS algorithm.

4.3.5 Simulation with the no-delay structure

We know that the difference between the proposed no-delay structure and the conventional structure lies in the different arrangement of the filter banks. Thus, to investigate the performance of the new subband AAEC, simulations are conducted by simply considering the filter banks as delay units (Chen 1988a)

The receive-in signal x_j used in the simulations is an averaged speech signal with high energy around 500 Hz. The near-end signal s_j is assumed to be absent. The impulse response of the echo path is measured in a small office with size of $3 \times 3 \times 2.7m^3$, only the first 100 samples are used for the simulations. The analysis/synthesis filter banks function as a delay unit of 16 samples. Thus 32 taps are used for the compensating adaptive filter. Adaptive filters in subbands, AFB, is composed of a single adaptive filter with 68 taps. Its weights are adjusted according to Eq(4.29).

Fig.4.12 shows the mean square value of e_j over 100 independent runs versus the adaptation number. From this figure we observe that the algorithm converges after 600 adaptations. The echo cancellation is shown in Fig.4.13, where the upper curve presents the power spectrum of the echo , the lower one, the echo cancellation output. From the figure more than 30 dB echo cancellation is observed at the dominant frequencies. It is also observed that the echo canceller does not converge well for the whole frequency range. This is because full-band instead of subband is applied in the simulations.

The simulation results in Fig.4.12 and Fig.4.13 show that the no-delay structure and the corresponding modified LMS algorithm is convergent and adequate for the acoustic echo cancellation.

In conclusion, the proposed new structure has the same performance as the conventional one, while having the advantage of no delay in the transmission line. Its disadvantage is that a compensating adaptive filter is required and therefore extra computations are involved.

This new structure has been successfully applied in the design of an acoustic echo canceller for hand-free telephone systems. It will be described in the following section.

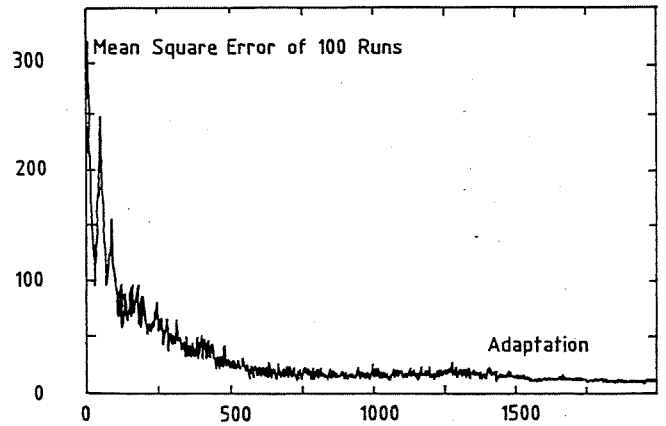


Figure 4.12: Convergence of the no-delay AAEC. MSE over 100 runs vs. adaptations.

4.4 Design of A No-delay Subband AAEC

In this section we give an example of how to design an acoustic echo canceller using the no-delay subband structure. The general structure of the proposed AAEC and the adaptation algorithm for the adaptive filters will be found in section 4.4.1. In section 4.4.2 we present the computational efficiency of the no-delay subband structure. Design considerations and simulation results are presented in section 4.4.3 and section 4.4.4, respectively.

4.4.1 General structure of the AAEC

The overall structure of the echo canceller is based on the no-delay subband method (see Fig.4.11) and the filter banks are implemented with a simplified weighted overlap-add method (Crochiere 1983). The main structure is shown in Fig.4.14 (Chen 1988d).

During the decimation period, M samples of the input signal are shifted into the input shift register with length of K. Its contents are multiplied by the analysis window and then an odd-FFT is performed on these weighted data, producing $K/2$ non-redundant outputs. These $K/2$ output are fed into AFB which contains $K/2$ complex adaptive filters. In a similar way

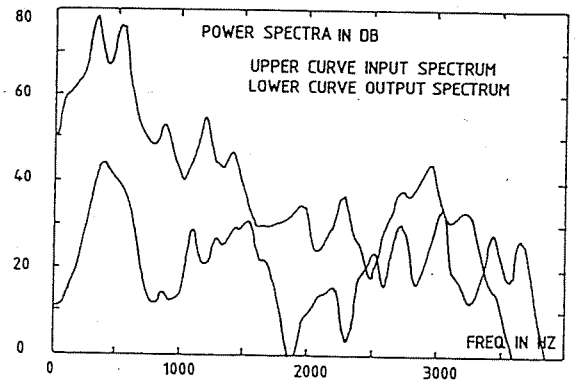


Figure 4.13: ECho cancellation output with the new structure. Upper line: power spectrum of the echo; Lower line: power spectrum of the echo-cancelled output.

the error signal is processed and then used to control the adaptation of the complex adaptive filters. The synthesizer performs reversely. The outputs of the AFB (adaptive filters in subbands) are fed into inverse odd-FFT processor and the results are weighted again by the same window. These weighted values are added to the running sum stored in the output shift register. During each decimated sample period M values are available at the output shift register at the original sampling rate. These values together with the output of the compensating adaptive filter are subtracted from the signal d_j to produce an echo-free error signal to be transmitted.

The main features of the AAEC are described as follows (Chen 1988d):

1. The odd-FFT allows to use a complex FFT of size $K/2$ to calculate a real FFT of size K at the cost of a complex modulation of the input signal (Vernet 1971). In Fig.4.14 this is emphasized by mentioning at the output of the FFT (IFFT) , "complex $K/2$".

2. To avoid aliasing problems in both time and frequency domains with the simplified weighted overlap-add method, oversampling is applied with $M = K/4$ (Crochiere 1983).

3. The synthesis filter (window) is the same as the analysis filter. It is

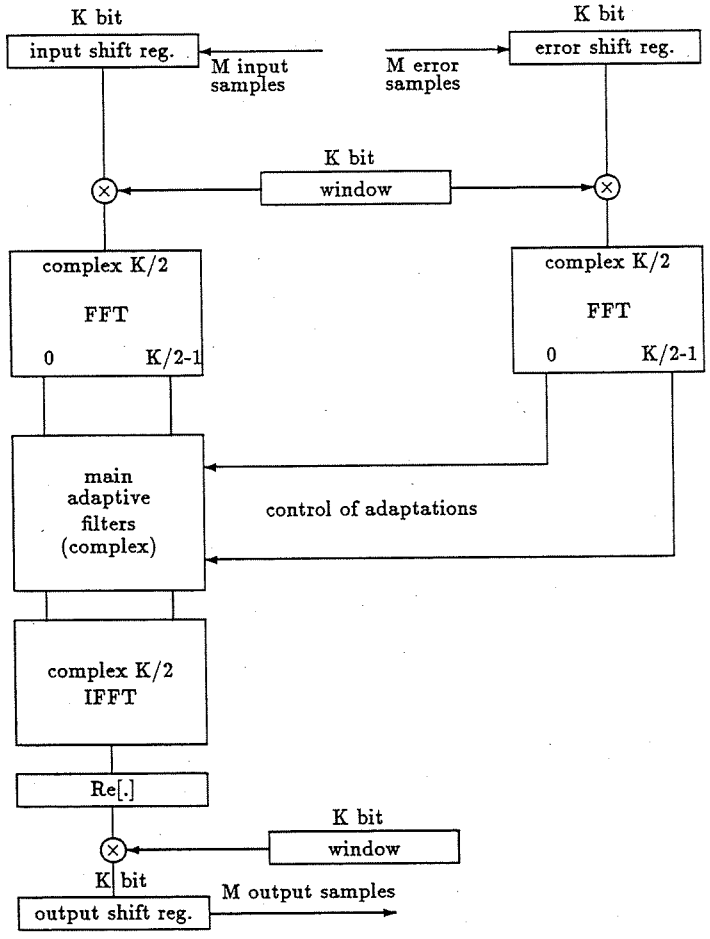


Figure 4.14: General structure of an no-delay subband AAEC. Window – prototype lowpass filter. Re[.] – real part of a complex value.

a lowpass filter with cutoff frequency of f_s/K. Fig.4.15 shows the frequency response of the analysis (synthesis) filter with $K = 128$.

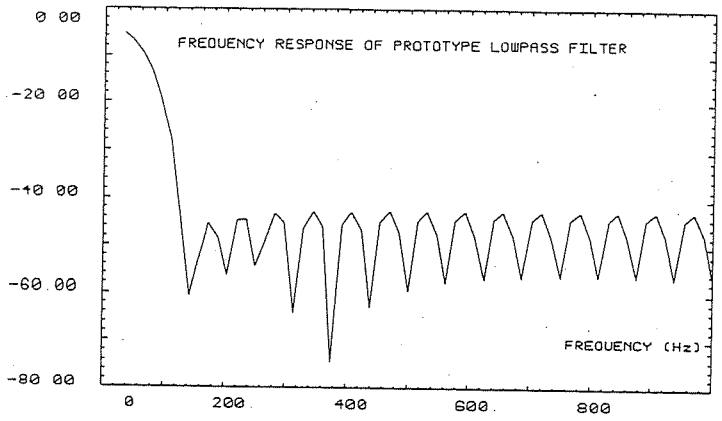


Figure 4.15: Frequency response of the prototype lowpass filter

4. The compensating adaptive filter is not depicted in Fig.4.14. It is a conventional LMS adaptive filter operating at the original sampling rate. The number N' of taps required is equal to the delay produced by block processing of the filter banks. The FFT processing generates K sample delay. There exists a delay of M samples in summing the output of the subbands and the output of the compensating adaptive filter. Thus the total delay is $K + M$.

Since the outputs of the FFT processor are complex, the complex adaptive filters are applied in the subbands. The time for a complex multiplication, taking I/O transfer into account, requires only twice the execution time of a real multiplication. These complex adaptive filters are operating at the decimated sampling time m and the used algorithm is a modified complex LMS algorithm:

$$W_{m+1} = W_m + 2\mu e_m \bar{\mathbf{X}}_{m-\delta} \tag{4.31}$$

where W_m is the complex weight vector of the adaptive filter at the decimated time m. e_m is the complex output of the error signal processed

by FFT, $\mathbf{X}_m$ is the complex input vector to the adaptive filter, $\bar{\mathbf{X}}_m$ is the complex conjugate of $\mathbf{X}_m$. δ is the delay equal to $(K + M)/M$. μ is normalized step-size.

$$\mathbf{X}_m^T = [X_m, X_{m-1}, ..., X_{m-N}] \tag{4.32}$$

where N is the number of taps required by the complex adaptive filter. It is calculated as follows:

$$N = (TAPS - N')/M \tag{4.33}$$

where $TAPS$ is the total number of taps required to achieve sufficient echo cancellation, N' is the number of taps of the compensating adaptive filter.

4.4.2 Optimal number of subbands

The number of subbands can be selected to reduce the overall number of multiplications per sample period. Since the subband adaptive filters operate at the decimated sampling frequency and the decimation factor M is equal to $K/4$, the multiplication required by the subband adaptive filters is inversely proportional to K. However, as the number of subbands increases, the delay introduced by the filter banks is getting larger, requiring a larger size (more taps) of the compensating adaptive filter, the FFT requires more calculations too. This means that an optimal value of K exists with respect to the number of multiplications per sample period for the no-delay subband acoustic echo cancellation (Chen 1988d).

If the total number of taps required is $TAPS$, the operation involved in a full band AAEC, O_{full}, is equal to

$$O_{full} = 2 \times TAPS \tag{4.34}$$

The operation O_{sub} involved in the no-delay subband AAEC contains mainly three parts:

- Multiplications required by the compensating adaptive filter O_c

$$O_c = 2 \times N' = 2(K + M) \tag{4.35}$$

- Multiplications required by the subband adaptive filters O_{AFB}, which are performed in the complex mode and at the decimated sampling rate. As we mentioned before that taking the I/O transfer into account, a complex multiplication is counted as 2 real ones. Thus,

$$O_{ABF} = \frac{1}{M}[\frac{K}{2} \times \frac{TAPS - N'}{M} \times 2 \times 2] \tag{4.36}$$

- Multiplications required by three FFT (or IFFT) processors, O_{fft}, which are also performed in the complex mode and at the decimated sampling rate.

$$O_{fft} = \frac{1}{M}[\frac{K}{2} \times \log_2(\frac{K}{2}) \times 2] \times 3 = 12 \times \log_2(\frac{K}{2}) \qquad (4.37)$$

where $\frac{K}{2}\log_2(\frac{K}{2})$ is the complex multiplication required by one FFT processor with $K/2$ complex inputs.

Noting that $M = K/4$, the total operations required by the no-delay subband AAEC can then be expressed as a function of the number of subbands K and the number of the total taps $TAPS$ as follows:

$$O_{sub} = O_c + O_{AFB} + O_{fft} = 2.5K + 12\log_2(\frac{K}{2}) + \frac{32 \times TAPS}{K} - 40 \qquad (4.38)$$

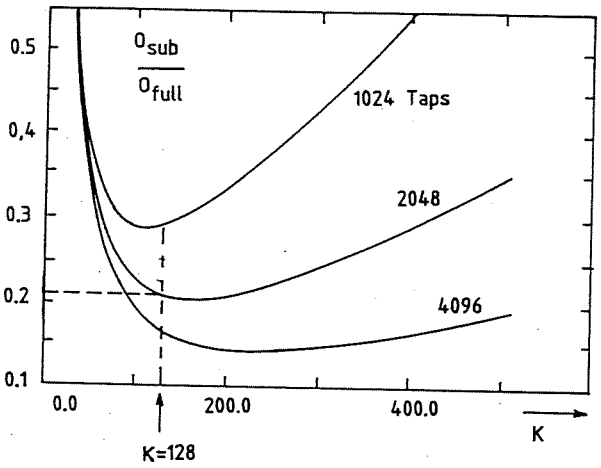


Figure 4.16: Computational reduction of the proposed AAEC. 1024, 2048 and 4096 stand for numbers of taps.

The ratio of the number of real multiplications for the proposed AAEC and the conventional full-band AAEC O_{sub}/O_{full} as a function of K is shown in Fig.4.16. The computational reduction of the proposed method over the conventional method can be clearly observed from this figure. It

can be seen that the optimal value of the number of the subbands K as well as the maximum reduction in computations depends on the length of the echo canceller, $TAPS$. For the length of 2048 taps the optimal value of K is near 128 and the computational saving factor is about 5. In this case 37% of the total number of the operations in the no-delay subband AAEC is required by the compensating adaptive filter ($O_{AFB} = 37\%O_{sub}$), which is only responsible for 8% of the total length of the AAEC; 56% for the subband adaptive filters and 7% for the filter banks.

4.4.3 Design consideration

The goal is to design an acoustic echo canceller for hand-free telephone systems with 2048 taps at 8 KHz sampling frequency, achieving an average ERLE of 30 dB using logarithmic A/D conversion (Chen 1988d).

The ERLE is the echo return loss enhancement defined as the ratio of the echo-combined incoming signal and the residual error signal (see Fig.4.11):

$$ERLE = 10\log\frac{E[d_j^2]}{E[e_j^2]} \qquad (4.39)$$

The compensating adaptive filter uses the conventional LMS algorithm and has a length of 160 taps. It can be realized by means of a single commercial component. For the subband adaptive filters, a custom IC can be developed, which should contain the modified LMS algorithm for the subband adaptive filters and the filter banks.

Since several issues have already been discussed in previous sections, here only the finite wordlength effect and the requirement of the RAM size will be discussed.

Required wordlength of filter weights

The required worldlength of the weights for an adaptive filter is given in Eq(4.9) and repeated here:

$$B = LOG2(1/2 * \lambda_{max}/\lambda_{min} * (1+\gamma)/\gamma * N * ERL) \qquad (4.40)$$

With B : number of bits, $\lambda_{max}/\lambda_{min}$: eigenvalue spread of input signal, γ : safety factor to guarantee convergence, N : number of taps and ERL : echo return loss.

Implementing 2048 taps using conventional LMS algorithm would require about 24 bits for the filter weights in order to get an echo return loss enhancement (ERLE) of 30 dB, using *speech* as an input signal. By making use of subbands the length of each filter is reduced by the decimation factor M and the ratio $\lambda_{max}/\lambda_{min}$ is approaching one when a large

number of subbands is used . According to the above equation the required wordlength of the filter weights is 14 bits for 2048 taps and $K = 128$, which means a saving of 9 bits when compared to the conventional LMS algorithm.

Required RAM size

Because the decimated sampling frequency used in the subbands is 4 times the critical sampling frequency (original sampling frequency divided by K) the RAM-space to store all data and filter weights of the subband adaptive filters, is increased with a factor of 4. For this reason all data and filter weights of the subbands are stored in an external 8 bit wide RAM, while a duplicated cache memory is provided in the custom chip. When a subband needs to be processed all required data and weights are downloaded into one of the cache memories by means of an I/O processor and uploaded again after processing.

In order to reduce the number of I/O cycles all data and weights are stored as floating point numbers.

4.4.4 Simulation results

The performance of the designed no-delay subband AAEC has been investigated by both off-line computer simulations and real-time simulations with DSP processors (TMS32020). The simulation results are shown in this section on the convergence speed of the designed AAEC, the echo cancellation performance in comparison with the conventional full-band AAEC and the influence of the time variations of the acoustic echo path (Chen 1989f).

Computer simulation

First the designed system is programed and simulated in VAX computer, using finite wordlength representations of the filter weights and data in floating point. Data are represented by 11 bits with 7 bits for signed mantissa and 4 bits for exponents; Filter weights are also represented by 11 bits, but with 8 bits for the signed mantissa and 3 bits for the exponent. The total taps of the echo canceller is $TAPS = 2048$, the number of subbands $K = 128$ and the decimation factor $M = 32$.

The input signal to the loudspeaker is a simulated speech which results from white noise filtered by the CCITT recommended filter (G.227). Its level is -10 dB. The impulse response of the acoustic echo path is real measurement. The near-end speech is not presented.

The convergence rate of the designed AAEC is shown in Fig.4.17, where the vertical axis is the mean square error and the horizontal one is the adaptation number. From this figure we see that the convergence speed is rather slow. It takes about 16000 adaptations (or 2 seconds) for the AAEC

to converge. This is because of the long (2048 taps) impulse response of the echo path.

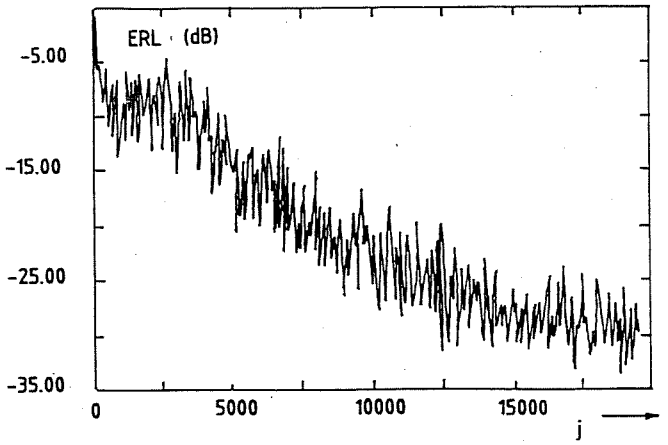


Figure 4.17: Convergence of the subband AAEC (echo return loss versus adaptations).

Fig.4.18 shows the power spectra of the incoming signal d_j before and after the echo removal. It can be seen that the echo is cancelled over the complete frequency spectrum. The condition of this simulation is the same as the previous one but the input signal to the loudspeaker is a real speech instead of the simulated one. In order to compare its performance with the conventional full-band AAEC, we present in Fig.4.19 the echo cancellation performance of the full-band AAEC under the same simulation conditions. From Fig.4.19 one can observe that the echo is removed only at the dominant frequencies around 500 Hz. The better performance of the proposed no-delay subband AAEC is evident.

Based on computer simulations, following conclusions are drawn:

1. The performance of the no-delay subband AAEC is better than that of the full-band AAEC.

2. There exists no aliasing problems.

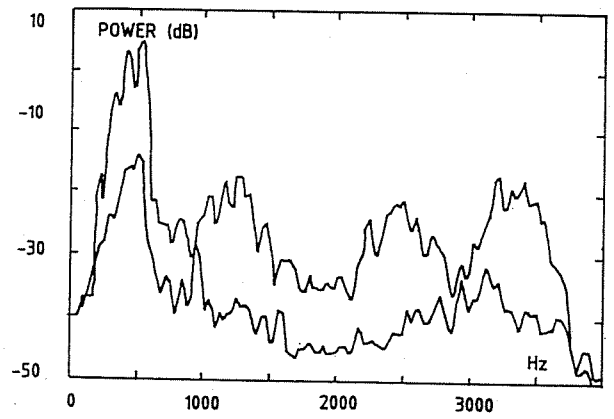


Figure 4.18: Echo cancellation performance of the proposed subband AAEC

3. The LMS adaptive filter, operating in a certain frequency band, always converges to the dominant frequencies in that band. The filter banks divide the input signal into different frequency subbands, and complete convergence at every frequency component in the whole band is obtained when the number of subbands gets infinity. However, it's found that if the input signal is white noise or has a flat spectrum, the full-band AAEC generates the same performance as the proposed new method.

4. Another advantage of the proposed method is that the the frequency components of the echo in different subbands have different power and thus different numbers of taps can be used for different adaptive filters. That is, if the statistical property of the input signal in power spectrum is known in advance, more taps can be applied to the adaptive filters in subbands where the echo has high level and less taps to the adaptive filters in other subbands. In this way better echo cancellation performance or more reduction in computations can be achieved.

5. Comparing with the subband method with critical sampling we attain less computational reduction because of the oversampling with a factor of 4.

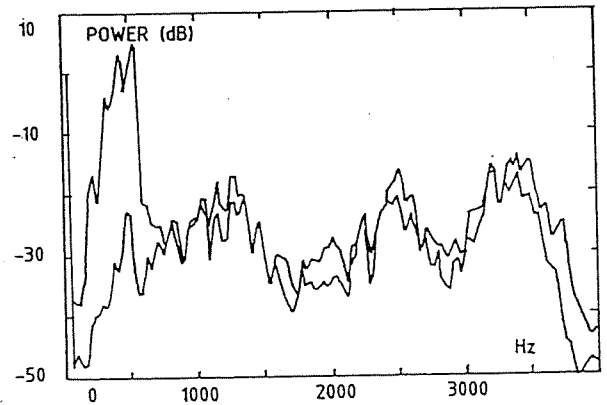


Figure 4.19: Echo cancellation performance of full-band AAEC

It should be pointed out that more reduction in computations can be achieved without severely affecting the echo cancellation performance of the proposed method. One example is the following: The proposed AAEC was once simulated by ignoring one out of two adjacent subband adaptive filters, and it performed well but with several dB degradation in the echo cancellation. An extra computational reduction with a factor of about 2 was, however obtained.

Real time simulation

The no-delay subband acoustic echo canceller has also been simulated in a multi-processor system (TMS32020). The simulation conditions are: $K = 128$ $M = 32$; Only limited bandwidth (half band) of the signal is used (200-2000Hz) in order to reduce the number of the adaptive filters in subbands. The microphone and the loudspeaker are installed in a normal-size office with a distance of 30 cm. The input signal is white noise. The compensating adaptive filter contains 192 taps and each subband adaptive filter has 24 taps. That is, the total taps $TAPS$ equals 960. Data and filter weights are represented by 15 bits.

Fig.4.20 shows the ERLE versus the adaptation with input signal level of -10 dB. From the figure we see that more than 30 dB ERLE is achieved. The AAEC converges after about 2 second adaptations.

Fig.4.21 and 4.22 show the effects of the time variations of the acoustic

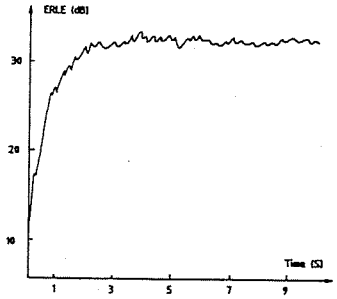


Figure 4.20: ERLE vs. adaptations in real-time simulation

echo path on the AAEC performance. It has been shown that the no-delay subband AAEC is stable in the nonstationary environments.

Fig.4.21 presents the influence of opening/closing the door. The whole process of opening/closing the door takes about 2 seconds. The degradation of the echo cancellation performance can be observed in this figure. However when the acoustic echo path is time-varying, the AAEC can still achieve more than 12 dB ERLE.

Fig.4.22 shows the influence of some one walking in front of the microphone and the loudspeaker. The performance of the AAEC is degraded, while still being stable.

The AAEC has also been simulated in real-time with a real speech as the input signal. Similar effects of the time variations of the acoustic echo path were observed.

In summary, the performance of the proposed AAEC in nonstationary environments is investigated by real-time simulations. It is found that while the acoustic echo path is time-varying, its impulse response has significant changes. The proposed AAEC is always stable in the nonstationary environments but its performance is degraded. This is because the convergence speed of the AAEC is not fast enough to follow the changes of the acoustic echo path.

A custom chip for the proposed no-delay AAEC has been designed. A detailed discussion can be found in (Chen 1988d).

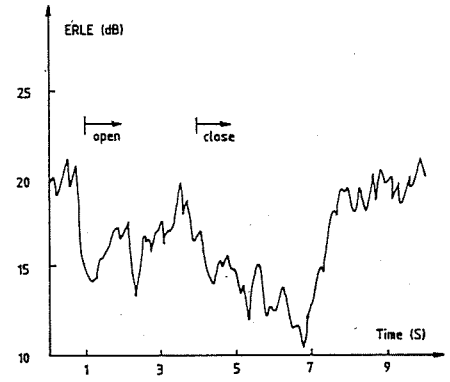


Figure 4.21: The influence of open/close the door

4.4.5 Summary of the no-delay subband AAEC

The design of the no-delay subband acoustic echo canceller is presented in this section. A new subband structure which introduces no delay in the transmission line is applied. The analysis and synthesis filter banks are realized, applying a simplified weighted overlap-add method and oversampling rate is applied in order to avoid aliasing problems. Complex adaptive filters with modified complex LMS algorithm are utilized in the subbands. the design considerations is discussed. External RAM is used because of the large amount of data and filter weights resulting from the oversampling with a factor of 4.

The proposed AAEC with $TAPS = 2048$ can be realized in a single custom chip plus two commercial devices, one for the compensating adaptive filter and the other for the external RAM (Chen 1988d).

The designed AAEC has been simulated both off-line on computers and real-time in a multi-processor system. The results show that the designed AAEC has advantages of sufficient ERL, echo cancellation in the whole frequency range, no aliasing problems and computational efficiency compared with the full-band method.

Real-time simulations show that the designed AAEC is stable in nonstationary environments. As expected, when the echo path is time-varying, the performance is degraded. This is because the AAEC involves a large

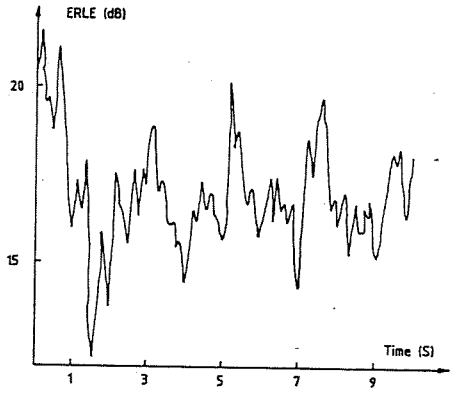


Figure 4.22: The influence of some one walking

number of taps and its convergence is not fast enough to track the statistical changes of the echo path.

It is also mentioned that a compromise can be made between better performance of the designed AAEC and higher computational reduction. That is, some simplifications may be made in practice.

4.5 Nonlinear Echo Cancellation

In the preceding sections of this chapter we discussed the echo cancellation on line telephone and the acoustic echo cancellation in teleconferencing and hand-free telephone systems, where the echo path is assumed to be linear. In practice, some nonlinear effects are involved in the echo path, such as the nonlinearity resulting from the A/D or D/A conversion.

In telephone lines and in teleconferencing systems, the level of the echo is usually lower than the interesting signal, thus the required echo return loss enhancement (ERLE) of the echo canceller is not higher than 50 dB. In two-wire full duplex data transmission systems, however, the level of the echo signal may be 30 to 40 dB higher than that of the interesting signal. Therefore if an SNR of 20 dB after the echo cancellation is required, the echo canceller should reduce the echo level by 50 to 60 dB. In order to have such a high echo reduction the nonlinear effect of the echo path must be

taken into account.

In this section we first discuss the echo source in the two-wire full duplex data transmission system and its nonlinearities. Some of common approaches for the nonlinear echo cancellation are described. Two methods, Wiener scheme and Volterra expansion, are discussed in some detail (Chen 1989a and 1989d).

4.5.1 Echoes in full duplex data transmission system

Fig.4.23 shows a two-wire full duplex data transmission system together with an adaptive echo canceller. Data are transmitted over the two-wire simultaneously in both directions. At each end a transmitter and a receiver are installed and a hybrid is provided to transfer the two-wire to four-wire connection. One may have noticed the difference between the data transmission system in Fig.4.24 and the telephone network shown in Fig.4.1. The hybrids in these two systems have the same function but with the opposite direction of the transform.

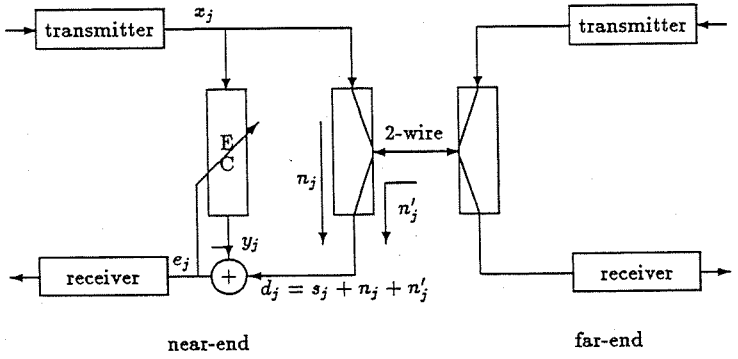


Figure 4.23: Echoes in full duplex data transmission system

When a signal x_j is transmitted by the transmitter at the near-end, the hybrid couples it to the full duplex two-wire line, while generating no leakage to its own receiver. However for the same reason as we discussed in section 4.2.1 an echo n_j is generated by the hybrid at the near-end. It is usually called near-end echo, n_j. Similarly, the impedance mis-match of the hybrid at the far-end generates a far-end echo n'_j. That is, in the

two-wire full duplex data transmission system, the receiver at the near-end receives not only signal s_j from the far-end transmitter but also near- and far-end echoes of the transmitted signal at the near-end.

The far-end echo is characterized by weak amplitude and by a significant delay (in milliseconds range) which depends on the length of the line. The near-end echo has a short delay and a high signal level because of the short distance between the transmitter and the hybrid at the same end. Typical hybrid attenuation is around 10 dB, while the line attenuation can be 40 to 50 dB. This means that the level of the near-end echo n_j is 30 to 40 dB higher than that of the incoming far-end signal s_j. Consequently, if a SNR of 20 dB is required, the echo canceller should attenuate the echo level by 50 to 60 dB.

Usually the echo path of the data transmission system is considered as linear. The effects of nonlinear distortions are completely neglected. Thus, the linear adaptive echo canceller is utilized as shown in Fig.4.23. Other possible realizations of the linear echo canceller were discussed in section 4.2.4.

To achieve better performance of the echo canceller in the full duplex data transmission system, the nonlinear effect of the echo path should be taken into account. In a practical data transmission system, following three nonlinear distortions can be identified (Agazzi 1982):

- Nonlinearity of A/D, D/A convertor. In a practical system an adaptive echo canceller itself requires A/D or D/A or both convertors. The input to the echo canceller is digital bit stream and therefore the echo canceller is usually implemented as a digital processor. The echo-combined incoming signal d_j to the subtractor, however is analog. Thus an A/D convertor is needed in front of the subtractor in the digital subtraction mode. In the analog subtraction mode an A/D convertor is required for the error signal and a D/A convertor for the output of the adaptive filter. These data convertors generate nonlinear distortions.

- Transmitted pulse asymmetry. In practice, nominally balanced positive and negative pulses are transmitted. But there always exists a slight unbalance which can not be compensated for by a conventional linear adaptive echo canceller.

- Saturation in transformers. It introduces only a slight nonlinearity.

4.5.2 Nonlinear echo cancellation

The first attempt to cancel the nonlinear distortion in the echo path was made by Thomas (Thomas 1971). He applied the Volterra representation

of nonlinear systems to the echo control problem and proposed a generalized adaptive echo canceller which compensates for nonlinear echo paths. Since then some developments have been achieved. Unlike the linear echo cancellation, only few papers can be found in the literature on the subject of the nonlinear echo cancellation. As far as we know, following approaches have been proposed:

Table look-up method
Distributed arithmetic architecture
Wiener sheme
Volterra expansion

Table look-up method was proposed in (Holte 1981). For transmitted binary data through an echo path with N tap impulse response, the echo canceller assigns an independent output to each possible combination of N transmitted bits. Thus all possible sorts of nonlinearities are completely taken into account and can be corrected. The price paid for this method is 2^N taps, rather than N and a structure in which at each sample time, only one tap weight can be updated. Consequently for a large N, the required memory becomes very large and the adaptation, very slow.

A thorough study (Agazzi 1982) was made, where a combinational structure based on a Volterra expansion of an arbitrary nonlinear function of N binary variables was proposed. That structure is intermediate between the linear and the completely general nonlinear table look-up algorithms.

Distributed arithmetic architecture was proposed in (Peled 1974 and Sicuranza 1986). It is based on the theory of the truncated discrete Volterra series. The memory oriented implementation exploiting distributed arithmetic is considered.

Wiener scheme proposed in (Corredera 1985) has a simple nonlinear structure. In that method, the nonlinear effect in the echo canceller is modeled by a memoryless nonlinear function. If a practical system is matched with the assumed structure, the nonlinear effect resulting from the D/A converter can be compensated. But the cancellation of the other nonlinear effects is not granted.

Volterra expansion is considered to be a general way of modeling nonlinear systems. It is of great interest for the nonlinear echo cancellation.

In next sections we discuss the Wiener scheme and the Volterra expansion methods because of their simplicity and generality, respectively.

4.5.3 Wiener scheme

It is assumed that the echo path is composed of a linear FIR filter with N taps followed by a nonlinear memoryless function $d(.)$. To identify the echo path, an echo canceller consisting of an adaptive FIR filter and a memoryless function $g(.)$ is proposed (see Fig.4.24).

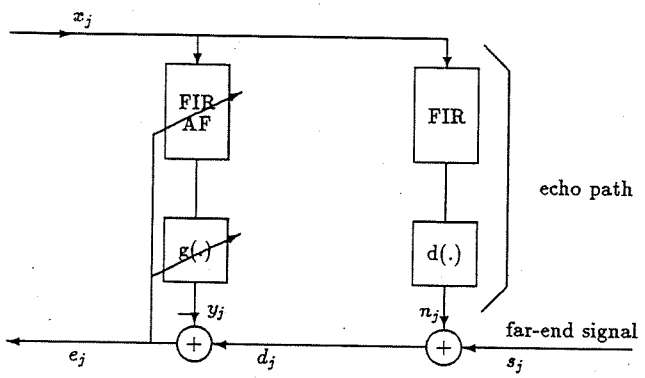


Figure 4.24: Nonlinear echo canceller with the Wiener scheme

The output of the adaptive filter y_j equals

$$y_j = \sum_{k=1}^{N} w_{kj} x_{j-k+1} \tag{4.41}$$

and the output of the nonlinear processor y'_j is expressed

$$y'_j = g(y_j) = \sum_{k=1}^{M} a_{kj} y_j^{k-1} \tag{4.42}$$

where w_{kj} $(k = 1, 2, ...N)$ are the weights of the adaptive FIR filter at time instant j. $g(.)$ is the nonlinear process which is assumed to be parameterized in polynomial form with parameters a_{kj} $(k = 1, 2..., M)$.

The residual error signal e_j is then equal to

$$e_j = d_j - y'_j \tag{4.43}$$

From the above equations, following the same process presented in chapter 2, the LMS algorithm can be derived as follows (Corredera 1985):

$$w_{k,j+1} = w_{kj} + 2\mu_w e_j x_{j-k+1} q_j \quad k = 1, 2, ..., N \tag{4.44}$$

$$a_{k,j+1} = a_{kj} + 2\mu_a e_j y_j^{k-1} \quad k = 1, 2, ..., M \tag{4.45}$$

where,

$$q_j = \sum_{k=1}^{M} a_{kj}(k-1) y_j^{k-2} \tag{4.46}$$

is the derivative of the instantaneous estimation of $g(y_j)$.

Comparing this method with the conventional LMS algorithm one can find two differences: First, a nonlinear processor is included and its parameters are adaptively adjusted according to the LMS Algorithm; Second, the adaptation of the FIR filter weights is modified. The quantity q_j is added to the modification term of Eq(4.44). This cross term makes the behavior of the echo cancellation more complicated and the analysis more difficult (Chen 1989a).

Generally speaking, the error performance surface of this method is not quadratic and the uniqueness of the minimum point is not guaranteed. A primitive discussion on the convergence can be found in (Corredera 1985).

It should be noted that this method is well suited for the adaptive echo canceller realized in the analog subtraction mode (see Fig.4.25). Since the subtraction is performed in analog mode, a D/A convertor is required after the nonlinear processor. This D/A convertor generates a nonlinear distortion which can be compensated for by the adaptive nonlinear processor $g(.)$.

4.5.4 Volterra expansion method

The Volterra expansion is a popular description of nonlinear circuits and systems with mild nonlinearities. The discrete Volterra series for a nonlinear function can be written as

$$\begin{aligned} y_j \;=\; & h^{(0)} + \textstyle\sum_{k=0}^{\infty} h_k^{(1)} x_{j-k} + \sum_{k_1=0}^{\infty} \sum_{k_2=0}^{\infty} h_{k_1,k_2}^{(2)} x_{j-k_1} x_{j-k_2} \\ & + \cdots + \textstyle\sum_{k_1=0}^{\infty} \cdots \sum_{k_n=0}^{\infty} h_{k_1 k_2 \cdots k_n}^{(n)} x_{j-k_1} x_{j-k_2} \cdots x_{j-k_n} + \cdots \end{aligned} \tag{4.47}$$

where $h^{(0)}$ is the dc output component when $x_k \equiv 0$. y_j and x_j represent the jth sample of the output and input signals, respectively. $h_{k_1 k_2 \cdots k_n}^{(n)}$ is the weight for the product of n input samples for the $k_1 \cdots k_n$ combination of indices. The superscripts (n) stand for the order of the Volterra series.

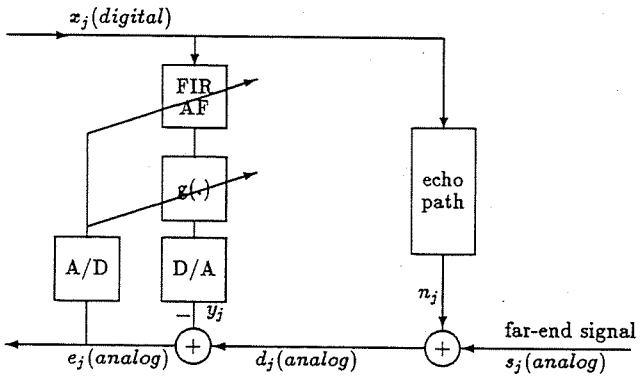


Figure 4.25: Analog subtraction NEC with the Wiener scheme

For the echo cancellation, a truncated version of the Volterra series is sufficient:

$$y_j = h^{(0)} + \sum_{k=1}^{N} h_k^{(1)} x_{j-k+1} + \sum_{k_1=1}^{N}\sum_{k_2=1}^{N} h_{k_1,k_2}^{(2)} x_{j-k_1+1}x_{j-k_2+1} \\ \sum_{k_1=1}^{N}\sum_{k_2=1}^{N}\sum_{k_3=1}^{N} h_{k_1,k_2,k_3}^{(3)} x_{j-k_1+1}x_{j-k_2+1}x_{j-k_3+1} + \cdots \tag{4.48}$$

The above equation can be further simplified by considering the symmetric properties of the nonlinear impulse response, i.e., $h_{k_1\cdots k_n}^{(n)}$ is the same for every permutation of given indices $k_1 \cdots k_n$. Then one attains,

$$y_j = \sum_{k=1}^{N} h_k^{(1)} x_{j-k+1} + \sum_{k_1=1}^{N}\sum_{k_2=k_1}^{N} h_{k_1,k_2}^{(2)} x_{j-k_1+1}x_{j-k_2+1} \\ + \sum_{k_1=1}^{N}\sum_{k_2=k_1}^{N}\sum_{k_3=k_2}^{N} h_{k_1,k_2,k_3}^{(3)} x_{j-k_1+1}x_{j-k_2+1}x_{j-k_3+1} + \cdots \tag{4.49}$$

In the above equation the *dc* component is omitted.

The nonlinear echo canceller can be realized by the Volterra series shown in Eq(4.49), where the x_j is the input signal to the adaptive echo canceller and y_j is its output to be subtracted from the echo-combined far-end signal d_j.

It should be noted that the first order Volterra term in Eq(4.49) is the same as the linear echo canceller. The second order, third order, $\cdots$ represent the nonlinear parts of the echo. The highest order used in the nonlinear echo canceller must be matched with that of the nonlinearities in the echo. For example, if the impulse response of the echo path has

contributions up to third order harmonics, a third order Volterra series expansion must be implemented for the echo canceller.

The length N in Eq(4.49) stands for how many previous (including current) input samples are taken into account for calculating the output. It can be observed that N for the first order term should be chosen equal to the effective length of the echo path impulse response. The value of N for other terms is associated to the level of the nonlinearity. As N gets larger, the computation increases dramatically. Thus it is reasonable to select different values of N for the first term and the others (Chen 1989d):

$$y_j = \sum_{k=1}^{N} h_k^{(1)}(j) x_{j-k+1} + \sum_{k_1=1}^{M}\sum_{k_2=k_1}^{M} h_{k_1,k_2}^{(2)}(j) x_{j-k_1+1}x_{j-k_2+1} \\ + \sum_{k_1=1}^{M}\sum_{k_2=k_1}^{M}\sum_{k_3=k_2}^{M} h_{k_1,k_2,k_3}^{(3)}(j) x_{j-k_1+1}x_{j-k_2+1}x_{j-k_3+1} + \cdots \tag{4.50}$$

where $h_{k_1\cdots k_n}^{(n)}$ are replaced by the adjustable weights $h_{k_1\cdots k_n}^{(n)}(j)$ (j is the time index). The larger M is chosen, the more nonlinearities that can be compensated.

The filter weights are adapted by the LMS algorithm as follows (Chen 1989a):

$$h_{k_1\cdots k_n}^{(n)}(j+1) = h_{k_1\cdots k_n}^{(n)}(j) + 2\mu_n e_j x_{j-k_1+1}x_{j-k_2+1}\cdots x_{j-k_n+1} \\ (n) = 1, 2, 3, .. \tag{4.51}$$

where (see Fig.4.23)

$$e_j = d_j - y_j \tag{4.52}$$

Since the Volterra series is a general (not special) representation of a nonlinear function, the nonlinear distortions of the echo path can be cancelled, using the above method as long as the order (n) is high enough and the value of M is large enough.

Another important feature of the Volterra expansion method is that for the elimination of nonlinear distortions, only extra nonlinear taps are required to be added into the existing linear echo cancellation. This is very practical for the purpose of improving an existing system.

It can be observed from Eq(4.52) and (4.50) that the mean square error is also a quadratic function of the weight vector defined as:

$$H^T(j) = [h_1(j), ..., h_N(j), h_{11}^{(2)}(j), ..., h_{1M}^{(2)}(j), ..., h_{MM}^{(2)}(j), ..., h_{MMM}^{(3)}(j), ...]$$

4.6 Design of A Nonlinear Echo Canceller

In this section we are going to design a nonlinear echo canceller for a data transmission system (ISDN) with more than 8 dB improvement in

the echo cancellation and with acceptable extra computational complexity (Vandeputte 1988, Chen 1989a).

A simulation model based on U-interface circuit on ISDN line is set up, the performance of the nonlinear echo cancellers with Wiener scheme and Volterra series are thoroughly investigated by simulations. Results showing influences of various parameters are presented in this section.

4.6.1 Model of simulation

Based on the μ-interface circuit on the ISDN line, a simulation model is set up and shown in Fig.4.26, where main components of the real system which may affect the performance of the nonlinear echo canceller are included (Vandeputte 1988, Chen 1989a).

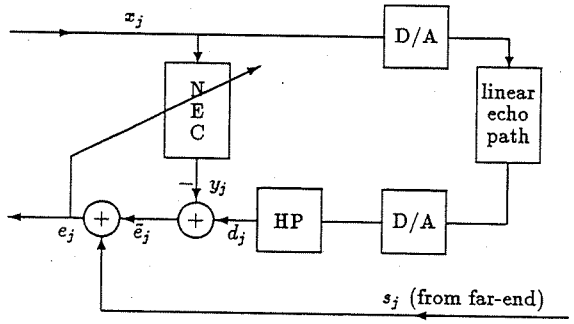


Figure 4.26: Simulation model based on U-interface on ISDN. HP – FIR highpass filter; x_j – signal to be transmitted.

In Fig.4.26 x_j is a random ternary (-1,0,+1) or random quaternary (-1,-3,+1,+3) signal to be transmitted. The linear echo path is simulated based on parameters of the real system. The nonlinear distortions are generated by A/D, D/A convertors, asymmetric of the transmitted pulse and the saturation of the transformer. Among these distortions, only the nonlinear behavior of the A/D and D/A convertors will be discussed. That is, we simulate only that part of the nonlinearities which is generally considered to be the main source of the nonlinearities.

The nonlinear behavior of a D/A convertor can be described as follows

(Agazzi 1982):

$$g(x) = 1.0133x - 0.0133x^3 \tag{4.53}$$

The equation states that the D/A convertor produces an third order harmonics.

In our experiments both A/D and D/A convertors are modeled by the following equation:

$$g(x) = x + bx^2 + cx^3 \tag{4.54}$$

Parameter b and c in Eq(4.54) are determined based on the measured powers of the second and third order harmonics from the real system in the following way:

Let $x_t = cos(\omega t)$ and denote P_1, P_2 as the powers (in dB) of the second and third order harmonics,

$$\begin{aligned} g(x) &= cos(\omega t) + bcos^2(\omega t) + ccos^3(\omega t) \\ &= \tfrac{b}{2} + (1 + \tfrac{3c}{4})cos(\omega t) + \tfrac{b}{2}cos(2\omega t) + \tfrac{c}{4}cos(3\omega t) \end{aligned} \tag{4.55}$$

The normalized powers P_1 P_2 of the second and third order harmonics can then be expressed:

$$\begin{aligned} P_1 &= 20\log\tfrac{b/2}{1+3c/4} \\ P_2 &= 20\log\tfrac{c/4}{1+3c/4} \end{aligned} \tag{4.56}$$

Once the powers of the second and third order harmonics are known, the parameters b and c can be determined from Eq(4.56).

"HP" in the model is a high pass filter. One may consider that its effect can be incorporated in the linear echo path. We'll see later that it can be considered in this way for the Volterra expansion. For the Wiener scheme, however, this highpass filter affects dramatically the performance of the echo canceller.

Far-end signal s_j will not be affected by the echo canceller but it introduces noise in the weights of the adaptive filter during the adaptation. In order to calculate the echo return loss enhancement (ERLE) consistently for different powers of the far-end signal, it is connected in the way as shown in Fig.4.26.

Recall that the ERLE is calculated according to:

$$ERLE = 10\log\frac{E[d_j^2]}{E[\tilde{e}_j^2]} \tag{4.57}$$

It can be seen that this ERLE reflects the pure degree of the echo cancellation. Different values of s_j do not affect the computation of the ERLE.

4.6.2 Simulations with Volterra expansion approach

Simulation results (Chen 1989a) to be shown in this section are based on the following simplifications: 1) The far-end signal is assumed to be absent 2) The effects of the "HP" and the D/A convertor are ignored (It is measured from the real system that the A/D convertor is the main nonlinear distortion).

Comparison between the linear and nonlinear echo canceller

First the performances of the linear and nonlinear echo cancellers are investigated and compared. The results is shown in Fig.4.27, where two learning curves are depicted. Curve 1 results from the linear echo canceller and curve 2 from the nonlinear one. The simulation conditions are:

x_j – quaternery data, μ=0.03, $P_1 = P_2$ = -50 dB
$N = 34$, $M = 3$, $(n) = 3$ (3rd order Volterra series)

From the figure 20 dB improvement in echo cancellation is observed by applying third order ((n)=3) Volterra series with $M = 3$. Since the total number (50) of taps in the nonlinear echo canceller is larger than that (34) in the linear echo canceller, the nonlinear echo canceller converges more slowly than the linear one, which can also be observed in the figure.

Influence of the step-size

It has been mentioned several times in this dissertation that the performance and the convergence of the LMS algorithm are controlled by the value of the step-size. In a stationary environment, the smaller the μ is chosen, the better performance the adaptive filter produces and the slower it converges. Our simulations with nonlinear echo canceller with different μ follow that observation.

Using ternary data as the input signal and the third order Volterra expansion with $M = 3$, a reasonable compromise value of μ between better performance and faster convergence is 0.007, with which the mean square error $E[\bar{e}_j^2]$ goes to -70.9 dB and the nonlinear echo canceller converges after 8500 adaptations.

Influence of the length M

As we mentioned before, the computational complexity of the nonlinear echo canceller is determined by the order of the Volterra expansion and the length M for the nonlinear summation, see Eq(4.50). Once the order (n) is fixed ($(n) = 3$), the computational complexity depends only on the value of M. As M gets larger, the computation increases dramatically, however in principle, better performance can be obtained. Therefore a good compromise must be made in choosing the value of M.

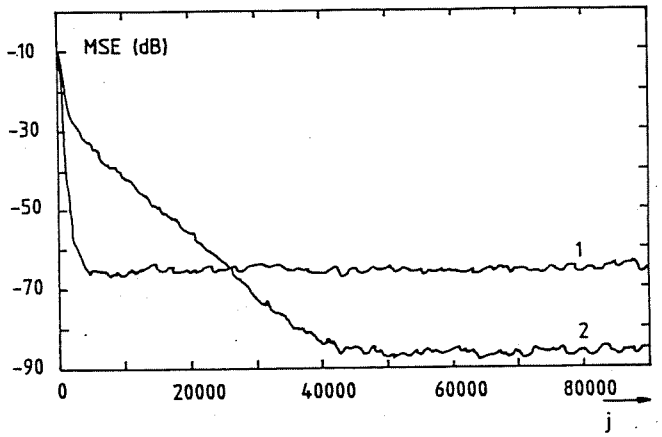


Figure 4.27: Comparison of a linear EC and a nolinear EC of Volterra expansion. MSE vs. adaptations. Curve 1: result of the linear echo canceller; Curve 2: result of the nonlinear echo canceller using 3rd order Volterra expansion.

A series of experiments are done with different values of M and under following conditions:

$$x_j \text{ – ternary data, } \mu = 0.007, P_1 = P2 = -57\ dB$$

The results are presented in table 4.2, where the first column represents the length M, the second column the total number of taps required by the third order nonlinear echo canceller, the third column the adaptation number at which the NEC converges, the fourth column the MSE in dB and the last column is the most important one which shows the gain per extra nonlinear tap.

The first row $M = 0$ means that the linear echo canceller is applied since no quadratic and higher order terms are present. As M gets larger we see that the total number of taps involved increases dramatically, the convergence speed slows down and the performance gets better. But from the last column we can see that increasing M from 0 to 2 produces a gain/tap of 0.756 and from 2 to 3, a gain/tap of 0.528. Starting from $M = 3$ only little improvement can be obtained by increasing the value of M. This can also be seen from the second column from the right: only 0.8 dB improvement in the echo cancellation is obtained by increasing M

Table 4.2: Influence of the length M on the NEC

M	Total taps	Convergence	MSE(dB)	gain (dB)/tap
0	34	5000	-60.76	
2	41	6000	-64.15	0.756
3	50	8500	-70.90	0.528
4	64	10000	-72.50	0.114
5	84	12000	-73.95	0.073
6	111	17500	-75.05	0.041
7	146	22000	-75.85	0.029

Table 4.3: Influence of the nonlinearity

P_1, P_2	MSE of NEC (dB)	MSE of LEC (dB)	Improvement(dB)
-70	-83.93	-74.61	9.32
-57	-70.90	-61.58	9.32
-50	-63.86	-54.53	9.33
-40	-53.67	-44.35	9.32
-30	-43.07	-33.70	9.37

from 6 to 7 (with extra taps of 35). The table serves as a good tool for the selection of M.

Influence of nonlinearity

To investigate the power of the nonlinearities on the performance of the nonlinear echo cancellation, following simulations are conducted:

$$x_j \text{ – ternary data, } \mu = 0.007,\ M = 3\ P_1 = P_2 = -70, -60, \cdots, -30$$

The results with different values of P_1 and P_2 are summarized in table 4.3, from which one can observe: 1) As the nonlinearity increases the performances of both NEC and the linear echo canceller (LEC) get worse; 2) The improvement of the NEC over the LEC is kept the same (about 9.3 dbB) for different values of P_1 and P_2. This means that once the order of Volterra series and the length M are fixed the improvement which can be achieved by the nonlinear echo canceller is determined. If better performance is desired, the value of M should be increased as shown in table 4.2.

4.6.3 Simulations with Wiener scheme

In this section the far-end signal s_j is assumed to be absent, the highpass filter is omitted. The echo path is composed of a linear echo path followed by a nonlinear function shown in Eq(4.54). The echo canceller has the same structure as the echo path while its parameters are adaptively adjusted by the LMS algorithm (Chen 1989a)

Comparison between linear and nonlinear echo canceller

Fig.4.28 shows the learning curves of the linear echo canceller (curve 1) and NEC (curve 2). An improvement of about 16 dB can be observed from the figure by using the Wiener scheme. The convergence of the NEC with Wiener scheme is slower than that of the linear echo canceller but is much faster than the NEC with Volterra expansion method due to less extra nonlinear taps. The simulation conditions are as follows:

x_j – ternary data, $P_1 = P_2$ =-57 dB
Parameters for NEC: N=20, M=3, $\mu_w = 0.03$, $\mu_a = 0.05$
Parameters for LEC: N=34, $\mu = 0.005$

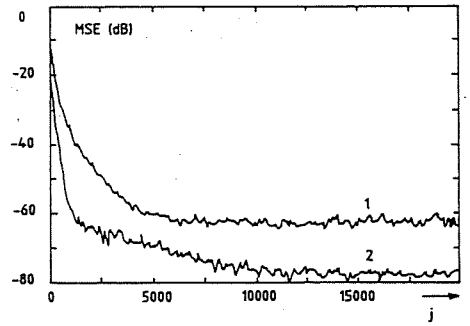


Figure 4.28: Comparison of linear EC and NEC of Wiener scheme

Influence of step-size μ_w and μ_a

Recall that in the Wiener scheme, there exists an inter-connected term between the adaptive FIR filter and the adaptive nonlinear processor. For convenience we repeat them here:

$$\begin{aligned} w_{k,j+1} &= w_{kj} + 2\mu_w e_j x_{j-k+1} q_j & k = 1, 2, ..., N \\ a_{k,j+1} &= a_{kj} + 2\mu_a e_j y_j^{k-1} & k = 1, 2, ..., M \\ q_j &= \textstyle\sum_{k=1}^{M} a_{kj}(k-1) y_j^{k-2} \end{aligned} \tag{4.58}$$

Table 4.4: The influence of step-size μ_w

μ_w	0.001	0.0025	0.004	0.007	0.03	0.05	0.07	0.08
MSE	-74.1	-78.2	-75.7	-73.6	-74.1	-75.4	-74.8	div.

Table 4.5: The influence of step-size μ_a

μ_a	>0.4	0.4	0.07	0.05	0.01	0.005	0.001	0.0005	0.0001
MSE	div.	-71.4	-74.7	-77.1	-74.8	-73.6	-67.6	-64.1	-64.4

In section 4.5.3 we mentioned that the error-performance surface is not guaranteed to have unique minimum point.

From Eq(4.58) we see that two parameters μ_w and μ_a should be optimized. This can only be done independently and in a trial-and-error manner. For the optimization of the μ_w we choose,

$$s_j \text{ – ternary data, } P_1 = P_2 = -57\ dB, \mu_a = 0.1,\ N = 20,\ M = 3$$

and change the value μ_w from 0.001 to 0.08. the results are listed in table 4.4, where the MSE's in dB with different μ's are shown. We see from this table that the minimum value of the MSE is not unique with fixed μ_a and variable μ_w. The MSE gets a minimum value (-74.1dB) with μ_w=0.03 and another minimum (-78.2dB) with $\mu_w = 0.0025$.

For the optimization of the step-size μ_a, we set μ_w equal to 0.03 while keeping the others unchanged. It is found that the echo canceller gets minimum value of MSE with μ_a equal to 0.05. The learning curves with different values of μ_a are shown in Fig.4.29, where curve a) results from $\mu_a = 0.001$, curve b) from $\mu_a = 0.05$ and curve c) from $\mu = 0.03$. From this figure one may have noticed that unlike the LMS adaptive filter, small value of the step-size μ_a does not always result in better performance. It can be seen more clearly in table 4.5. As the decrease of the μ_a from 0.4 to 0.05, the performance of the NEC is getting better, but getting worse as μ_a decreases from 0.05 to 0.0001.

It's found in simulations that the value of μ_a has bigger influence on the NEC performance than that of μ_w. This can be observed in table 4.4 and table 4.5. In table 4.4 we see that different values of μ_w have less influence on the MSE's while in table 4.5 the changes of μ_a result in bigger changes of the MSE. On the other hand, the value of μ_w has bigger influence on

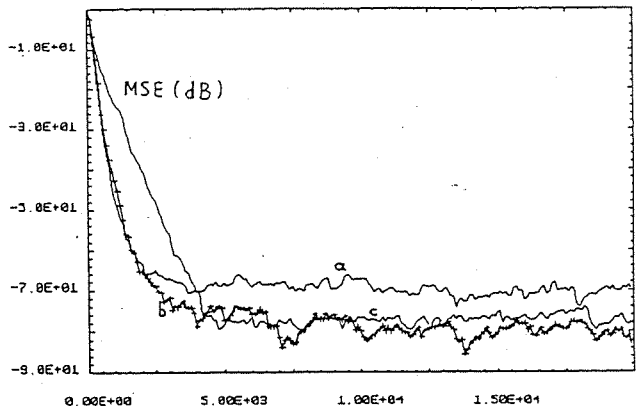


Figure 4.29: Learning curves of the NEC with different μ_a. Curve (a): μ=0.001; (b): 0.05; (c): 0.03.

the NEC convergence than that of μ_a (Vandeputte 1988). This leads to our conclusion that the convergence speed of the NEC with Wiener scheme is mainly determined by the step-size μ_w but its performance is mainly dependent on the step-size μ_a.

Influence of the nonlinearity

In the simulations of the NEC with the Volterra expansion we found that the cancellation of the nonlinear distortions is nearly a constant once the order of the Volterra series and the length for the nonlinear terms, M are fixed. In the following similar simulations are proposed to show the influence of the nonlinearities on the performance of the NEC with Wiener scheme.

The condition of the simulation is as follows:

$$x_j \text{ –ternary data,}$$
$$\mu_w = 0.03\ \mu_a = 0.05,\ N = 20M = 3,\ P_1 = P_2 = -30, \cdots, -90dB$$

The results obtained are presented in table 4.6.

From the table we see that the MSE is nearly constant with different powers of the nonlinearity. This means that the nonlinear distortion can efficiently be cancelled with the Wiener scheme no matter how strong the

Table 4.6: Influence of the nonlinearities (Wiener scheme)

P_1, P_2 (dB)	-20	-30	-40	-50	-60	-70,-80,-90
MSE (dB)	-67.5	-75.5	-74.6	-77.0	-77.1	-77.2

nonlinearity is. This is understandable since the nonlinear model in the echo path is exactly identified in the Wiener scheme.

The only significant effect of the different powers of the nonlinearity within certain range we observed is that the convergence rate decreases as the nonlinearity gets stronger.

Influence of the length N

In table 4.5 one may have observed that the minimum MSE achieved by the nonlinear echo canceller with the Wiener scheme is -77.2 dB no matter how low the nonlinear power is. This implies that the linear echo has not yet been completely eliminated. This is evident if one has noticed that the number of linear taps we have chosen in the simulations was N=20 which is smaller than the effective length, N=34 of the linear echo path. As we have already pointed in the discussion of the linear echo cancellation, the length of the linear taps must be equal to that of the linear echo path. That is, N must be set to 34 instead of 20. With $N = 34$, the MSE of the NEC with the Wiener scheme is -134.1 dB. This means perfect cancellation of the echo. It is reasonable since the structure of the echo canceller is exactly the same as that of the echo path.

4.6.4 Comparison of Volterra expansion and Wiener scheme

Based on the simulation results shown in section 4.4.2 and 4.4.3, it is now easy to compare the performances of the Volterra expansion method and the Wiener scheme (Chen 1989a).

With the simplified echo path, the Wiener scheme has advantages of 1) Less computation, 3 extra taps are required by the Wiener scheme and 16 by the Volterra expansion with $(n) = 3$, $M = 3$; 2) Better performance; 3) Efficient nonlinear echo cancellation. With Wiener scheme nonlinear distortions can almost be completely cancelled while with the Volterra expansion only partial nonlinear distortions can be cancelled if they are strong.

The Volterra expansion method uses the LMS algorithm to minimize the residual error between the echo and its replica produced by the NEC. It is a method of minimization of the error. Thus it is less dependent on

the functional structure of the real echo path. Since the Volterra series is a good representation of nonlinear functions, the NEC with the Volterra expansion is then a general method. That is, if the real system is not the same as the model we simulated, the NEC with the Volterra expansion may still produce nice performance.

The Wiener scheme, on the other hand is a system parameter identification method. Therefore its performance is highly dependent on the functional structure of the real echo path.. If the echo path is well modeled, the NEC produces nice performance, otherwise the effective reduction of the nonlinear echo can not be guaranteed.

To verify the above statement, two experiments are done with the same NEC's as in section 4.4.2 and 4.4.3, respectively and with the same echo path structure but with the inclusion of the FIR highpass filter (see Fig.4.26).

The results are shown in Fig.4.30 where line c is the learning curve of the linear echo canceller, line a) is that of the NEC with Volterra expansion and line b) with the Wiener scheme. From the figure it is seen that the Volterra expansion method still performs well but the Wiener scheme does not give any improvement over the linear echo cancellation.

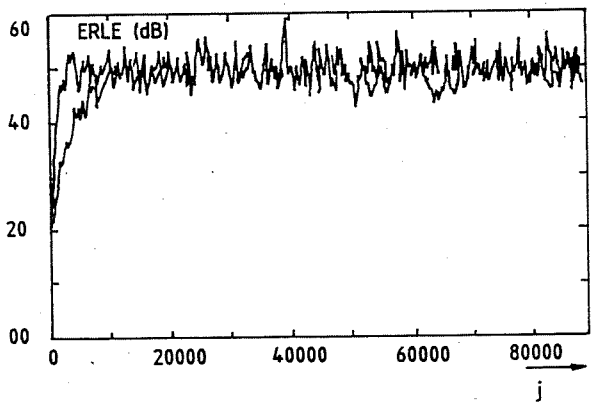


Figure 4.30: Influence of the far-end signal on the NEC

In conclusion, when the model of the echo path is known in advance, the Wiener scheme or other similar system identification methods can be used efficiently. If the exact behavior of the echo path is unknown, the Volterra

expansion is a good candidate for the implementation of the nonlinear echo cancellation.

4.6.5 Design of an NEC with Volterra expansion

In the full duplex data transmission systems, sufficient reduction of the echo is often desired. It is rather difficult to reduce the echo level by more than 60 dB with the linear echo canceller. Thus nonlinear distortions in the echo path should be taken into account in the design of the echo canceller. This leads to the design of a nonlinear echo canceller (Chen 1989d).

In the previous section we concluded that the Wiener scheme provides better performance in the echo cancellation if the echo path can be well identified. For the echo canceller with analog subtraction configuration, the Wiener scheme is very efficient in the cancellation of the nonlinear distortion resulting from the D/A convertor. In practice, however one may observe that 1) the echo path has the structure of FIR linear filter followed by nonlinear component and then followed by another FIR linear filter as the the μ-interface on the ISDN; 2) the linear echo canceller has already been installed in the digital mode and may not be changed. Therefore, the Wiener scheme may not be utilized.

In this section we design an NEC with Volterra expansion method for the data transmission system. The model shown in Fig.4.26 is used and no simplifications are made (Chen 1989d).

The performance of the Volterra expansion method has been thoroughly investigated in previous sections, assuming the absence of the far-end signal. In real full duplex data transmission system, however this is not the case and it is the far-end signal that one wants to receive. Thus, the influence of this far-end signal on the performance of the NEC will be investigated in this section.

The parameters are chosen as follows:

$$\mu = 0.007,\ (n) = 3,\ M = 3, P_1 = P_2 = -57\ dB\ \text{(A/D)},$$
$$P_1 = P_2 = -65\ dB\ \text{(D/A)}\ x_j\ \text{- quatenary data, Power of}\ s_j = \text{-40}\ dB$$

The simulation result is shown in Fig.4.30. From this figure we can see that the NEC does not have any improvement over the linear echo canceller. The effect of the far-end signal can be explained in the following way.

The adaptation of the filter weights is expressed:

$$W_{j+1} = W_j + 2\mu e_j X_j \tag{4.59}$$

Rewrite the above equation as follows (see Fig.4.26):

$$W_{j+1} = W_j + 2\mu \tilde{e}_j X_j + 2\mu s_j X_j \tag{4.60}$$

where $\tilde{e}_j$ is the residual between the echo and its replica, s_j is the far-end signal.

From Eq(4.60) we observe that during the transient period, the second term on the right of the equation is a factor which controls the weight vector to reach its optimal value, while the last term is a noise which disturbs the optimization process.

Let's define a signal-to-noise ratio (SNR) as,

$$SNR = 10\log\frac{E[\tilde{e}_j^2]}{E[s_j^2]} \tag{4.61}$$

It is not difficult to see that as the SNR decreases (s_j increases) it becomes more and more difficult for the weight vector W_j to reach the optimal value.

For an NEC, the effective error signal $\tilde{e}_j$ consists of two parts, e_j^l, the residual error between the linear echo and its replica and e_j^{nl}, the residual error between the nonlinear echo and its replica. Since the nonlinear echo usually has the power of -50 dB to -70 dB, the e_j^{nl} is then less than -50 to -70 dB. This means that the SNR of the adaptation of the nonlinear weights, SNR_{nl} is much lower than that for the adaptation of the linear weights.

$$SNR_{nl} = 10\log\frac{E[(e_j^{nl})^2}{E[s_j^2]} \tag{4.62}$$

Assume the nonlinear distortion has the power of -60 dB and far-end signal s_j , -40 dB, the SNR_{nl} is then less than -20 dB. This means that the nonlinear weights may stay far away from their optimal values, resulting in no cancellation of the nonlinear distortions.

In the steady-state, i.e., $W_{j+1} = W_j$ both the second and the last terms on the right of Eq(4.60) generate the noise.

From the above discussion we can see that to reduce the influence of the far-end signal, either s_j should be set to zero (no full duplex) or the step size μ should be as small as possible.

The elimination of the far-end signal is, of course ridiculous. However it may be possible to start with half-duplex (no far-end signal) or training period. After the nonlinear weights get their optimal values (nearly), the full-duplex or real data transmission begins.

Small μ results in better performance in the steady-state, while slowing the convergence. Accordingly, two steps can be taken: starting with sending a training period with relatively larger μ and switching to the full-duplex with smaller μ after the NEC converges. The value of μ in the steady-state should be chosen as small as possible, but large enough to follow the slow time-variations of the echo path.

Simulation results

Fig.4.31 shows the ERLE of the NEC with the Volterra expansion method with a training period.

The simulation conditions are the same as the previous ones except the step-size. During the training period (0 – 50000 adaptations) no far-end signal is presented and $\mu = \mu_1 = 0.01$. After 50000 adaptations, the far-end signal s_j is connected and the step-size $\mu = \mu_2 = 0.0001$. The improvement (about 15 dB for the quaternary data) of the NEC (curve b) over the linear EC (curve a) is clearly seen in the figure for the full-duplex data transmission.

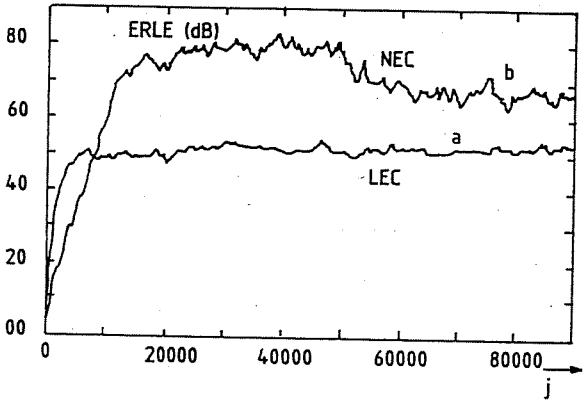


Figure 4.31: ERLE of the NEC with a training period. Training period: 0 – 50000; Curve a: ERLE results from linear EC; Curve b: ERLE results from nonlinear EC.

The performance of the nonlinear echo canceller without the training period is also investigated as follows: the NEC starts with full-duplex with $\mu = \mu_1 = 0.01$ for the first 20000 adaptation and with $\mu = \mu_2 = 0.0001$ after 20000 adaptations. The result shows that an improvement of about 8 dB in echo cancellation can be achieved.

Required wordlength for the filter weights

The effect of finite wordlength of the filter weights is investigated with different bits under the following conditions:

x_j – quaternary data, $P_1 = P_2 = -57$ (A/D), $P_1 = P_2 = -65$ (D/A)
Power of s_j=-40 dB (After training period), μ_1=0.01, μ_2=0.0001

The results are shown in Fig.4.32, where the ERLE's of the linear EC and the NEC with different bit representations are plotted. In a) 15 bits are used, an improvement of about 12 dB for the full-duplex is obtained; In b) 13 bits are used and an improvement of about 10 dB obtained; With 11 bit, we see in c) that the performance of the NEC becomes unacceptable: nearly no improvement can be achieved. From the figure it is observed that the finite wordlength representation of the weights has stronger influence on the NEC than on the linear EC.

Computational complexity

It has been proved that the performance of the NEC with Volterra expansion method is related to the order (n) of the Volterra series used to represent the nonlinearities of the echo path and the length M. It is also been mentioned that the computational complexity is determined by these two parameters M and (n). Thus, a compromise must be made in the design of the NEC with the Volterra expansion.

The order (n) of the Volterra expansion should be chosen equal or higher than the highest order of the harmonics measured in the real data transmission system. The length M for the nonlinear terms should be large enough to cancel sufficiently the nonlinear distortions. For a fixed value of $(n) = 3$, a series of simulations have been done with different values of M and the results are shown in Fig.4.33, where the computational complexity is also illustrated. Fig.4.33a shows the total operations required versus the M, where the operations required increase exponentially. The MSE's resulting from different values of M are presented in Fig.4.33b. As M gets larger the MSE of the NEC becomes smaller, i.e., the performance becomes better.

Fig.4.33 is very helpful in the design of the NEC. A compromised value of M can be chosen between the acceptable computational complexity and the specified performance of the NEC according to this figure.

4.7 Conclusion

This chapter shows the applications of the adaptive filter to the echo cancellation. The general problems of different echoes in telephone networks, data transmission systems and teleconferencing and hand-free telephone systems were outlined. An overview of various adaptive echo cancellation techniques was given. Two difficult subjects in the echo control, acoustic echo cancellation and nonlinear echo cancellation were discussed in detail and comprehensive solutions were given.

For controlling the acoustic echo in teleconferencing and hand-free telephone systems, the main problem is the long impulse response of the acoustic echo path which leads to heavy computational burden for an echo can-

celler. To reduce the computational complexity the subband AAEC is proved to be a good solution. The conventional subband AAEC, however introduces delay in the transmission line which should be avoided. In this chapter we proposed a no-delay subband AAEC. The detailed discussion of the new subband AAEC was given, such as, the optimal number of subbands, design considerations and hardware implementation. Both off-line and on-line simulation results were given.

In full duplex data transmission systems, the main problem is that the level of the echo is usually much higher than that of the interested signal to be received. Thus high echo reduction is required and the nonlinear effect of the echo path should be taken into account. In this chapter thorough investigations on the nonlinear echo cancellers applying the Volterra expansion and the Wiener scheme methods were given. Some useful results for the design of a nonlinear echo canceller were presented.

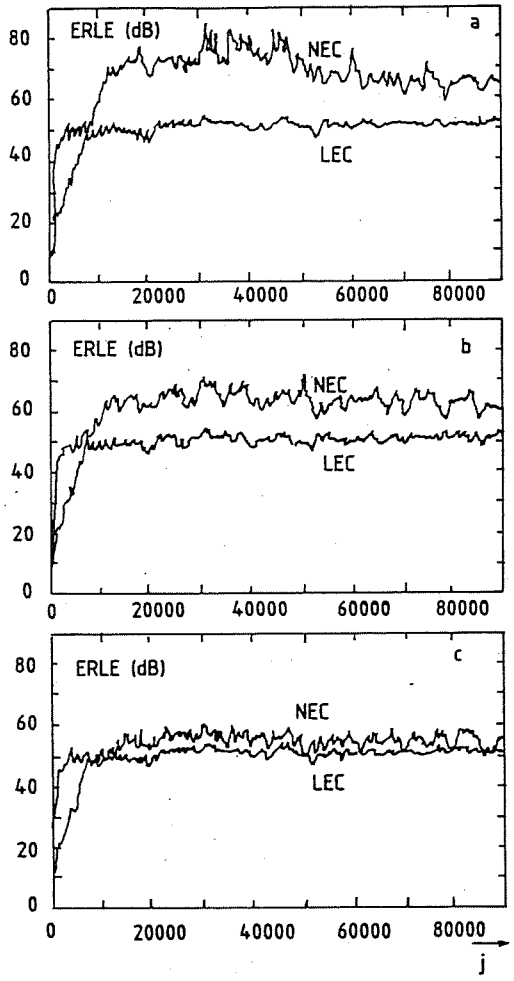


Figure 4.32: Effect of the finite wordlength of weights. a) 15 bits, b) 13 bits, c)11 bits

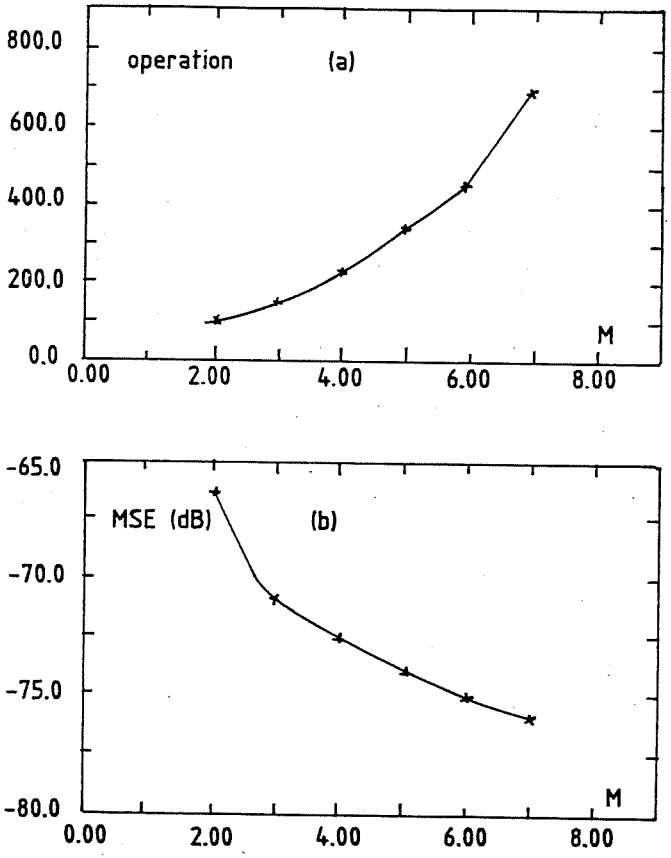


Figure 4.33: Effect of length M on performance and complexity of the NEC.
a) Computational complexity vs. M; b)MSE vs. M

Chapter 5

Adaptive Gastric Signal Processing

5.1 Introduction

As in the human heart, there are electric activities in the stomach. These electrogastric activities can be detected both internally and cutaneously. The cutaneous measurement made by attaching electrodes on the abdominal skin is usually called electrogastrography (EGG) in analogy with electrocardiography (ECG) (Alvarez 1922 and Stern 1985). The cutaneous electrogastrography is especially attractive for medical research and clinical applications since it is non-invasive, completely harmless and does not disturb the on-going process of the stomach.

The first cutaneous EGG was made in 1922 by Alvarez (Alvarez 1922). Since then a lot of research efforts have been expended on investigating the relationship between recorded gastric signals and specific activities of the stomach in question. Unlike other electrophysiological measurements, such as the ECG, however, the progress of the applicability of the methods has been very slow. Generally speaking, the research on the EGG is still on experimental level, not for clinical diagnosis like the ECG. One of the main reasons for this is the poor quality of the cutaneous EGG. The cutaneous EGG contains heavy disturbances and noise, such as respiratory artifact, ECG and motion artifacts, especially, the respiratory disturbance, which superimposes on most of the EGG recordings and may completely obscure the gastric signal.

In order to make great progress in the research of the EGG, better recording techniques and suitable signal processing and analysis methods

have to be developed. Lowpass filtering techniques have been commonly used among researchers for years to eliminate the disturbance and noise (Goodman 1955, Nelsen 1968, Stoddard, 1981) . Fast Fourier transform (Brown 1975, Van der Schee 1983 and 1987), phase lock filtering (Smallwood 1978) and autoregressive modeling (Linkens 1978) techniques have been applied for the frequency analysis of the EGG. However, the improvements of the recording and processing techniques are still one of main topics as Abell and others said: "We must await future improvement in EGG recording techniques and waveform analysis" (p87, Stern 1985).

The main problem with the use of the lowpass filter is that the frequency (or it harmonics) of the interesting gastric signal may overlap with that of some disturbance and noise. Thus, when a lowpss filter is used, the waveform of the gastric signal will be distorted. In order to solve the problem properly, i.e., eliminating the disturbance and noise while keeping the waveform of the gastric signal undistorted, we developed several adaptive filtering techniques which have been tested with a lot of experiments (Chen 1987b, 1987c and 1988e).

The gastric signal is nonstationary. Both its amplitude and its frequency are changing over time. In order to have an on-line monitoring of the frequency of the gastric signal, the adaptive ARMA spectral estimation technique proposed in chapter 3 has been applied (Chen 1988f).

This chapter is structured as follows: The electrogastric activities in the stomach are described in the next section. In section 5.3 we discuss the method for the measurement and the characteristics of the EGG. An adaptive gastric signal enhancing system is developed in section 5.4. In section 5.5 we present an adaptive technique for the cancellation of the respiratory artifact. In section 5.6 computer simulations on the transfer of the internal gastric signals from the stomach to the abdominal skin can be found. The detection of the propagation of the gastric signal from the cutaneous EGG is described in section 5.5. In section 5.8 we show the on-line gastric spectral analysis method and its application in post-prandial EGG analysis.

5.2 Electrical Activities in the Stomach

In this section we discuss electric activities in the stomach. We start with a brief description of the anatomy of the stomach and then describe how an action potential is generated in the muscle cell. Finally, the electric activities in the stomach are discussed.

5.2.1 Anatomy of the stomach

The stomach consists of three main parts: fundus, corpus and antrum, see figure 5.1. The fundus is the part oral to the gastroesophageal junction. The corpus is the main body of the stomach and the antrum is the electrically active region of the stomach. The junction between the stomach and the duodenum is called pylorus.

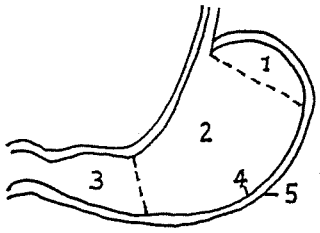


Figure 5.1: The anatomy of the stomach. 1 – fundus, 2 – corpus, 3 – antrum, 4 – mucosa, 5 – serosa.

The concave right border of the stomach is called the less curvature and the left one is the great curvature.

In each region, the wall of the stomach has three major layers: the mucosa, which is the epithelial line of the gastric cavity, the muscularis, which is the smooth muscle coat and the serosa, which is a thin membranous outer line of the stomach. The muscularis is divided into an outer longitudinal muscle layer and an inner circular muscle layer that is thickest in the antrum.

The function of each region of the stomach can be described as follows: The fundus and the proximal part of the corpus function as a temporary storage of a large meal. The gastric contents are then moved by the tonic contractile activity to the distal part of the stomach, where phasic contractions occur. Small portions of the chyme are propelled into the duodenum depending on the momentary diameter of the pyloric sphincter, while most part of the chyme is retropropelled in oral direction for mixing and grinding.

The underlying control mechanism, especially with respect to the distal part of the stomach, is of electrical nature. It is observed that the smooth muscle cells of the distal two-third of the stomach (in the corpus) generate cyclic recurring electrical signals, which propagate circumferentially and

distally toward the pylorus as shown by the arrow in figure 5.1. It will be discussed later at length.

5.2.2 Electrical signaling in nerve or muscle cells

The voltage difference across a cell's plasma membrane, that is, the membrane potential, depends on the distribution of electric charges. Charge is carried back and forth across the cell membrane by small inorganic ions, mainly Na^+, K^+, Cl^- and Ca^{2+}.

The most important ions involved in the propagation of the action potential in the cell are Na^+ and K^+. Muscle cells, like all other cells, expend a great deal of metabolic energy pumping Na^+ out and K^+ in by means of an $Na^+ - K^+$ ATPase in the plasma membrane (Alberts 1983). As a result, the concentration of Na^+ is about ten times lower inside the cell than it is outside, while the distribution of K^+ is roughly the reverse. These concentration differences represent a storage of free energy available to drive fluxes of ions across the plasma membrane.

The ion concentration gradient across the membrane can be balanced by a voltage gradient as shown in figure 5.2, where the "+" sign stands for K^+, and $\bigoplus$ sign for Na^+. The K^+ concentration is high outside the cell and low inside. In (A), the membrane channels allow free passage of K^+ but not of Na^+, so that the K^+ distribution is equilibrated between the two sides of the membrane, but the Na^+ distribution is not. The passage of a few K^+ ions arcoss the membrane to the outside of the cell creates a charged layer on each side of the membrane. The flow of K^+ continues until a voltage difference is created that just opposes the effect of the K^+ concentration gradient. At equilibrium, the electrochemical gradient for K^+ is zero. In (B) just conversely, the membrane channels allow free passage to Na^+ but not K^+. This results in a voltage difference being set up that is opposite in direction to that shown in (A) and just balances the Na^+ concentration difference between the two sides.

In the resting state, the leak channels are much more permeable to K^+ than to Na^+, and the membrane potential is consequently close to the K^+ equilibrium potential of about -70 mv.

The electrical signaling in the cell depends on channels whose permeability is regulated: the so-called voltage-gated channel. The voltage-gated channel, by definition is the one that opens and closes in response to changes in the voltage across the membrane. It makes the cell electrically excitable and enables them to conduct action potentials. Figure 5.3 shows an example of the triggering of an action potential by a brief pulse of current that partially depolarizes the membrane. The upper graph shows the stimulating current. In the middle, the solid curve shows the course of the action

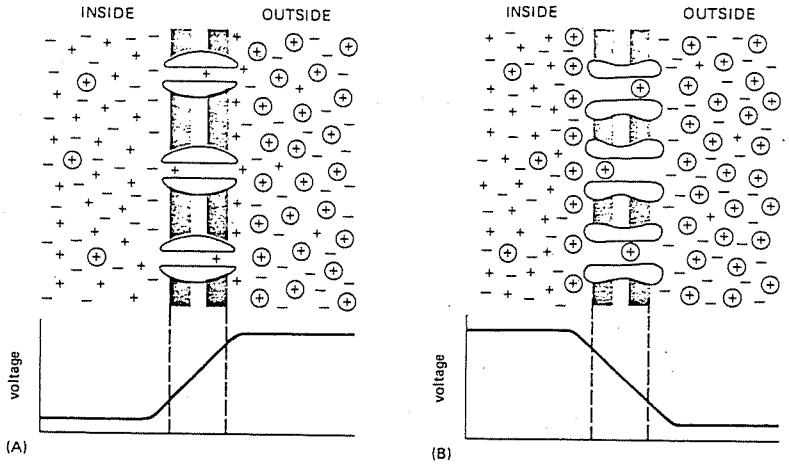


Figure 5.2: Ion concentration gradient and voltage gradient

potential due to the opening and subsequent inactivation of the voltage-gated Na^+ channels; the dashed curve shows how the membrane potential would have simply relaxed back to the resting value after the initial depolarizing stimulus if there had been no voltage-gated channels. When the membrane of a cell with many Na^+ channels is partially depolarized by a momentary stimulus, some of the voltage-gated Na^+ channels are open, allowing Na^+ ions to enter the cell. The influx of positive charge depolarizes the membrane further thereby opening more channels, which admits more Na^+ ions, causing still further depolarization. This process continues till the Na^+ equilibrium potential is reached. At that point, the net electrochemical driving force is zero. Then the Na^+ channel is automatically inactivated and gradually close and stay closed until the membrane potential has returned to its negative resting value, repolarization (Alberts 1983).

5.2.3 Slow wave (electrical control activity)

There are different ways of measuring electric activities in the stomach, which provide different information. **Intracellularly** measured myoelec-

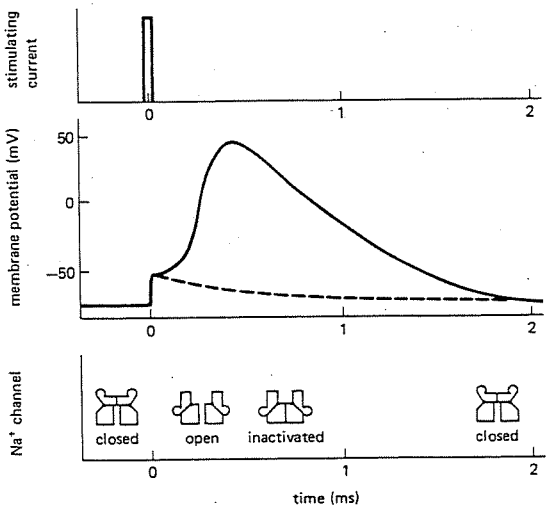


Figure 5.3: The triggering of an action potential

trical activity of the stomach is a reflection of the intracellular electrical activity of the smooth muscle cells, resulting from ion shifts from the inside of the cell to the outside and vice-versa. Whereas **extracellular** recording techniques (often called gastroelectromyography) with electrodes located in the immediate proximity of the muscle layers provides detailed information about the electrical activity of groups of cells. **Cutaneous** EGG with electrodes attached on the abdominal skin provides only global information about the electrical activity of the stomach.

Two kinds of electrical activities have been observed in the stomach, omnipresent periodic potentials and contraction related activities. In this section we discuss the omnipresent periodic potentials, while leaving the discussion of the contraction related activities can be found in the next section.

The omnipresent periodic potential can be recorded by either serosal or mucosal electrodes. Many names have been given to this potential. One may encounter the terms: slow wave, electrical control activity, basic electrical rhythm and pace setter potentials. In this dissertation we use the

first two terms.

The slow wave is originated in a region near the junction of the proximal one third and distal two-thirds of the gastric body along the great curvature. It is characterized by regular recurring changes in potential, propagating circumferentially and distally towards the pylorus at increasing velocity. It was believed that the slow wave only performs an electrical pacing function, but some studies (Morgan 1978, You 1984) indicate that the slow wave is associated with low-amplitude contraction of the antral smooth muscle.

Each cycle of the slow wave consists of two parts. The first portion of the cycle is usually triphasic, consisting of a small positive, a large negative and then a small positive deflection. It depends, in part, on the depth of the electrode in muscular coasts. As a role, when detecting electrodes lie in the most superficial fibers of the longitudinal muscle and just beneath the serosa, the slow wave shows only a positive deflection. As the detecting needle is advanced deeper into the muscle, a biphasic wave is often obtained, and the deepest insertion of the needle in the muscle is frequently associated with a predominantly negative wave (Bass 1961).

In the second portion of the cycle, the potential changes little under the resting condition, being represented by a nearly horizontal line which continues until the beginning of the next cycle. The duration of this portion is much longer than that of the first portion.

It is generally accepted that the frequency of the slow wave is 5 cycles/min in dog although there is a little difference between different dogs. In humans the normal frequency of the slow wave is about 3 cycles/min (0.05 Hz). However, tachygastria with frequencies higher than that value has been observed (Chen 1988g, 1989c) in the cutaneous EGG. Lower frequencies (lower than 2cycle/min) have also been observed (Van der Schee 1983).

The slow wave propagates from the orad corpus to the pylorus with increasing amplitude and velocity. In dog, the maximum amplitude of the slow wave is about 1 *mv* in the corpus and 2-3 *mv* in the antrum. The velocity of the propagation is about 0.1-0.2 cm/second in the orad corpus and 1.5-4.0 cm/s in the antrum (Kelly 1969). Figure 5.4 shows the propagation of the slow wave in a canine stomach. From the figure we can see the variations of the amplitude and of the propagation velocity in different positions of the stomach. The average velocity of the slow wave in the distal antrum of the human stomach is about 4 cm/s (Stern 1985).

5.2.4 Contraction related activities

A gastric contraction is usually a mechanical manifestation of an electrical process occurring at the surface membrane of smooth muscle cells. Dur-

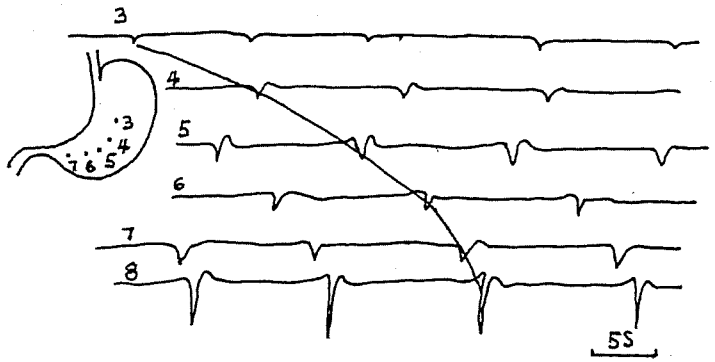


Figure 5.4: The propagation of electrogastric signal in the stomach

ing each peristalic contraction, electrical currents flow through the affected muscles. These currents are not incidental to contractions, they in fact cause the stomach to contract. The origin of a phasic gastric contraction is an electrical event.

One may encounter several terms for the contraction related gastric activities. Slow contraction related deflection: second potential, plateau potential; Fast contraction related oscillatory deflection: spike potentials, fast activity, electrical response activity and action potential. The term action potential was used by Smout (Smout 1980) to denote the first portion of the slow wave.

The main electrical wave, the slow wave, is present all the time in the stomach even when the muscle is not contracting, as described in section 5.2.3. During episodes of motor quiescence, the segments of the signal between the triphasic complexes are isoelectric or nearly isoelectric. When phasic contractions occur, potential changes take place in the first part of the isoelectric segment, just after the triphasic complex. With regard to the characteristics of these contraction related potential changes, different opinions can be found in the literature.

In (Daniel 1968) Daniel and Irwin say, "In the contracting stomach, a second electrical deflection (the second potential) is seen on conventional monopolar records..., The second potential is typically recorded as a prolonged (4-8 seconds) negative deflection. It may, however be a series of

negative spikes. Spikes are usually seen in the terminal 2 or 3 cm of the dog antrum." The description in (Kelly 1969) reads, "Simultaneous recordings of an electrical event, the changes in intragastric balloon pressure, and motility as seen fluoroscopically show that contractions occurred only when action potentials (spikes) were recorded.... They (the spike bursts) always occurred during the second portion of the slow wave cycle just after the triphasic complex, and were usually accompanied by a monophasic negative deflection."

Figure 5.5 illustrates the configuration of the potential changes in gastric smooth muscle cells. The resting membrane potential of the muscle cells involved in about -70 *mv* (portion (a) in the figure). The amplitude of the depolarization (b) in the corpus and in the antrum is of the order of 30 and 45 *mv*, respectively (El-Sharkawy 1978). The depolarization rate also increases in distal direction. In a mechanically inactive tissue, the plateau (c) with or without spikes is completely absent (Daniel 1965). Stronger contractions are associated with a higher plateau of longer duration and of higher velocity of repolarization (d).

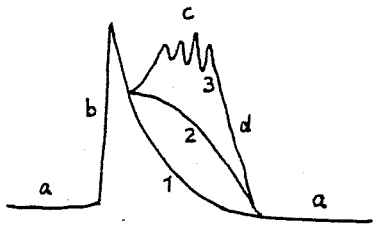


Figure 5.5: Configuration of gastric potentials

Figure 5.6 shows schematically the relations between the intracellular electrical activity, extracellular electrical activity (monopolar) and contractile force as may occur in the canine distal antrum. From the figure we can see that contractions are associated with the second potential. Strong contractions are related to the spike activities.

In conclusion, electrical gastric activities in the different regions of the stomach can be described as follows: muscle cells in any layer of the fundus are usually electrically silent, there being no spontaneous electrical activity. Recently, however electrical activities from that region has been recorded.

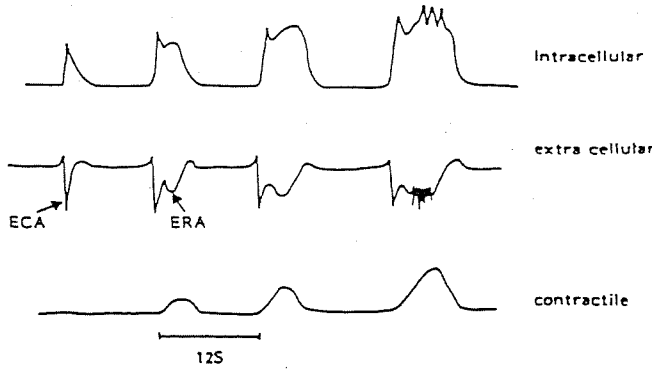


Figure 5.6: Relation between intra-cellular, extra-cellular electrical activities and contractile force

The slow wave propagates from the corpus to the pylorus with increasing amplitude and velocity. The contractions occurring in the corpus and in the orad antrum are associated with the second potential following the initial depolarization. The contractions in the distal antrum are related to the second potential with spikes.

5.3 Electrogastrography

In the previous section we discussed myoelectrical activities in the stomach. These internally measured electrical activities are very useful for medical research and clinical diagnoses. The main disadvantage of the gastromyography is its invasiveness.

Electrical gastric activities can also be measured cutaneously by attaching electrodes on the abdominal skin. The cutaneous measurement is called electrogastrography (EGG). The EGG is a very attractive tool for medical research and medical applications because of its non-invasiveness.

5.3.1 Measurement of EGG

Healthy volunteers or patients fasted over night are asked to lie on their back and to keep as still as possible. Ag/AgCl (red dot, 3M) electrodes are attached on the abdominal skin outside the stomach. Bipolar signals are derived by connecting electrodes in pairs or by connecting each electrode with a common reference electrode also on the abdomen. Up to 6 bipolar signals are amplified by a Universal Amplifier 854 with a time constant of 5 seconds (corresponding 0.031 Hz) and an upper frequency of 5 Hz. The amplified signals are simultaneously displayed on Mingograf paper (paper speed 2.5 mm/s) and stored on an analog tape by a tape recorder (TEAC). They are then digitized by an 8 channel 12-bit A/D convertor with a sampling frequency of 12 Hz. The digital gastric signals are lowpass (FIR) filtered with a cutoff frequency of 1 Hz (or 0.5 Hz). and down-sampled again with a frequency of 2 Hz (or 1 Hz) (Chen 1988e and 1989e). The general block diagram of the whole process is shown in figure 5.7, where the adaptive signal processing techniques will be discussed in the following sections.

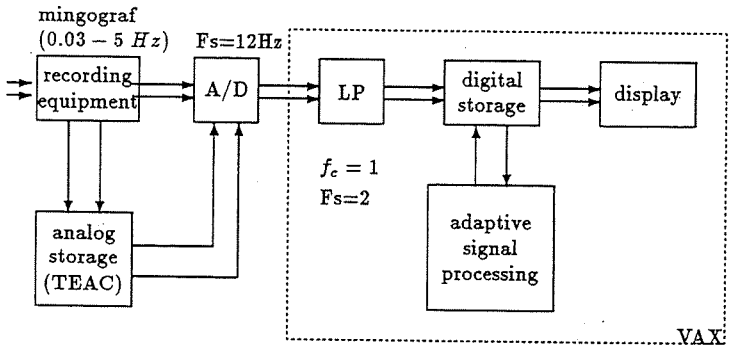


Figure 5.7: Block diagram of the overall system. LP – lowpass filter

5.3.2 Characteristics of EGG

Figure 5.8a and c) show two typical different positional bipolar EGG measurements from a normal fasted volunteer. The signals are lowpass filtered

with a cutoff frequency of 5 Hz. The slow wave of which the period equals about 20 seconds is the gastric signal component, the spike-like activity is the ECG and the superimposed sinusoidal disturbance is the respiratory artifact. Figure 5.8b shows the simultaneously recorded respiration with a pressure sensor (it will be described in section 5.5). From figure 5.8 we can see that different positional EGG's have different qualities. It can also be seen that the respiratory artifact is the main disturbance source.

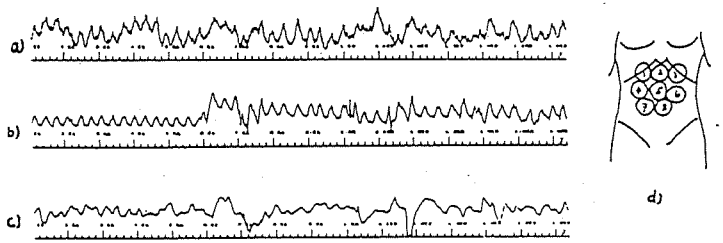


Figure 5.8: Cutaneous electrogastrographies. a) Bipolar cutaneous electrogastric measurement (electrodes 6 and 7); b) Simultaneously measured breathing pressure; c) Bipolar cutaneous electrogastric measurement (electrodes 4 and 8); d) Positions of electrodes.

Figure 5.9 presents the power spectrum of the signal shown in figure 5.8a lowpass filtered with a cutoff frequency of 1 Hz and sampled at 2 Hz. The first peak from the left at around 0.05 Hz shows the frequency of the gastric signal and the second peak from the left around 0.3 Hz is that of the respiratory artifact.

From these two figures we see that the EGG is a mixture of the gastric signal component and disturbance. Generally, the latter is composed of respiratory artifact, ECG, noise resulting from electrode-skin interface (Tam 1977), motion artifacts and other possible unknown noise. The frequencies of different components in an EGG are listed in table 5.1 (Chen 1988e).

The frequency of the gastric signal component is about 0.05 Hz. However in some cases, it can be higher as we have already mentioned before. The respiratory artifact has a frequency of about 0.2-0.4 Hz, varying from person to person. It is usually strong since the stomach is close to the diaphram, although the bipolar connection may reduce its amplitude. ECG

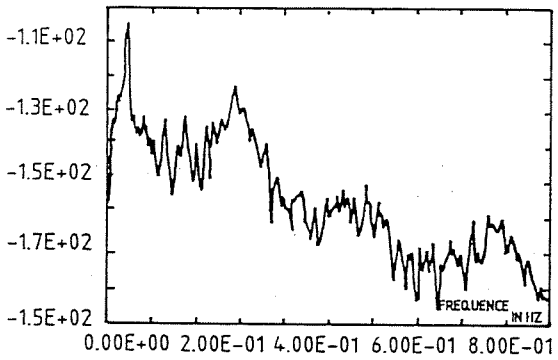


Figure 5.9: Power spectrum (dB) of an EGG

Table 5.1: Composition of cutaneous EGG

	Component	*Frequency (Hz)*
Interesting component	Gastric signal component	0.05
Disturbance	Respiratory disturbance	0.2 - 0.4
	Electrocardiography	0.8 - 1.0
	Electrode-skin noise	less than 0.03
	Motion artifacts	whole range
	Other possible noise	unknown

is not a big problem for signal processing because its frequency is about 1 Hz or higher, which is far apart from that of the gastric signal, and thus can be eliminated by a lowpass filter without introducing waveform distortion of the gastric signal. However it does cause problems in the preparation of the measurement. Its peak amplitude can be much higher than that of the gastric signal. Consequently, most bits of the A/D convertor are used to satisfy its dynamic range, while only few bits of the converter are really used for the gastric signal. Motion artifacts are within the full frequency band. It's very hard to cope with it. But it can be limited by simply asking volunteers or patients to keep as calm as possible during the recording time. The electrode-skin noise has a lower frequency and does not affect the gastric signal much according to our experiences.

The characteristics of the EGG are summarized as follows (Chen 1989e):

- The cutaneous EGG provides global information about the electrical activities of the stomach. The gastric signal in the EGG at certain time is a weighted summation of all the internal electrogastric activities at that time. Its waveform is related to the position of electrodes, to the connection of the electrodes and most importantly, to the condition of the stomach, such as contracting or not.

- Gastric signals have a low fundamental frequency. But they may also contain higher frequencies. It can be seen from figure 5.10 which shows part of an EGG measured from a volunteer. From the figure we see the sudden increase of the EGG' amplitude like the depolarization measured intracellularly. These sharp edges imply the existence of higher frequency components.

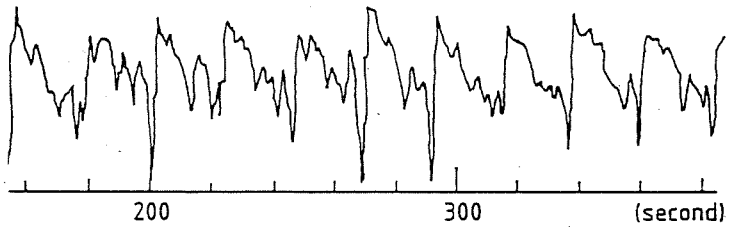


Figure 5.10: A cutaneous EGG

Moreover, in some other situations, such as in the case of tachygastria, the frequency of the EGG can be much higher than its normal frequency. Figure 5.11 shows the power spectrum of a gastric signal in this case. The signal is measured from a patient with mild gastrites, who claimed feeling nausea sometimes during the measurement. From the figure we can observe that the frequency of the gastric signal is about 0.15 Hz. It is rather close to that of the respiratory disturbance (Chen 1989c).

- The SNR of the EGG is low. The respiratory disturbance may be considered to be periodic and is usually a main problem in the waveform analysis of the EGG.
- Some noise, such as the motion artifacts, are within the frequency range of the gastric signal.
- The amplitude and the frequency of the gastric signal component change over time within certain limits according to our clinical experience. This means that the EGG is a nonstationary signal.
- Different positions of electrodes result in different qualities of the EGG's measurements. The best positions for the electrodes are along the vertical axis of the stomach (Mirizzi 1983, Chen 1984). However, the position of the stomach in the human torso changes from person to person and changes from one time to another for the same person. This implies that the best locations of the electrodes are unknown unless a special localization technique is provided.

5.4 Adaptive Enhancement of EGG

From the above discussion we observe that the frequency of the gastric signal (or its harmonics) may overlap with (or close to) that of the respiratory disturbance and motion artifacts. If a lowpass filter is applied to eliminate the respiratory disturbance, the cutoff frequency should be set lower than 0.2 Hz (the frequency of the respiration is about 0.2-04 Hz) as most of researchers did. This will certainly result in waveform distortion of the gastric signal. For an EGG shown in figure 5.10, after lowpass filtering, the signal would be too "smoothed", i.e., the sharp edges would disappear. Therefore we conclude here that lowpass filtering with cutoff frequency lower than 0.2 Hz should not be applied if the waveform analysis of the EGG is to be performed.

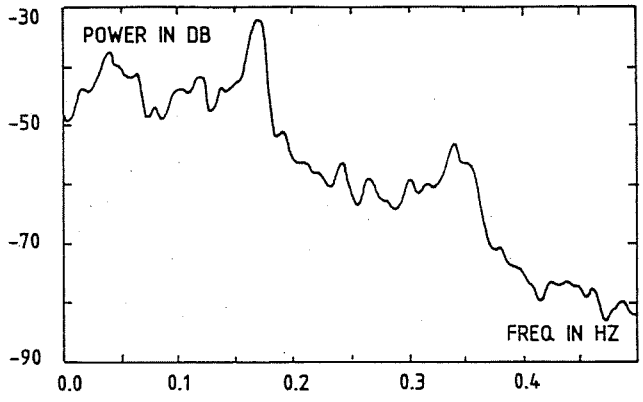


Figure 5.11: Power spectrum of a tachygastrial EGG

In this section we present an adaptive enhancing system for the EGG. First we introduce the principle of adaptive signal enhancement and then propose an adaptive system for the enhancement of the EGG. Both simulation results and EGG signal processing results can be found in this section.

5.4.1 Principle of adaptive signal enhancement

Figure 5.12 illustrates the LMS adaptive signal enhancer (Ferrara 1981), where AF is the LMS adaptive filter. For simplicity the time index j is dropped. Assume that the primary input contains a signal s_0 and a noise n_0. The reference input contains a signal s_1 and a noise n_1. Among these signals and noise, only two signals s_0 and s_1 are correlated with each other.

According to the LMS algorithm described in chapter 2, the weight vector of the adaptive filter at time $j+1$ is adapted as,

$$W_{j+1} = W_j + 2\mu e_j X_j \tag{5.1}$$

From figure 5.12, squaring the residual error

$$e = s_0 + n_0 - y \tag{5.2}$$

one attains

$$e^2 = (s_0 - y)^2 + n_0^2 + 2n_0(s_0 - y) \tag{5.3}$$

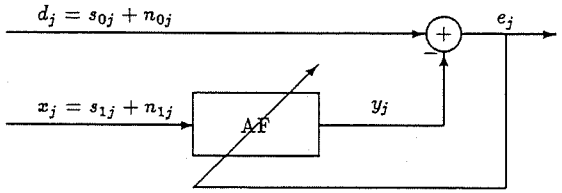


Figure 5.12: An adaptive signal enhancer

Taking the expectation and considering that n_0 is uncorrelated with either of s_0, s_1 and n_1, one gets,

$$\begin{aligned} E[e^2] &= E[(s_0 - y)^2] + E[n_0^2] + 2E[n_0(s_0 - y)] \\ &= E[(s_0 - y)^2] + E[n_0^2] \end{aligned} \tag{5.4}$$

Since $E[n_0^2]$ can not be affected during the adaptation, the necessary and sufficient condition of minimizing the mean square error is

$$E[(s_0 - y)^2] = 0 \tag{5.5}$$

That is, the filter output y is a best estimate of the signal s_0 contained in the primary input in the sense of the mean square error.

5.4.2 Adaptive enhancement system

Having discussed both the characteristics of human EGG and the principle of the adaptive signal enhancement, we are now ready to present the adaptive gastric signal enhancement system (Chen 1987c, 1988e).

Figure 5.13 shows the block diagram of the adaptive system. It contains two stages. The first stage (called pre-processing) is an adaptive line enhancer which is used to improve the SNR of the EGG signal and to eliminate some uncorrelated noise.

The second stage is a modified multi-channel adaptive signal enhancer. We know that the conventional FIR lowpass filter can keep the main characteristics of the signal unchanged although it may affect the waveform of the underlying signal. For the adaptive signal enhancer, it is known that the reference input signal x_j should contain some information which is correlated to the signal involved in the primary input, but is not necessary to have the same waveform. Therefore we use a conventional FIR lowpass filter (LP) to eliminate the periodic respiratory disturbance in order to have a relevant reference input.

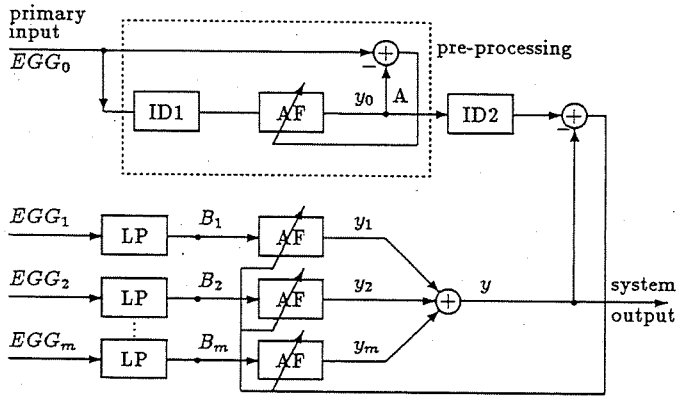


Figure 5.13: Adaptive system of EGG signal enhancment. Time index j is omitted. ID1 and ID2 : delay units. LP – lowpass filter.

Since the best positions of the electrodes are generally unknown in practice, we use multi-channel references (Ferrara 1981). The adaptive filter in each reference channel is adapted according to the μ-vector LMS algorithm proposed in chapter 2, and the summation of these adaptive filters produces a better estimate of the gastric signal in the primary input. It has been proved (Ferrara 1981) that the more reference inputs available containing correlated signal components, the better the system performance will be.

Pre-processing

In section 5.3 we indicated that the EGG is nonstationary and the SNR is low. So when the LMS algorithm is used, the convergence speed should be fast enough to follow the variations of the EGG statistics, that is, the value of the step-size should be larger. However, larger μ will result in stronger gradient noise. In order to keep the gradient noise within a tolerable limit when a fast adaptation is needed an alternative way is to reduce noise components in the input signal. For this reason the pre-processing is introduced.

The pre-processing (dashed part in figure 5.13) is simply an adaptive line enhancer. The input signal to the pre-processing is a cutaneous EGG to be filtered and the reference input is its delayed version. Properly choosing

the length of the filter, step-size μ and bulk delay $ID1$, the output of the pre-processing y_0, after convergence of the adaptive filer, contains little uncorrelated noise. However, the gastric signal component is not affected because of its periodicity. The SNR of the signal is then considerably increased, which relieves the "burden" of the next stage processing.

Figure 5.14 shows the power spectra of a cutaneous EGG before and after the pre-processing. Line 1 is the power spectrum of the signal before the pre-processing and line 2, after the pre-processing. From the figure we can see that the gastric signal component around 0.05 Hz is little affected. However, the power spectrum of the noise component with frequency greater than 0.1 Hz is reduced 30 dB or more.

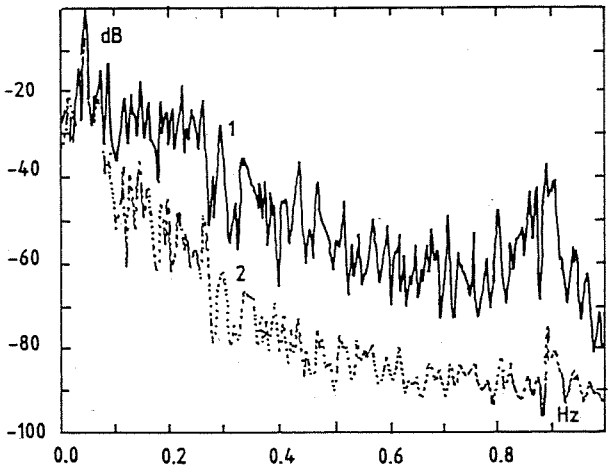


Figure 5.14: Curve 1: power spectrum of the input signal; Curve 2: output (after pre-processing) power spectrum.

Modified Multi-channel Adaptive Enhancing

The remainder of the system shown in figure 5.13 is a modified multi-channel adaptive enhancer. Its primary input is the output of the pre-processing and the reference inputs EGG_1–EGG_m are different positional

cutaneous EGG. All of the reference inputs are first filtered by an FIR digital lowpass filters in order to extract only the gastric signal component in the primary input. A delay $ID2$ is included in the primary input to compensate the time delay introduced by the FIR filter in the reference inputs.

"LP" in figure 5.13 is the lowpass FIR filter with a cutoff frequency of 0.1 Hz (it can be up to 0.2 Hz if necessary). It has linear phase characteristics so the phase characteristics of the gastric signal component will not be affected except the time delay.

The adaptive filter in figure 5.13 is realized by a tapped delay line. The tapping space time is one sample, that is, 0.5 second and the number of weights will be discussed later.

The gastric signal components in different positional EGG's may have different waveform, amplitude and phase. However, they must have the same time-varying characteristics, such as possible time variations of the frequency and the amplitude because they originate from the same source. In other words, they must be highly correlated with each other.

Assume that the primary input EGG_0 contains a gastric signal, an uncorrelated noise and a correlated noise (mainly the respiratory artifact). After the pre-processing, at point A in the primary input we have the gastric signal and some correlated noise (mainly respiratory artifact). After lowpass filtering, at points $B_1, B_2, ...B_m$ we have the gastric signals related to that in the primary input and little noise mostly uncorrelated with that in y_0. Properly choosing the parameters of the system, the output y is then, after convergence, a best estimate of the gastric signal component in the primary input.

Recall that the adaptive filter generates a replica of that part of the primary input which is correlated with the reference input to the adaptive filter. From the proposed system the following conclusions can be made:

> *The system output y is a best estimate of the gastric signal component in the primary input. The respiratory artifact, the ECG, the electrode-skin noise and some of the motion artifacts can be efficiently reduced by the proposed system.*

Although the respiratory artifact (and the ECG) are correlated signals, they can not be extracted from the primary input by the adaptive filters since they don't appear at the points $B_1, ..., B_m$.

The electrode-skin noise can be eliminated if no common reference electrode is used since this class of the noise in one EGG is uncorrelated with that in another EGG.

The motion artifacts are not periodic and thus some of them can be reduced by the pre-processing if the delay $ID1$ is properly chosen. Some

of them which are uncorrelated in different EGG can also be reduced. The complete reduction of the motion artifacts is, however not guaranteed by the proposed system.

System Parameters

Several parameters need to be determined in the system shown in figure 5.13. They are step-size μ, the length of the adaptive filter and the delay units, $ID1, ID2$. The most crucial parameter is the step-size μ.
Step-size The necessary and sufficient condition for the convergence of the LMS algorithm is:

$$0 < \mu < \frac{1}{G^2} \tag{5.6}$$

where G^2 is the total input power to the adaptive filter.

Since the electrogastrographical signal is nonstationary, a μ-vector LMS algorithm (Chen 1987c, 1988e) is used for all of the adaptive filters in the system.

In general a faster adaptation leads to a more noisy adaptation process. When the input environment is statistically stationary the best steady-state performance results from a slow adaptation. In this application, however, the input statistics are time varying. Hence a fast adaptation is needed in order to follow the variations. After trials the value of μ' is chosen to be 0.062, which is a good compromise between fast and slow adaptation. The best value of the β is about 0.04 (see μ-vector LMS algorithm in chapter 2).
Length of the adaptive filter The length of the tapped delay line, namely the number of weights, should be at least the reciprocal of the desired filter resolution (Widrow 1975). Since the normal period of the gastric signal is 20 seconds (40 samples), this value is chosen to be 60 in our experiments.

Time delay

The delay $ID1$ is used to decorrelate the noise in the primary input. For a white noise it can be set to be 1. For the EGG application we have found that if the motion artifacts are not strong the change of its value within a certain range does not affect the system performance. It is usually chosen to be 1. The delay $ID2$ is inserted to compensate the delay introduced by the FIR filters.

5.4.3 Performance analysis

To investigate the performance of the proposed system quantitatively, simulations have been conducted based on the following conditions:

The input signals to the system shown in Fig.5.13 (only two channels are considered) are generated as,

$$EGG_{0j} = s_j + br_j + cn_j \tag{5.7}$$

$$EGG_{1j} = s_{1j} + br_{1j} + cn_{1j} \tag{5.8}$$

where, r_j and r_{1j} are simulated respiratory artifacts. They are sinusoids with a frequency of 0.3 Hz. n_j and n_{1j} are uniformly distributed (-0.5,0.5) white noise. s_j and s_{1j} are simulated gastric signals in the primary input and in the reference input, respectively. They are nonstationary.

s_j is a sequence of sinus signals

$$s_j = \tilde{a} sin(2\pi \tilde{f}_s j) \tag{5.9}$$

each considered over one full period. The amplitude, $\tilde{a}$ and the frequency, $\tilde{f}_s$ of each sinusoid vary as follows:

$$\tilde{a} = a(1 + d_a n') \tag{5.10}$$

$$\tilde{f} = f_s(1 + d_f n') \tag{5.11}$$

where, n' is a white noise, having the same nature as n_j and n_{1j}. Parameters a, b, and c in Eq(18), (19) and (22) are constants controlling the SNR of the simulated signals. d_a and d_f are nonstationary factors determining the variation degree of the frequency and of the amplitude of the gastric signal, respectively. When they are equal to zero, the gastric signal, s_j turns out to be a sinusoid.

s_{1j} has different waveform from s_j, but its frequency follows the same changes as s_j. It is also a sequence of sinus signals,

$$s_{1j} = sin(\pi \tilde{f}_s j) \tag{5.12}$$

but each considered over half a period.

Fig.5.15a and Fig.5.15b show the simulated gastric signals s_j and s_{1j}, respectively. The simulated primary input EGG_0 is shown in Fig.5.15c (SNR=-7.8 dB).

To give some quantitative measures on the performance of the proposed adaptive system, we define terms, "mean square error" (MSE_j) and "misadjustment" (M) as follows:

$$MSE_j = E[(s_j - y_j)^2] \tag{5.13}$$

$$M = \frac{\sum_{j=K}^{K+L}(s_j - y_j)^2}{\sum_{j=K}^{K+L} s_j^2} \tag{5.14}$$

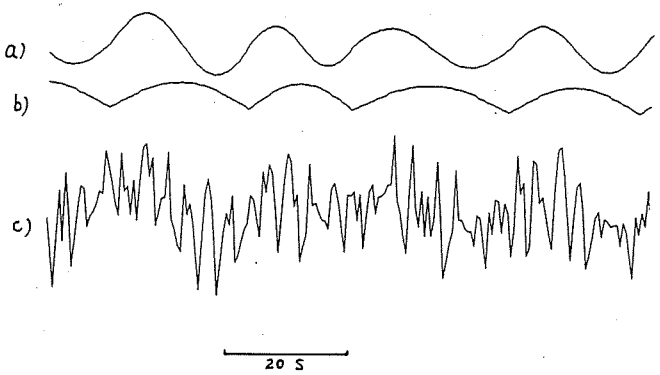


Figure 5.15: Simulated signals. a) and b) Simulated gastric signals, s_j and s_{1j}, c) simulated primary input EGG_0.

where, s_j is the gastric signal in the primary input EGG_0 and y_j is the system ouput. The misadjustment, M, is an averaged relative square error in the steady-state. K should be large enough such that after K adaptations, the system has already converged.

In the following experiments, the parameters are chosen as follows (if not specially mentioned):

Sample frequency: 2 Hz; Length of the adaptive filters N=60; Order of the FIR lowpass filters: 50; Cutoff frequency of the FIR lowpass filter: 0.2 Hz;

$f_s = 0.05Hz$, f_r (frequency of respiration) $= 0.3$, $ID1 = 1$,

$ID2 = 25$, $d_a = d_v = 0.5$, $SNR = -7.8$, $\mu' = 0.04$, $\beta = 0.04$

Convergence of the system

Fig.5.16 shows the convergence of the system with the stationary inputs ($d_a = d_f = 0$), the mean square error, MSE_j vs. the number of the adaptations over 100 independent runs. The step-size μ' is chosen to be 0.04 for curve 1 and 0.1 for curve 2. From the these two curves we can see that for the stationary inputs, larger μ' results in faster convergence and

larger mean square error in the steady-state. Smaller μ', on the other hand, results in slower convergence and better performance.

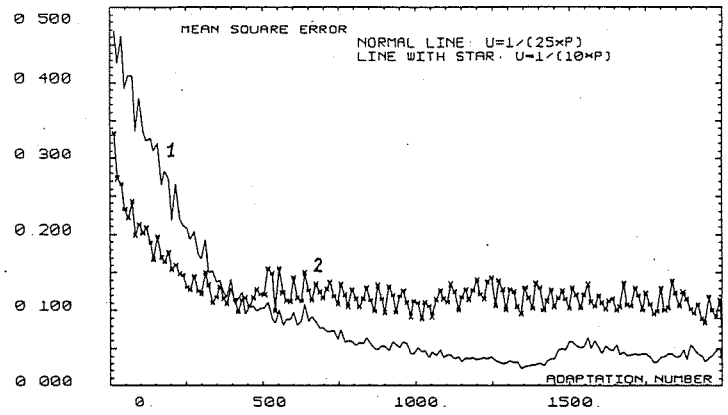


Figure 5.16: Convergence of the system. Curve 1: MSE with a smaller step-size; Curve 2: MSE with a larger step-size.

For nonstationary inputs, however, this is not always the case since the system has to follow the changes of the input signals. Smaller μ' may result in worse performance, as shown on table 5.2, where $d_a = d_f = 0.5$. The first row on the table shows different values of μ' and the second, the misadjustment, M in the steady-state. It can be observed that for the nonstationary inputs smaller μ' does not lead to better performance. The optimum value of μ' for the simulated nonstationary inputs with $d_a = d_f = 0.5$ is 0.1-0.2.

Optimization of the μ-vector LMS algorithm

Table 5.3 shows the performance of the system with different values of β ($d_a = d_v = 0.5$). It can be seen in the table that for $d_a = d_f = 0.5$, the optimum value of β is equal to 0.6, which leads to a minimum misadjustment.

Table 5.2: Effect of μ' on the system performance with nonstationary inputs ($d_a = d_f = 0.5$, $\beta = 0.04$, SNR=-7.8dB)

Values of the step-size μ'	0.005	0.01	0.02	0.04	0.1	0.2
Misadjustment, M	0.630	0.473	0.417	0.398	0.357	0.358

Table 5.3: Effect of β on the system performance

Nonstationary factor, β	0.8	0.6	0.4	0.2	0.0
Misadjustment, M	0.359	0.343	0.357	0.462	0.788

Fig.5.17 shows the performance of the system with different β in the frequency domain. Curve 1 is the power spectrum of the primary input (512 s data). Curve 2 and 3 are the system outputs with $\beta = 0$ and $\beta = 0.04$, respectively. From this figure we can see that the power of the simulated gastric signal is little affected by the system: 2.5 dB reduction for the maximum value with $\beta = 0$; 3.5 dB with $\beta = 0.04$. The power of the respiratory artifact and the white noise is substantially reduced: 44 dB reduction of the maximum power of the respiratory artifact with $\beta = 0$ and 59 dB reduction with $\beta = 0.04$. The noise level is reduced by about 55 dB. We can also observe that better performance (15 dB more reduction of the respiratory artifact) is achieved by the μ-vector LMS algorithm.

Effect of the SNR

Experiments with different SNR of the primary input have been conducted and the results are shown in table 5.4. It can be seen that as the SNR of the input signal increases the misadjustment gets smaller and smaller, i.e., better performance can be obtained with higher SNR.

Table 5.4: Effect of SNR of the primary input on the system performance. ($d_a = d_f = 0.5$, $\mu' = 0.04$, $\alpha = 0.04$)

Signal-to-noise Ratio,SNR (dB)	-16.7	-7.8	-1.2	10.8	17.8
Misadjustment, M	0.708	0.398	0.157	0.149	0.148

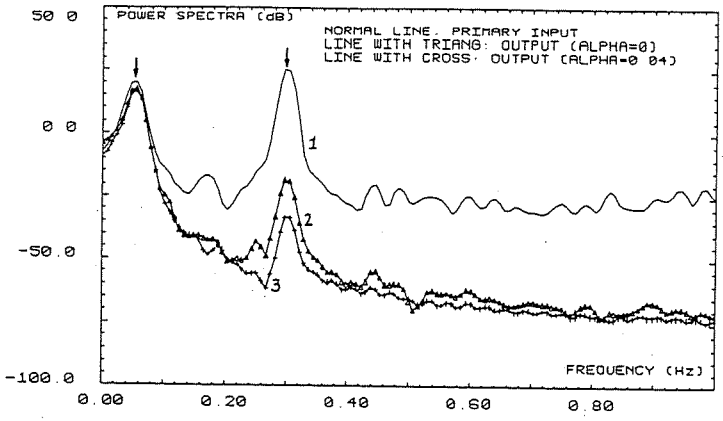


Figure 5.17: Performance of the system. Curve 1: power spectrum of the primary input; Curve 2: output power spectrum with LMS algorithm; Curve 3: output power spectrum with μ-LMS algorithm ($\beta = 0.04$).

Nonstationary effect

We have shown in Fig.5.16 and that with stationary inputs better performance can always be achieved by choosing smaller μ'. With nonstationary inputs this is not always true because smaller μ' results in slower convergence and makes the system less able to follow the changes of the input signal and thus leads to larger misadjustment (see table 2). Optimum values of β can be found for different nonstationary signals. To see this several experiments have been done. In table 5.5 we fix the value of β (=0.04), but vary the parameters d_a and d_f. From the table we can see that $\beta = 0.04$ is more suitable for $d_a = d_f = 0.3$ than for others. When the deviations of the frequency and of the amplitude of the signal are further away from 0.3, the performance of the system with $\beta = 0.04$ becomes worse. The last column in the table means that the input signals are stationary and thus the best performance is obtained.

Table 5.5: Effect of time variations of the frequency and the amplitude of the signal on the system performance. ($\mu' = 0.04$, $\beta = 0.04$, SNR=-7.8 dB)

Variation degree, d_a, d_f	0.7	0.5	0.3	0.2	0.1	0.0
Misadjustment, M	0.488	0.398	0.319	0.398	0.414	0.2

Effect of the pre-processing

Fig.5.14 has already shown the performance of the pre-processing. It is known that some uncorrelated noise (not necessarily white noise as in the simulations) can be reduced by the pre-processing. Fig.5.18 presents the improvement achieved by the pre-processing for the simulated signals. Curve 1 is the power spectrum (512s data) of the system output without the pre-processing and curve 2 is that with the pre-processing. In the figure we can find that the power of the simulated gastric signal and the simulated respiratory artifact is not affected by the pre-processing but more white noise reduction is obtained by the pre-processing.

It should be noted that in most of the above experiments bad conditions were simulated:

1. Very low SNR (-7.8dB).
2. Big changes of the frequency and the amplitude of the gastric signal (50% deviations)
3. Bad reference signal (the waveform of the gastric signal, s_{1j} in the reference input is completely different from that, s_j, in the primary input).

In reality, however the SNR is normally higher than -7.8 dB, the time variations of the gastric signal may not be so fast and the waveform of the gastric signals in different EGG recordings are more similar with each other than in the above simulations.

Assuming better conditions, $d_a = d_f = 0$, SNR=-1.1, and choosing a smaller μ'(=0.01), we have conducted one more experiment. The results are shown in Fig.5.19 and Fig.5.20. Fig.5.19 shows the power spectra of the primary input (curve 1) and the system output (curve 2). It is seen that the gastric signal is hardly affected while the respiratory artifact and the white noise are significantly reduced. In Fig.5.20 we present the original gastric signal in the primary input and the system output in time domain, from which we can see that the waveform of the gastric signal is little affected.

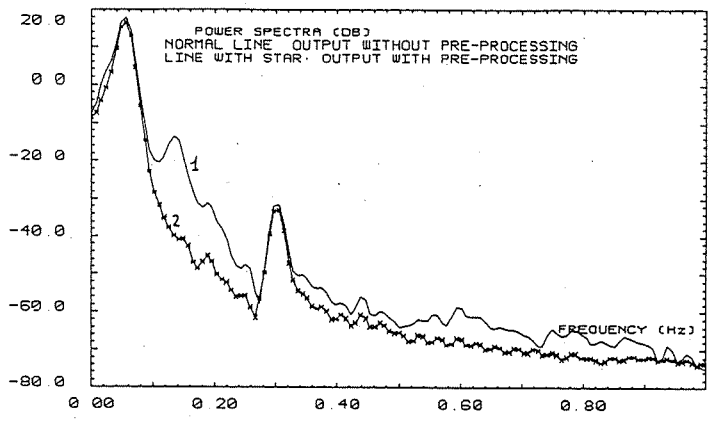


Figure 5.18: Effect of the pre-processing. Curve 1: power spectrum of the system output without the pre-processing; Curve 2: with the pre-processing.

5.4.4 Result and application

The proposed adaptive signal enhancing system has been successfully used for real cutaneous gastric signal processing. Our experiments with more than 15 measurements (each more than 1 hour) have shown that the system is efficient and is simple to use or to implement.

With sampling frequency of 2Hz, following suitable values have been found: the length of the adaptive filter, N=50-60; the step-size $\mu' = 0.06$ and the nonstationary factor, $\beta = 0.04$.

Fig.5.21 shows one of the results. Fig.5.21a–21d show four different positional EGG's and Fig.5.21e and 5.21f are the adaptive enhancing outputs of the signal EGG_0. In Fig.5.21e only EGG_1 is used as the reference input and in Fig.5.21f, three reference inputs EGG_1, EGG_2 and EGG_3 are used. The improvement of the system output quality by using more reference inputs can be seen by comparing Fig.5.21e and Fig.5.21f.

As we have mentioned that the quality of the EGG is usually poor and the waveform analysis of the EGG is difficult. Applying the adaptive system

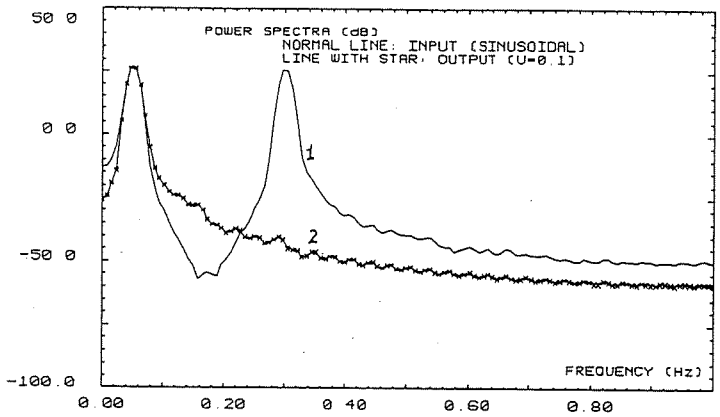


Figure 5.19: Performance of the system in a stationary environment. Curve 1: power spectrum of the primary input signal; Curve 2: system output.

in this paper, however, we can improve the SNR of the EGG significantly. This makes the direct waveform analysis of the EGG easier, and more information can be extracted from the EGG, such as the changes of the frequency and the amplitude of the gastric signal, the different patterns of the EGG waveform associated to different subjects (if there are any) and so on. In words, the importance of making detailed waveform analysis feasible can not be overstressed.

5.4.5 Summary

In this section an adaptive signal enhancing system is proposed for the human EGG. The performance of the proposed system has been thoroughly investigated. It has been shown that the system can substantially reduce the respiratory artifact, the ECG, the noise resulting from electrode-skin interface and some motion artifacts. The gastric signal component in the EGG is, however little affected by the system. Consequently, the signal-to-noise ratio of the EGG can be significantly improved.

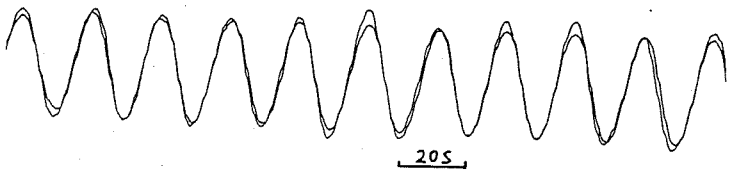


Figure 5.20: Comparison of the input signal waveform and the output signal waveform

5.5 Adaptive Cancellation of Respiratory Artifact

The respiratory disturbance superimposes upon almost all of the EGG recordings and even internal gastric recordings. Sometimes, it may completely obscure the electrogastric signal. Thus "the importance of ruling out respiratory artifact, especially upon the external EGG but also on the internal recording can not be overstressed" (p83, Stern 1985).

In section 5.4 we proposed an adaptive enhancing system to eliminate most of the noise including respiratory disturbance. From the previous discussion we know that the adaptive enhancing system can only work properly if the fundamental frequency of the gastric signal does not overlap with that of the respiratory disturbance. This may happen in some abnormal situations, as we mentioned previously. In that case the proposed adaptive enhancing system becomes impractical since the lowpass FIR filter in the reference channels will also filter out the gastric signal component.

In this section we propose an adaptive method for the cancellation of the respiratory artifact in both EGG and intraluminal recordings (chen 1987b, 1989b). The technique to be discussed is suitable for the cancellation of the respiratory artifact not only in the EGG but also in the ECG and in electrointestinal recordings. This section is structured as follows: We first describe the methods for measuring the intraluminal gastric signal and the reference respiratory signal, and then the basic principle of the adaptive noise cancellation and finally the results.

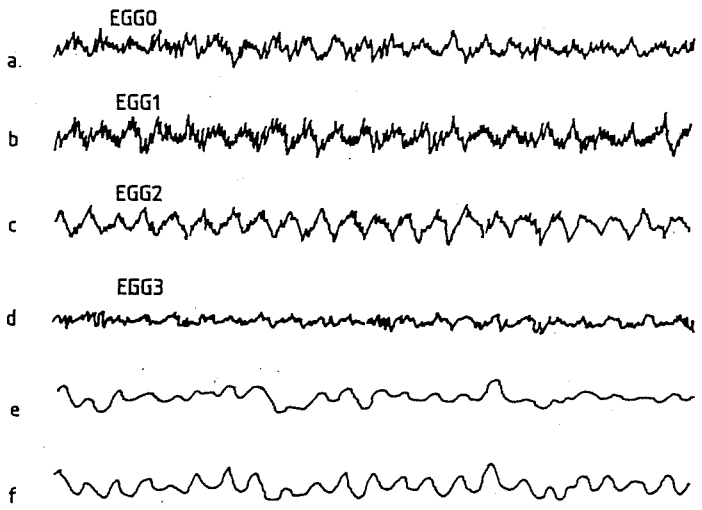


Figure 5.21: Results of the adaptive enhancement of the EGG. a)–d) Four channel EGG signals; e) Enhanced output signal with one reference signal; d) Enhanced output signal with three reference signals.

5.5.1 Measurement

The way of measuring the cutaneous EGG was described in section 5.3 and is not repeated here.

The intraluminal bipolar gastric signal is measured by asking volunteers to swallow down a small tube with suction electrodes in it. The distance between each pair of the electrodes in 3 *mm*. The electrodes are placed in the distal antrum, facing the mucosa under the monitoring of fluoroscopy.

The reference respiratory signal is measured by fastening a small balloon filled with water, on the abdomen near the diaphram, but away from the stomach. The small balloon is connected to a pressure sensor.

Both the intraluminal gastric recording and the reference respiratory

signal are amplified, displayed on Mingograf paper and stored on an analog tape in the same way as for the EGG recordings.

Some typical measurements are shown in figure 5.22, where all three tracings were simultaneously measured from a volunteer. Tracing a) is a bipolar cutaneous EGG, b) an intraluminal gastric signal and c) the respiration. From b) we see that even the intraluminal recording has heavy respiratory artifact.

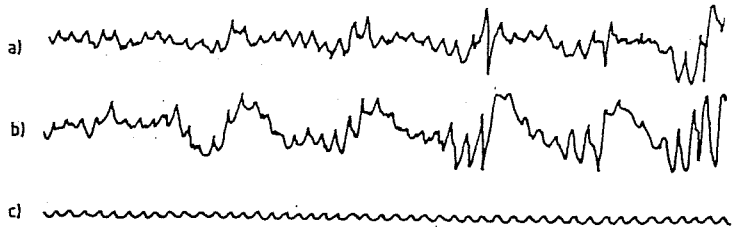


Figure 5.22: Cutaneous (a) and intraluminal (b) electrogastric signals and respiratory signal (c)

In section 5.3 we claimed that slow activity in the EGG is originated from the stomach. Now comparing the tracing a) and b) we can be convinced about that statement since the slow activities in these two tracings have the same characteristics. Figure 5.23 shows the cross-correlation power spectrum between the EGG and the intraluminal recording. From this figure we observe a peak at the frequency of the gastric signal. This shows more evidently that the slow wave in the EGG does originate from the stomach.

The power spectrum of the correlation function between the EGG and the respiratory signal is shown in figure 5.24. It has a higher value at around 0.3 Hz, which shows that the frequency component around 0.3 Hz in the EGG is really the respiratory artifact.

5.5.2 Adaptive cancellation of the respiratory artifact

The adaptive cancellation system is shown in figure 5.25, where Δ stands for delay in samples, "AF" for the adaptive filter. The system contains

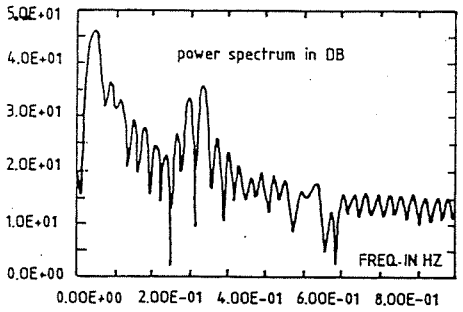


Figure 5.23: Power spectrum of the cross correlation between the cutaneous and the intraluminal gastric signals

two stages of which the first stage is the ALE and the second stage is an adaptive noise canceller.

The input to the ALE is the EGG measurement. It contains the gastric signal s, the respiratory disturbance r and some non-periodic noise n. Ideally, the output of the ALE contains only $s + r$, which is used as the primary input of the second stage. The reference input of the second stage is a measured respiratory signal $\tilde{r}$. The coefficients of the adaptive filters are adapted according to the LMS algorithm. After the convergence, the mean square error is minimized. From the figure the mean square error of the last stage can be written as

$$E[e^2] = e[s^2] + 2E[s(r-y)] + E[(r-y)^2] \tag{5.15}$$

Since y is the convolution of the filter input and the filter weights and since the filter input $\tilde{r}$ is not correlated with the gastric signal s, therefore the second term in the right hand side of Eq(5.15) turns out to be zero and

$$E[e^2] = e[s^2] + E[(r-y)^2] \tag{5.16}$$

Consequently, the mean square error can only be minimized if and only if:

$$E[(r-y)^2] = 0 \tag{5.17}$$

Then,

$$E[e^2] = E[s^2] \tag{5.18}$$

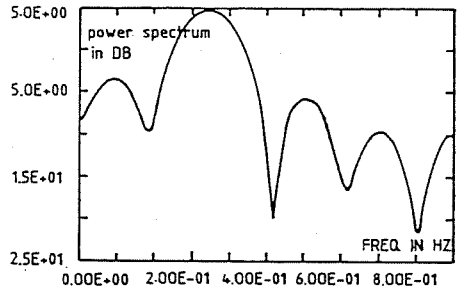


Figure 5.24: Power spectrum of the cross correlation between the cutaneous EGG and the respiratory signal

That is, the system output e_j is a best estimate of the gastric signal s_j in the sense of the mean square error.

In a similar way as we did in section 5.4, the performance of the proposed adaptive respiratory artifact cancellation system was investigated. A detailed discussion can be found in (Chen 1989b).

5.5.3 Results

Experiments with both the intraluminal recordings and the cutaneous EGG's have been done by applying the system shown in Fig.5.25. The results are shown in figures 5.26 – 5.28.

The length of the adaptive filter in the ALE is chosen to be 50, For the second adaptive filter, the aim is to produce a replica of the respiratory disturbance and the possible longest period of the respiration is about 5 seconds (10 samples), thus its length is set to be 10.

The delay Δ is chosen to be 1 (this value is not sensitive according to the experiments). The step-size μ is set to be $0.01/G$ (G is the input power to the adaptive filter) for the first stage and $0.05/G$ for the last stage.

The processed result of the cutaneous EGG is shown in Fig.5.26, where the upper line is the power spectrum (in dB) of the input signal and the lower line is that of the filtered output. We see that the frequency component of the respiratory disturbance is eliminated. Fig.5.27 shows the result

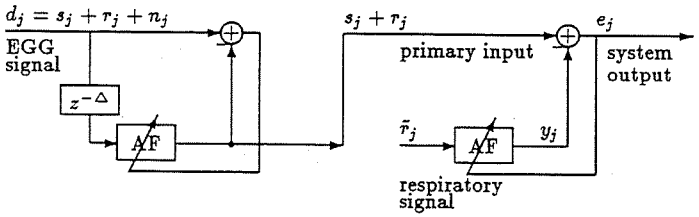


Figure 5.25: Adaptive system for the cancellation of respiratory disturbance. d_j – input EGG signal to be processed; $\tilde{r}_j$ – referencing respiratory signal.

for the intraluminal recording. The upper line is the power spectrum of the input and the lower line, the output. It can be seen that the respiratory disturbance is completely cancelled. The gastric signal component (around 0.05 Hz) is, however not affected by the system. The cancellation of the respiratory artifact in the intraluminal recording in time domain is presented in Fig.5.28, where a) is the input and b), the filtered output. The cancellation of the respiratory artifact can be clearly observed in this figure.

5.5.4 Discussion and Conclusion

We have shown both intraluminal and cutaneous gastric recordings. The cross correlations between the cutaneous EGG and the intraluminal gastric recording and between the EGG and the respiratory signal have been calculated. Thereby, the origins of the main components of the cutaneous EGG are shown.

The adaptive system for the cancellation of the respiratory artifact is developed and shown to be very efficient, i.e., respiratory artifact is almost completely removed, while the interesting gastric component is not affected.

Besides the cancellation of the respiratory artifact in the gastric recordings, the proposed system is also applicable to other biomedical signal analysis. One of the other attractive applications is the cancellation of the respiratory artifact in intestinal measurements, where the frequencies of the intestinal signal overlaps with that of the respiration. Another possible application may be the cancellation of the baseline drift in ECG signals.

The drawback of the system proposed in this section compared with that in section 5.4 is that an additional sensor is needed. Another possible problem in practice is that the measurements of the EGG and the respiration

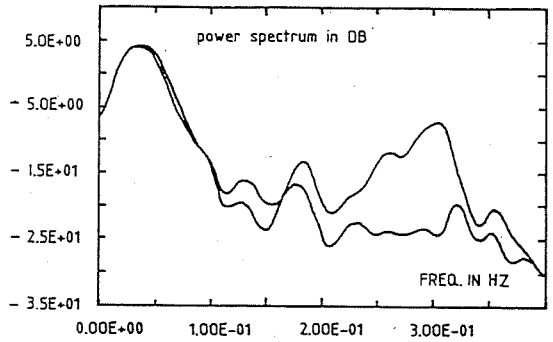


Figure 5.26: Cancellation of the respiratory artifact in the cutaneous EGG. Upper curve: power spectrum of the input; Lower curve: the output.

have different dynamic ranges. Therefore different factors of amplifications are needed in order to use one single multi-channel A/D convertor.

5.6 Information Available to be Extracted in an EGG

As we have discussed in previous sections, the electrogastric signal can be successfully measured from the abdomen. Using the proposed adaptive filtering techniques waveform analysis can be performed. Now at this point we'd like to raise a question: "what can be expected from a cutaneous EGG?"

Assuming that the cutaneous EGG is a combination of all of the internal gastric activities, we start with simulations of internal (serosal) gastric signals and then transfer those simulated gastric signals on to the abdomen to construct cutaneous EGG's according to the volume conduct theory.

Based on the characteristics of serosal measurements, we simulate gastric signals in section 5.6.1, and then in section 5.6.2 we discuss the transfer of the gastric signals from the stomach to the abdominal skin. The simulated results, assuming that only slow wave exists in the stomach are shown in section 5.6.3. The simultions with both slow wave and second potential taken into account are presented in section 5.6.4. Finally the conclusion on

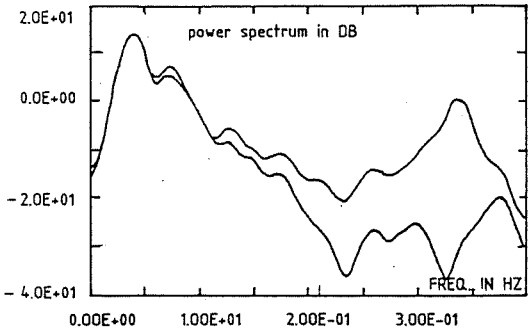


Figure 5.27: Cancellation of the respiratory artifact in the intraluminal recording. Upper curve: power spectrum of the input; Lower curve: the output.

what we may expect from the EGG can be found in section 5.6.5.

Since the information about the myoelectrical gastric activities is much more available for dogs than for humans, internal gastric signals are simulated according to canine gastric activities. However, it is believed (Stern 1985) that there is no big difference between canine gastric activities and human gastric activities except the difference in frequency. We believe that results and conclusion obtained from the simulations are relevant to the research on the human EGG.

5.6.1 Simulation of internal gastric signal

In section 5.2 we discussed that there are two sorts of electric signals in the stomach: the slow wave and the contraction related second potential with or without spikes. In this and the next sections, we assume the latter is absent.

The frequency of the slow wave in the canine stomach is about 5 cycles/min. It propagates from the corpus to the pylorus with increasing amplitude and velocity. The maximum amplitude is about 0-1 *mv* in the corpus and 2-3 *mv* in the antrum. The propagation velocity is about 0.1-0.2 cm/second in the orad corpus and 1.5-4.0 cm/second in the antrum. The total phase lag from the originating point in the corpus to the pylorus

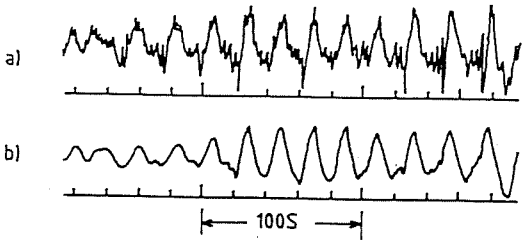


Figure 5.28: Cancellation of the respiratory artifact (time domain). Upper curve: the intraluminal recording; Lower curve: the output.

is about 3 cycles. Sarna (Sarna 1972) stated that the longitudinal phase lag(degrees/cm) is around 70-100 degrees/cm near the most proximal site and around 8-20 degrees/cm near the pylorus in different dogs.

For the simulation of the slow wave, we simply assume that the stomach is cylindrical and all slow waves concentrate in one vertical line, propagating from the top, corresponding to the origin in the corpus, to the bottom, corresponding to the pylorus. The circumferential propagation is ignored.

The internal gastric signal is simulated as follows (Chen 1984): The first portion of the slow wave is assumed to be a rectified sinusoid with duration of 1.6 seconds, followed by zeroes with duration of 10.4 seconds. Both the amplitude and the propagation velocity increase acceleratively distally from 0 to 1 *mv* in the corpus and 2 to 3 *mv* in the antrum. The total phase shift is designed to be 3 cycles, 2.5 cycles in the corpus and 0.5 in the antrum.

The simulated signals are shown in Fig.5.29. Number 1 to 9 stand for different positions in the stomach with 1 referring to the originating point of the slow wave, 5 to the junction between the corpus and the antrum and 9 to the pylorus.

5.6.2 Transfer from the stomach to the abdomen

The EGG at a certain point on the abdomen is a summation of contributions of all internal gastric activities to that point. In order to simulate the EGG, we first discuss the relevant electrical properties of the biological materials and their effects.

The propagation of the electric activity in the smooth muscle results from the depolarizing effect of action currents on surrounding resting membranes. When a membrane is activated, the current density is strongest

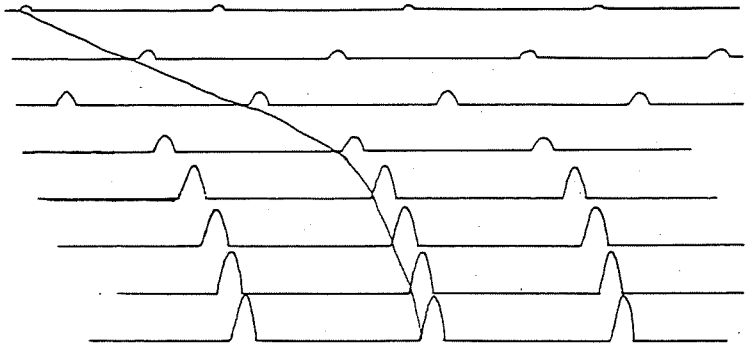


Figure 5.29: Simuled gastric signals in the stomach. From top to bottom: corpus to pylorus

in the immediate vicinity, but there will be current everywhere in the surrounding medium.

Assume the medium is linear, homogenous, isotropic and characterized by physical parameters, $\tilde{\mu}, \tilde{\sigma}$ and ξ, the potential φ at point (x', y', z') due to a volume current source density $I_v(x, y, z)$ can be calculated according to the following formula (Plonsey 1969):

$$\varphi(x', y', z') = \frac{1}{4\pi(\tilde{\sigma} + i\omega\xi)} \int \frac{I_v(x, y, z)e^{-ikr}}{r} dv \tag{5.19}$$

where, $\tilde{\mu}$ – permeabilty, $\tilde{\sigma}$ – conductivity, ξ – dielectric constant, $i = \sqrt{-1}$ and ω – angular frequency.

$$k^2 = -i\omega\tilde{\mu}\tilde{\sigma}(1 + \frac{i\omega\xi}{\tilde{\sigma}}) \tag{5.20}$$

r is the distance between the source point and the field point,

$$r^2 = (x - x')^2 + (y - y')^2 + (z - z')^2 \tag{5.21}$$

The unprimed variables referring to the source point, the primed variables to the field point.

Table 5.6: Conductivity of biological tissues

Tissue	*Mean conductivity (mhos/m)*
Blood	0.67
Lung	0.05
Liver	0.14
Fat	0.04
Human trunk	0.21

According to the electrical properties of biological material (Schuan 1957, Plonsey 1961, Rush 1963). The ratio of displacement to conduction current

$$\frac{i\omega\xi}{\tilde{\sigma}} << 1 \tag{5.22}$$

That is,

$$\tilde{\sigma} + i\omega\xi \doteq \sigma \tag{5.23}$$

The term e^{-ikr} in Eq(5.19) represents the phase delay, the time required for changes at the source to "propagate" to a field point. It can be written as:

$$e^{-ikr} = 1 - ikr - \frac{(kr)^2}{2!} - i\frac{(kr)^3}{3!} + \cdots \tag{5.24}$$

Table 5.6 lists the conductivity of biological tissues, from which we see that the conductivity of fat is low. Since the media for the propagation of slow waves from the serosa of the stomach to the abdominal skin is mainly fat and human trunk, we choose an average value of 0.125.

Because of the absence of magnetic materials in the media, the permeability, $\tilde{\mu}$ is the free space value of $4\pi \times 10^{-7}$ $henry/m$. The maximum distance r_{max} between the stomach and the abdomen is less than 0.5 m.

According to the above values of $\tilde{\mu}, \tilde{\sigma}$ and r_{max} we have

$$kr = \sqrt{-i\omega\tilde{\mu}\tilde{\sigma}(1 + \frac{i\omega\xi}{\tilde{\sigma}})}\, r < 0.00157(1 - i) \tag{5.25}$$

where the value $(1 + \frac{i\omega\xi}{\tilde{\sigma}})$ is conservatively set to be 2 and e^{-ikr} is set to be 1 and $\omega_{max}, 2\pi \times 10$ since the highest frequency component of the gastric signal is less than 10 Hz.

Finally, the potential at field points (x,y,z) can be simplified as

$$\varphi(x', y', z') = \frac{1}{4\pi\tilde{\sigma}} \int_v \frac{I_v(x, y, z)}{r} dv \tag{5.26}$$

Now assume there exist M current sources along the vertical axis of the stomach and these current sources are simulated gastric signals shown in Fig.5.29. Denote the kth internal gastric signal at discrete time j as $ECA(k,j)$ and the nth cutaneous gastric signal as $EGG(n,j)$, we have

$$EGG(n,j) = b\sum_{k=1}^{M}\frac{ECA(k,j)}{r_{n,k}} \tag{5.27}$$

where b is a constant factor, $r_{n,k}$ is the distance between the measure point on the abdomen and the kth internal source signal. $r_{n,k}$ is associated with the width of the fat in between the stomach and the abdomen and with the size of the stomach.

From Eq(5.27) we see that the cutaneous EGG is a weighted summation of internal gastric activities.

Results

Based on Eq(5.27) and simulated internal gastric signal $ECA(k,j)$ cutaneous gastric signals on the different positions can be calculated. Figure 5.30 shows the simulated EGG's outside the stomach. The number of the curves corresponds to the positions of the EGG from the corpus to the pylorus. From this figure we observe that there are no phase shifts among the EGG signals outside the corpus (curve 1 to 4), but there exist phase shifts among those outside the antrum (curve 5 to 9). This phenomenon can be explained in the following way: The cutaneous signal at point n is a weighted summation of all the internal signals. But the weight for nth internal signal $ECA(n,j)$ has a maximum value. That is, the nth internal signal has a dominant contribution to the $EGG(n,j)$ at point n, which makes different positional EGG's to have different characteristics. Therefore phase shifts may be observable.

For the EGG's outside the corpus, however the internal signals with larger weights are those in the corpus, which are much weaker. Consequently, the cutaneous EGG's outside the corpus are not dominated by their corresponding internal signals, but by ensemble internal signals in the antrum. This strengthens the common feature of the different positional EGG's outside the corpus and thus phase shifts are hardly observable.

An important factor that determines whether phase shifts can be observed or not is the ratio of the longitudinal size of the stomach to the width of the fat in between the stomach and the skin. We call it the observability factor denoted by γ

$$\gamma = \frac{\text{longitudinal size of the stomach}}{\text{fat width}} \tag{5.28}$$

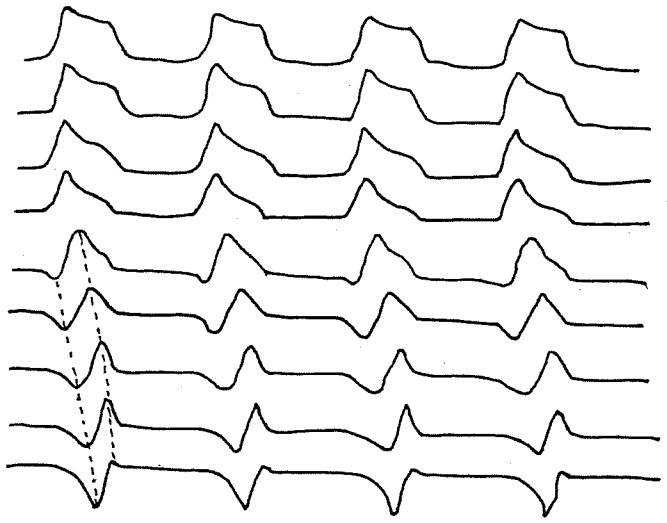


Figure 5.30: Simulated cutaneous electrogastric signals

The observability of phase shifts among cutaneous gastric signals increases as γ gets larger. If γ is infinity, the cutaneous EGG becomes an internal signal and obviously phase shifts are observable. On the other hand, if γ is zero, then no phase shifts can be detected since the internal electrogastric signal becomes a point source. In figure 5.30, γ is set to be 10. More details on the effect of the parameter γ can be read in (Chen 1984).

5.6.3 Simulation with contractions

In the following we simulate cutaneous EGG's by including contraction related gastric activities. The purposes are twofolds: 1) whether spikes can be observed; 2) whether phase shifts are still observable (Chen 1985).

Simulation of the internal signal

It is generally accepted that phasic contractions in the terminal antrum are initiated by discrete spike potentials, whereas phasic contractions in the corpus and in the orad antrum are regulated by plateau potentials. being different from the slow wave, the spikes occur at random and do not propagate from one region to another. The mean duration of the bursts of spikes is approximately 5 seconds and the mean number of undulations in each burst is about 5 (Bass 1961).

The configuration of simulated internal gastric signals in the corpus and in the antrum are shown in figure 5.31a and 5.31b, respectively. In the corpus the slow wave is followed by a prolonged plateau with duration of 4 seconds and a times the maximum amplitude of the corresponding slow wave. In the antrum the slow wave is followed by 5 discrete spikes superimposed on the plateau potential. The initial phase of each spike is random and the amplitude is also random within the range of 0-0.5 times the maximum amplitude of the slow wave. The duration of each spike is 0.75 seconds.

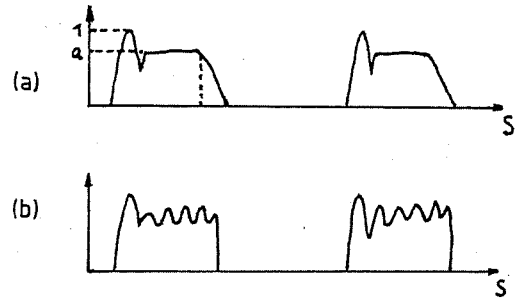


Figure 5.31: Configurations of gastric signals in the antrum

Results

Assume the observability factor γ equal to 10 and a equal to 0.5, the simulated cutaneous EGG at different positions are shown in figure 5.32. They are very different from those resulting from the simulation without second potentials. Instead of having a quiescent interval in each period, the waveform of the EGG looks like sinusoidal. It is clear from this figure that the different positional EGG's have different amplitudes. The values of the

EGG's are bigger outside the antrum than those outside the corpus (different scales are used for different EGG signals). The EGG's outside the corpus (upper 4 tracings) have very similar waveform and phase shifts are not observable. From the EGG's outside the antrum (lower 4 curves) we can see visually the distal shift of the total signal energy in each period although the phase shifts among the peaks are hardly seen. Comparing this figure with Fig.5.30 (with no contractions) we can see that the propagation of the gastric signal is more difficult to be detected when contractions (or second potentials) occur in the stomach.

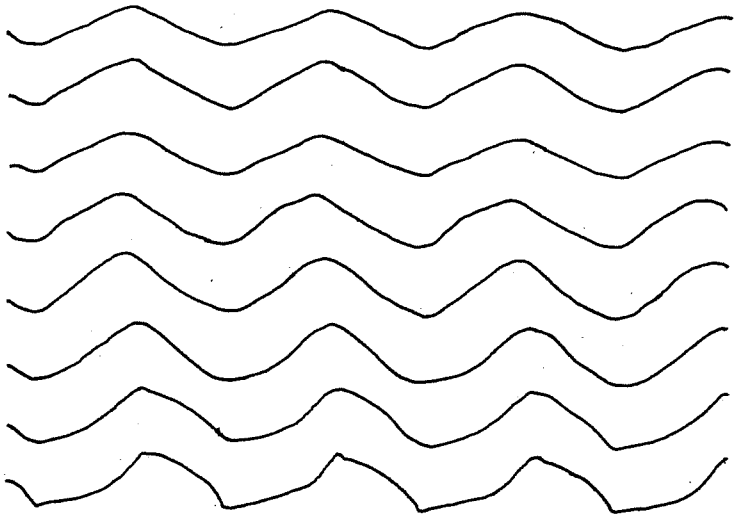


Figure 5.32: Simulated cutaneous electrogastric signals when contractions occur in the stomach

Another interesting result we can observe from Fig.5.32 is that almost no spike activities are observed in the EGG's. This is reasonable because spikes have random phase and do not propagate. They are cancelled with each other when being summed.

5.6.4 Discussion and conclusion

In order to know what we can expect from an EGG, simulations with or without contractions occurring in the stomach have been conducted. The following conclusions are made:

- The cutaneous EGG is a weighted summation of internal gastric activities.
- Phase shifs may not be observable among cutaneous EGG's outside the corpus of the stomach.
- Phase shifts may be observable among the EGG's outside the antrum.
- The observability is associated with the ratio of the longitudinal length of the antrum and the fat width. This is, it's easier to detect phase shifts from thin volunteers than from fat ones.
- The observability of phase shifts is related to the condition of the stomach. It becomes more difficult when contractions (second potentials) occur in the stomach.
- Spikes are not observable in cutaneous EGG's
- Cutaneous EGG's outside the antrum have higher amplitude than those outside the corpus.

5.7 Detection of Slow Wave Propagation

In the previous section it was concluded that phase shifts (that is, the propagation of the gastric activity) can be observed from cutaneous EGG's outside the antrum. However, it has been claimed by several researchers (Stern 1985, Familoni 1987) that the propagation of the slow wave could not be detected from the EGG' recordings. To the best of our knowledge no positive results have been reported on the human stomach.

Inspired by the computer simulation results we have done several clinical experiments and found the opposite answer: *the propagation of the slow wave can be detected from cutaneous EGG's.*

The reason why the propagation has never been observed from the cutaneous EGG's is that all the reported methods are not adequate for that purpose. In this section we'd like to point out that the stomach should be localized before the measurement and electrodes should be attached along the longitudinal axis of the stomach. By using an X-ray we observed the slow wave propagation in all 11 volunteers and diabetic patients (Chen 1988e, Van Cutsem 1988)

5.7.1 Localization of the stomach

Since the aim of the experiments is to detect the propagation of the slow wave, electrodes should be attached along the longitudinal axis of the stomach. The position of the stomach is, however different from one to another and even from time to time, especially before and after a meal. According to our experience no standard position, size and orientation of the stomach can be drawn. Therefore, before attaching electrodes to the abdomen, the stomach is first localized either by an ultra-sonic instrument or by an X-ray machine. Then four electrodes are attached on the abdomen along the longitudinal axis of the stomach. Bipolar signals are derived by connecting each electrode with a common reference electrode (position 0 in figure 5.33). In most of experiments, one or two intraluminal recordings are also made in order to check the origin of the cutaneous EGG's.

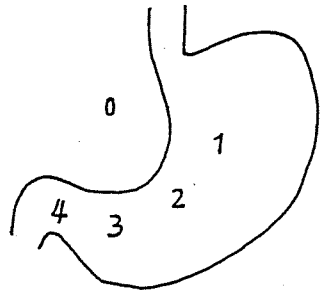


Figure 5.33: Positions of electrodes

It has been shown that with the localization of the stomach, the quality of the EGG's recorded is much higher (Chen 1989c). By using the same equipment and the same measurement set-up, we recorded EGG's from 15 volunteers without the localization of the stomach, no clear slow waves were recorded in about half of the measurements. With the localization by an ultra-sonic machine we recorded clear EGG's from all 10 volunteers, among which 2 are obese patients. With the localization by the x-ray we recorded very nice EGG's and observed the propagation of the slow wave from all the volunteers and patients during most of the recording time (Chen 1989c).

It should be noted that the localization of the stomach with the ultra-

sonic machine is very difficult, especially in the fasted state of the stomach, the position of the stomach can only roughly be localized.

5.7.2 Running cross correlation

A running cross correlation analysis method is developed (Chen 1988g) for calculating time lags among EGG's from different abdominal positions. It is explained as follows:

Suppose x_j and y_j are two discrete time signals at time j. The running cross correlation function $\Re_j(k)$ with lag k at time j is expressed as:

$$\Re_j(k) = \sum_{m=-N}^{N} x_{j+m} y_{j+m+k} \tag{5.29}$$

$$k = -p, -p+1, 0, 1, ..., p \text{ and } j = 0, M, 2M, 3M, ...$$

Where $(2N+1)$ is the length over which the cross correlation is calculated, p is the possible maximum absolute time lag between the signals x_j and y_j, M is the step-size for calculating the time lag (if it is chosen to be 1 the time lag is then calculated at each input sample).

The time lag ρ_j between signal x_j and y_j at time j is defined as:

$$\rho_j = l \text{ if } \Re_j(l) \geq \Re_j(k) \text{ for } -p \leq k \leq p, k \neq l \tag{5.30}$$

The above equations can be interpreted as follows: First a segment of each signal with length of $(2N+1)$ is selected, cross correlations with lag from $-p$ to p are calculated and compared with each other. The lag l with which the cross correlation attains its maximum is assigned as the time lag at that time. Next the process is repeated by shifting M samples forward and selecting a new segment of each signal.

5.7.3 Results

Two different ways of the localization of the stomach are applied: the ultrasound localization and x-ray localization.

Using the localization technique of the stomach by an ultra-sonic instrument, following experiments have been conducted and the results are given:

1. Thin fasted volunteers: 3 volunteers fasted over night with weight a little bit less than normal persons were asked for measurements. Slow waves were clearly recorded from all these 3 volunteers. Phase shifts among the different EGG's were observed from 2 volunteers during most of the recording time (1-2 hour).

2. Fat fasted volunteers: Slow waves were well recorded from two obese volunteers (one with weight of 190 kg and the other 120 kg) fasted over night. But no phase shifts were observed from the EGG's.

3. Postprandial volunteers: Phase shifts were observed from 2 thin volunteers (60kg/180cm) during about 50% of the recording time (0.5 hour). The EGG's were measured half an hour after having a normal meal. No phase shifts were observed postprandially from a volunteer with normal weight.

Using the localization by the x-ray machine, 2 sets of experiments were done:

1. Thin fasted volunteers: Slow waves were clearly recorded from 6 thin volunteers fasted over night (two females with average weight/height = 33kg/m, four males with average=39.3kg/m). Phase shifts were observed from all volunteers for more than 85% of the recording time (1-2 hour for each).

2. Fasted diabetic patients: Phase shifts were observed from all 5 patients for about 80% of the recording time (1-2 hour for each). No obvious difference was observed in the EGG's between the normal volunteers and the diabetic patients.

Figure 5.34 shows 4 channel cutaneous recordings from a fasted diabetic patient. The electrode positions are shown in figure 5.33. These recordings were lowpass filtered with a cutoff frequency of 0.5 Hz. Visually we can observe phase shifts between channel 1 and 2, and between channel 2 and 3. Channel 1 and 4 have about the opposite phase.

Figure 5.35 shows a portion of the adaptively enhanced EGG's shown in Fig.5.34 by using the technique described in section 5.4. From this figure we can clearly see the phase shifts among different channels.

The time lags calculated by the running cross correlation method are shown from figure 5.36. where the horizontal axis stands for time in seconds and the vertical axis for the time lag in seconds. In the calculations a segment of 40 second samples is selected at each time and the possible maximum time lag between two adjacent channels is assumed to be 15 seconds (p equals 15 times the sampling frequency). The time lags are calculated for every 10 seconds. Fig.5.36a shows the time lag between channel 1 and channel 2. The average time lag is about 4 seconds. The time lag between channel 2 and channel 3 is shown in Fig.5.36b and the average time lag is about 4 seconds. In Fig.5.36c we observe that the time lag between channel 3 and channel 4 is about 0.5-1 second.

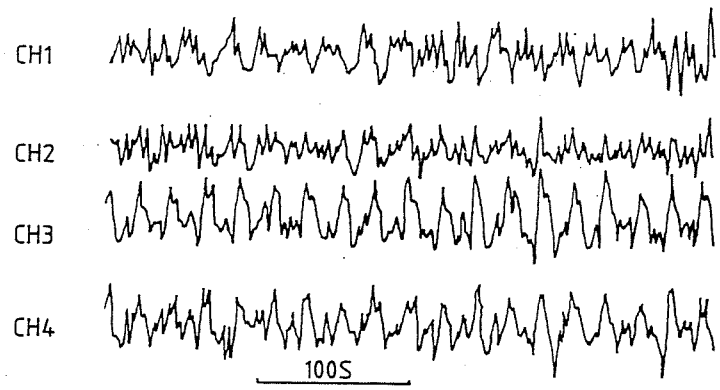


Figure 5.34: Four channel cutaneous electrogastric signals

5.7.4 Discussion and Conclusion

We have experimentally shown in this section that the propagation of the slow wave in the stomach can be detected from cutaneous recordings. The conventional methods found in the literature are not adequate for the detection of the propagation. The stomach should be carefully localized before the measurement. Electrodes should be attached along the longitudinal axis of the stomach.

Four electrodes are attached along the vertical axis of the stomach. Generally the upper two electrodes are outside the corpus while the lower two are outside the antrum. According to a statistical investigation of all experiments, we have found that usually there is no phase shift between channel 1 and channel 2, bigger phase shift between channel 2 and 3, small phase shif between channel 3 and 4. This is coincident with the computer simulation results shown in section 5.6. The results illustrated in Fig.5.36 show one of few counter examples to the above statistical conclusion.

The average total phase shift observed among 4 channels is about 7-8 seconds which agrees with the simulation results. This may imply the total

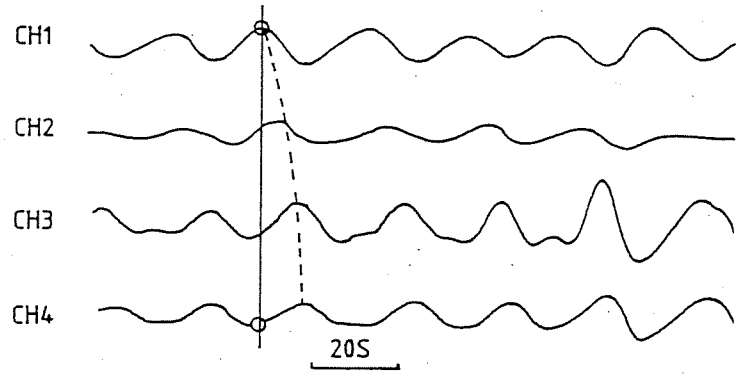


Figure 5.35: A portion of the filtered signals shown in Fig.5.34

phase shift of internal slow waves in the antrum.

The experimental results show that it is easier to detect phase shifts from thin volunteers than from thick ones. It becomes very difficult for very thick volunteers.

We have observed that it is easier to detect phase shifts in a fasted situation than in a postprandial situation. The reason could be that there exist more contractions in the postprandial case. The contraction related gastric activities make it more difficult to detect phase shifts from EGG's.

Spikes are sometimes recorded from intraluminal electrodes, but have not been observed in any cutaneous EGG's.

5.8 Adaptive Spectral Analysis

In the previous sections we have discussed adaptive signal processing techniques in time domain. In this section we will shift our attention to the frequency domain: spectral analysis of cutaneous EGG's.

The gastric frequency component can be extracted from the EGG by means of Fourier analysis (Linkens 1974, Brown 1975, Smallwood 1975, Smout 1980). Its disadvantage is, however that the time information is

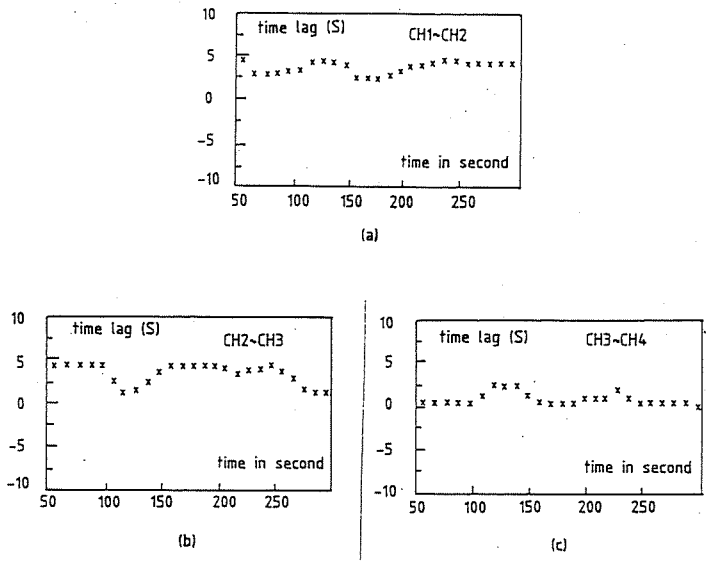


Figure 5.36: Time lags among different channel EGG signals

completely missing.

In order to extract both time and frequency information from the EGG, the autoregression modelling method (Linken 1978) and the running spectral analysis method (Van der Schee 1987) were applied.

In this section we apply the adaptive ARMA spectral analysis method proposed in chapter 5 to analyze EGG signals (Chen 1988f).

5.8.1 Gastric dysrhythmias

Three sorts of electrogastric activities have been found in the stomach: slow wave, plateau potential and spikes. The only rhythm which can be detected by cutaneous electrodes is that of the slow wave. The normal frequency of the slow wave is about 0.05 Hz. It is slightly varying over time.

Some abnormal electrical behaviors have been found such as tachygastria (Telander 1978, Cullikson 1980, You 1981, Bellahsene 1986, Chen

1989c), which seems to be related to gastric disorders. Figure 5.37 shows a tachygastrial tracing recorded from a patient with mild gastrites who claimed feeling nausea sometimes during the measurement. Tracing a) is the cutaneous EGG and b) is the respiratory signal. From this figure we see that in certain periods the slow wave has a normal frequency while in some other periods, it has a much higher frequency. The power spectrum of the signal is shown in figure 5.11, where different gastric components can be seen but the information about alternations of the frequency is missing.

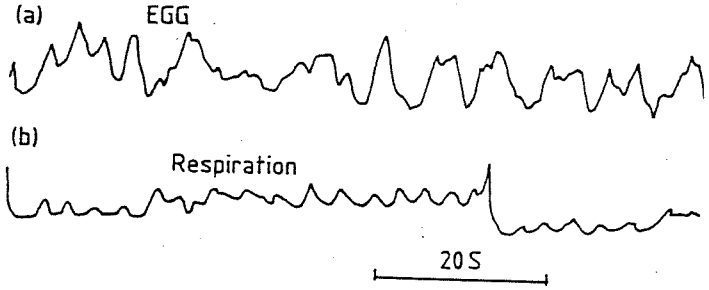


Figure 5.37: Tachygastrial EGG signal (a) and simultaneously recorded respiration.

In a postprandial situation, electrogastric activities become complicated because of the contractions of the smooth muscle. Lower frequency components (< 2 cycle/min) have been observed (Van der Schee 1983, Stern 1985). Recently we have observed higher frequency components in a postprandial study of the EGG (Chen 1988f).

In summary the frequency of the slow wave in the stomach is not time invariant. In some abnormal and postprandial situations, the rhythm of the gastric signal is time varying. In order to investigate the change of the gastric frequency over time, some techniques which can provide both time and frequency information are required.

5.8.2 Adaptive spectral analysis

The running spectral analysis method was applied in the analysis of EGG signals (Van der Schee 1987). The principle of the running spectral analysis is explained as follows: For a time series x_j at time j, first a window with

a length of L is applied then an FFT with length N (assuming $N = L$) is calculated. Therefore the spectrum at time j is obtained. To calculate the spectrum at the next step, the window is shifted $\triangle T$ samples ahead and the same process is repeated.

It is obvious that the spectrum at time j calculated in this way provides only the averaged information of the signal within the range of the N samples around the time instant j. As the length of the FFT becomes smaller, the averaging effect decreases, but the resolution of the spectrum decreases too. Thus, it is not possible to reduce the averaging effect by choosing a smaller length of the FFT. This effect can be reduced by selecting a suitable window, such as a Hamming window which gives a broadening of the main lobe of the spectrum but reduces leakage to side lobes.

Recall the adaptive ARMA spectral analysis method proposed in chapter 3. A time series can be modelled as an ARMA process, while the adaptive ARMA filter generates an ARMA estimate of the time series. Consequently, the power spectrum of the time series can be calculated from the weights of the adaptive ARMA filter. Since the weights of the adaptive ARMA filter are adaptively adjusted for every input sample according to the LMS algorithm, the power spectrum calculated from the current weights, therefore does not have any averaging effect as the running spectral analysis method.

For the application of the adaptive ARMA filter in the EGG's spectral analysis, the order of p (length of the forward tapped delay line) should be long enough to cover the lowest possible period of the slow wave. A suitable value of q (the length of the backward tapped delay line) is 10 according to our experiments. With small values of μ_a and μ_c, the adaptive ARMA filter always works properly.

Since the algorithm converges only after a certain amount of adaptations, say M adaptations, the power spectrum can only be calculated after M samples. Following that period the power spectrum can be calculated for each time instant. In the case that only short data are available or the signal has to be analyzed right at the beginning, the adaptive ARMA filter can provide correct power spectra by processing the data or a segment of the data several times.

If an averaged power spectrum within a certain interval is required, the weights of the adaptive filter at each time instant should be averaged and then the power spectrum is calculated from the averaged weights. In reality it is not necessary to provide a power spectrum for every input sample and the power spectrum is calculated only for a certain time shift. Therefore the averaged weights over a small range of time are usually used for the adaptive spectral analysis in order to reduce the gradient noise in the filter weights.

Figure 5.38 shows running power spectra of an EGG measured from a normal fasted volunteer. The sampling frequency of the EGG is 2 Hz, $p = 50$, $q = 10$. The interval between two spectra is 20 seconds. The frequency component at around 0.3 Hz is the respiratory disturbance and that around 0.05 Hz is the gastric signal. From the figure we can see the evolution of the gastric signal frequency. It is fairly stationary.

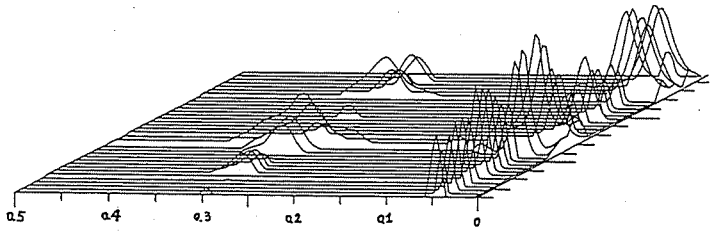


Figure 5.38: Running power spectra of a normal EGG. Horizontal: frequency in Hz; Depth: time; Vertical: power spectrum.

The running spectra of the tachygastrial EGG is shown in Fig.5.39, where the time interval between two successive spectra is 50 seconds. The frequency component of the gastric signal spreads from 0.05 to 0.2 Hz. The frequency of the respiratory artifact is about 0.25 to 0.3 Hz. It is relatively weak and not shown in the figure (we can observe it only in two power spectra). From this figure we can see that the frequency of the gastric signal changes over time. In some periods the dominant frequency of the gastric signal equals 0.05 Hz and sometimes it equals 0.17 Hz. The power changes of different gastric frequency components over time can also be observed in the figure.

5.8.3 Postprandial EGG spectral analysis

One of interesting research subjects on the EGG is the postprandial study since the stomach really does its job only after the intake of the meal. From the postprandial study, one may obtain information about the function of the stomach. After the intake of the meal, the stomach starts to work, its smooth muscles begin to contract, and the electrical behavior becomes

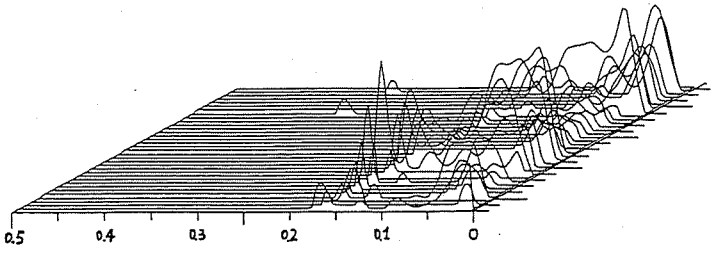


Figure 5.39: Running power spectra of a tachygastrial EGG. Horizontal: frequency in Hz; Depth: time; Vertical: power spectrum.

complicated. We mentioned at the beginning of section 5.8 that in the postprandial situations the EGG becomes complicated too. The frequency of the gastric signal changes postprandially, which requires the adaptive technique for the spectral analysis.

Previous work

In the pre-postprandial research on the electrogastric activities in dogs, Smout et al (Smout 1980) recorded both serosal and cutaneous signals while simultaneously examining the mechanical activity. During the motile quiescent period only the slow wave was recorded. When contractions occurred, the cutaneous EGG was found to increase in amplitude over periods of motile quiescience.

In a pre-postprandial EGG study in human (Jones 1985), it is found that (1) the amplitude of the EGG after the intake of the meal (60 minutes) is much higher than that before the meal; (2) The number of 3 cycles/min waves per block (10 min) after the meal (3 blocks) is about 5 times higher than that before the meal (2 blocks); (3) The mean amplitude of the EGG in each block decreases postprandially (6 blocks).

In the investigation of the effect of the ingestion of a barium sulfate meal, Stewart et al (Stern 1985, Koch 1987) found that during the period (5.5min) before the ingestion only 3 cycles/min gastric waves were found while during the period (5.5 min) after the ingestion an additional peak on the spectrum at a frequency of 1 cycle/min was found. The amplitude of the 1 cycle/min frequency component was associated with the density of

the barium.

Our study

Fig.5.40 shows the running spectra of a postprandial EGG, which was measured from a male volunteer 30 minutes after the normal meal (meat with potato) (Chen 1988f). The interval between two spectra is 50 seconds. From this figure we can clearly see that at the beginning of the measurement the gastric signal is composed of two dominant frequencies (0.05 and 0.1Hz). Postprandially the amplitude of the higher frequency component decreases while the amplitude of the lower frequency component increases. At the end of the measurement, the dominant frequency of the gastric signal is lower than the normal frequency (0.05 Hz).

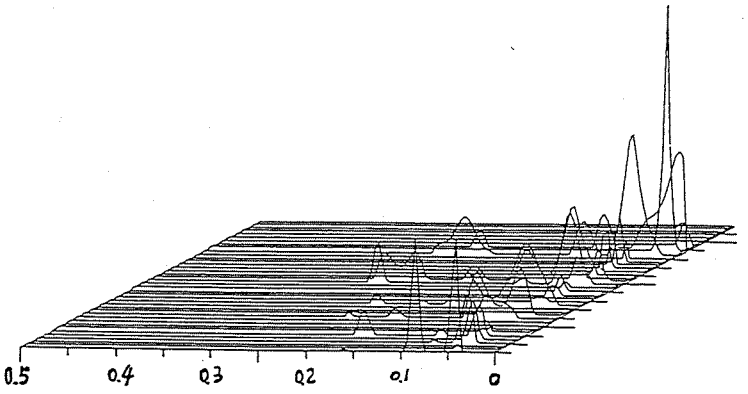


Figure 5.40: Running power spectra of a postprandial EGG. Horizontal: frequency in Hz; Depth: time; Vertical: power spectrum.

The above example is not intended to give a conclusion about the evolution of the postprandial EGG, but to show the usefulness and advantages of the adaptive spectral analysis method proposed in chapter 3.

In Fig.5.40 significant difference between two successive spectra (only 50 second time interval) can be observed. This implies that any FFT based spectral analysis methods may not be suitable because of the averaging effect.

5.9 Conclusion

In this chapter we presented novel methods for the analyses of the electrogastric signals. First, we introduced the electrical behavior of the smooth muscles of the stomach. Then, the measurement and the characteristics of the EGG were described. An adaptive gastric signal enhancement system and an adaptive respiratory artifact cancellation method were proposed. Promising results were obtained and shown in the chapter. To answer some important questions in the research on the EGG, computer simulations were conducted based on the model derived from the volume conduct theory and suggestive conclusions were made. Stimulated by the simulation results, experiments were carried out on the detection of the slow wave propagation. Some new important results have been attained. Finally, the adaptive ARMA spectral analysis method proposed in chapter 3 was successfully applied to the running spectral analysis of the EGG. Comprehensive results were obtained on the tachygastria and the postprandial EGG.

Chapter 6

Conclusions

In this thesis, we have presented adaptive filters, adaptive algorithms, structures and their applications in telecommunications and in biomedical signal processing. In this chapter we would like to summarize our main contributions and further work related to the subjects of the thesis.

Our main contributions include three parts: new adaptive algorithms, adaptive echo cancellation and adaptive gastric signal processing.

New adaptive algorithms In chapter 2 we proposed two new adaptive algorithms for nonstationary signal processing: **the μ-vector LMS algorithm and the lattice form time-sequenced LMS algorithm.**

The μ-vector LMS algorithm is an extension of the LMS algorithm. It uses different values of the step-size for different input samples. To track statistical changes of input signals, a nonstationary factor (similar to the forgetting factor in the RLS algorithm) is introduced. The step-size corresponding to the most recent input sample is given the largest value and the step-size corresponding to older input samples is given exponentially decreasing values. It has been shown that for given nonstationary input signals, there exists an optimal value for the nonstationary factor. The μ-vector LMS algorithm gives a better performance than the LMS algorithm for nonstationary signal processing. In a stationary environment, however, the nonstationary factor can be set 0 and the μ-vector LMS algorithm turns out to be the LMS algorithm.

The TSAF proposed by Ferrara and Widrow produces a better performance for some nonstationary signals having a recurring statistical character. Since it uses multiple weight vectors for different intervals between the recurring points and only one of the weight vectors is adapted for each input sample, it converges very slowly. This limits its applications. To

improve its convergence we proposed to implement the TSAF in a lattice form. In the proposed lattice form TSAF, the tapped delay line of the adaptive filter is replaced by a lattice structure. The backward errors of the lattice filter are used as the inputs of the TSAF. Since the backward errors are uncorrelated with each other, the convergence speed of the TSAF is dramatically increased.

In chapter 3 **an adaptive ARMA filter was proposed. An LMS algorithm and a RLS algorithm have been derived for the adaptive ARMA filter.** The LMS-ARMA and the RLS-ARMA methods were successfully applied in spectra estimation and the results were presented. **Comparisons** between the adaptive IIR filters and the adaptive FIR filter were given. It was concluded that the convergence of the adaptive FIR filter is always guaranteed but that of the adaptive IIR filters (except the constrained adaptive IIR filter) can never be guaranteed. However our experience has shown that the adaptive IIR filters do not diverge if the step-size is chosen to be fairly small. In contrast to the conclusion made in the literature we have observed that the recursive adaptive filter may converge faster than the adaptive FIR filter in the applications of adaptive noise cancellation and of adaptive line enhancement. In adaptive spectral estimation we found that the adaptive LMS-ARMA method provides a better performance than the adaptive LMS-AR method proposed by Griffiths for input signals which can be modeled as ARMA processes.

Adaptive acoustic echo cancellation and adaptive nonlinear echo cancellation In chapter 4 we presented our contributions in adaptive echo cancellation. Two different problems (the acoustic echo and the nonlinear echo) in the echo cancellation were discussed and promising results were obtained.

The adaptive echo cancellation includes adaptive linear echo cancellation, adaptive acoustic echo cancellation and adaptive nonlinear echo cancellation. The adaptive linear echo canceller has been commercially available. The progress of the research on the adaptive acoustic echo cancellation and the adaptive nonlinear echo cancellation has been slow.

The main problems with the acoustic echo are that the acoustic echo path has a long impulse response (more than 1000 taps) and is nonstationary. The nonstationary echo path requires fast adaptations. The long impulse response, however, makes fast adaptation algorithms impractical (too high computational complexity). The subband AAEC was shown to be a good solution. The existing subband AAEC, however, introduces delays in the transmission line, which should be avoided in practical applications.

In chapter 4 we proposed a no-delay subband structure. An AAEC using the no-delay structure has completely been designed. The simplified

weighted overlap-add method is applied to realize the analysis/synthesis filter banks. To avoid aliasing problems, an oversampling rate with a factor of 4 is used. For the adaptive filtering in subbands, a modified complex LMS algorithm was developed.

The proposed new subband AAEC has been simulated both off-line on computers and on-line in a multi-processor system. Promising results were obtained: sufficient ERLE, sufficient echo reduction in the whole frequency band, no aliasing problems and a computational saving with a factor of 5 over the conventional full band AAEC.

On-line simulations have shown that the proposed AAEC is stable in nonstationary environments. When the echo path is time-varying, the performance is, however, degraded. This is because the convergence of the AAEC is not fast enough to track well the changes of the acoustic echo path.

On telephone networks and in hand-free telephone and teleconferencing systems, the level of the echo is usually lower than that of the interesting signal. The required ERLE of the adaptive echo canceller is not higher than 50 dB. In two-wire full duplex data transmission system, however, the level of the echo may be 30 to 40 dB higher than that of the interesting signal. Thus a high echo reduction (may be more than 60 db) is required. In order to have high echo reduction, the nonlinear effect of the echo path should be taken into account. In the thesis two methods for adaptive nonlinear echo cancellation were discussed and their performances were exhaustively investigated. A comparison between the Wiener scheme and the Volterra expansion method was given. It was found that the Wiener scheme (a system identification method) results in a better performance than the Volterra expansion method only if the echo path is exactly known and modeled. In practice, however, this is not the case. We have observed that the performance of an adaptive nonlinear echo canceller with the Wiener scheme is not better than an adaptive linear echo canceller if the echo path is not exactly modeled. The Volterra expansion has been shown to be a good method. To cancel the nonlinear effect resulting from A/D and D/A convertors we designed an adaptive nonlinear echo canceller using a 3rd order Volterra series. An improvement of more than 8 dB echo reduction was achieved with extra 16 taps. Its performance and computational complexity were investigated. The effect of the far-end signal and the finite wordlength representation of the filter weights was shown and the methods to alleviate the problems were given.

Adaptive electrogastric signal processing In chapter 5 novel methods for the detection and the analysis of electrogastric signals were proposed and some important results were presented.

As in the human heart, there is electric activity in the stomach. The electrogastric activity can be cutaneously measured and the cutaneous signal (EGG) is very attractive because it is non-invasive, completely harmless to patients or volunteers and does not disturb the on-going gastric activities. Unlike other electrophysiological measurements, such as ECG, however, the medical and diagnostic use of the EGG is very limited. One of the important reasons for that is the poor quality of the EGG.

To make great progress in the research on the EGG, better signal processing techniques have to be developed. In the literature it was observed that the lowpass filtering is the most commonly used method. The main problem with the lowpass filtering however, is that the frequency (or harmonics) of the interesting gastric signal may overlap with that of some noise contained in the EGG. In this thesis adaptive filtering techniques have been applied to filter and to analyze EGG signals.

In the aspect of signal processing, our contributions include the adaptive enhancement of the EGG, the adaptive cancellation of the respiratory artifact in the EGG and the on-line spectral analysis of the EGG. The performance of the proposed adaptive systems was thoroughly investigated. It has been shown that the respiratory artifact, the ECG and some other noise can be substantially reduced, applying the proposed adaptive systems. The gastric signal component in the EGG is, however, little affected. The SNR of the EGG is significantly improved and the direct waveform analysis is made possible.

The EGG is a nonstationary signal. The normal frequency of the gastric signal is about 0.05 Hz. However, sudden changes of its frequency have been observed and they are generally considered to be related to gastric motility disorders. The LMS-ARMA spectral analysis method, we proposed, provides a good tool for on-line monitoring the frequency changes of the EGG. It is especially useful for the postprandial study.

In the area of biomedical research, our contributions include the analysis of the characteristics of the EGG, the new method for the measurement of the EGG, the observation of the propagation direction of the gastric slow wave and the analysis of the postprandial EGG.

Based on measurements, the characteristics of the EGG was well exploited. In order to answer the question, "what can be expected from an EGG", a simulation model for the transfer of internal electrogastric activities to the abdomen was derived based on the volume conduct theory, and cutaneous EGG signals were simulated. Some interesting conclusions were made based on simulation results and were shown in clinical experiments to be true: 1) Spike activities are not observable in the EGG; 2) The propagation direction of the gastric slow wave can be detected in EGG signals. This has been considered to be impossible for years. In a postprandial EGG

study we found some interesting phenomena in frequency domain, which are more comprehensive than those explained in the literature.

Further work The whole thesis has been devoted to the development of new adaptive algorithms and new applications in the echo cancellation and biomedical signal processing. To conclude the thesis we would like to give some suggestions on further work related to this thesis.

- Convergence analysis of the adaptive IIR filter. We have mentioned that the adaptive IIR filter is more suitable than the adaptive FIR filter for identifying an unknown recursive system and for modeling a noisy signal. One may find many other potential applications of the adaptive IIR filter. The convergence of the adaptive IIR filter is, however, not guaranteed. More efforts still have to be made on the analysis of the convergence both theoretically and experimentally.

- More efficient and faster methods for acoustic echo cancellation. In this thesis we proposed a new subband AAEC. We believe the proposed AAEC gives a better performance than other methods described in the literature. But this does not imply that it is the optimal solution for the acoustic echo cancellation. Some other methods are worth investigating:

  1) Adaptive acoustic echo canceller using an adaptive IIR filter. We know that the main problem in the acoustic echo cancellation is the long impulse response. In z-transform domain, this impulse response can be represented by a long polynomial as follows:

  $$H(z) = a_0 + a_1 z^{-1} + a_2 z^{-2} + \cdots + a_N z^{-N} \qquad (6.1)$$

  However, the transfer function of a recursive adaptive filter has a rational expression:

  $$H_{IIR}(z) = \frac{a_{1j} + a_{2j} z^{-1} + \cdots + a_{pj} z^{-p}}{1 - c_{1j} z^{-1} - \cdots - c_{qj} z^{-q}} \qquad (6.2)$$

  Dividing the numerator in Eq(6.2) by its denominator one can have a long polynomial like the one expressed in (6.1). Thus it is clear that the adaptive IIR filter may be used to model the acoustic echo path and a computational reduction may be achieved, i.e., $p + q <$ (or $<< N$. Moreover it may also be possible that the acoustic echo path has a recursive nature. If this is true, the adaptive IIR filter is certainly more suitable than the adaptive FIR filter.

  2) Frequency domain AAEC. Adaptive filtering in frequency domain has an advantage of less computation. Its convergence is, however

very slow. Thus, we would like to suggest to realize an acoustic echo canceller using frequency domain fast adaptive algorithms, e.g., frequency domain RLS algorithm since less taps are required by the adaptive filter in each frequency bin.

- Potential research on the EGG. There are several things that can be done. First we believe it is very useful to install all of the adaptive systems and methods proposed in this thesis on a personal computer so on-line processing and monitoring of the EGG can be performed. Second, the neural network may find applications in the analysis of the EGG signal, e.g., a multi-layer neural network may be used to classify and to recognize different patterns of the postprandial EGG in frequency domain. Third, more clinical experiments may be done for medical research, such as postprandial study of the EGG and study of the correlations between EGG signals and contractions in the stomach.

Bibliography

[1] O. Agazzi (1982), D.G. Messerschmitt and D.A. Hodges, "Nonlinear echo cancellation of data signals," IEEE Trans. Comm., vol.COM-30, pp2421-2433

[2] B. Alberts (1983) et al., Molecular biology of the cell, Garland Publishing, ICC., New York

[3] S.T. Alexander (1986), Adaptive signal processing: theory and applications, Springer-Verlag

[4] W.C. Alvarez (1922), "The electrogastrogram and what it shows," Journal of American Medical Ass., vol.78, pp1116-1118

[5] C. M. Anderson (1983) et al., "Adaptive enhancement of finite bandwidth signals in white Gaussian noise," IEEE Trans. Acoust., Speech, Signal Processing, vol. ASSP-31, pp.17-27

[6] A. Barbe (1971), "Behaviour of the LMS adaptive algorithm in the identification of a linear discrete finite-memory system," Review A, Vol.13, No.2, pp53-62

[7] P. Bass (1961), "Electric activity of gastroduodenal junction," Amer. J. Physiol. vol.21, pp587

[8] B.E. Bellahsene (1985), J.W. Hamilton, J.G. Webster, P. Bass and M. Reichelderfer, "An improved method for recording and analyzing the electrical activity of the human stomach", IEEE Trans., MBE-32, pp911-915

[9] M. Bellanger (1976) et al.,"Digital filtering by polyphase network: application to sample-rate alteration and filter banks," IEEE Trans. ASSP, vol.ASSP-24, No.2, pp109-114

[10] M. Bellanger (1987), Adaptive digital filters and signal analysis, Marcel Dekker Inc., New York

[11] N. Bershad (1980) et al., "Tracking characteristics of the LMS adaptive line enhancer–Response to a linear chirp signal in noise." IEEE Trans. Acoust., Speech, Signal Processing, vol. ASSP-28, pp.504-517

[12] R.B. Blackman (1959) and J.W. Tukey, The measurement of power spectra from the point of view of communications engineering. New York: Dover

[13] B.H. Brown (1975), R.H. Smallwood, H.L. Duthie, and C.J. Stoddard, "Intestinal smooth muscle electrical potentials recorded from surface electrodes",Med. and Biol. Eng., Vol. 13, pp97-102

[14] J.P. Burg (1967), "Maximum entropy spectral analysis," 37th Ann. Ineter. Meeting, Soc. Explor. Geophysics. Oklahamo City, Okla

[15] J.P. Burg (1975), "Maximum entropy spectral analysis", Ph.D dissertation, Geophysics Dept., Stanford Univ., CA, May 1975

[16] T.E. Carter (1978), "Study of an adaptive lattice structure for linear prediction analysis of speech," Proc of ICASSP-1978, Tulsa, OK

[17] J. Chen (1984), "Computer simulation of the transfer of the electrogastrogram from stomach to the abdominal skin," (part 1), Internal report, Lab. ESAT, Dept. Electr. Eng. KU Leuven

[18] J. Chen (1985), "Computer simulation of the transfer of the electrogastrogram from stomach to the abdominal skin," (part 2), Internal report, Lab. ESAT, Dept. Electr. Eng. KU Leuven

[19] J. Chen (1986), "Time sequenced adaptive filtering of the computer simulated abdominal cutaneous signals," Internal report, Lab. ESAT, Dept. Electr. Eng. KU Leuven

[20] J. Chen (1987a) and J. Vandewalle, "Lattice Form Time Sequenced Adaptive Filter" in Digital Signal Processing - 87, V. Cappellini and A.G. Constantinides (eds.), North-Holland, pp766-770

[21] J. Chen (1987b), J. Vandewalle, W. Sansen, G. Vantrappen and J. Janssens, "Adaptive Cancellation of Respiratory Disturbance in Electrogastric Signals", in Digital Signal Processing - 87, V. Cappellini and A.G. Constantinides (eds.), North-Holland, pp901-905

[22] J. Chen (1987c), J. Vandewalle, W. Sansen, G. Vantrappen and J. Janssens, "Adaptive Enhancement of Human Electrogastrography", Proc. of IEEE Int. Conf. on Biomed. Eng., Vol.2, pp858-859

[23] J.Chen (1987d), J. Vandewalle and B. De Moor, "ARMA Spectral Estimation by an Adaptive IIR Filter", to appear in Linear Algebra and Application

[24] J. Chen (1988a), H. Bes, J. Vandewalle and P. Janssens, "A New Structure for Sub-Band Acoustic Echo Canceller", Proc. of IEEE Int. Conf. on Acoustic, Speech and Signal Processing, Vol.5, pp2574-2577,

[25] J. Chen (1988b) and J. Vandewalle,"A comparison Between Adaptive IIR and Adaptive FIR Filter", Proc. of Ninth Symposium on Information Theory in the Benelux, pp163-169

[26] J. Chen (1988c) and J. Vandewalle, "An μ–Vector LMS Adaptive System for Enhancing Nonstationary Narrow Band signals", Proc. of IEEE Int. Symp. on Circuit and System, Vol.1, pp771-774

[27] J. Chen (1988d), J. Vandewalle, P. Janssens and H. Bes "Design of Sub-Band Acoustic Echo Canceller", Proc. of IEEE Int. Symp. on Circuit and System, Vol.2, pp1325-1328

[28] J. Chen (1988e), J. Vandewalle, W. Sansen, G. Vantrappen and J. Janssens, "Detection of Gastric Signals From Cutaneous Abdominal Measurements" in Analysis and Optimization of Systems, A. Bensoussan & J.L. Lions (Eds.), Springer-Verlag, pp1117-1128

[29] E. Vancutsem (1988), J. Janssens, G. Coremans, G. Vantrappen, J. Chen, J. Vandewalle and W. Sansen, "Detection of Gastric Slow Wave Propagation by Cutaneous Electrogastrography," Gastroenterology, Vol.92, No.5.2, p475

[30] J. Chen (1988f), J. Vandewalle, W. Sansen, G. Vantrappen and J. Janssen, "On-line Spectral Analysis of Electrogastrographical Signals", Proc. of IEEE Int Conf on Biomedical Engineering, Vol.10:1988, pp1186-1187

[31] J. Chen (1988g), J. Vandewalle, W. Sansen, E. Vancutsem, G. Vantrappen and J. Janssen, "Observation of Phase Shifts from Cutaneous Electrogastrographies", Proc. of IEEE Int. Conf. on Biomedical Engineering, Vol.10:1988, pp992-993

[32] J. Chen (1989a) J. Vandewalle, D. Van De Putte, M. Vandeurzen, and D. Sallaerts, "Adaptive cancellation of nonlinear echo in datacommunication systems," to appear in Mathematics in Signal Processing, J. Mcwhirter (ed.), Oxford University Press

[33] J. Chen (1989b), J. Vandewalle, W. Sansen, G. Vantrappen and J. Janssens, "An Adaptive Method for Cancellation of Respiratory Artifact in Electrogastric Measurements", Medical & Biological Eng. & Computing., Vol.27, pp57-63

[34] J. Chen (1989c), J. Vandewalle, W. Sansen, E. Van Cutsem, G. Vantrappen and J. Janssens, "Observation of the Propagation of Human Electrogastric Activity from Cutaneous Recordings", to appear in Medical & Biological Eng. & Computing., Vol.27

[35] J. Chen (1989d) and J. Vandewalle, "Study of Adaptive Nonlinear Echo Canceller With Volterra Expansion," in Proc. of ICASSP-1989

[36] J. Chen (1989e), J. Vandewalle, W. Sansen, G. Vantrappen and J. Janssens, "Multi-Channel Adaptive Enhancement of Human Electrogastrogram," submitted to IEEE trans. on Biomedical Engineering

[37] J.Chen (1989f), H. Bes, J. Vandewalle, I. Evers and P. Janssens, "A new subband acoustic echo canceller," submitted to IEEE Trans. on Acoustic, Speech and Signal Processing.

[38] J. Chen (1989g), J. Vandewalle, H. Bes, I. Evers and P. Janssens, "No-delay subband acoustic echo canceller", to appear in Proc. of 1989 Workshop on Applications of Signal Processing to Audio and Acoustics, New York, (invited paper).

[39] J. Chen (1989h) and J. Vandewalle, "Adaptive nonlinear echo cancellation using Volterra expansion," submitted to IEEE Trans. on Acoustic Speech and Signal Processing

[40] J. Chen (1989i) and J. Vandewalle, "On the convergence of the time-sequenced adaptive filter" submitted to Electronics Letters

[41] J. Chen (1989j), J. Vandewalle, W. Sansen, G. Vantrappen, J. Janssens, "Adaptive spectral analysis of cutaneous electrogastric signal using autoregressive moving average modelling," submitted to Med. & Biol. Eng. & Comp.

[42] J. Chen (1989k) and J. Vandewalle, "Adaptive filters: structures, algorithms and applications," submitted to Journal A

[43] J.C Chow (1972), "On estimating the order of an autoregressive moving average process with uncertain ocservations," IEEE Trans. on Autoamatic Control, vol.AC-17, pp707-709

[44] J.M. Cioffi (1983) and T. Kailath, "Fast, fixed-order, least-square algorithms for adaptive filtering," ICASSP-1983, pp679-682

[45] J.M. Cioffi (1984) and T. Kailath, "Fast recursive least squares filters for adaptive filtering," IEEE Trans. on Acoustic, Speech and Signal Processing, vol.ASSP-32, pp304-338

[46] A.B. Clark (1925) and R.C. Mathes, "Echo suppressors for long telephone circuits", Proc. AIEE, vol.44, pp481-490

[47] G.A. Clark (1981) et al,"Block implementation of adaptive digital filters" IEEE Trans. Acoust., Speech, Signal processing, Vol. ASSP-29, No.3, pp.744-752

[48] J.R. Caser-Corredera (1985) et al., "Data echo nonlinear cancellation," ICASSP-1985, pp1245-1247

[49] R.E. Crochiere (1983) and L.R. Rabiner, Multirate digital signal processing, Prentice-Hall, Inc., Englwood Cliffs, New Jersey

[50] E.E. Daniel (1965), "Electrical and contractile activity of pyloric region in dogs and effects of drugs administered intra-artrially," Gastroenterology, vol 49, pp403-418

[51] E.E. Daniel (1968) and Irwin: Handbook of physiology

[52] R.A. David (1978) and S.D. Stearns, "Adaptive IIR algorithms based on gradient search," Proc. 24th Midwest Sympo. Circuits Syst.

[53] M. Dentino (1978), J. McCool and B. Widrow, "Adaptive filtering in the frequency domain," Proc. IEEE, vol.66, pp1658-1659

[54] J.D. Durbin (1959), "Efficient estimation of parameters in moving average models," Biometrika, vol.46, pp306-316

[55] T.Y El-Sharkawy (1978) et al., "Intracellular electrical activity of canine and human gastric smooth muscle," J. Physiol. (London), vol.279, pp291-307

[56] D.D. Falconer (1978) and L. Ljung, "Application of fast Kalman estimation to adaptive equalization", IEEE Trans. Comm., vol. COM-26, pp1439-1446

[57] B.O. Familoni (1987), Y.J. Kingma and K.L. Bowes, "Study of transcutaneous and intraluminal measurement of gastric electrical activity in humans", Med. Biol. Eng. Compt., Vol. 25, pp397-402

[58] H. Fan (1988), "Counter examples to Stearn's conjecture on error surfaces of adaptive IIR filters," IEEE Int. Conf. on ASSP, vol.3, pp1568-1571

[59] P. L. Feintuch (1976) "An adaptive recursive LMS filter", Proc. of IEEE, vol.64, pp1622-1624

[60] E. R. Ferrara Jr (1981). and B. Widrow, "Multichannel adaptive filtering for signal enhancement" IEEE-ASSP-29, No.3, pp766-700

[61] E.R. Ferrara (1981) JR and B. Widrow, "The time-sequenced adaptive filter" IEEE Trans. Acoust., Speech, Signal processing, Vol. ASSP-29, No.3, pp.679-683,

[62] E.R. Ferrara (1982) and B. Widrow, "Fetal electrocardiogram enhancement by time sequenced adaptive filtering," IEEE Trans. on Biomed. Eng., vol.BME-29, pp458-460

[63] B. Friedlander (1982), "Lattice filters for adaptive processing," Proc. of IEEE, vol.70, pp990

[64] B. Friedlander (1982), "A recursive maximum likelihood algorithm for ARMA line enhancement", IEEE trans. Acoustic, Speech, Signal Processing, vol.ASSP-30, pp651-65

[65] A. Fuch (1988), "Adaptieve recursieve filters – Toepasbaarheid bij het verwijderen van een acoustische echo," Endwork thesis of Hoger Instituut der Kempen (Geel), Belgium

[66] J.J. Fuchs (1987), "ARMA order estimation via matrix perturbation theory," IEEE Trans. Automatic Control, Vol.AC-32, pp359-361

[67] N. Furuya (1985) et al., "Audio conference equipment with acoustic echo canceller," NEC Res. & Develop., No.76, pp18-23

[68] C. Galand (1984), "New quadrature mirror filter srtuctures," IEEE Trans. ASSP, vol.ASSP-32, pp522-531

[69] C. Gibson (1980) and S. Haykin, "Learning characteristics of adaptive lattice filtering algorithms," IEEE Trans. ASSP, vol.ASSP-28, pp681-691

[70] A. Gilloire (1987), "Experiments with sub-band echo cancellers for teleconferencing," ICASSP-1987, pp49-12-1

[71] A. Gilloire (1988) and M. Vetterli, "Adaptive filtering in sub-bands," ICASSP-1988, vol.D

[72] R.D. Giltin (1976) and J.S. Thompson, "A new structure for adaptive digital echo cancellation," Conf. Rec. Nat. Telecommun. Conf., pp8.2.1-8.2.7

[73] E.N. Goodman (1955), H. Colcher, G.M. Katz and C.L. Dangler, "The clinical significance of the electrogastrogram", Gastroenterology, Vol. 29, pp598-607

[74] L.J. Griffith (1975), "Rapid measurement of digital instantaneous frequency", IEEE Trans. Acoust., Speech, Signal processing, Vol. ASSP-23, pp207-222

[75] L.J. Griffiths (1977), "An adaptive lattice structure for noise cancelling applications", Proc.IEEE Int. conf. on Acoust.,Speech, Signal processing, Hartford, CT, pp.683-686

[76] C.W.K. Gritton (1984) and D.W. Lin, "Echo cancellation algorithms" IEEE ASSP Magazine, pp30-38

[77] G.W. Gullikso (1980), H. Okuda, M. Shimizum and P. Bass, "Electrical arrhythmias in gastric antrum of the dog," Amer. J. Physiol., vol.239, ppG59-G68

[78] R. W. Harris (1986) et al. "A variable step (VS) adaptive filter algorithm," IEEE Trans. Acoust., Speech, Signal Processing, vol. ASSP-34, pp.309-316

[79] S. Haykin (1985), "Radar signal processing, IEEE ASSP Magazine vol.2 pp2-18

[80] S. Haykin (1986), Adaptive filter theory, Prentice-Hall

[81] N. Holte (1981) and S. Stueflotten, "A new digital echo canceler for two-wire subsriber lines," IEEE Trans. Comm., vol.COM-29, pp1573-1580

[82] H. Holtz (1973), "Prony's method and related approaches to exponential approximation," Aerospace Corp., Rep. ATR-73 (9990)-5, June 15, 1973

[83] M.J. Honig (1981) and D.D. Messerschmitt, "Convergence properties of an adaptive digital lattice filter", IEEE Trans. Acoust., Speech, Signal processing Vol. ASSP-29, June 1981, pp. 642-653

[84] M.J. Honig (1984) and D.D. Messerschmitt, Adaptive filters: structures, algorithms and applications, Kluwer Academic Publishers

[85] O. Horna (1982), "Cancellation of acoustic feedback," COMSAT Tech. Review, vol.12 pp319-333

[86] T.C. Hsia (1981), "A simplified adaptive recursive filter design," Proc. of IEEE, vol.69, No.9, pp1153-1155

[87] W. Hsu (1986), D.A. Hodges and D.G. Messerschmitt, "Acoustic echo cancellation for loudspeaker telephones," IEEE Trans. Comm., December

[88] D.R. Hush (1986), N. Ahmed, R. David and S.D. Stearn, "An adaptive IIR structure for sinusoidal enhancement, frequency estimation and detection," IEEE Trans. on ASSP, vol.ASSP-34, pp1380-1390

[89] F. Itakura (1971) and S. Saito, "Digital filtering techniques for speech analysis and synthesis," Proc. of Int. Conf. Acoustics, Paper 25-c-1, Budapest

[90] C.R. Johnson (1981) et al., " SHARF convergence properties," IEEE Trans. on ASSP, vol.ASSP-29, p659

[91] K.R. Jones (1985) and G.E. Jones, "Pre- and postprandial EGG Variation", in "Electrogastrography" eds by Stern, R. M. and Koch, K. L. New York, Praeger

[92] S. M. Kay (1981) and S. L. Marple, JR "Spectrum analysis – a modern perspective", Proc. of IEEE, vol.69, pp1380-1419c

[93] W. Kellermann (1985), "Kompensation akustischer echos in frequenzteilbandern," Frequenz, vol.39, No. 7/8, pp209-215

[94] JR. Kelly (1970) et al., "Self-adaptive echo canceler", U.S. patent , No. 3,500,000

[95] K. Kelly (1969) and C.F. Code, "Effect of transthoracic vagotomy on canine electrical activity," Gastroenterology, vol.55, pp51-58

[96] M.A. Kentie (1981), E.J. van der Schee, E.J. Grashuis, and A.J.P.M. Smout, "Adaptive filtering of canine electrogastrographic signals", Part 1 and 2. Med. and Biol. Eng. and Comput. Vol. 19, pp759-769

[97] K.L. Koch (1987), W. R. Stewart and R.M. Stern, "Effect of barium meals on gastric electromechanical activity in man", Digestive Diseases and Sciences, Vol. 32 No.11, pp1217-1222

[98] A.N. Kolmogorov (1939), "Sur l'interpolation et extrapolation des suites stationaires," Comptes Rendus de l'Acad. Sci., Paris, vol.208, pp2043-2045

[99] M.G. Frein (1945), "On a problem of extrapolation of A.N. Kolmorov," C.R. (Dokl.) Akad. Nauk SSSR, Vol.46, pp306-309

[100] M.G. Larimore (1980) et al, "SHARF: An algorithm for adaptive IIR digital filters", IEEE trans. on Acoustic, Speech, Signal Processing, vol.ASSP-28, pp428-439

[101] M.G Larimore (1978a) et al., "Adaptive cancelling using SHARF," Proc. 21st Midwest Symp. Circuits Syst.

[102] M.G Larimore (1978b) et al., "Multipath cancellation by adaptive recursive filtering, Proc. 12th Asilomar Conf. Circuits Syst. Comput.

[103] D.T. Lee (1981), M. Morf and B. Friedlander, "Recursive least square ladder estimation algorithms," IEEE Trans. ASSP, vol.ASSP-29, pp467-481

[104] N. Levinson (1947), "The Wiener RMS (root mean square) error criteria in filter design and prediction," J. Math. Phys., vol.25, pp261-278

[105] D.A. Linkens (1974) and A.E. Cannell, "Interactive graphic analysis of gastrointestinal electrical signal," IEEE Trans. Biomedical Eng., vol.21, pp335-339

[106] D.A. Linkens (1978) and S.P. Datardina, "Estimation of frequencies of gastrointestinal electrical rhythms using autoregressive modelling," Med. and Biol. Eng. and Comput., vol.16, 262-268

[107] L. Ljung (1978), M. Morf and D.D. Falconer, "Fast calculation of gain matrices for recursive estimation schemes," Int. J. of Control, pp1-17

[108] L. Ljung (1983) and T. Soderstrom, Theory and practice of recursive identification, MIT Press, Cambridge, Mass.

[109] D. Long (1987), D. Shwed and D.D. Falconer, "Study of a pole-zero adaptive echo canceller," IEEE Trans. Circuit and System, vol.CAS-34, pp765-769

[110] R.W. Lucky (1968), J. Salz and E.J. Weldon JR., Principles of data communication, McGraw-Hill, New York

[111] J. Makhoul (1977), "Stable and efficient lattice methods for linear prediction," IEEE Trans. ASSP, vol.ASSP-25, pp423-428

[112] J. Makhoul (1978), "A class of all zero lattice digital filters: principles and applications," IEEE Trans. ASSP, vol.ASSP-26, pp304-413

[113] J. Makhoul (1981)and L.K. Cosell, "Adaptive lattice analysis of speech," IEEE Trans. ASSP, vol.ASSP-29, pp654

[114] D. Mansour (1982) and A.H. Gray Jr., "Unconstrained frequency-domain adaptive filter," IEEE Trans. on ASSP, vol. ASSP-30, pp726-734

[115] S.L. Marple (1980), "A new autoregressive spectrum analysis algorithm," IEEE Trans. on ASSP, vol.ASSP-28, pp441-454

[116] J.D Markel (1975) and A.H. Gray, Linear prediction of speech, Springer-Verlag, New York

[117] R.S. Medaugh (1981) and L.J. Griffiths, "A comparison of two fast linear predictors," Proc of ICASSP-1981, Atlanta GA

[118] D.V. Messerschmitt (1984), "Echo cancellation in speech and data transmission" IEEE J. on Selected Areas in Communications, vol. SAC-2, No.2, pp283-297

[119] P.C. Millar (1985), "Recursive quadrature mirror filters – criteria specification and design method," IEEE Trans. ASSP, vol.ASSP-33, No.2, pp413-420

[120] S. Minami (1985) and T. Kawasaki, "A double talk detection method for an echo canceller", ICASSP-1985 pp46.5.1-pp46.5.5

[121] M. Morf (1978) and D.T. Lee, "Recursive least square ladder forms for fast parameter tracking," Proc. of Int. Conf. on Dec. and Control, San Diego, CA

[122] D. R. Morgan (1983), "Effect of gradient noise on the adaptive cancellation of a sinusoid in white noise," IEEE Trans. Acoust., Speech, Signal Processing, vol. ASSP-31, pp.1043-1045

[123] K.G. Morgan (1978) P.F. Schmalz and J.H. Szurszewski, "The inhibitory effects of vasoactive intestinal polypeptide on the mechanical and electrical activity of canine antral smooth muscle," J. of Physiology (London), vol.282, pp437-450

[124] W. Murray (1972) ed., Numerical Methods for Unconstrained Optimization, Academic Press, New York

[125] S.S. Narayan (1983) et al., "Transform domain LMS algorithm," IEEE Trans. ASSP, vol. ASSP-31 pp609-615

[126] T.S. Nelsen (1968) and S. Kohatsu, "Clinical electrogastrography and its relationship to gastric surgery", American Journal of Surgery, Vol. 116, pp215-222

[127] A.V. Oppenheim (1975) and R.W. Schafer, Digital Signal Processing, Prentice-Hall, Inc.

[128] A. Peled (1974) and B. Liu, "A new hardware realization of digital filters," IEEE Trans. ASSP, vol.ASSP-22, pp456-462

[129] V.F. Pisarenko (1973), "The retrieval of harmonics from a covariance function," Geophysical J. Royal Astronomical Soc., vol.33, pp346-366

[130] R.L. Plackett (1950), "Some theorems in least squares," Biometrika, vol.37, p149

[131] R. Plonsey (1961) and R. Collin, Principles and applications of electromagnetic fields, McGraw-Hill Book Company, NY, 1961

[132] R. Plonsey (1969) and D. Fleming, Bioelectric Phenomena, McGraw-Hill Book Company, New York

[133] J.G. Proakis (1983), Digital Communications, McGraw-Hill, New York

[134] L.R. Rabiner (1978) and R.W. Scharfer, Digital processing of speech signals, Prentice-Hall, Englewood Cliffs, N.J, USA

[135] B.D. Rao (1988) and R. Peng, "Tracking characteristics of the constrained IIR adaptive notch filter," IEEE Trans. on ASSP, vol.ASSP-36, pp1466-1479

[136] J. T. Rickard (1979) and J. R. Zeidler, "Second-order output statistics of the adaptive line enhancer," IEEE Trans. Acoust., Speech, Signal Processing, vol. ASSP-27, pp.31-39

[137] S.Rush (1963) et al., "Resistivity of body tissues at low frequencies," Circulation Res., vol.12, p40

[138] J. Salz (1983), " On the start-up problem in digital echo cancellers", Bell Syst. Tech. J., vol.62, pp1353-1364

[139] E.H. Satorius and S.T. Alexander, "Channel equalization using adaptive lattice algorithms", IEEE Trans. Communications, Vol. COM-27, No.6, June 1979, pp.899-905

[140] S.K. Sarna (1972), "Simulation of the electrical control activity of the stomach by an array of relaxation oscillators," Dig. Diseases, vol.17, No.4, pp299

[141] A. Schuster (1898), "On the investigation of hidden periodicities with applications to a supposed 26-day period of meterological phenomena," Terr. Mag. Atmos. Elect., vol.3, pp13-41

[142] H.P. Schuwan (1957) and C.F. kay, "The conductivity of living tissues," Ann. N.Y., Acad. Sci., vol.65, p1007

[143] G.L. Sicuranza (1986) and G. Ramponi, "Adaptive nonlinear digital filters using distributed arithmetic," IEEE Trans. ASSP, vol.ASSP-34, pp518-526

[144] R.H. Smallwood (1975) B.H. Brown and H.L. Duthie, "An approach to the objective analysis of intestinal smooth muscle potential recorded from surface electrodes," Proc. 5th Int. Symp. Gastrointestinal Motility, Leuven, Belgium

[145] R.H. Smallwood (1978), "Analysis of gastric electrical signals from surface electrodes using phaselock techniques," Med. and Biol. Eng. and Comput., vol.16, pp507-518

[146] A.J.P.M. Smout (1980), E.J. Van der Schee and J.L. Grashuis, "What is measured in electrogastrography?" Dig. Dis. Sci., vol.25, pp179-187

[147] M.M. Sondhi (1967), "An adaptive echo canceller", Bell Syst. Tech. J., vol.46, pp487-511

[148] M.M. Sondhi (1980) and D.A. Berkley, "Silencing echoes on the telephone network", Proc. of IEEE, vol.68, pp948-963

[149] S.D. Stearns (1981), "Error surfaces of recursive adaptive filters," IEEE Trans. on Cirsuits Syst., vol.CAS-28, June 1981

[150] R.M. Stern (1985), and K.L. Koch, (eds) Electrogastrography. New York, Praeger

[151] C.J. Stoddard (1981), R.H. Smallwood and H.L. Duthie, "Electrical arrythmias in the human stomach", Gut, Vol. 22, pp705-712

[152] P. Stoica (1988) and A. Nehorai, "Performance analysis of an adaptive notch filter with constrained poles and zeroes," IEEE Trans. on ASSP, vol.ASSP-36, pp911-919

[153] T.M. Sullivan (1978) et al., "High resolution signal estimation," ARGO Systems, Internal Rep. June

[154] H.W. Tam (1977), J.G. Webster, "Minimizing electrode motion artifact by skin abrasion," IEEE Trans on Biomedical Engineering, Vol. BME-24, No.2

[155] R.L. Telander (1978) et. al., "Human gastric atony with tachygastria and gastric relention," Gastroenterol., vol.75, pp495-501

[156] E.J. Thomas (1971), " Some considerations on the application of the Volterra representation of nonlinear networks to adaptive echo cancellers," Bell Syst. Tech. J., vol.50, pp2797-2805

[157] D.A. Thompson (1978), "A constrained recursive adaptive filter for enhancement of narrow-band signals in white noise," in Proc. of 12th Asilimar Conf. Circuits Syst. Comput., pp214-218

[158] H. Tong(1976), "Fitting a smooth moving average to noisy data," IEEE Trans. on Inform. Theory, vol.IT-22, pp493-496

[159] J. Treichler (1979), "Transient and convergent behavior of the ALE," IEEE Trans. Acoust., Speech, Signal Processing, vol. ASSP-27, pp.53-63

[160] D. Vandeputte (1988) and M. Vandeurzen, "Ontwerp van een adaptieve niet-lineaire echo-canceler voor toepassing op ISDN-lijnen," Master thesis, Dept. Electrotechnieke, KUL, Belgium

[161] E.J. van der Schee, and J.L. Grashuis, "Contraction-related, low-frequency components in canine electrogastrographic signals", American Journal of Physiology, Vol. 245, ppG470-G475, 1983

[162] E.J. van der Schee, and J.T Grashuis, "Running spectrum analysis as an aid in the representation and interpretation of electrogastrographic signals", Med. and Biol. Eng. and Comput., Vol. 25 pp57-62, 1987

[163] P. Vary (1983) and G. Wachersreuther, "A unified approach to digital polyphase filter banks," AEU, Band 37, Heft 1/2, pp29-34

[164] N.A.M. Verhoeckx (1979) et al., "Digital echo cancellation for baseband data transmission, IEEE Trans. ASSP, vol.ASSP-27, No.6, pp768-781

[165] J.L. Vernet (1971), "Real signals fast Fourier transform: storage capacity and step number reduction by means an odd discrete Fourier transform," Proc. of IEEE, Oct.

[166] P. D. Welch (1967), "The use of fast Fourier transform for the estimation of power spectra: a method based on time averaging over short, modified periodograms," IEEE trans. Audio Electroacoust., AU-15:70-73

[167] B. Widrow (1960) and M.E. Hoff Jr., "Adaptive switching circuits," IRE WESCON Conv. Rec., Part 4, pp96-104

[168] B. Widrow (1975) et al., "Adaptive noise cancelling: Principles and applications," Proc. IEEE, vol. 63, pp.1692-1716

[169] B. Widrow (1976) et al., "Stationary and nonstationary learning characteristics of the LMS adaptive filter", Proc. IEEE, vol.64, pp.1151-1162

[170] B. Widrow (1985) and S.D. Stearn, Adaptive Signal Processing, Prentice-Hall Englewood Cliffs, N.J.

[171] B. Widrow (1987) and R. Giltlin, "1987 Annual international seminars on circuit design and signal processing," CEI course 709, book 2, ppVII-3-9

[172] N. Wiener (1949), Extrapolation, Interpolation, and Smoothing of Stationary Time Series, with Engineering Applications, MIT Press, Cambridge, Mass.

[173] N. Wiener (1931) and E. Hopf, "On a class of singular integral equations," Proc. Prussian Acad. Math-Phys. Ser., p696

[174] S.A. White (1975), "An adaptive recursive digital filter," Proc. 9th Asilomar Conf. Circuits Syst. Comput., p21

[175] H. Wold (1938) A study in the analysis od stationary time series," Almqvist and Wicksells, Uppsala, Sweden

[176] C.H. You (1981) et al., "Gastric and small intestinal myoelectrical dysrhythmia associated with chronic intractable nausea and vomitting," Ann. It. Med., vol.95, pp449-451

[177] C.H. You (1984) and W.Y. Chey, "Study of electromechanical activity of the stomach in human and dogs with particular attention to tachygastria," Gastroenterology, vol.86, pp1460-1468

[178] G.U. Yule (1927), "On a method of investigating periodicities in disturbed series, with special reference to Wolfer's sunspot nembers," Phil. Trans. Royal Soc. (London), vol.A226, pp267-298

[179] J. Zeidler (1978) et al., "Adaptive enhancement of multiple sinusoids in uncorrelated noise," IEEE Trans. Acoust., Speech, Signal Processing, vol. ASSP-26, pp.240-254